BENCHTOP NMR METABOLOMICS: AN EXPLORATION OF BIOFLUIDS AND DISEASES

Oliver James Megram

A thesis submitted in partial fulfilment of the requirements of Nottingham Trent University for the degree of Doctor of Philosophy

July 2025

Copyright Statement

The copyright and intellectual property of this work is held by the author. You may copy up to 5% of this work for private study, or personal, non-commercial research. Any re-use of the information contained within this document should be fully referenced, quoting the author, title, university, degree level and pagination. Queries or requests for any other use, or if a more substantial copy is required, should be directed to the author.

Abstract

With ageing populations and increasing healthcare demands, there has been a growing need for cost-efficient diagnostic tools that enable early disease detection and intervention. Metabolomics has demonstrated significant potential in identifying disease-associated biomarkers, providing a valuable approach for early diagnosis and monitoring. Nuclear magnetic resonance (NMR) spectroscopy has been widely used in metabolomics; however, high-field (HF) NMR spectrometers are expensive, requiring specialised infrastructure, limiting accessibility. Recent advances in benchtop NMR (bNMR) spectroscopy have offered a more affordable technique, though its diagnostic utility across a broader range of diseases remains underexplored.

This research investigated bNMR's potential for disease detection through metabolomic profiling across multiple biofluids and pathological conditions. Using optimised pulse sequences and minimal sample preparation, bNMR's ability to differentiate between health states was evaluated. The study examined its performance in distinguishing metabolic signatures in diabetes, asthma and epilepsy using urine, blood plasma, and cerebrospinal fluid (CSF), respectively.

The findings demonstrated that bNMR successfully differentiated diabetic patients from healthy controls in urine-based analysis. However, it could not distinguish pre-diabetic individuals, a distinction HF-NMR achieved, suggesting a limitation in bNMR's sensitivity. Similarly, in blood plasma, bNMR identified metabolic differences between individuals with well-managed asthma, though differentiation between a more severe asthma type and controls remained challenging. In CSF, bNMR could not effectively distinguish between idiopathic epilepsy and control samples, highlighting potential limitations in detecting subtle metabolic changes in this biofluid. Metabolites were detected using bNMR, with only minor differences compared to HF-NMR. These findings suggested that bNMR could help guide targeted disease analysis.

This research highlighted bNMR's potential as a cost-effective tool while emphasising the need for further refinement in sensitivity and validation across diverse disease cohorts. While applications of bNMR are promising, future research

should explore its applicability in detecting comorbid populations and assess its clinical viability for early disease detection.

Acknowledgements

I would like to express my deepest gratitude to those who have supported me on this PhD journey. First and foremost, I am profoundly grateful to Dr. Elena Hunter, thank you for the countless hours of supervision and unwavering support you have provided throughout my research. This is extended to Professor John Hunt for his invaluable guidance and insightful feedback over the years. A special thank you to Professor Philippe B. Wilson, for believing in me as a Ph.D. candidate, introducing me to the field of benchtop NMR, and bringing together collaborators. I am also grateful for the camaraderie of the wider research group, including Simmie, Dantherine, Stefan, Kate, Leilah, Sam, Daniella, and Connor.

I am grateful for the financial support from NTU through the Pro Vice Chancellor's studentship award. This research was made possible by contributions from Oxford Instruments for their technical support, Dr. Luisa De Risio, Dr. Oliver Marsh, and Associate Professor Giunio Cherubini on the CSF study, as well as Dr. Cristina Panetti, Dr. Neil Williams, Dr. Alice Murphy, and Professor Philip McTernan at NTU for their work on blood plasma and diabetes urine samples.

My heartfelt thanks go to Dr. Benita Percival and Professor Martin Grootveld for introducing me to NMR metabolomics and teaching me "NMR is great". I am also grateful to the MTIF team, especially Associate Professor Samantha McLean and Dr. Adam Varney, for their support—I owe you many bags of Haribo! I am deeply indebted to Dr. Baptiste Busi and Dr. Marshall Smith for their mentorship, especially to Marshall for his patience guiding me through the "basics" of NMR.

To my friends: Ed, CT, Liam, Callum, Lewis, Libby, and Kieran, thank you for providing me with perspective and inspiration to push this research further, on our many coffee crawl catch-ups.

I am here today based on the strong foundation built upon me by my family. To my whole family, past and present, especially to my grandparents, thank you. I would like to extend my thanks to my now extended family: Charlie, Lavinia, Arthur, and Auntie, thank you all for being there for me and being so supportive.

To my parents, you joke about how you “don’t know how I got my brains”. The skills I needed were hard work, determination, a good work ethic, and a drive for what you love to do to make a difference to people. These skills I learnt from you, although “brains” would have been helpful at times to have. You gave me the power to do whatever I wanted, to achieve whatever I wanted. I hope you will get to understand more about my work further than the “bits in your bloods”. This thesis reflects your support, for this, my work is dedicated to you.

Finally, I would not have made it through this journey without my other half, Megan. Thank you for putting up with my frustrations, for reminding me to step back when I got too immersed, and for always “being right” (as much as I hate to admit it!). Your unwavering support, endless patience, and encouragement have meant everything to me.

Declaration

I declare that the work presented in this thesis is my own unless explicitly stated otherwise. None of the work included in this thesis has previously been submitted for a degree or other qualification.

Patient Recruitment and Sample Collection

Blood plasma samples for the asthma study were provided by collaborators in ISTEC, Nottingham Trent University (NTU) (Dr. Cristina Parenti and Dr. Neil Williams). Clinical difficult-to-control samples were drawn by clinicians at Southampton University Hospital. All other blood plasma samples were recruited at NTU.

Cerebrospinal fluid samples were supplied by the Dick White Referrals (DWR) Centre. All clinical laboratory analyses were conducted at DWR, with Idiopathic Epilepsy Stage II conformation analysis performed by clinicians Dr. Luisa De Risio, Dr. Oliver Marsh, and Associate Professor Giunio Cherubini.

Additional research presented in the appendices was also contributed by collaborators. Blood serum samples, displayed in Appendices 25 - 26, were collected by Associate Professor Jessica Piasecki and Dr. Mathew Piasecki at NTU. Bacterial media was grown at NTU (Appendices 23 - 24) by Dr. Felix Dafhnis-Calas, while chronic kidney disease (CKD) urine samples were collected by veterinarians at the University of Bristol Medical School and Langford Vets. The CKD samples were provided to NTU through collaboration with Dr. Natalie Finch.

Sample Preparation

Leillah Madhau assisted with sample preparation and acquisition of the chronic kidney disease urine samples presented in the appendices (19 - 22). Kevin Butler and Huw Williams at the University of Nottingham (Centre for Biomolecular Sciences, University Park) conducted sample acquisition on the 800MHz NMR spectrometer for the CKD and cerebrospinal fluid studies.

List of Abstracts

The following review abstracts have been presented at conferences as part of this research:

Busi B, **Megram O**, Madhau L, Hunter E, & Wilson P. (2022) Toward Quality Control and Contaminant Analysis of Spices. Poster presented at the 18th Annual Conference of the Metabolomics Society. Metabolomics 2022. Palacio de Congresos de Valencia, Valencia, Spain. 19-23 June, 2022.

Megram O, Busi O, Hunter E, Hunt J, & Wilson P. (2022) Optimising Benchtop NMR**:** A comparison of tubes for improved spectra. Poster presented at the School of Animal, Rural and Environmental Sciences: Research Conference Programme 23rd September 2022 Brackenhurst Campus, Nottingham Trent University.

Megram O, Busi B, Hunter E, Smith M, Finch N, & Wilson P. (2023) Chronic Kidney Disease Analysis *via* High-field and Benchtop NMR. Poster presented at the 19th European Magnetic Resonance Congress, EUROMAR, Scottish Event Campus, Glasgow, Scotland, Abstract P-014.

Megram O, Hunt J, & Hunter E. (2025) Benchtop NMR metabolomics: an exploration of biofluids and diseases. Presentation presented at the 12th Analytical Biosciences Group Early Career Researcher Meeting, University of Sheffield (24th-25th April 2025)

Megram O, Hunt J, & Hunter E. (2025) Towards Accessible Metabolomics: Disease Detection using Benchtop NMR. Presentation presented at the 2025 Systems Health and Integrated Metabolic Research Symposium, City Campus, Nottingham Trent University (2nd July 2025)

Abbreviations and Acronyms:

1D	One Dimensional
2D	Two Dimensional
AA	Amino Acids
ABCD	Age, BMI, C-peptide levels, and Duration of Diabetes
ANOVA	Analysis of Variance
AT	Adipose Tissue
ATP	Adenosine Triphosphate
AUC	Area Under the Curve
AUCROC	Area Under the Curve of the Receiver Operating Characteristic
BCAA	Branch Chain Amino Acid
BMI	Body Mass Index
bNMR	Benchtop Nuclear Magnetic Resonance
BPD	Biliopancreatic Diversion
BTB	Bovine Tuberculosis
CHD	Coronary Heart Disease
CI	Confidence Intervals
CKD	Chronic Kidney Disease
CNS	Central Nervous System
CoA	Acetyl Coenzyme A
COPD	Chronic Obstructive Pulmonary Disease
COSY	Correlation Spectroscopy
CP	Composite Pulse
CPMG	Carr-Purcell-Meiboom-Gill
CSF	Cerebrospinal Fluid
D_2O	Deuterium
DI	Diameter Inner
DiaRem	The Diabetes Remission Prediction Score Model
DO	Diameter Outer
DPFGE	Double Pulsed Field Gradient Spin Echo
DSS	Sodium trimethylsilylpropanesulfonate

DTC	Difficult To Control Asthma
DWR	Dick White Referral Centre
EBC	Exhaled Breath Condensate
EDTA	Ethylenediaminetetraacetic acid
FADH2	Flavin Adenine Dinucleotide
FC	Fold Change
FDR	False Discovery Rate
FID	Free Induction Decay
FT	Fourier Transformation
GC	Gas Chromatography
GC-MS	Gas Chromatography-Mass Spectrometry
HbA1c	Glycated Haemoglobin
HC	Healthy Controls
HF	High-Field NMR
HF-NMR	High-Field Nuclear Magnetic Resonance
HIV	Human Immunodeficiency Virus
HMDB	Human Metabolome Database
HMQC	Heteronuclear Multiple Quantum Correlation
HOMA-IR	Homeostatic Model Assessment for Insulin Resistance
HSQC	Heteronuclear Single Quantum Correlation
Hz	Hertz
IE	Idiopathic Epilepsy
IFG	Impaired Fasting Glucose
IGT	Impaired Glucose Tolerance
IMS	Individualised Metabolic Surgery
INEPT	Insensitive Nuclei Enhanced by Polarization Transfer
IQR	Interquartile Range
IR	Insulin Resistance
IVETF	International Veterinary Epilepsy Task Force
J	Joules
K	Kelvin
LAGB	Laparoscopic Adjustable Gastric Banding
LC	Liquid Chromatography

LGCP	Laparoscopic Greater Curvature Plication
LTBI	Latent TB Infection
MA	Well Managed Asthma
MHz	Mega Hertz
MLTC	Multiple Long Term Conditions
MRI	Magnetic Resonance Imaging
MS	Mass Spectrometry
MVA	Multivariate Analysis
NADH	Nicotinamide Adenine Dinucleotide
NADPH	Nicotinamide Adenine Dinucleotide Phosphate
NfL	Neurofilament Light chain
NHS	National Health Service
NMR	Nuclear Magnetic Resonance
NOE	Nuclear Overhauser Effect
NOESY	Nuclear Overhauser Effect Spectroscopy
NTU	Nottingham Trent University
ONS	The Office for National Statistics
OPLS-DA	Orthogonal Partial Least Squares Discriminant Analysis
PC	Principal Component
PCA	Principal Component Analysis
PCR	Polymerase Chain Reaction
PFG	Pulsed Field Gradient
PLS-DA	Partial Least Squares Discriminant Analysis
ppm	Parts Per Million
PPP	Pentose Phosphate Pathway
Pre-Sat	Presaturation
PRISMA	Preferred Reporting Items for Systematic Reviews and Meta-Analyses
PROJECT	Periodic Refocusing of J Evolution by Coherence Transfer
PTB	Paratuberculosis
qNMR	quantitative NMR
RCF	Relative Centrifugal Force
RD	Relaxation Delay

RF	Radio Frequency
RPM	Revolutions Per Minute
ROC	Receiver Operating Curve
RYGB	Roux-en-Y Gastric Bypass
S/N	Signal to Noise
SARS-CoV-2	Severe Acute Respiratory Syndrome Coronavirus 2
SE	Structural Epilepsy
SNR	Signal to Noise Ratio
SOP	Standard Operating Procedure
SPLS-DA	Sparse Partial Least Squares Discriminant Analysis
SST	School of Science and Technology
T	Tesla
T1DM	Type 1 Diabetes Mellitus
T2DM	Type 2 Diabetes Mellitus
TB	Tuberculosis
TMAO	Trimethylamine-N-Oxide
TMS	Tetramethylsilane
TOCSY	Total Correlation Spectroscopy
TSP	Trimethylsilylpropanoic acid
UK	United Kingdom
USA	United States of America
V/V	Volume / Volume
VIP	Variable Importance in Projection
W/V	Weight / Volume
WASTED-II	WAter Suppression with a Transverse relaxation filter that Eliminates Distortions
WATERGATE	WATER suppression by GrAdient Tailored Excitation
WET	Water Suppression Enhanced Through T1 Effects
WET-CP	Water Suppression Enhanced Through T1 Effects with a Composite Pulse
WHO	World Health Organisation
$\boldsymbol{B}$	Magnetic Field
B_0	External Magnetic Field

$\boldsymbol{B}_1$	Applied Magnetic Field
h	Planck's constant
$\hbar$	Planck's constant divided by 2π
$\boldsymbol{I}$	nuclear spin angular momentum
$\boldsymbol{M}$	Magnetization Vector
PW	Peak Width
T	Temperature
μ	Magnetic Moment
ω^0	Larmor Frequency (Radians per second)
γ	Gyromagnetic Ratio
υ^0	Larmor Frequency (Hertz)
ΔE	Energy Difference

Table of Contents

List of Figures:

List of Tables:

Chapter 1 Introduction

This research aims to explore the utility of metabolomics, *via* benchtop nuclear magnetic resonance (bNMR) spectroscopy for studying diseases through analysis of mammalian biological fluids. Therein, Chapter 1 will introduce the research question and topic. This comprises an introduction to the research topic, the motivations behind this research, and a literature review of the use of bNMR for metabolomic studies shown in Chapter 2. The pulse sequences utilised in these studies will also be presented. More in-depth NMR theory will be provided in Chapter 3 to ensure the reader is equipped with the knowledge needed to understand the work undertaken and presented in subsequent chapters. Chapter 4 will cover the experimental methodology, offering a detailed explanation of the methods used. Following that, Chapters 5, 6, and 7 will present the research findings, exploring a different disease and biofluid. To conclude, this research will provide a final discussion of the research findings, an outlook on the future of bNMR metabolomics, and a conclusion.

1.1. Practical Motivations

The cost of healthcare in the United Kingdom's (UK) National Health Service (NHS) has increased significantly, rising fourteen-fold between 1950 and 2023.[1] This rise is linked to the growing and ageing population in the UK, which has led to increased demand and strain on the NHS.[1,2] Despite the advances in healthcare, 54% of people aged 65 or older live with multiple long term conditions requiring managed long term care, which is projected to increase to 68% by 2035.[3] This growing burden of disease is associated with the current fundamentally flawed ethos in healthcare; treat diseases once they become an issue or symptoms show, yet this approach can lead to worse health outcomes and largely neglects to prevent diseases before they present.[3]

The World Health Organisation (WHO) and the NHS have proposed intervention and prevention plans to address the increasing demand for earlier detection and improved monitoring of diseases.[4–6] To implement such fundamental changes to

healthcare operations, research should prioritise the development of new detection models. Such strategies must implement the collection or use of biobanks (collection of biological samples) of varied populations (age, gender, and ethnicity) for covering large-scale health screen monitoring.

One such example is the Our Future Health research programme, which is currently recruiting up to five million adult volunteers to obtain a detailed picture of the nation's health that truly reflects the UK's population.[3,7] Recruitment started in July 2022, with preliminary work on the Our Future Health cohort revealing that over half of the first 100,000 volunteers had untreated high cholesterol.[7] Left untreated, high cholesterol could apply further stress to health services, further reinforcing the existing cycle of reactive rather than preventative treatment measures.[7,8]

To transform the current healthcare strategy, testing must be performed quickly and cost-effectively to detect and monitor diseases, enabling preventative treatments. Therefore, research supporting preventative care and detection initiatives should focus on improved usability and practicality. While highly specific and sensitive disease detection techniques are valuable, their impact is limited if the cost of testing exceeds the economic burden of the disease itself. Consequently, research efforts should be balanced between understanding disease aetiology and developing efficient, accessible detection methods. This approach ensures that innovative healthcare solutions are not only scientifically sound but also economically viable and widely implementable.

The worldwide rising cost of care has also been steadily increasing for animals, driven partially by advancements in veterinary medicine and a rising demand for comprehensive animal healthcare.[9] The Office for National Statistics (ONS) reported a 60% increase in the cost of veterinary and other pet services from 2015 to 2024.[10] Furthermore, the detection and prevention of diseases can provide broader benefits for public health and food security, particularly in regions where livestock plays a crucial role in the economy.[11] Investing in animal health is, therefore, not only a matter of improving the quality of life for animals but also a critical component of global health security.

As with human disease detection, to address such a need, this research is focused on the investigation of a cost-effective and fast method for the detection, monitoring and potential prognosis of diseases and care. To assess the methods capabilities three commonly extracted biofluids with differing topographic/anatomic disease aetiologies were selected.

1.1.1. Asthma

Asthma is a chronic lung disease caused by muscle tightening and the inflammation of airways often triggered by allergies, occupational exposures, air pollution, obesity, irritants, and infections. An estimated 80,000 asthma cases are diagnosed in the UK each year, with clinical evidence suggesting improved outcomes are observed with earlier diagnosis and interventions.[12–14] One review of the deaths of patients diagnosed with mild asthma identified that 30% of patients should have been diagnosed with moderate or severe asthma.[13] False positive and negative diagnoses of respiratory conditions further delay the implementation of treatments and increase the chance of acute admissions.[15–17] Moreover, asthma costs the NHS approximately £3 billion a year.[12,13] This cost is partly due to false positive and negative diagnoses; with an estimated £1.5-7.5 million that could be saved by the NHS by reducing misdiagnoses of asthma alone.[13] Therefore, asthma prevention through earlier diagnoses and interventions could help reduce costs from admissions and pharmaceuticals.[13]

One method of reducing misdiagnoses of asthma is to distinguish between asthma phenotypes, such as difficult-to-control asthma, severe asthma, seasonal asthma and childhood asthma, for personalised healthcare strategies.[18] The results from an asthma study distinguishing between phenotypes will later be discussed in Chapter 6 along with a more in-depth introduction to previous research into asthma detection.

1.1.2. Bariatric Surgery and Type 2 Diabetes Mellitus

Type 2 diabetes mellitus (T2DM) is a largely preventable disease, characterised by high levels of glucose in the blood, which accounts for approximately 10% of the NHS budget.[19] Alarmingly, an additional two million people in England alone are at

high risk of developing the disease.[19] A low-cost fast solution to detect T2DM is therefore highly advantageous to the financial stability of healthcare providers. One method used to help manage glycaemic control and obesity is through weight loss surgery, also known as bariatric surgery. However, patients respond differently to the surgery. Therefore, there is a need for screening tools that can predict surgery outcomes. This could be achieved using metabolomics and such research aligns with the research strategy goals of the Our Future Health research programme.[18] This subject is further discussed in the third research chapter (Chapter 7).

1.1.3. Epilepsy

Neurological disorders, such as epilepsy, can be extremely disruptive for both humans and animals. Epilepsy is one of the most prolific neurological disorders in the world with 50 million people having the disease; 80% of which live in low- and middle-income countries and rural areas which coincide with the highest rates of premature mortality.[20] The WHO estimates there to be five million diagnoses of epilepsy every year.[20] Epilepsy is prevalent in humans and dogs, with an estimated 0.75% of all dogs having the condition.[21] Idiopathic Epilepsy (IE) is the most common form of epilepsy clinically diagnosed in dogs from an expensive process of elimination.[22,23] With IE reportedly hard to diagnose due to the numerous disorders that mimic epileptic seizure activity the disease will be investigated in Chapter 5 to explore if an accurate detection model can be obtained.[23]

1.2. Omics

Omics refers to the study of a biological system to explore how it functions. By examining the collective interactions of genes, proteins, metabolites, RNA transcripts, and epigenetic modifications, omics offer a comprehensive understanding of biological systems.[24] By analysing large-scale molecular data, researchers and clinicians can explore disease mechanisms, identify novel biomarkers for accurate detection and staging, and tailor treatment plans based on individual patient's molecular profiles.[24] The main omics approaches include genomics, transcriptomics, proteomics, and metabolomics.[24] For instance, genomics can pinpoint genetic mutations linked to cancer, while proteomics can track protein alterations associated with autoimmune diseases.[24] Omics

approaches hold great potential for improving diagnosis, prognosis, and the development of targeted interventions, driving the progress of modern healthcare.[24] Among these, metabolomics is essential for assessing the current metabolic state of an organism. As the youngest of the major omics techniques, metabolomics is also considered one of the most promising for clinical application.[25]

1.3. Metabolomics

The simultaneous analysis of multiple analytes in biological fluids was first explored in the 1980's.[26] Although the term metabolomics was not coined until 1998, this early research laid the foundation for the field.[26,27] Metabolomics is the study of small molecules less than 1.5kDa in size (metabolites) found within cells, biofluids, tissues and organisms to provide insight into a system's biological status.[28] The complete set of metabolites within a system is known as the metabolome, which can be influenced by factors such as environment, genetics, drugs, age, gender, and diet.[27–29] While the metabolome is constantly changing, metabolomics captures a snapshot of a systems biochemical activity.[28,29] Metabolism encompasses all chemical and physical processes within a system that uses or converts energy and the term metabolic refers to anything related to or affected by these processes. [30]

Metabolomics has been applied across various fields, including toxicology and environmental studies; however its primary focus remains on mechanistic understanding, diagnosis, and prevention.[26,28,31] The first metabolomic study completed using nuclear magnetic resonance (NMR) was conducted in 1983, by Nicholson *et al.*, who demonstrated diabetes mellitus may have a unique metabolic fingerprint that could potentially be used for diagnosis and treatment.[32] Metabolomics was developed further with the integration of chemometric and bioinformatic methods, enabling the differentiation of complex biological profiles. Common classification models used in metabolomics include principal component analysis (PCA) and partial least squares-discriminant analysis (PLS-DA).[33,34] Modern metabolomics continues to follow this trend, employing multivariate statistical analysis (discussed further in Chapter 4.9) to enhance the understanding of biological phenotypes, deciphering mechanisms, and identifying biomarkers.[31]

Since its inception, metabolomics has expanded to encompass a wide range of studies, including research on various cancers,[35,36] neurological diseases such as Parkinson's[37,38] and Alzheimer's disease[39], as well as cardiovascular diseases.[40,41] This has not only provided a deeper mechanistic understanding of disrupted pathways, but has also driven research into novel detection methods through biomarker discovery.

1.4. Metabolites and pathways

Metabolic investigations mainly study amino acids, carbohydrates, organic acids, and lipids, all of which are either produced by the body or obtained through dietary intake. The cocktail of metabolites present, and the concentration in which they are found reflects an organism's physiological state, as well as provide insights into the ongoing metabolic processes.

1.4.1. Amino Acids

Amino acids serve as the fundamental building blocks to proteins and play a vital role in various metabolic pathways. They are classified as either essential or non-essential. The essential amino acids (histidine, isoleucine, leucine, lysine, methionine, phenylalanine, threonine, tryptophan, and valine) cannot be synthesised by the body and must be acquired through diet.[42] In contrast non-essential amino acids (alanine, arginine, asparagine, aspartate, glutamate, glutamine, glycine, proline, serine, tyrosine, and cysteine) can be produced from metabolic intermediates during pathways such as glycolysis.[42] These amino acids are involved in numerous physiological functions, including neurotransmission, immune response, and energy production.

1.4.2. Carbohydrates

Carbohydrates, comprising sugars, starches and fibres represent the primary source of energy for cellular function. Beyond their role in energy metabolism, carbohydrates contribute to cellular structure, for example as components of glycoproteins and glycolipids that stabilise cell membranes and mediate cell-cell interactions. They also play key roles in biochemical signalling, such as during

immune recognition and hormone regulation, where carbohydrate moieties on cell surfaces enable communication between cells and the detection of foreign antigens. Several key metabolic pathways involve carbohydrates, including glycolysis and gluconeogenesis.[43] Glycolysis breaks down glucose into pyruvate, generating ATP and NADH, serving as a primary energy-producing process, particularly under anaerobic conditions.[43] Gluconeogenesis enables the synthesis of glucose from non-carbohydrate precursors such as lactate, glycerol, and amino acids, ensuring glucose availability during fasting or intense exercise.[43] Dysregulation of glycogenesis has been implicated in conditions such as hyperglycaemia, commonly observed in type 1 and 2 diabetes mellitus.

1.4.3. Organic Acids

Organic acids, a broad group of compounds containing one or more carboxyl groups, serve as key intermediates in cellular respiration and metabolic regulation.[44] They are integral to energy production, pH balance, and various biosynthetic processes.[44] Citric acid and succinate are central to the Krebs cycle, where they contribute to ATP generation through oxidative phosphorylation. Lactic acid and pyruvic acid are involved in glycolysis, facilitating energy production under anaerobic conditions. Acetic acid plays a key role in the fatty acid cycle, supporting lipid metabolism and energy homeostasis. Organic acids are particularly relevant in urine metabolomics, as they are excreted as metabolic waste products, providing insights into systemic biochemical activity.[44]

1.4.4. Lipids

Lipids, encompassing fats and oils, serve critical functions in energy storage, cell membrane integrity and cell signalling. They are fundamental to the organisation of life, forming the structural matrix of biological membranes that enable the compartmentalisation of metabolic processes and the establishment of controlled microenvironments. This compartmentalisation allows for the spatial and temporal regulation of biochemical reactions, maintaining homeostasis and facilitating complex cellular functions such as protein sorting, ion transport, and signal transduction.

Beyond structural roles, lipids also act as key mediators in cellular communication. Phospholipids, sphingolipids, and sterols contribute to membrane fluidity and serve as precursors to potent signalling molecules, including prostaglandins, eicosanoids, and steroid hormones. These bioactive lipids regulate diverse physiological processes, from inflammation and immune response to growth and metabolism.

The diversity of lipid species, collectively known as the lipidome, is immense, encompassing thousands of structurally distinct molecules. This complexity reflects their extensive involvement in nearly all aspects of cell biology, from energy metabolism and membrane trafficking to signal transduction and apoptosis. Lipids are primarily synthesised in the liver but can also be acquired through dietary intake. Lipid metabolism is tightly regulated, as imbalances can contribute to metabolic disorders such as obesity, non-alcoholic fatty liver disease, and cardiovascular disease.

1.5. Biological Fluids

A biological fluid, shortened to biofluid, is any liquid found within an organism.[45] Biofluids, such as urine and blood, are routinely used in healthcare settings to monitor patients' health and diagnose diseases. The diversity of biofluids produced by mammals allow for the examination of a wide range of physiological conditions and pathologies.[46]

1.5.1. Blood

Blood is produced in the bone marrow through haematopoiesis. It consists of plasma (liquid component), red blood cells (carrier of oxygen), white blood cells (immune system cells), and platelets (facilitating clotting).[47–49] Functionally, blood is central to maintaining homeostasis, including transporting nutrients from the digestive tract to tissues, delivering oxygen to cells, and removing metabolic waste, including carbon dioxide expelled through the lungs.[48]

Blood circulates throughout the body and interacts with all organs and tissues; it provides a snapshot of the body’s overall metabolic state at any given time. The blood metabolome is composed of glucose, lipids, and amino acids, along with other

biomolecules, such as haemoglobin and plasma proteins, that reflect physiological and pathological conditions.[50] The composition makes blood an invaluable biofluid for studying systemic diseases such as cancer, multiple sclerosis, cardiovascular disease, and Alzheimer's disease.[51–53]

However, while blood is a valuable biofluid for diagnosing multiple diseases, it also has its limitations. The collection procedure is invasive, and the high abundance of proteins can also interfere with the detection of low-abundance metabolites.[54] The most common method of blood collection is venipuncture, where a needle is inserted into a vein, typically in the arm, to draw blood. This procedure can cause discomfort and pain and requires a trained specialist. Additionally, if not performed correctly, it carries a risk of infection. Another method is the fingerstick, a minimally invasive procedure where a small, sharp lancet is used to prick the finger to obtain a drop of blood. This method is commonly used for small-volume samples, such as blood glucose testing or certain rapid tests.[55] However, this method is limited by the small volume of blood collected and variations in metabolite concentrations based on the sample's collection location.

Blood is often processed in its serum or plasma form. To obtain serum, blood is drawn and allowed to clot. The clot is then removed by centrifugation, leaving the clear, yellowish fluid called serum. In contrast, plasma is the liquid portion of blood in which blood cells are suspended. Plasma is obtained by drawing blood and adding an anticoagulant to prevent clotting. The blood is then centrifuged to separate the plasma from the blood cells. Common anticoagulants include ethylenediaminetetraacetic acid (EDTA), heparin, and citrate. However, these additives can interact with the sample and influence analytical outcomes. For instance, EDTA chelates divalent metal ions such as Ca2+ and Mg2+, potentially altering enzyme activity and metabolite stability. Heparin can interfere with lipid and protein binding assays, while citrate dilution can affect ion balance and metabolite quantification. In NMR metabolomics, such interferences are particularly important, as EDTA and citrate produce characteristic spectral peaks that can obscure nearby metabolite resonances and complicate spectral interpretation. These can interact with the sample causing issues in correctly interpreting the results leading to misdiagnoses.

1.5.2. Urine

Urine is a waste product produced by the kidneys through a process of filtration, reabsorption, and secretion.[56] This process removes metabolic waste, toxins, and excess water from the bloodstream, maintaining electrolyte balance and homeostasis.[56] Unlike blood, which circulates continuously throughout the body, urine is an excretory biofluid that reflects metabolic waste products rather than ongoing systemic activity. Urine contains a diverse array of water-soluble metabolites, including urea, creatinine, citrate, and amino acids. Urea is a byproduct of amino acid metabolism to detoxify ammonia. This prevents ammonia accumulation, which could otherwise lead to neurotoxicity.

Urines metabolic composition is primarily influenced by renal function, hydration status and diet rather than direct interactions with all tissues, as seen with blood. This makes urine a particularly valuable biofluid for assessing renal function, metabolic disorders, and systemic toxin accumulation. Urine has been widely used in metabolomic studies, particularly to investigate diseases like diabetes, kidney diseases and cancer. [57–60]

Since the kidneys filter blood plasma and excrete waste, many metabolic disruptions associated with disease, such as altered glucose metabolism in diabetes or abnormal protein excretion in kidney disease, are reflected in urine composition. Unlike blood, where proteins and cells are abundant, urine from healthy individuals is typically devoid of these compounds. The presence of proteins or blood cells can indicate underlying health conditions, such as proteinuria in diabetic nephropathy or glomerulonephritis, and haematuria associated with urinary tract infections, kidney stones, or malignancies of the urinary tract. This makes urine a sensitive marker for renal and systemic disease.[61] One of urine's major advantages in metabolomics is its non-invasive collection method. Unlike blood, which requires venipuncture or fingerprick sampling, urine can be collected easily, painlessly, and in large volumes, making it an ideal biofluid for longitudinal studies that require multiple time-points collections. However, urine has inherent challenges from highly variable metabolites depending on the individual's hydration status, diet and physical activity which can pose challenges in data interpretation.

1.5.3. Cerebrospinal Fluid

Cerebrospinal fluid (CSF) is a clear, colourless biofluid that surrounds and protects the brain and spinal cord, providing both mechanical cushioning and nutrient exchange system for the central nervous system (CNS).[62] CSF plays a crucial role in removing metabolic waste, maintaining intracranial pressure, and transporting signalling molecules, nutrients, and metabolites between the brain and bloodstream.[62]

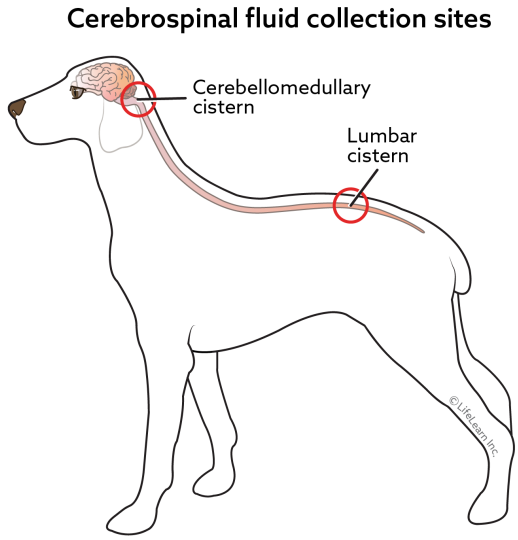

Figure 1 - Cerebrospinal fluid collection sites on canines.

Due to its direct interaction with the CNS, CSF is a highly relevant biofluid for diagnosing and studying neurological diseases. It has been widely used in the investigation of conditions such as Alzheimer's disease, Parkinson's disease, and multiple sclerosis as well as CNS infections like meningitis and encephalitis.[62–65] Unlike blood, and urine, which reflect systemic metabolic activity, CSF is unique in its ability to provide a direct biochemical snapshot of brain metabolism, making it a powerful tool in metabolomics.

CSF is primarily produced by the choroid plexus within the ventricles of the brain and circulates through the ventricular system, subarachnoid space, and spinal canal before being reabsorbed into the bloodstream.[66] Its composition is tightly regulated and includes key metabolites such as glucose, lactate, and amino acids.[66]

In diseased states, CSF composition can be altered exhibiting proteins, abnormal metabolite profiles, and inflammatory markers, providing insights into

neurodegenerative and neuroinflammatory processes.[67] Since the blood-brain barrier (BBB) tightly regulates molecular exchange between the blood and CSF, many brain-specific diseases can be detected in CSF rather than in blood. [62,65]

Despite its diagnostic value, CSF extraction is highly invasive, requiring lumbar puncture (spinal tap) to collect the fluid. This procedure carries risk such as headaches, infections nerve damaged and, in rare cases, brain herniation, making it a less frequently utilised biofluid compared to blood and urine. Due to these risks, CSF sampling is generally reserved for critical cases where brain-related pathology is suspected.[67]

Additionally, while CSF is an excellent medium for detecting neurological biomarkers, its lower metabolite concentration compared to blood and urine requires highly sensitive analytical techniques, posing challenges for metabolomics studies. Typically, total metabolite concentrations in CSF fall within the tens to hundreds of micromolar range, roughly one to two orders of magnitude lower than those in plasma or urine, where concentrations commonly reach millimolar levels. This reduced abundance reflects the restrictive nature of the blood-brain barrier but also ensures that detected metabolites are closely associated with central nervous system metabolism. However, its low protein content compared to blood makes it advantageous for detecting small molecules without significant interference.

1.5.4. Saliva

Saliva is a readily accessible, non-invasive biofluid that has gained increasing interest in clinical and metabolomic research.[68–70] Compared to other biofluids, saliva contains fewer NMR detectable metabolites with approximately 20–50 metabolites identified, depending on the sensitivity of the analytical technique used.[68–70] The metabolomic composition of saliva includes electrolytes, amino acids, organic acids, and enzymes, though their concentrations are significantly lower than in blood or urine.

Table 1 - Comparison of common biofluids used in NMR-based metabolomics

Biofluid	Detectable metabolites (^{1}H NMR)	Metabolite range	Advantages	Disadvantages
Blood	100–150: Amino acids, organic acids, glucose, lactate, lipids, ketone bodies, creatinine, choline-containing compounds	100 μM – 10 mM	Reflects systemic metabolism; widely validated; good reproducibility	Invasive collection; high protein and lipid content can obscure low-abundance metabolites
Urine	150–300: Amino acids, organic acids, sugars, creatinine, urea, hippurate, citrate, phenolic compounds	1 mM – 100 mM	Non-invasive; large sample volume; suitable for longitudinal studies; rich metabolite diversity	High variability due to hydration, diet, and diurnal effects
CSF	50–100: Amino acids, neurotransmitters (glutamate, GABA), lactate, glucose, ketone bodies, choline derivatives	10 μM – 500 μM	Direct insight into central nervous system metabolism; low protein content reduces interference	Invasive collection; low metabolite concentrations require sensitive methods
Saliva	20–50: Amino acids, organic acids, urea, lactate, sugars, ethanol, acetate	1 μM – 100 μM	Easy, non-invasive collection; useful for stress, infection, and oral disease studies	Fewer detectable metabolites; influenced by flow rate, oral microbiome, and contamination

Due to its ease of collection, saliva has been widely utilised in virology through polymerase chain reaction (PCR) for the detection of viruses such as SARS-CoV-2, HIV, and hepatitis.[71] In addition, saliva has been employed in metabolomic studies for distinguishing cigarette smokers from non-smokers, as well as to investigate conditions such as Parkinson's disease.[68–70]

Despite its advantages, saliva presents several challenges that limit its utility in metabolomic research. The fluid has a lower concentration and diversity of metabolites compared to blood, urine and CSF making it harder to detect meaningful biochemical changes. In addition to this environmental and dietary contamination plagues the biofluid. Furthermore, salivary metabolite levels can fluctuate based upon factors such as hydration, stress, circadian rhythms and food intake, reducing reproducibility in metabolomic studies.

While saliva remains a promising biofluid, these limitations reduced its suitability for detecting systemic metabolic changes, particularly in diseases that affect multiple organ systems.[69,72] As such saliva was not included in this research due to its lower diagnostic potential compared to blood, urine and CSF.

In addition to saliva, other biofluids such as breastmilk, nipple aspirate, synovial fluid, sweat, tears, bile, and stool were not analysed in this research. These fluids were excluded due to factors relating to limited sample availability due to potential invasive procedures, smaller sample volumes making it harder to detect metabolites at bNMR scale as well as reduced widespread clinical application. By focusing on blood, urine, and CSF this study prioritises biofluids with the highest metabolic information content and clinical relevance, ensuring a comprehensive yet feasible approach to disease biomarker discovery.

1.6. Analytical techniques in metabolomics

The selection of an appropriate analytical platform is fundamental to effective metabolite analysis, with each method offering distinct advantages and limitation that must be evaluated within the context of specific research objectives. Metabolomic studies can be conducted using either targeted or untargeted

approaches. Untargeted analysis examines the entire metabolome, without requiring prior knowledge of specific compounds, rendering it particularly valuable for novel biomarker discovery.

Conversely, targeted analysis focuses on the identification and quantification of predefined metabolites, making it well suited for diagnostic applications where disease biomarkers or substantial system knowledge has been previously examined. Due to the exploratory nature of this research, an untargeted approach was implemented to maximise discovery potential of new disease biomarkers.

For a technique to be best suited for widescale adoption for detection, diagnostics and prevention in a clinical setting, the methodology must demonstrate suitable sensitivity with high reproducibility, cost-effectiveness, and robust high-throughput capabilities. The following section explores different analytical techniques employed in metabolomic research, along with examining their respective attributes.

1.6.1. Raman Spectroscopy

Raman spectroscopy (RS) provides chemical structural information through observation of light scattering and molecular interactions. This non-destructive technique demonstrates versatility in both organic and non-organic analysis establishing the device as a universal detector.[73] While RS offers quantitative capabilities, accurate calibration with reference standards are required for reliable quantification. A significant methodological limitation arises from florescence interference, which compromises spectral integrity due to the techniques inability to distinguish fluorescent interference and Raman scattering.[73] This is especially problematic for metabolomics as fluorescence is frequently observed in biological matrices containing proteins, lipids, and pigments present in blood samples. Therefore, more complex sample preparation is required to mitigate these challenges.

The method also faces significant sensitivity limitations due to the minimal proportion of light (0.0000001%) that undergoes Raman scattering.[73] Enhanced detection sensitivity can be achieved through increased laser intensity; although, this introduces the potential risk of sample degradation, increased instrument costs

and increased sample processing costs. Surface-enhanced Raman spectroscopy (SERS) employs this principle to deliver improved sensitivity in the nanomolar range compared to conventional RS operating in the micromolar detection range. Nevertheless, this improved detection limit requires complex and costly nanoparticle preparation procedures. Despite these technical considerations SERS has been used for diverse metabolomic applications, including the analysis of glucose and lactate in CSF, lactic acid in blood, as well as creatinine and urea in urine.[74–76] Even though RS has demonstrated research application in metabolomic investigation, widespread clinical implementation remains constrained by the absence of standardised preprocessing protocol and enhanced reproducibility.[77]

1.6.2. Infrared spectroscopy

Infrared spectroscopy (IR), particularly Fourier transform infrared spectroscopy (FTIR) offers advantages within the metabolomic landscape, including minimal operating costs and sample preparation requirements as well as high-throughput capabilities.

However, the technique demonstrates inherent limitation with ambiguous metabolite identification in complex biofluids occurring due to overlapping IR bands, much like the challenges observed in RS. Furthermore, IR methodologies yield semi-quantitative analysis requiring calibration against known standards and cannot provide detailed structural information like that available through NMR.

Notable research applications of IR encompass the differentiation of enantiomeric N-acetylhexosamines in biological fluids and the identification of oxidative stress biomarkers in plasma specimens obtained from patients exhibiting cognitive impairment, thus demonstrating potential diagnostic utility for neurodegenerative conditions such as Alzheimer's disease.[78]

1.6.3. Ultraviolet-Visible Spectroscopy

Ultraviolet-visible spectroscopy (UV-Vis) represents a relatively underutilised analytical platform within the metabolomics landscape, with comparatively limited implementation in comprehensive metabolomic investigations. The technique

operates through the measurement of electromagnetic radiation absorption within the ultraviolet and visible spectral regions, facilitating the identification and quantification of specific metabolic entities based on their characteristic absorption profiles.[79]

UV-Vis methodologies offer several advantageous attributes, including operational simplicity, rapid analytical throughput, minimal sample preparation requirements, non-destructive analytical capabilities, and favourable cost-effectiveness compared to more sophisticated instrumental platforms such as mass spectrometry.[79] However, these benefits are counterbalanced by inherent limitations regarding analytical sensitivity and molecular selectivity, alongside restricted structural elucidation capabilities.[79] The intrinsically complex spectral matrices encountered in biological fluids present significant analytical challenges due to the presence of multiple absorbing compounds that generate substantial spectral overlap phenomena, thereby complicating accurate metabolite quantification.[79] Despite these methodological constraints, the straightforward implementation and economic accessibility of UV-Vis spectroscopy render it potentially valuable for routine analytical applications where metabolite specificity requirements are less stringent.

Research applications of UV-Vis in metabolomic investigations include haemoglobin quantification in biological specimens and the detection of stress-related biomarkers including cortisol, serotonin, dopamine, norepinephrine, and neuropeptide Y.[80,81] [31]These applications demonstrate the technique's potential utility in specific metabolomic contexts, particularly when implemented as a complementary analytical approach within multi-platform investigative frameworks.

1.6.4. Mass Spectrometry

Mass spectrometry (MS) is an analytical technique used to measure the mass-to-charge (m/z) ratio of ions present in a sample. This method is highly sensitive and can detect and quantify over a thousand metabolites, making it an invaluable tool in various scientific fields.[82] MS works by ionizing chemical compounds to generate charged molecules or molecule fragments and measuring their mass-to-charge ratios. The resulting data provides detailed information about the molecular weight and structure of the analytes, which can be used to identify and quantify them.

The integration of chromatographic techniques, especially gas chromatography (GC) and liquid chromatography (LC), enhances the ability of MS to provide a highly quantitative and precise analysis of compounds in a sample. Each coupled technique exhibits distinct strengths and weaknesses.[83] The capabilities of GC coupled with MS (GC-MS) demonstrates analytical ability for volatile and low-molecular-weight metabolites, establishing utility in lipidomic analysis, fatty acid profiling, and characterisation of volatile organic compounds.[84]

For instance, GC-MS has been employed to investigate serum fatty acid profiles to identify potential biomarkers for Alzheimer's disease.[85] Additionally, it has been utilised to study alterations in host metabolism due to gut microbiota changes in mice, revealing key pathway modifications associated with aging.[86] Furthermore, GC-MS has shown promise in breathomics, demonstrating potential in diagnosing influenza infections through the analysis of breath condensate.[87] However, GC-MS's application is limited to thermally stable compounds due to the high temperatures (up to 400˚C) involved, resulting in a comparatively narrower metabolite coverage than LC-based platforms.85

LC-MS encompasses a broader spectrum of metabolites, from small polar molecules to complex lipids and peptides.[88] While LC methodologies demonstrate excellent sensitivity parameters and widespread implementation in targeted metabolomic investigations, they require sophisticated method development protocols for the optimisation of stationary phases, mobile phase compositions, and elution gradients. Significant methodological challenges include retention time variability across analytical sequences, matrix-induced ion suppression phenomena, and labour-intensive sample preparation requirements for the elimination of interfering proteins and lipids from biological matrices. LC-MS has been applied in metabolomics to explore pathways in Huntington disease, cardiovascular diseases, as well as in gum diseases like gingivitis.[89–91]

Capillary electrophoresis (CE) coupled with MS is another technique gaining traction in metabolomics. CE-MS provides high separation efficiency for ionic and highly polar metabolic, including amino acids, nucleotides, and organic acids, while requiring minimal sample preparation.[92,93] However, the methodology may exhibit

sensitivity limitations and reproducibility challenges attributable to migration time fluctuations. Although CE-MS has shown to have relative low running costs with good quantification accuracy, the technique currently lacks a sufficient database of studies and metabolites available for use in current widespread metabolomics applications.[93,94] Moreover, while praised for simpler sample preparation compared to other coupled MS techniques, these procedures can still be more involved and time-consuming than those used in IR and NMR spectroscopy.[92]

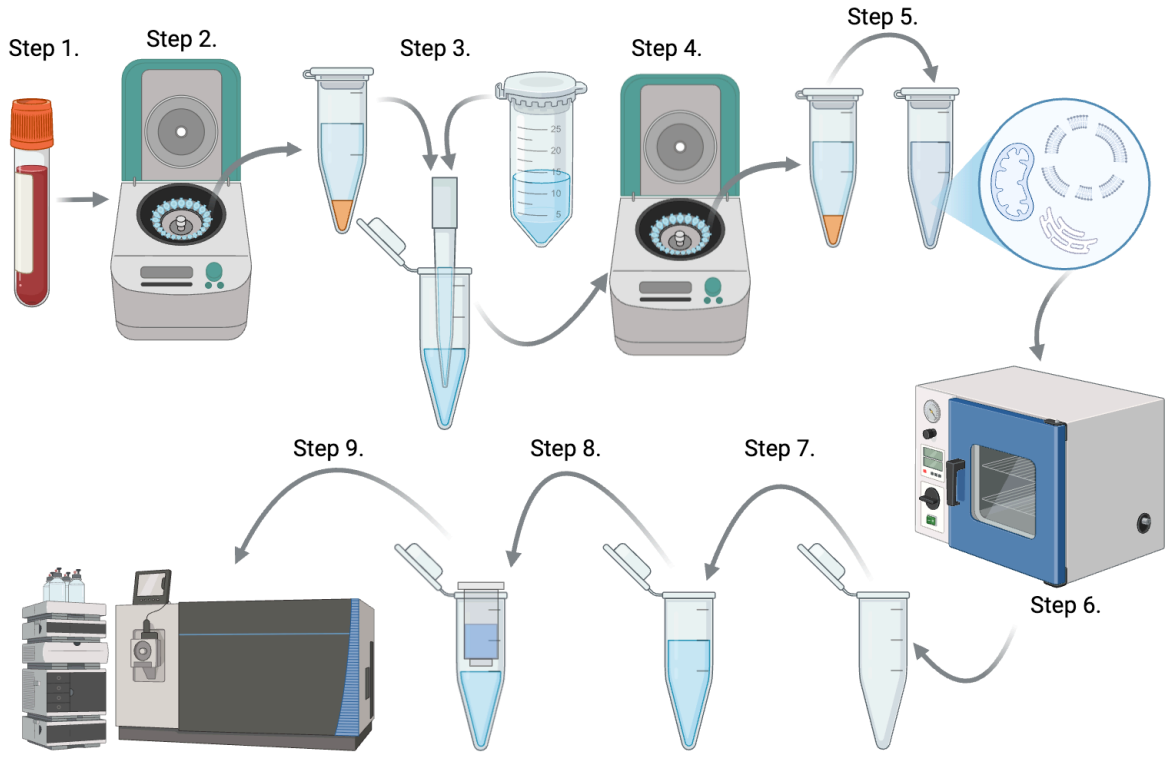

Figure 2 - Workflow for blood sample preparation for mass spectrometry (MS) metabolomics. Whole blood is collected in anticoagulant tubes (e.g., EDTA) and centrifuged to separate plasma or serum from cells. Proteins are precipitated using organic solvents, and the metabolite-containing supernatant is collected. Optional lipid extraction and sample concentration/drying steps can be performed before reconstitution in an MS-compatible solvent. Additional steps such as filtration may be included to remove particulates. Prepared samples are then analysed by LC-MS to profile the metabolome.

A notable advantage of MS and its coupled techniques have been its suitability for targeted analysis when the specific analytes of interest are known, allowing for accurate detection and quantification of targeted metabolites. While the initial cost of a mass spectrometer is relatively affordable and the instrument is more space-efficient compared to high-field NMR (HF-NMR) spectrometers, typically MS platforms range from approximately £150,000 - £600,000 depending on resolution and configuration, whereas HF-NMR systems often exceed £400,000 - £1,000,000. However, the per-sample cost for MS analysis is considerably higher, typically £10 - £30 per sample due to consumables, solvents, and derivatisation steps, compared to under £5 per sample for NMR, which requires minimal preparation steps.[95]

1.6.5. Nuclear Magnetic Resonance

NMR is a widely used analytical technique employed across various fields, including chemistry, pharmaceutical testing, and the food industry.[26] It operates on the principle that certain atomic nuclei, when placed in a strong external magnetic field, absorb and re-emit electromagnetic radiation, producing a spectrum that can be recorded and analysed.[96–99] More information on NMR theory is provided in Chapter 3. NMR is a versatile, non-destructive analytical tool with excellent capability for providing detailed structural information, even in complex samples.[31] One of its key advantages over MS is the simplicity of sample preparation, which enhances reproducibility and enables rapid analysis.[31] Due to these strengths, NMR has become a popular techniques for metabolomic analysis.[100]

The most commonly used nuclei in NMR metabolomic studies is ^{1}H, due to its high natural abundance and strong signal intensity. However other active nuclei, such as ^{13}C, ^{15}N, and ^{31}P, have also been used for metabolomic studies.[100] This versatility of the technique has led to a wide range of biofluids being analysed, including blood plasma, urine and saliva, as well as less conventional samples like CSF, nipple aspirate and breath condensate.[100,101]

Despite its advantages, NMR's minimal sample preparation protocols have drawbacks. Limited removal of macromolecules and other interfering substances can introduce unwanted signals, negatively impacting nearby compounds.[31,100] To mitigate these issues, researchers have developed improved sample preparation methods and applied specialised pulse sequences.[102] A key limitation of NMR compared to MS is its lower sensitivity. While the cost of high-field instruments increases exponentially, NMR resolution scales linearly with magnetic field strength.[100] At current field strengths, NMR is 10 to 100 times less sensitive than LC-MS and GC-MS. While NMR typically detects 50-100 metabolites at concentrations >1μM, LC-MS can identify over a thousand metabolites at levels as low as 10-100 nM.[100]

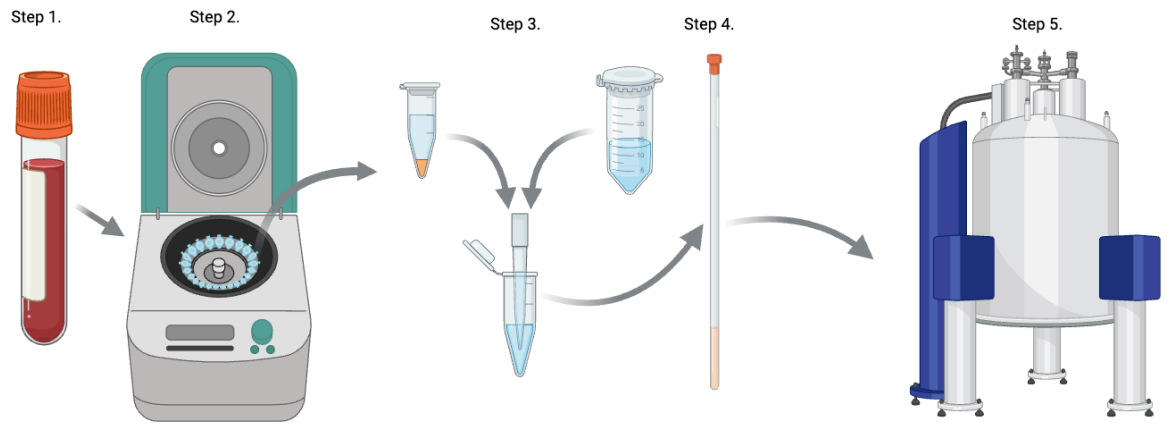

Figure 3 – Workflow for biofluid sample preparation for ¹H NMR metabolomics. Samples (urine, plasma, saliva, or CSF) are first centrifuged or filtered to remove cells and debris. A deuterated buffer containing a chemical shift reference (e.g., TSP or formate) and preservatives (e.g., NaN_3) is prepared and mixed with the sample, typically in a 9:1 or 8:2 ratio. The mixture is transferred to an NMR tube (e.g., 550 µL in a 5 mm tube or a volume compatible with benchtop NMR) for spectral acquisition. The ¹H NMR spectrum can then be directly recorded without further sample processing.

Although magnetic resonance imaging (MRI), NMR's closely related counterpart, is extensively utilised in healthcare, NMR itself has not yet seen widespread adoption.[103] This is largely due to the high cost of high-field NMR (HF-NMR) instruments, lower sensitivity, their substantial space requirements, and the ongoing expenses of cryogenic maintenance with liquid nitrogen and helium.[104] However, recent developments have increased interest in NMR-based metabolomics for private healthcare assessments, with companies like Nightingale Health offering diagnostic services.[105]

Despite these advancements, NMR remains expensive and is not yet viable as a cost-effective screening tool.[105] Nonetheless, ongoing innovations are driving reductions in the cost of NMR analysis.

1.6.6. Benchtop NMR

Over the past two decades, major developments in permanent magnet systems have led to the development of small, inexpensive benchtop NMR (bNMR) spectrometers.[106] While the reduced cost and size of these machines could allow for their implementation in local healthcare settings, they have lower sensitivity and resolution compared to their superconducting counterpart HF-NMR spectrometers. These instruments, typically operating at 0.5 – 2.5 Tesla (T), offer a practical alternative to HF-NMR systems, particularly in settings where cost, space (shown in Figure 4), and accessibility are limiting factors.[106,107] While bNMR has the potential

to be integrated into local healthcare settings, its lower sensitivity and resolution compared to HF-NMR raise questions about its effectiveness for metabolic analysis and disease diagnostics.

Figure 4 - HF-NMR (left) compared to Benchtop NMR (right) in size.

Ongoing research seeks to determine whether bNMR can reliably detect clinically relevant metabolites and whether it could supplement or even replace current diagnostic techniques. Although its capabilities are still being evaluated, recent studies have explored bNMR's applications in metabolomics, particularly in areas such as diabetes and tuberculosis.[72,108–114] These studies highlight the growing interest in leveraging bNMR for reduced sensitivity biomarker discovery and clinical decision-making.

Given the expanding range of potential applications for bNMR, it is crucial to assess the breadth and depth of existing research in this field. The following chapter presents a literature review of bNMR applications, examining its use across various domains from biomedical research to quality control in pharmaceuticals and food science. By reviewing the current state of bNMR research, its strengths, limitations and future prospects in metabolomics and beyond can be evaluated.

Chapter 2 Review of bNMR applications

A systematic literature search was conducted to explore the applications of bNMR in academia over the past decade, spanning from 2014 to 2024. The investigation employed a rigorous, multi-database approach to ensure a comprehensive coverage of scientific literature with emphasis on metabolomics.

Three databases were used for this review: Scopus,[115] PubMed,[116] and Web of Science.[117] Each database was constructed with search terms designed to capture relevant applications of bNMR. These specific search terms, which can be found in Table 2, focus on the liquid state application of small-scale permanent magnet systems with MRI applications excluded from this search.

Table 2 - Search strategy and results for the systematic review across three databases.

Database	Keywords	Results
Web of Science	(((benchtop NMR) OR (Low-field NMR)) NOT (MRI) NOT (Imaging) NOT (solid) NOT (gas) NOT (relax*))	(n= 387)
PubMed	(((benchtop NMR) OR (Low-field NMR)) NOT (MRI) NOT (Imaging) NOT (solid) NOT (gas) NOT (relax*))	(n = 613)
Scopus	TITLE-ABS-KEY ("benchtop NMR" OR "Low-field NMR") AND TITLE-ABS-KEY ("Metab*" OR "detect" OR "diagnose") AND NOT ("MRI" OR "Imaging" OR "solid" OR "gas" OR "relax*" OR "rock" OR "moist*")	(n = 35)

Following an initial search of journal articles Web of Science produced 387 articles, PubMed generated 613 articles, and Scopus identified 35 articles. The Scopus search incorporated additional refinement by including keywords related to metabolic analysis, detection, and diagnostic applications. Selection criteria were applied to ensure the review's focus and quality. Only full English-language journal articles and reviews published between January 1, 2014, and December 31, 2024, were considered. This allowed for a comprehensive examination of recent technological developments and research trends in bNMR applications.

The corresponding papers were then exported to the reference management software Zotero (version 6.0.37) with duplicates removed.[118] The data was then exported to Rayyan to facilitate screening, selection and categorisation.[119] A full breakdown of the number of papers that were identified, screened and included can be found in Figure 5.

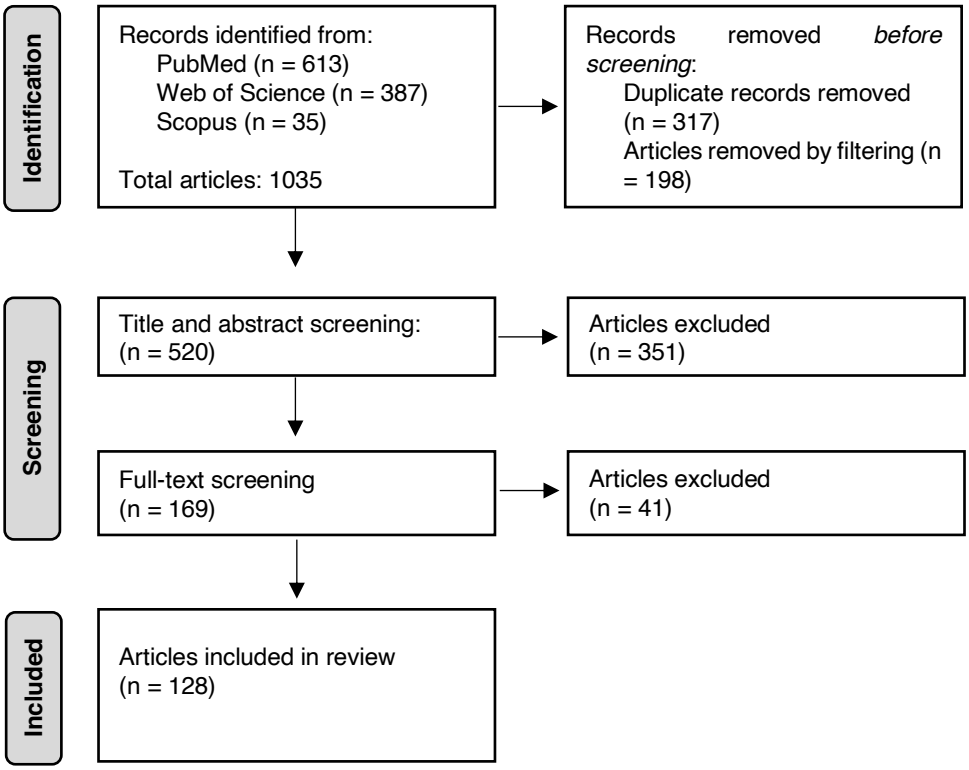

Figure 5 - PRISMA flow diagram of the included journal articles and how they were processed.

The initial search identified 1,035 articles. After removing duplicates, and screening for relevance, the final analysis focused on 118 primary research articles, supplemented by 10 review papers.

A data extraction protocol was implemented to capture research parameters including the publication year, research category, investigated nuclei, pulse sequences, acquisition parameters, and magnetic field strengths. The extracted data revealed insights into the evolution of bNMR technology and its interdisciplinary applications. Notably, an observable correlation emerged between technological advancements, magnetic field strength improvements (Figure 6), and increased research output (Figure 7). The research landscape demonstrated remarkable breadth, encompassing diverse scientific domains including food science, method

development, forensic science, flow and reaction monitoring, quality control, pharmaceutical research, material science, hyperpolarization, metabolomics, and environmental analysis.

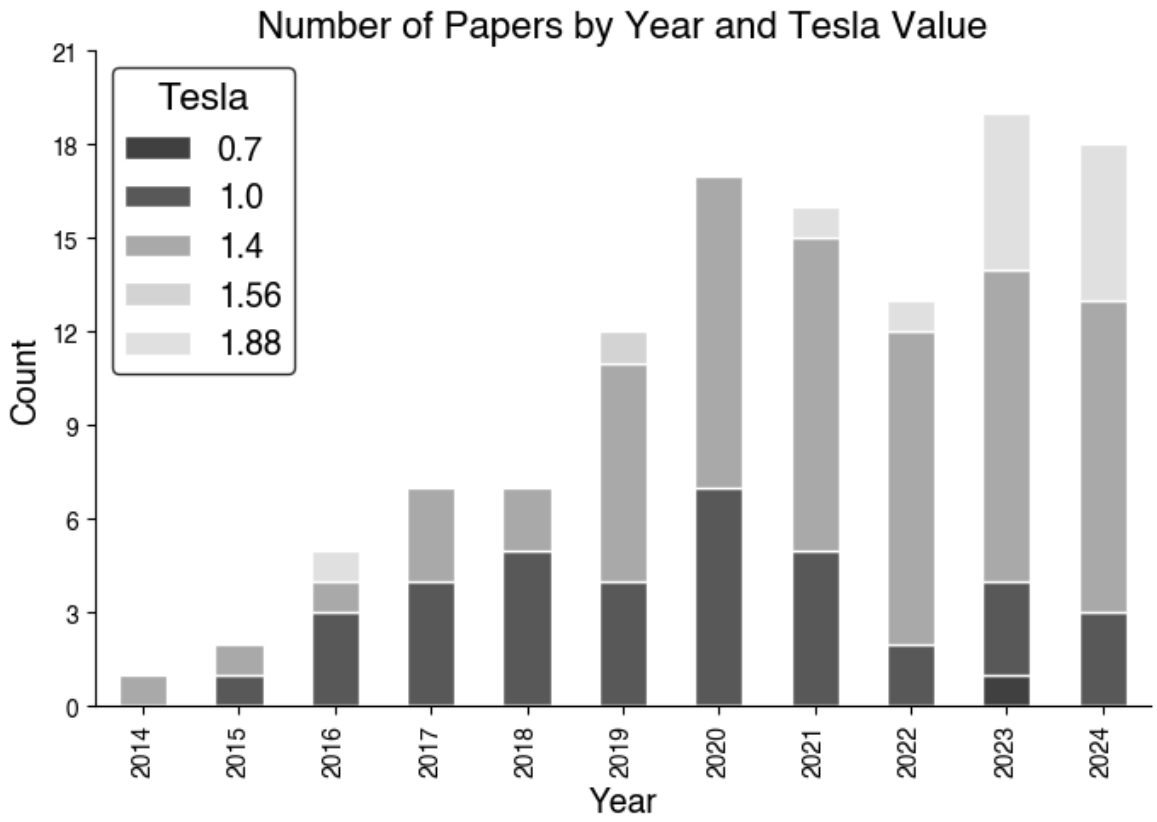

Figure 6 - Yearly breakdown of bNMR magnet strengths present in journal articles from 2014 to 2024.

The data presented in Figure 7 shows a steady increase in bNMR research, particularly in applied sciences such as food science, metabolomics and method development. The sharp increase in research from 2020, and its decrease in the subsequent two years, is most likely due to the pandemic at the time limiting the time allowed for researchers to conduct experiments in labs.

It should be noted that more than one category could be present from each article. From the topics discussed in the articles 34 were related to food science, 25 on method development, 25 on forensic science, 23 on flow and reaction monitoring, 22 were on quality control, 21 about pharmaceuticals and drugs, 18 on material science, 16 on hyperpolarization, 10 on metabolomics, and 10 on environmental analysis. The emergence of hyperpolarization techniques aligns with technological advancements, enhancing bNMR sensitivity and extending its practical applications. This increasing trend suggests that bNMR is evolving into a widely adopted tool for

diverse scientific fields, bridging fundamental research and real-world applications. Each category will be subsequently discussed on its applications and development.

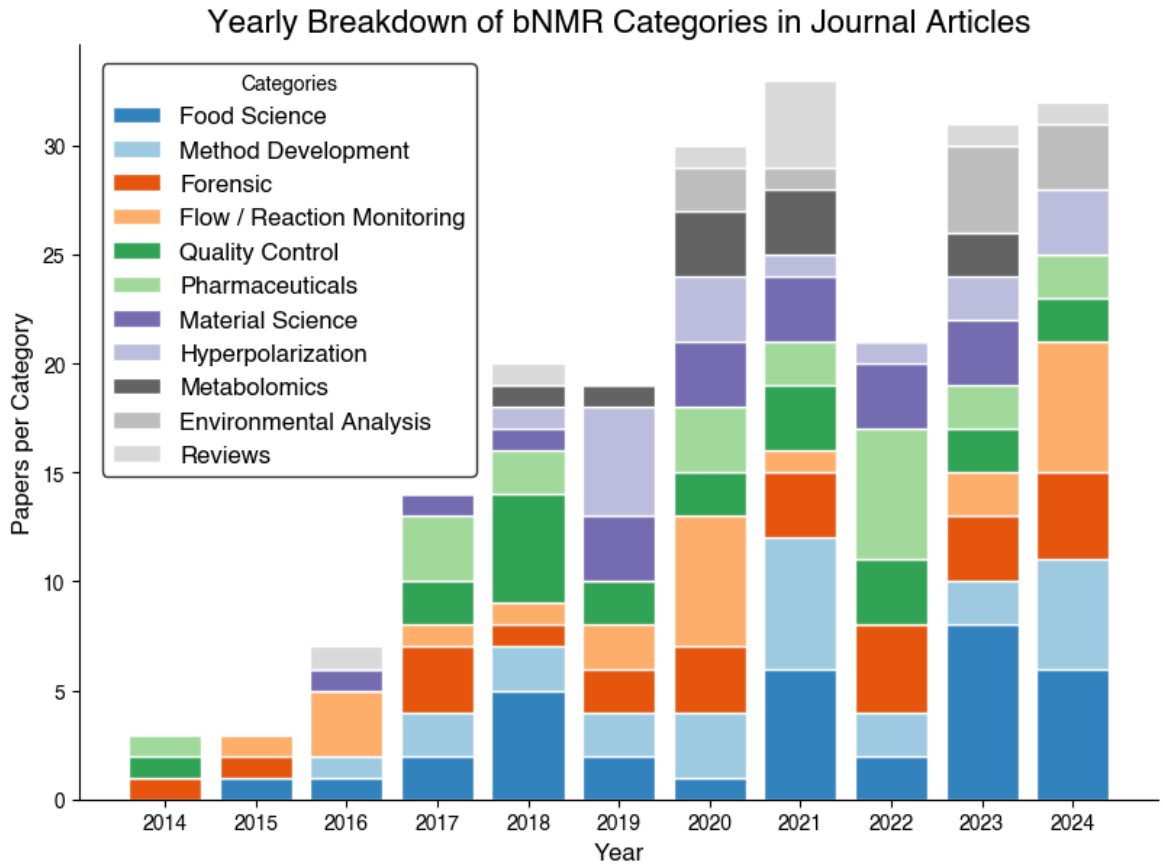

Figure 7 - Yearly breakdown of bNMR research categories present in journal articles from 2014 to 2024.

2.1. Food Science

The food industry faces increasing pressure to ensure product authenticity, quality and safety.[120,121] bNMR emerges as a transformative analytical technique, offering rapid, cost-effective analysis, with minimal sample preparation requirements. This is highly advantageous to food science analysis. Notably, this systematic literature review revealed food science as the most prominent application of bNMR in academic research over the past decade which showed emphasised research efforts towards detecting food fraud and verifying product authenticity.[120–123] Several compelling case studies illustrate the technique's detection capabilities across various foods.

One early example is bNMR's use to detect horse meat.[121] During the deliberate horsemeat substitution scandal, researchers Jakes *et al.* (2015) developed a new

method capable of distinguishing between legitimate beef and counterfeit horsemeat within ten minutes.[121] Furthermore, they showed that the quicker analysis times, including freeze-thaw cycles of the meat, did not compromise the precision.[121]

The authentication of high-value commodities represents another crucial application especially due to the potential health implications illegitimate food sources can have on the health of animals and humans.[121] Saffron has been particularly susceptible to fraudulent adulteration due to its high cost.[124–126] Utilising a 60 MHz bNMR spectrometer, researchers successfully developed a detection protocol revealing systemic adulteration patterns.[120] A comprehensive study by Gunning *et al.* (2023) examined 33 saffron samples, identifying abnormalities in seven suggesting widespread adulteration practices.

bNMR has also shown utility in distinguishing between Arabica and Robusta coffee. Arabica coffee is more expensive due to its complex flavour and more challenging cultivation process, while Robusta coffee is generally cheaper because it is easier to grow and produces higher yields. Therefore, Arabica coffee can sometimes be supplemented with Robusta beans for financial gains. A key finding, found by Gunning *et al.* (2018), showed that the presence of 16-O-methylcafestol could be used as a marker for Arabica coffee.[122] The methodology reliably identified Robusta content at 20% concentration, with partial detection capabilities even at 10% adulteration levels.[122] These results were exemplified at both 600 MHz and the aforementioned 60 MHz spectrometers with comparable precision achieved.[122]

Additionally, bNMR has shown its application in identifying the location of origin of food products. Ozbay *et al.* (2024) revealed that bNMR coupled with chemometrics could authenticate honey based on botanical origin and detect adulteration with inexpensive sugar syrups.[123] Using 95 genuine honey samples (monofloral, polyfloral, and honeydew) and adulterated sets, multivariate models achieved 100% classification accuracy for monofloral honeys.[123] Supervised partial least squares (S-PLS) models demonstrated high sensitivity for quantifying adulterants, with detection limits as low as 0.96% in monofloral honeys.[123]

The emergence of bNMR as a powerful food authentication tool presents significant implications for regulatory frameworks and quality control practices. These studies highlight the effectiveness of bNMR as a cost-efficient, rapid tool for food authentication and fraud detection, with significant implications for quality control and regulatory practices.[123] As technological capabilities expand, legislative approaches must correspondingly evolve to incorporate these advanced verification methodologies.

2.2. Method Development

The evolving landscape of bNMR has had continuous methodological refinement, addressing fundamental technological limitations through innovative analytical approaches. Technological improvements in hardware and software have catalysed methodological developments, enabling further analytical capabilities.

One of the most significant challenges inherent in bNMR spectroscopy is signal overlap, particularly when solvent signals such as water obscure surrounding chemical signals. Gouilleux *et al.* (2020) conducted an assessment of the optimal pulse sequence to be used on a 45 MHz spectrometer, with the application of metabolomics in mind.[127] Their research showed that the WET-180-NOESY (water suppression enhanced through T1 effects with 180˚ pulse and nuclear Overhauser effect spectroscopy) pulse sequence as the most effective technique, with WATERGATE (water suppression by gradient tailored excitation) and WET-CP (water suppression enhanced through T1 effects with composite pulse) demonstrating comparable performance.[127] A more comprehensive study of solvent suppression pulse sequences is explored in chapter 3.7.

The field of bNMR has also been extensively explored through hyperpolarization to enhance the sensitivity of the device.[128] Hyperpolarization works by enhancing the NMR signal by increasing the population difference between nuclear spin states. Normally, the Boltzmann distribution (discussed in Chapter 3.1) results in only a very small excess of nuclear spins in the lower energy state, leading to inherently weak NMR signals. Hyperpolarization boosts this population difference, increasing signal intensities by several orders of magnitude, making previously undetectable metabolites visible.[129] Current methods that have been applied to bNMR include

dynamic nuclear polarization (DNP), parahydrogen-induced polarization (PHIP), and pure shift.[128]

The enhanced molecular detection capabilities of hyperpolarization therefore mitigates the persisting issues of sensitivity from bNMR.[128] While hyperpolarization offers unprecedented molecular detection capabilities, significant implementation challenges persist. Hyperpolarization remains expensive and complex, limiting its widespread industrial adoption.[128] Current applications remain predominantly confined to academic research environments, although companies such as NVISION are introducing the technology to the broad market.[128]

The Duckett research group pioneered signal amplification by reversible exchange (SABRE), a hyperpolarization technique with signal enhancement capabilities.[128] Comparative studies by the Duckett group demonstrated a 250-fold signal enhancement in 400 MHz 9.4T experiments and a 3,100-fold signal enhancement in a 43 MHz 1T benchtop system.[128,129] The Duckett group further exemplified SABRE by combining it with another sensitivity-enhancing approach through sensitive, homogeneous, and resolved peaks in real time (SHARPER).[130] By removing the multiplicity signals could be further enhanced. This was demonstrated using ^{19}F to enhance three fluoropyridines.[130] The researchers were then able to achieve a signal-to-noise ratio of 1370 using SABRE which was further increased to 23400 with SABRE-SHARPER.[130] This selective enhancement could be further developed into methods for routine micromolar limits of detection, which could be especially important in domains traditionally dominated by mass spectrometry techniques.[130] However, hyperpolarization techniques often require additional and expensive equipment. Furthermore, protocols can be complex with significant method development needed for optimising new experiments with the resulting sample processing capacity reduced.

2.3. Forensic and Pharmaceutical applications

Drug identification, quantitative analysis, and compound characterisation are further applications of bNMR over the past ten years. A study by Nowroozi *et al.* (2022) demonstrated bNMR's potential for pharmaceutical compound quantification. The research successfully determined phenytoin and phenobarbital concentrations with

accuracy comparable to high-performance liquid chromatography (HPLC).[131] Critically, the bNMR methodology offered significant methodological advantages with minimal sample preparation requirements and quick experimental setup which could substantially reduce overall analysis times.[131]

The rapidly evolving landscape of psychoactive substances presents significant challenges for forensic and pharmaceutical researchers. bNMR has emerged as a powerful analytical tool for addressing these complex identification challenges.[132] Lee *et al.* (2022) conducted a comprehensive investigation of methamphetamine and associated impurities, demonstrating bNMR's capability to perform quantitative analysis even in scenarios with substantial spectral overlap. This research underscores the technique's potential for forensic investigations involving complex chemical mixtures.[132]

Multiple studies have explored bNMR's utility in analysing cannabinoid compounds and synthetic drugs. Aranda *et al.* (2020) successfully quantified tetrahydrocannabinol (THC) and cannabidiol (CBD) concentrations using bNMR techniques, providing a robust methodology for cannabinoid analysis.[133] Wu et al. (2021) presented a novel application of ^{19}F bNMR for the detection of fluorinated synthetic cannabinoids. Their findings highlight the potential of this technique in routine forensic investigations, particularly for the identification of emerging synthetic drug compounds.[134] By offering rapid, precise, and versatile chemical analysis, bNMR addresses critical challenges in compound identification and quantification.

2.4. Flow/ Reaction Monitoring

Although samples are traditionally added to an NMR *via* a tube, they can also be flowed through the spectrometer. This is especially advantageous when you want to track and monitor a reaction. With a more cost-effective, easy-to-use, and movable device, both academics and industry have been able to apply this field to monitor reactions.

Two-dimensional (2D) NMR experiments can encounter significant time-acquisition challenges, particularly at lower sensitivity ranges. Giraudeau's research group

pioneered an ultra-fast 2D method specifically designed to address this limitation. Their investigation demonstrated rapid correlation spectroscopy (COSY – later discussed in chapter 3.8.1) analysis using a 45 MHz (1T) bNMR, successfully analysing ethanol and executing complex reaction monitoring during the Heck-Matsuda reaction.[135]

Sagmeister *et al.* (2020) took a different approach to overcome the hurdle of overlapping peaks. By using multivariate analysis overlapping signals were able to be distinguished.[136] They also noted how removing buckets with background noise, reduced the error of the model.[136] Overall, Sagmeister et al. (2020) confirmed this application in four different validation mixtures (salicylic acid, 3-nitro- salicylic acid, 5-nitro- salicylic acid and dinitrated salicylic acid).[136] They concluded that short acquisition and relaxation times were advantageous to increase precision and real-time measuring while maintaining accuracy.[136]

Reaction monitoring has also been explored in other contexts. Claaßen *et al.* (2019) used the technique to monitor the conversion of an aromatic aldehyde to an aromatic amino alcohol.[137] The study further proposed that this approach holds significant potential for future applications, including the self-regulation of reactions involving toxic substrates and the tracking of catalyst modifications.[137]

Hyperpolarization has also been employed in reaction monitoring to help increase bNMR's sensitivity. Using the aforementioned SABRE technique, Jeong *et al.* (2023) showed how previously hidden proton signals in a drug molecule could be detected during a reaction with SABRE reaction monitoring.[138] This further increases the potential for bNMR to be used for reaction monitoring, especially where low concentrations may need to be detected like in drug development or toxicological applications.[138] However, research on reaction monitoring using bNMR has predominantly focused on simpler reactions that are easier to model. Therefore some gaps in the technologies limitations are still to be discovered.

2.5. Material Science

As regulatory requirements continue to adapt, the financial burden that can come with more robust legislation can become problematic for consumer providers. As

such, the industry adapts and pivots to explore techniques that can fulfil these legislative requirements while maintaining a low cost to analyse.

Block *et al.* (2023) conducted a comprehensive study comparing multiple spectroscopic techniques for analysing organic acids and polysaccharides. Using Aloe Vera as a model system, Block *et al.* (2023) evaluated common techniques ultraviolet-visible (UV-vis) spectroscopy, near-infrared (NIR) spectroscopy, attenuated total reflectance Fourier-transformed infrared (ATR-FTIR) spectroscopy, high-performance liquid chromatography (HPLC), and bNMR with HF-NMR serving as a reference.[139] Their findings demonstrated bNMR to be the most effective technique for analysing the majority of organic acids and sugars.[139] Furthermore, the study highlighted how bNMR can be used quantitatively and remarked bNMR's robustness, stability, precision, and reproducibility.[139] The experiments were conducted using an 80 MHz (1.88T) spectrometer, though the researchers encountered challenges due to signal overlap between isocitric acid and citric acid signals which rendered these metabolites unquantifiable.[139] However other key components, including aloverose, glucose, malic acid, lactic acid, acetic acid, magnesium, and calcium, were successfully validated for qNMR at the benchtop scale.[139]

Microplastics remains a topic of serious environmental debate due to its potential hazard to the environment and food chain. Researchers Peez *et al.* (2022) used an 80 MHz (1.88T) bNMR to find the limits of detection of three plastics, polyvinylchloride, polyethylene terephthalate, and polystyrene which are common plastics used in food packaging.[140] Impressively the researchers were able to confirm similar limits of detection to that employed at HF-NMR.[140] However, a critical methodological consideration emerged: while high-field NMR facilitated analysis within minutes, benchtop techniques required extended experimental durations exceeding two hours.[140] Nevertheless, they were able to show the quantitative use of bNMR for microplastic detection and further could help another important area in environmental analysis. This raises an important discussion on whether the extended analysis time is justified by the reduced cost and accessibility of benchtop systems.

2.6. Environmental Analysis

Magnetic resonance in environmental analysis has been widely employed, especially for relaxometry based experiments in soil samples. However, these such studies were outside of the scope of this literature review and not investigated further due to their different bore size, magnetic strength and homogeneity.

Chen *et al.* (2024) investigated toxic components found in wastewater. Using ^{19}F COSY experiment the researchers were able to quickly (~two hours) quantify toxic compounds (fluorosurfactants).[141] The researchers opted for bNMR due to the technique's ability to potentially quickly and cost-effectively detect toxic compounds in wastewater.[141] However, the previously used techniques LC-MS boasts a more impressive sensitivity than NMR and even more so than bNMR (1.4T magnet), therefore this study wanted to investigate if bNMR was sensitive enough to detect these compounds.[141] The study concluded that bNMR could effectively detect the fluorosurfactants.

The production of bio-oils produced from the decomposition process of plant-based matter represents a significant advancement in the development of sustainable fuel alternatives.[138] Tang *et al.* (2023) employed ^{19}F bNMR to analyse pyrolysis oils, successfully identifying key carbonyl-containing compounds, such as aldehydes, ketones and quinones, information that is not traditionally obtained through elemental analysis.[142] Similarly, Makarova *et al.* (2021) investigated the polyphenol content and antioxidant capacity of Polish St John's wort flowers, demonstrating the utility of bNMR in the compositional analysis of natural product extracts.[143]

Environmental pollutants also require effective monitoring, particularly as traditional analytical techniques can be limited by their cost and accessibility. In this context, bNMR spectroscopy emerges as a more cost effective and accessible tool. Heerah *et al.* (2020) investigated the degradation of a persistent organic pollutant, perfluorooctanoic acid, providing a critical framework for understanding bNMR's potential in environmental analytical.[144] While the study demonstrated significant promise, further technological refinement is needed to overcome current analytical limitations.[144]

Critical evaluation suggests that bNMR spectroscopy represents an emerging analytical paradigm with considerable potential for environmental research and remediation technologies, contingent upon continued methodological innovation and technological advancement.

2.7. Metabolomics

The first published use of bNMR metabolomics was the analysis of urine from type II diabetes mellitus (T2DM) patients. Percival *et al.* (2019) identified 15 biomarkers for the disease at 60 MHz, concluding that bNMR was able to distinguish between diabetic and healthy controls, as well as quantify key biomarkers including glucose and creatinine.[108] However, the study also noted that intensity dampening of glucose was occurring due to the presaturation pulse sequence. This study was also reviewed and further tested by Leenders *et al.* (2020) and Edgar *et al.* (2021), which agreed that bNMRs' can be used for T2DM detection. In particular, Edgar *et al.* (2021) suggested its future use for prediabetes detection.[109,110] One downside to these studies was the relatively low sample numbers, however this is more largely a problem in the field of metabolomics and health studies to have a high enough *n* number to meet sufficient statistical power.

Sepsis is another disease which has been explored using bNMR. Stocchero *et al.* (2023) analysed urine to detect sepsis in newborn babies.[145] The researchers used the NOESY Presaturation experiment over 64 scans to acquire spectra in 10 minutes.[145] Only 18 samples were collected for this study, ten of which were a sepsis group and eight of which were the control group.[145] They opted for intelligent binning to bucket the data with subsequent OPLS-DA analysis conducted.[145] Of particular interest were regions between 7.65–7.48, 1.58–1.47, and 1.47–1.40 ppm. Which achieved the significance threshold of $p < 0.05$ with area under the curve values above 0.8 that all had significant fold change increase in sepsis compared to the controls.[145] Stocchero *et al.* (2023) stated that they were unable to elucidate the metabolites in question that were responsible using bNMR and instead this was completed at HF-NMR.[145] The study concluded that it was able to generate similar prediction performance to the MS data set and also agreed with Leenders *et al.* (2020) that both the bNMR and HF-NMR spectra share similar strong correlations

of metabolites. These researchers also say how bNMR meets the requirements for clinical applications.[145]

Grootveld *et al.* (2022) were also the first to analyse saliva using bNMR. They used (^{1}H) bNMR to detect 19 metabolites, with only five biomolecules being reliably quantifiable.[68] This can increase to a total of eight in the absence of signal overlap.[68] The research suggests that salivary metabolomics could also be a valuable tool for early detection and prevention of dental cavities in T2DM patients.[68] Although the study identified potential biomarkers that could be used for various diseases, further research is necessary to determine if these biomarkers can predict the development of dental cavities.[68]

Studies have also been conducted on animal-based models for metabolomics. One such study is a preliminary study investigating chronic kidney disease (CKD) in the urine of cats.[60] Although the study was limited as only four samples (two healthy and two CKD) were used, the study still identified 15 metabolites, with results suggesting bNMR has the potential to be used for the detection of CKD.[60] Three metabolites, namely glycine, serine and threonine were identified as statistically significant in distinguishing CKD in the sample cohort, however, threonine and serine may be harder to detect as they were not identified in the annotated spectra.

Tuberculosis (TB) was detected in the first bNMR blood study. Bovine TB (BTB) was distinguishable in the plasma bNMR profile of cows as compared to those diagnosed with paratuberculosis, paratuberculosis-vaccinated healthy controls, and healthy paratuberculosis-unvaccinated controls.[112] The authors did not identify the specific metabolites contributing to the significance of the bNMR PLS-DA model but did suggest a high correlation and predictive potential (R^2 = 0.97, and Q^2 = 0.36) from the model. The same research group also investigated TB in the urine of humans. Using bNMR they were able to identify 9 metabolites in the urine, 7 of which were biomarkers for TB distinction.[113] From PLS-DA, cases of TB were able to be discriminated from cases of pneumococcal pneumonia, latent TB infection (LTBI) and uninfected cases with an accuracy of 87.3%, 85.2% and 100% accuracy, respectively.[113] The same group also completed a study where TB in children was distinguished from healthy controls in urinary analysis using bNMR.[111]

Another blood study was conducted by Stolz *et al.* (2020) who investigated if glucose was still quantifiable using a 1 Telsa spectrometer in whole blood and plasma.[146] Heparin tubes were used for sample collection instead of EDTA tubes to avoid the large overlap of signals observed form EDTA tubes.145 Signals in spectra were fitted with a Gaussian or Lorentzian function and then integrated for quantification. The researchers opted to not use a T2 filter or solvent suppression technique in their acquisition, instead opting for a simple pulse acquire.[146] As a result signals are hard to decipher with only methanolic acid (internal standard), water, proteins, lipids and glucose being named as identifiable from the spectra at 1.5 Tesla.145 These researchers were ultimately able to confirm that quantitative glucose analysis of whole blood and plasma is achievable by bNMR.

Colitis has been investigated using faecal extracts from a mouse model, where a total of 19 metabolites were identified through bNMR.[114] The non-targeted multivariate analysis allowed for effective differentiation between healthy mice and those with ulcerative colitis.[114] The metabolite acetate emerged as particularly significant due to its large concentration in the diseased mice.113 This demonstrates the potential of bNMR in enhancing the understanding of colonic inflammation and dysbiosis, and its promise for point-of-care diagnostics. By using this non-invasive and efficient analytical technique, Song *et al.* (2023) were able to profile metabolites and gain valuable insights into potential biomarkers and underlying pathways.

The research conducted in this field has been commendable in selecting diseases where bNMR analysis could significantly enhance detection capabilities. The chosen diseases are not only well-suited to this technique but also have high prevalence rates. For instance, T2DM affects 10.5% of the population, ulcerative colitis has a prevalence of 0.1%, CKD impacts up to 49% of cats aged 15 years and older, and TB remains one of the top 10 causes of death worldwide.[147–152] Nevertheless, to fully explore the potential and limitations of these techniques, studies with larger cohorts, including a wider range of diseases, biofluids, and pulse sequences, are essential.

One of metabolomics' main challenges is achieving sufficient water suppression due to the high concentration of water in biolfuids. There are three main physical and chemical attributes that contribute to making solvent suppression hard: radiation

dampening, the ‘faraway solvent’ effect, and the frequency instabilities.152 Radiation dampening is proportional to the magnetic field strength and therefore has a reduced effect at the lower operating frequency of current bNMR spectrometers.[153,154]

From the current published research of bNMR metabolomics, only three pulse sequences have been used. These are the presaturation (1D-Presat) pulsed sequence on the 60 MHz Magritek bNMR spectrometer [72,108–114], the NOESY presaturation pulse sequence on the 80 MHz Bruker bNMR spectrometer,[145] and the water suppression enhanced through T1 effects with a composite pulse (WET-CP) on Oxford Instruments 60 MHz spectrometer.[60]

Overall, more work can be done with the exploration of other pulse sequences for metabolomics.[153] Pulse sequences which can “filter out” proteins and other macromolecules such as the Carr-Purcell-Meiboom-Gill (CPMG) pulse sequence have also been absent from bNMR metabolomic studies. Therefore, future studies should employ an expanded range of pulse sequences. However, to understand the theory behind these pulse sequences, the theory of NMR needs to be discussed.

2.8. Research Aims

This research aims to evaluate the potential of bNMR spectroscopy for disease detection through metabolomic profiling across multiple biofluids and pathological conditions. Specifically, it seeks to determine whether bNMR can effectively distinguish between healthy and diseased states by analysing metabolic signatures in urine, blood plasma, and cerebrospinal fluid. Additionally, the study compares bNMR’s diagnostic performance to HF-NMR to assess its ability to detect disease-associated metabolites. A key objective is to investigate whether bNMR can differentiate between varying disease severities, such as pre-diabetes and diabetes or different asthma severity levels. Furthermore, this research aims to identify the specific metabolites detectable by bNMR to be used for disease analysis. Finally, the study explores the broader applicability of bNMR as a cost-effective and scalable diagnostic tool, identifying potential refinements in sensitivity, pulse sequences, and sample preparation to enhance its clinical utility.

Chapter 3 NMR Theory

The following chapter will lay the foundational knowledge of NMR spectroscopy necessary to understand its core concepts. By establishing a solid understanding of these principles, the reader will be equipped to comprehend the methodology, results and discussions presented in subsequent chapters.

3.1. Energy Levels

An object with a rotational motion has angular momentum.[96,97] Spin is a form of angular momentum and is an intrinsic property of magnetic nuclei.[98] The nuclear spin angular momentum ($\boldsymbol{I}$) is influenced by the arrangement of protons and neutrons in the nucleus. Nuclei with no angular momentum, where both the number of neutrons and protons are even, are unobservable in NMR.[98] On the other hand, nuclei with unpaired nucleons have a spin angular momentum of a half-integer. The spin angular momentum is a positive integer if both the number of neutrons and protons are odd.[98]

The spin quantum number, $\boldsymbol{I}$, has $2I + 1$ allowed energy levels, characterized by the magnetic quantum number m.[96] These energy transitions can only occur between adjacent m-states in singular integer steps, ranging from $+I$ and $-I$.[96,98] The magnitude of spin angular momentum is calculated by Equation 1, where $\hbar$ is Planck's constant (h) divided by 2π.[96–98]

$$\hbar\sqrt{I(I+1)} \qquad \text{Equation 1}$$

^{1}H nuclei have a spin angular momentum of ½ with two allowed energy transitions, the higher energy β state ($m = -\frac{1}{2}$), and the lower energy α state ($m = +\frac{1}{2}$). The spin angular momentum is also linked to the magnetic moment (μ), which describes the magnetic dipole's strength and orientation depending on the spin angular momentum and the gyromagnetic ratio (γ), as shown in Equation 2.[96–98]

$$\boldsymbol{\mu} = \gamma \boldsymbol{I} \qquad \text{Equation 2}$$

The magnetic moment can align with the magnetic field where the gyromagnetic ratio is positive, or an alignment against the magnetic field where the gyromagnetic ratio is negative. In the absence of a magnetic field, the energy levels are degenerate and so there is no energy difference (ΔE). The energy difference is related to the external magnetic field ($\boldsymbol{B_0}$), the gyromagnetic ratio and Planck's constant, as described in Equation 3.[97,98]

$$\Delta E = \frac{h\gamma \boldsymbol{B}_0}{2\pi} \qquad \text{Equation 3}$$

The two energy levels for a single spin-half nucleus in a magnetic field are shown in Equation 4 with the energy states dependent on m, where m can be ±½.

$$E_m = -m\hbar\gamma \boldsymbol{B}_0 \qquad \text{Equation 4}$$

The magnetization vector precesses around the magnetic field at a constant angle.[98] The frequency of this precession is known as the Larmor frequency (υ^0 or ω^0) and can be calculated by dividing the energy difference (as described in Equation 3) by Planck's constant, as shown in the Equation 5 below.

$$\upsilon^0 = \frac{-\gamma \boldsymbol{B}_0}{2\pi} \qquad \text{Equation 5}$$

The units for Equation 5 are expressed in Hertz, however, the Larmor frequency can also be provided in radians per second as presented in Equation 6 by the multiplication of 2π. Nuclei with a positive gyromagnetic ratio, such as ^{1}H, ^{13}C, and ^{19}F, correspond to a negative Larmor frequency and, therefore, experience a clockwise rotation.

$$\omega^0 = -\gamma \boldsymbol{B}_0 \qquad \text{Equation 6}$$

When in a state of thermal equilibrium, where no relative change occurs to the energy levels, the population of two energy states is dependent on the energy difference (as previously defined ΔE in Equation 3) and the thermal energy. Using N_a and N_b to label the lower and upper energy levels, respectively, the population

ratio is defined by the Boltzmann distribution as in Equation 7 where k_B is the Boltzmann constant (1.380649 x 10^{-23} J/K) and T is the temperature.[97,98]

$$\frac{N_\mathrm{b}}{N_\mathrm{a}} = exp\,(\frac{-\Delta E}{k_B T}) \qquad \text{Equation 7}$$

The relative population difference given by the Boltzmann distribution provides only a small excess of spins in the lower energy level for spectrometers operating at 300 K.[98] For example, the population difference for protons in a 60 MHz spectrometer is only 1 in 10^6, but close to 6 in 10^5 in a 400 MHz instrument.[155] Higher-field instruments therefore are inherently more sensitive due to the larger population difference.[155]

However, this difference between N_a and N_b can be increased by either changing the strength of the static magnetic field or by decreasing the temperature of the spins. However, achieving a significantly improved distribution of energy levels would require temperatures below freezing, leading to relaxation problems.

The Boltzmann distribution describes the relative population of nuclei in different energy levels at thermal equilibrium. For spin ½ nuclei, such as ^{1}H and ^{13}C, there are only two energy levels: one with the magnetic moment aligned with the external magnetic field and one opposed to it. While individual spins can only be aligned to or against the field, the sum of the magnetic moments results in a small net alignment with the static magnetic field for nuclei with a positive gyromagnetic ratio. This net alignment produces what is called the bulk magnetization.

3.2. Chemical Shift

The magnetic field, $\boldsymbol{B}$, of a nucleus in an atom or molecule is unique, which can differ from the external field to provide varying resonances. This local environment that surrounds a nucleus is influenced by the electrons in nearby chemical bonds, which generate their own small magnetic fields. These electron-generated fields, often denoted as $\boldsymbol{B'}$, partially shield the nucleus from the full strength of the external magnetic field.[97,98] This shielding effect causes the nucleus to experience a reduced net magnetic field, referred to as chemical shift. The relationship between

the external magnetic field, the shielding effect, and the net field is given by Equation 8.[98]

$$\boldsymbol{B} = \boldsymbol{B}_0 - \boldsymbol{B}' \qquad \text{Equation 8}$$

The shielding constant (σ) shows the constant of proportionality between $\boldsymbol{B}'$ and $\boldsymbol{B}_0$. As such, the field at the nucleus can be presented as shown in Equation 9.[97,155]

$$\boldsymbol{B} = \boldsymbol{B}_0(1 - \sigma) \qquad \text{Equation 9}$$

The chemical shift (δ) is a normalized measure of a signals frequency. The chemical shift axis is provided in parts per million (ppm) instead of hertz to help with easy comparisons between spectrometer frequencies.[97] With varying spectrometer frequencies, the shielding constant becomes inefficient to measure nuclei's frequencies, due to the conversion. Instead, chemical shift is practically defined, in Equation 10, as the difference between the Larmor frequency of a nucleus in question (u) and a given reference standard (u_{ref}).

$$\delta(ppm) = 10^6 \times \frac{u - u_{ref}}{u_{ref}} \qquad \text{Equation 10}$$

The distribution of a compounds chemical shift can be associated with different functional groups, shown in Figure 8.

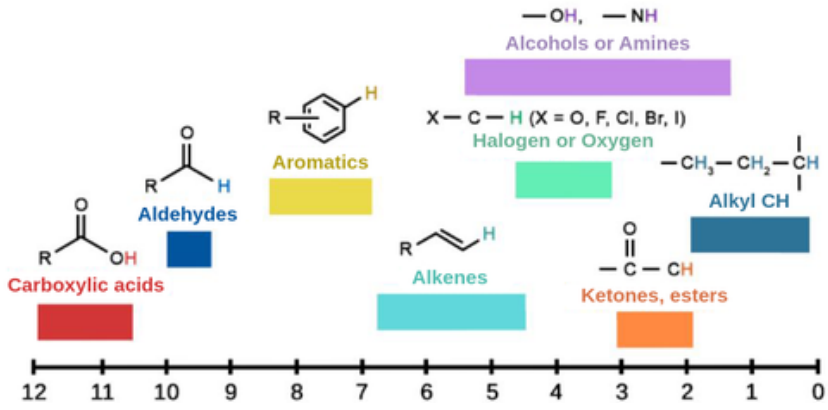

Figure 8 - ^{1}H Chemical shift ranges (in ppm) for some common organic functional groups 155

As observed in Figure 8, the high-frequency end of the spectrum (left side) is described as downfield with the nuclei de-shielded and the right side as upfield and shielded nuclei.

3.3. *J* Coupling

Each nuclear environment provides further information to a spectrum, allowing to interpret the magnetic interaction of two nuclei through chemical bonds. Nuclei in the absence of coupling (the interaction of connected nuclei) do not experience splitting peaks, however, the interaction of magnetic moments of neighbouring, non-equivalent nuclei that are spin-active create splitting patterns called multiplets in NMR spectra.[97] A multiplet has equally spaced components; the chemical shift of which is defined as the coupling constant J.

As defined in Chapter 3.1, nuclei with a spin angular momentum of ½, like ^{1}H, have two energy transitions: the higher β state, and the lower energy α state. In a two-spin system there are four possible α and β spin combinations: a_1a_2, a_1b_2, b_1a_2, and b_1b_2. This makes three different frequencies in a spectrum. The ratio of the heights of lines in spin-half multiplicity splitting pattern is observed in Pascal's triangle Figure 9 as well as in Figure 10.

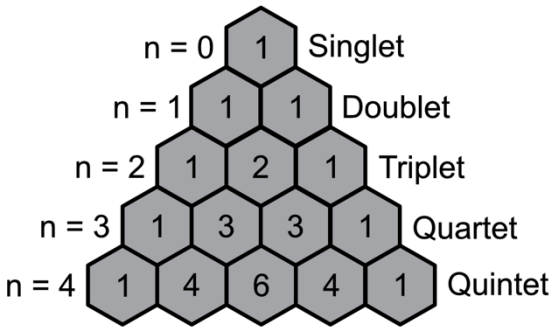

Figure 9 - Pascals triangle annotated with spin ½ nuclei ratio multiplets

The number of nuclei is also represented in a signal by its integration. In ethanol (Figure 10), the triplicate's integral (area of a signal) will be three times larger than that of the singlet and two times larger for the doublet compared to the singlet.

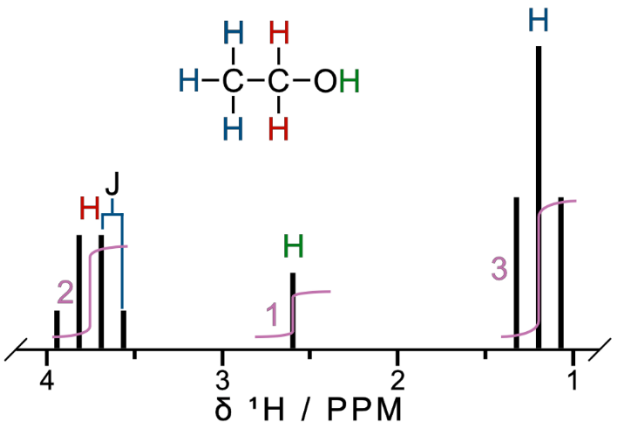

Figure 10 - ¹H NMR spectra showing Ethanol annotated with multiplets and integrals marked in pink

3.4. The Vector Model

When nuclei are placed in a magnetic field, there is an interaction between the nuclear magnetic moment and the external magnetic field. The net magnetization vector slowly increases until it reaches its thermal equilibrium, where no further change to the magnetization occurs. This total magnetization can be represented by the vector $\boldsymbol{M}$.

The vector model provides a simplistic view of the bulk magnetization and can help to understand how the magnetization vector is being manipulated in an NMR experiment for a large number of isolated, non-interacting spins. The magnetization vector is manipulated by applying a radio frequency (RF) pulse, which generates oscillating magnetic fields. This is sometimes named the applied magnetic field or $\boldsymbol{B}_1$.

When using the vector model, a rotating frame of reference is utilised where the Larmor frequency of $\boldsymbol{M}$ is not observable and instead observes the stationary vector $\boldsymbol{B}_1$ without oscillation or rotation. [96,97] This is employed in the vector model to simplify the description of how the spins are being manipulated during an experiment.

3.5. The Bloch Equations

To observe the interaction of the nuclei with the electric field, the bulk magnetization needs to be perturbed from its equilibrium state into the transverse (x and y) plane using an RF pulse. The angle by which the magnetization vector is rotated is called the flip angle (β) as defined by Equation 11, where t is the duration of the pulse and $\boldsymbol{B}_1$ is the applied magnetic field.

$$\mathrm{b} = \gamma \boldsymbol{B}_1 t \qquad \text{Equation 11}$$

The Bloch equations govern the rate of change of the x- , y-, and z- components of the magnetization vector. As an example, applying an RF pulse along the x axis rotates the magnetization away from its equilibrium (z-axis) towards the $-y$ axis, at a given flip angle. The rotation along each axis during a RF pulse is provided in Equation 12 - Equation 14.

$$M_y(t) = -M_0 sin\mathrm{b} \qquad \text{Equation 12}$$

$$M_z(t) = M_0 cos\mathrm{b} \qquad \text{Equation 13}$$

$$M_x(t) = 0 \qquad \text{Equation 14}$$

The precession of the magnetization vector induces a current in the coil that surrounds the sample tube after perturbation, which intern produces a free induction decay (FID), appearing as a damped sinusoidal wave. The FID is a time-domain signal that contains information of the relative resonance signals of a spectrum when converted into the frequency-domain after being Fourier transformed (FT).

3.6. Relaxation

The process where perturbed spins return to their thermal equilibrium is called relaxation. There are two processes by which relaxation occurs: the recovery of the z component of the bulk magnetization is Longitudinal or T_1 relaxation, and the decay of the transverse component of the bulk magnetization is transverse or T_2 relaxation. The vector model is also described by the Bloch equations through relaxation, as shown in Equation 15 -Equation 17.[157]

$$\frac{d\boldsymbol{M}_x}{dt} = \gamma \boldsymbol{B}_1 \boldsymbol{M}_y - \frac{\boldsymbol{M}_x}{T_2} \qquad \textit{Equation 15}$$

$$\frac{d\boldsymbol{M}_y}{dt} = -\gamma \boldsymbol{B}_1 \boldsymbol{M}_x - \frac{\boldsymbol{M}_y}{T_2} \qquad \textit{Equation 16}$$

$$\frac{d\boldsymbol{M}_z}{dt} = \gamma \boldsymbol{B}_1 \boldsymbol{M}_y - \frac{(\boldsymbol{M}_0 - \boldsymbol{M}_z)}{T_1} \qquad \textit{Equation 17}$$

Equation 15 and Equation 16 describe the change in magnetization over time along the x and y planes, and how it is characterised by transverse relaxation. Equation 17 is characterised by longitudinal relaxation during time evolution.[157]

3.6.1. Longitudinal Relaxation

Longitudinal relaxation is the recovery of the net magnetization after the spin's perturbation, back to its thermal equilibrium. This relaxation recovers exponentially. T_1 is a time constant, as previously seen in Equation 17, that denotes the time requires for the z component of $\boldsymbol{M}$ to recover to 63% of its maximum value.

A spin can interact with the magnetic fields generated by surrounding spins, collectively this environment is named the local field. This interaction provides thermal contact between spins and the random thermal motion of molecules which drives z magnetization back to its equilibrium value and hence T_1 relaxation. It is the transverse oscillation, at the Larmor frequency, in the local field that drives longitudinal relaxation.[97]

The value of T_1 can range from milliseconds to seconds depending on the properties of the sample, including its viscosity, molecular mobility, and structure.[97] In general, samples with higher mobility and lower viscosity tend to have shorter T_1 relaxation times. For quantitative studies, the magnetization needs to have recovered by 99% before being re-excited. For this to occur, the relaxation delay (RD) between experiments needs to be five times the value of T_1. As a result, quantitative NMR (qNMR) studies can have relaxation delays of over 20 seconds.

To measure the value of T_1, the exponential recovery of the z magnetization needs to be recorded. This can be recorded by using an inversion recovery experiment as seen in Figure 11.

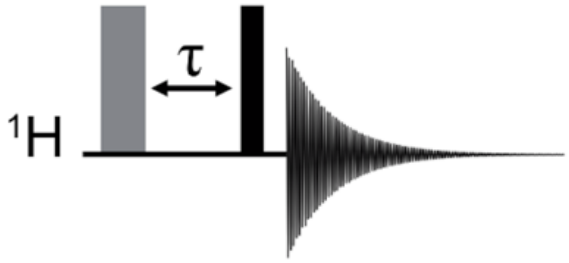

Figure 11 - A schematic diagram of an inversion recovery experiment used to record T_1. The 180˚ and 90˚ pulses are shown in grey and black rectangles respectively. The time in between the pulses is displayed by τ.

By inverting the magnetization with a 180˚ pulse (the light grey rectangle), magnetization relaxes back to its thermal equilibrium over a time tau (τ) before being rotated back into the transverse plane by a 90˚ pulse (the black rectangle) to be recorded. The length of τ is arrayed until the magnetization $(t > 5T_1)$ has reached its thermal equilibrium.

3.6.2. Transverse Relaxation

Equation 15 and Equation 16 show how the transverse magnetization decays exponentially with the T_2 time constant. Over time individual magnetic moments start to dephase, due to some spins precessing faster and slower than others. This creates a loss of phase coherence meaning that the direction of spins become scrambled.

There are two contributions to transverse relaxation. The first is comparable to longitudinal relaxation, where the local magnetic fields' transverse oscillation at the

Larmor frequency contributes to transverse relaxation. The second is the effect of magnetic field inhomogeneities, where slight variations in the magnetic field strength across the sample cause different spins to precess at different rates, further contributing to dephasing. Inhomogeneities in the magnetic field can accelerate the decay of transverse magnetization.[97,158]

3.6.2.1 Spin Echo

The more inhomogeneities present during an experiment, the shorter the T_2.[97] Due to magnetic field inhomogeneities, T_2 relaxation can be hard to record. To overcome the field inhomogeneities a spin echo pulse sequence (Figure 12) can be used to record the T_2 relaxation times. Irreversible fluctuations occur to the phase coherence during tau that cannot be refocused by a 180˚ pulse. As a result, the signal intensity of a spectrum decays with time. The spin echo pulse sequence (Figure 12) can be repeated with the length of τ arrayed to increase. As shown in Figure 13, this results in a decrease in the signal in the FID.

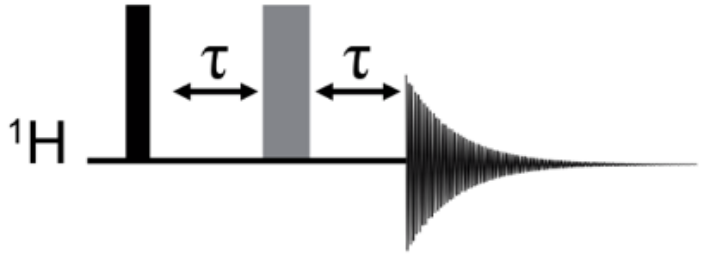

Figure 12 - A schematic of the spin echo pulse sequence. The black rectangle is a 90˚ pulse, τ which is the time in between the 180˚ pulse (grey rectangle) before the FID.

Following a 90˚ pulse, the magnetization is perturbed, with the magnetic moments precessing freely during the period of τ. During this interval, the slower precessing spins lag behind the faster ones. A 180˚ pulse is then applied, inverting the spins so that the slower precessing spins are in front of the faster precessing spins. As a result, after the second tau, the phase coherence is refocused. There is always some loss in phase coherence due to T2 relaxation during the spin-echo pulse sequence as the time-dependent fluctuations in the magnetic field cannot be refocussed.

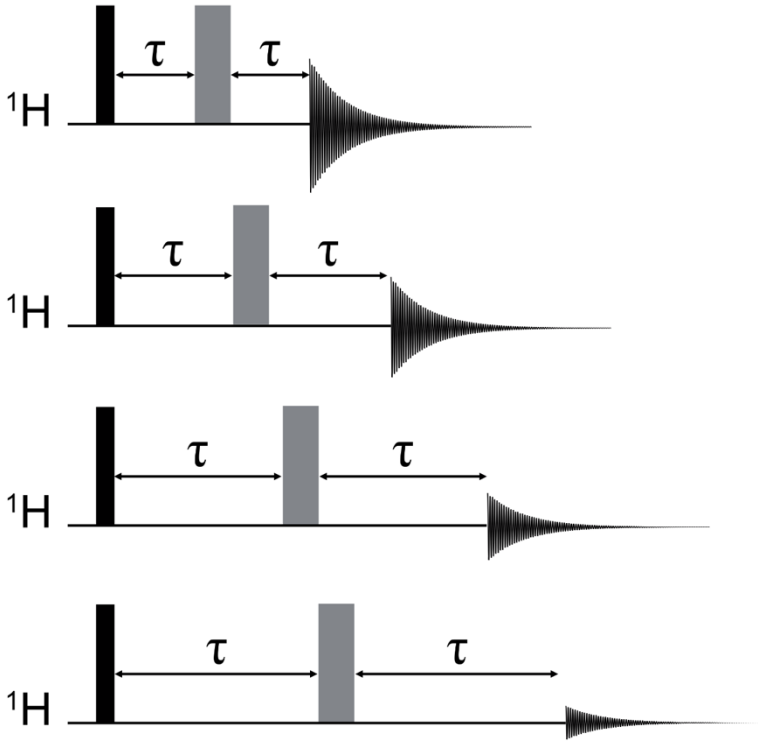

Figure 13 - A schematical pulse sequence diagram of measuring T2 relaxation

3.6.3. CPMG

Meiboom and Gill improved upon the initial work completed by Hahn in 1950, Carr and Purcell in 1954 with a pulse sequence named Carr-Purcell-Meiboom-Gill (CPMG).[159] The spin echo applied all RF pulses along the same axis, this meant phase errors were being introduced from imperfect 180˚ pulses, as well as applied magnetic field inhomogeneities. By applying a 180˚ pulse along an alternate axis to the initial 90˚ excitation e.g. along the ± x axis instead of the y axis, the pulse-related errors could be reduced.[159] The CPMG pulse sequence also improved the spin-echo sequence by fixing tau and increasing the number of cycles.

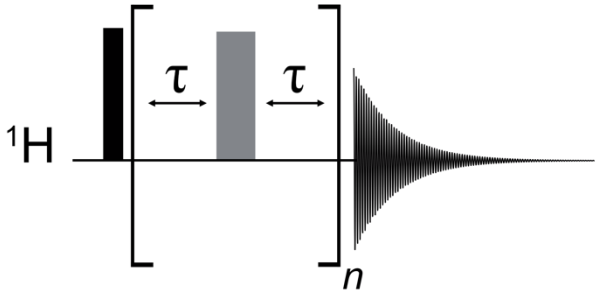

Figure 14 - Schematic diagram of the CPMG Pulse sequence

The CPMG pulse sequence (Figure 14) does, however, have some limitations, concerning echo modulations by scalar couplings J (J coupling). While the refocusing pulses correct for dephasing due to inhomogeneities in the external magnetic field, they do not cancel out the evolution caused by scalar J couplings

between spins.[160] Echo modulations can be overcome by decreasing tau and increasing the number of echoes. However, this can have the undesirable effect of sample heating, increasing the line widths.

3.6.3.1 PROJECT

Challenges outlined above were addressed by Aguilar *et al.* (2012) by Periodic Refocusing Of J Evolution by Coherence Transfer (PROJECT) as shown in Figure 15.

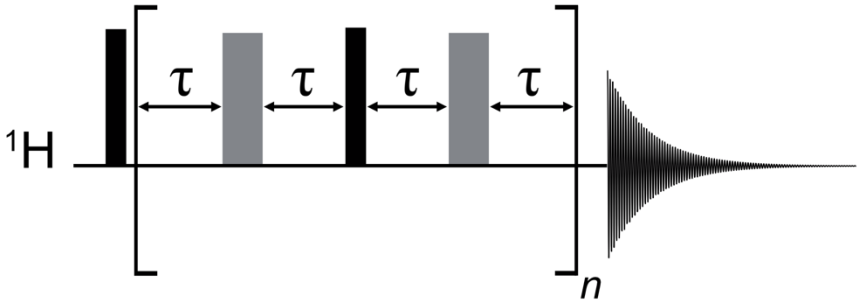

Figure 15 - Schematical diagram of the PROJECT pulse sequence

By adding a 90˚ pulse in between two spin echoes, it refocuses J and the chemical shift while also allowing for an increased length of τ to be employed.[160]

3.6.4. 1D NOESY

The Nuclear Overhauser Effect (NOE) is the change of one dipolar coupled spin intensities upon irradiation with another nearby spin (<5Å). This transfer of energy between two closely spaced spins can have a positive or negative enhancement on the intensity of the signal of energy transferred spin. The interaction of proteins and large molecules leads to a negative NOE enhancement due to their slower tumbling speeds, which leads to a longer correlation time (t_c). This slower motion leads to a negative NOE, where signal intensity decreases. In contrast, smaller molecules, with their faster tumbling and shorter correlation times, exhibit a positive NOE enhancement, leading to an increase in signal intensity.

The one-dimensional (1D) NOE spectroscopy (NOESY) experiment (Figure 16) is widely used in metabolomics due to its enhancements to solvent suppression and small molecule signals.

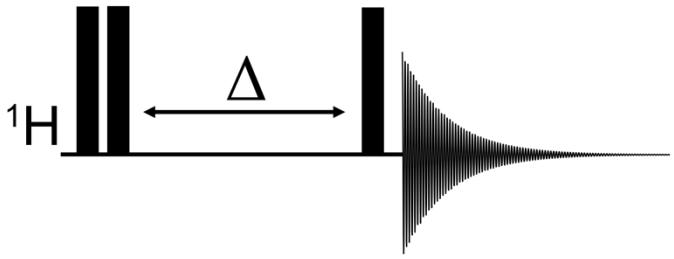

Figure 16 - 1D NOESY Pulse Sequence Schematic diagram

A two-dimensional (2D) NOESY experiment is also often used, where the purpose of this pulse sequence would be for the identification of spatial proximity between different protons. However, this pulse sequence can support solvent suppression and signal enhancement in the 1D variant.[161,162]

3.7. Water Suppression Pulse Sequences

The presence of large solvent signals (for instance the water signal observed in biofluids) in a sample can overshadow metabolites. Therefore, it is crucial to suppress solvent signals. Intense solvent resonances can also cause distortions to the baseline and phase roll if the solvent signal is saturating the NMR receiver and is not correctly suppressed.[163] Several different pulse sequences that supress solvents are discussed below.

3.7.1.1 WATERGATE

One such method for suppressing solvents is through coherence selection by pulse field gradients (PFG), observed in Figure 17. The core concept involves using a pulsed z-field gradient to dephase the coherences along the z-axes.[164] By doing so, only the selected signals are detected by the receiver. The WATERGATE (WATER suppression by GrAdient Tailored Excitation) technique is not affected by line shape, exchangeable protons or a change of phase around the water resonance. However, signals close to the water resonance can also be suppressed.[164] During the sequence (Figure 17), the first gradient dephases all coherences. Next, hard pulses with varying lengths excite all resonances, except those at the offset frequency. Finally, during the last gradient, the solvent signal is dephased further with all other resonances being refocused.[164]

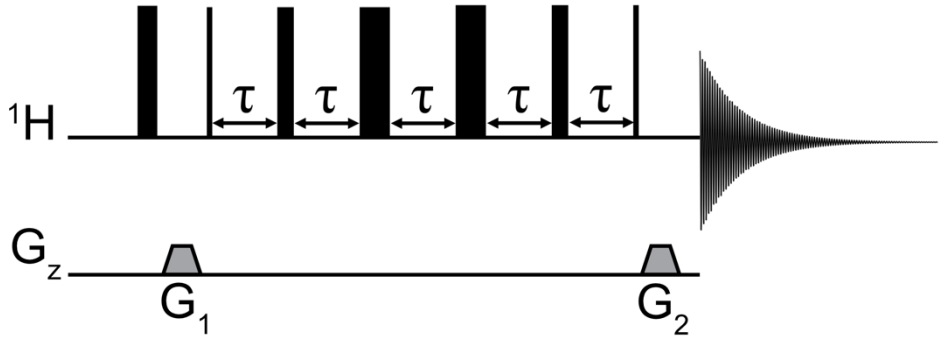

Figure 17 – WATERGATE-5 pulse sequence schematical diagram.

Even though WATERGATE is commended for its excellent solvent suppression, it has its problems, including base-line roll and signal phasing that were later addressed by Robust-5.[165,166]

3.7.1.2 Robust-5

For a pulse sequence to be robust, it needs to be able to handle sample inhomogeneities, radiation dampening and pulse miscalibrations.[165,166] These attributes were considered in the making of Robust-5 (Figure 18), to ensure the pulse sequence is well-equipped for chemometric work where general-purpose solvent suppression is needed.[166]

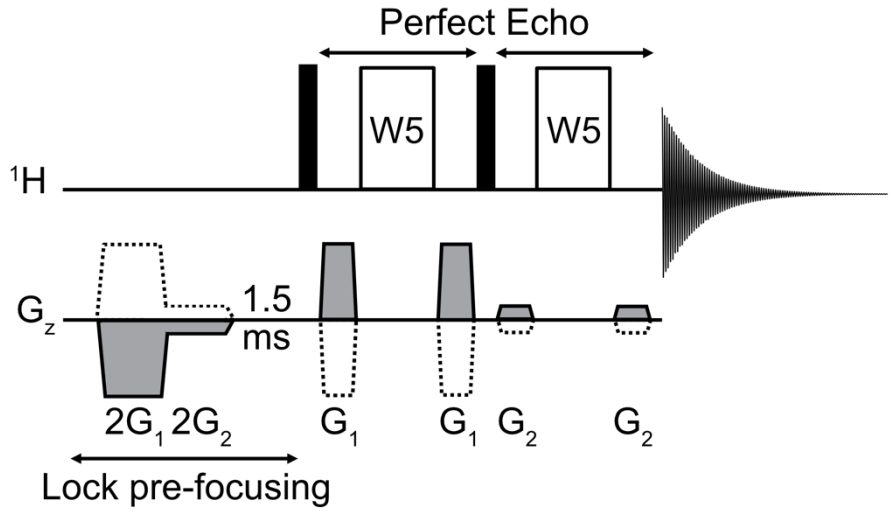

Figure 18 - Robust-5 Pulse sequence diagram schematic. G_z is the gradient applied to the z axis. The dotted lines are to signify the reverse is used for every other pulse. W5 refers to the WATERGATE 5 hard pulses.

By implementing lock pre-focusing pulse gradients, before the start of the water suppression, both eddy currents and lock disturbances are minimised.[166] The distortion of *J* modulation, as previously mentioned in 3.6.3.1, can be reduced by using a perfect echo. A similar water suppression pulse sequence that includes a

perfect echo, but without the pre-focusing lock, is called double pulsed field gradient spin echo (DPFGE).[164] Ultimately, the advantages of Robust-5 led to the decision not to further investigate DPFGE in this research.[164]

3.7.1.3 WET

Water suppression enhanced through T_1 effects (WET) is another PFG solvent suppression technique. The technique (observed in Figure 19), which has been frequently employed in MRI and hyphenated technique studies, applies selective on resonance gradient pulses and PFGs to dephase solvent transverse magnetization.[164] Subsequently, hard pulses perturb the remaining spins into the transverse plane before the acquisition takes place.[164]

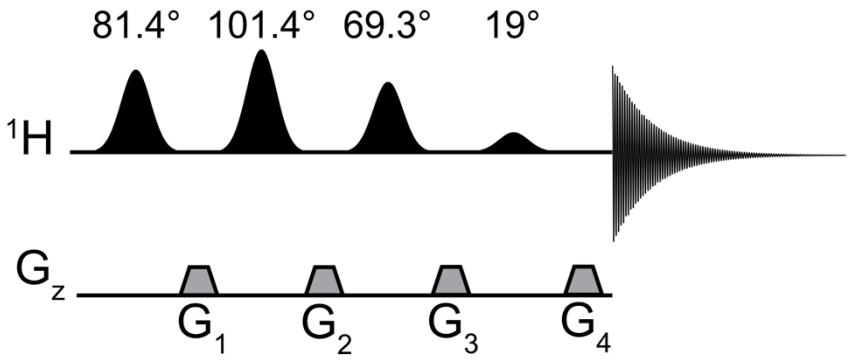

Figure 19 - WET Pulse Sequence schematical diagram.

3.7.2. Presaturation

The presaturation pulse sequence, also named PreSat for short, is the most widely used solvent suppression technique in metabolomics.[163] Presaturation (Figure 20) uses a saturation block, where a low-powered pulse is applied to reduce the solvent signal. The undesired magnetization is dephased on the applied $\boldsymbol{B}_1$ field; this is instead of the $\boldsymbol{B}_0$ field as with PFG pulse sequences.[164,167] To effectively irradiate the solvent signal, the spectrometer must be well-shimmed.[164]

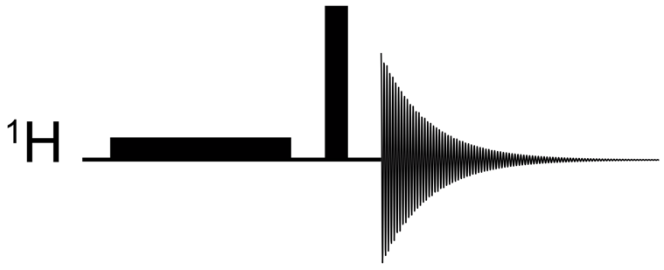

Figure 20 - Presaturation Pulse sequence

Solvent molecules that are found further away from the RF coil can experience lower RF field strength.[167] This can result in non-uniform flip angles which are unable to follow the designed coherence transfer pathways leaving behind a residue solvent signal. This term is also called the “far away” solvent effect.[163] The saturation block is robust but less efficient in suppressing on-resonance signals, such as the dominant water signal.[153] This can lead to residual water signals, especially when the solvent is water, which resonates on-resonance near 4.7 ppm. This is why it is often used with the 1D NOESY (Figure 16) pulse sequence. On the other hand, the WET-composite pulse (CP) pulse sequence (Figure 21) uses four 90˚ hard pulses (x, y, $-x$, $-y$), to reduce the effect of the faraway solvent and lead to a narrower residual water signal.[153]

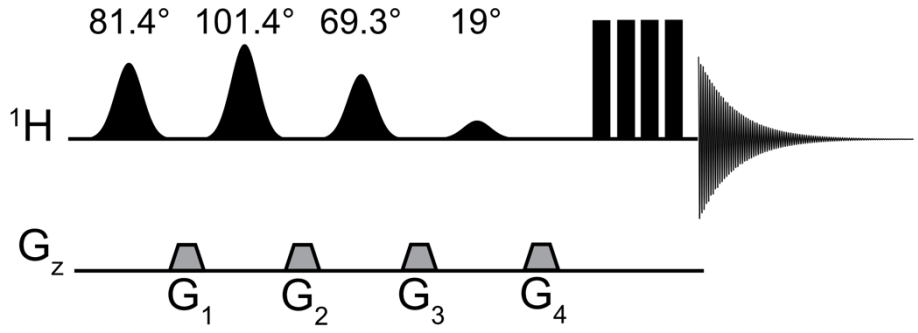

Figure 21 - WET-CP Pulse Sequence

Another limitation associated with the presaturation pulse sequence is the exchangeable NH protons that can be saturated and disappear from the spectrum.[163,167] This can be problematic in biofluids such as CSF and blood plasma, where observing NH signals is important, which is why WATERGATE is often preferred in these cases, as it allows for effective water suppression without saturating exchangeable NH protons.

3.8. 2D NMR

In 1D NMR, intensity is plotted against a single frequency axis, whereas in 2D NMR, two frequency axes are plotted, with the signal intensity represented by the contour levels. The peaks in a 2D NMR spectrum can represent a variety of information.

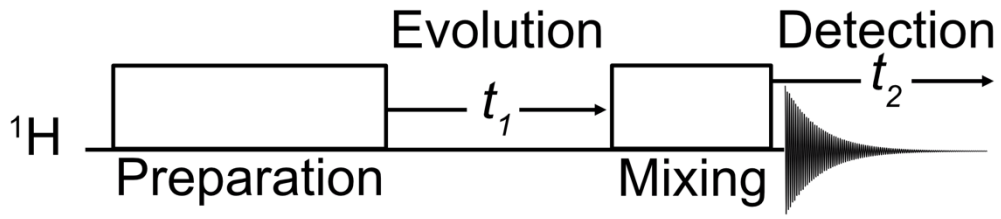

Figure 22 - Building blocks of a 2D pulse sequence

2D experiments are split into four steps: preparation, evolution, mixing, and detection (Figure 22).[97,99] During the preparation period, pulses generate coherence of spins.[97] During the evolution period, spins are allowed to evolve for a period t_1. The evolution time is varied between experiments. The mixing period transfers the coherence to be observable and then is followed by detecting the corresponding free induction decay (FID).[97,99]

3.8.1. COSY

Correlation spectroscopy (COSY) was first developed in 1971 and uses two proton dimensions.[97] Cross peaks indicate which spins are coupled together as a result, this method is used for spectral assignment. For COSY (Figure 23) there are two types of peaks: diagonal and cross. Diagonal peaks in COSY indicate that the frequencies (chemical shifts) during both evolution times are the same. This occurs because these peaks correspond to nuclei that are not *J* -coupled to other spins, so their chemical shifts remain constant during both the initial and indirect evolution periods. In contrast, cross peaks appear between *J* -coupled pairs of spins, reflecting correlations between nuclei that influence each other through scalar (*J*) coupling.

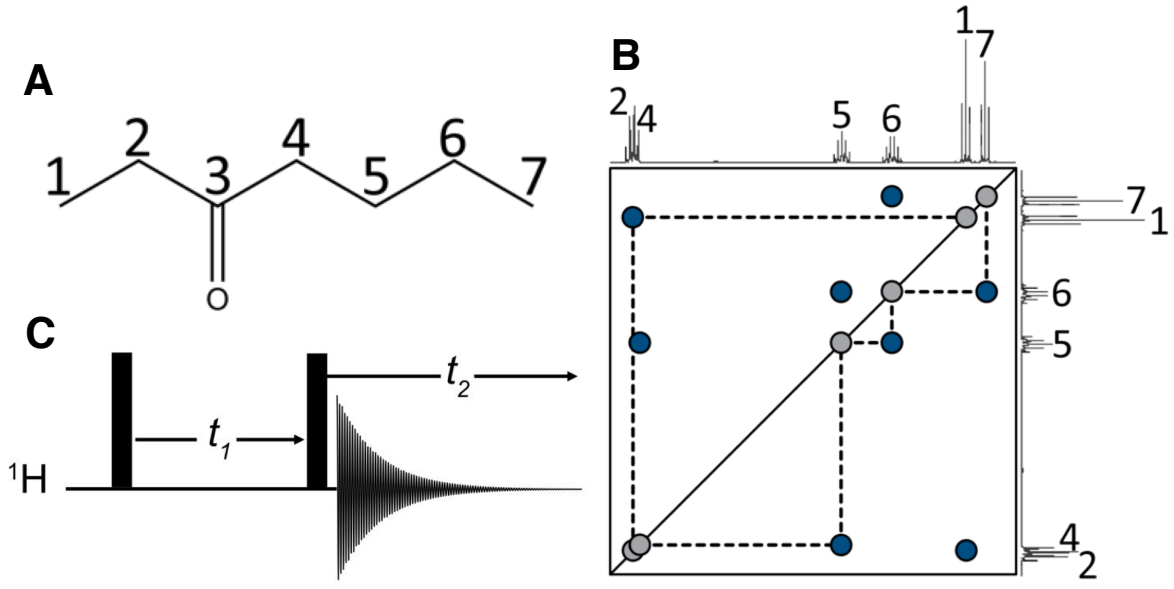

Figure 23 - 2D COSY Pulse Sequence Schematic. A) Chemical Formula for 3-Heptanone, B) A Schematic of a COSY spectrum for 3-Heptanone with annotated peaks, C) COSY Pulse Sequence Schematic. [168]

3.8.2. TOCSY

Total correlation spectroscopy (TOCSY) is a homo-nuclear pulse sequence that connects spins within a spin system, both those that are directly J -coupled and those that are indirectly connected through relay pathways of multiple J couplings. To achieve this, spin-locking is employed to transfer magnetization between these spins, as observed in Figure 24. A side-by-side comparison of COSY and TOCSY experiments is shown in the appendix chapter 9.1.

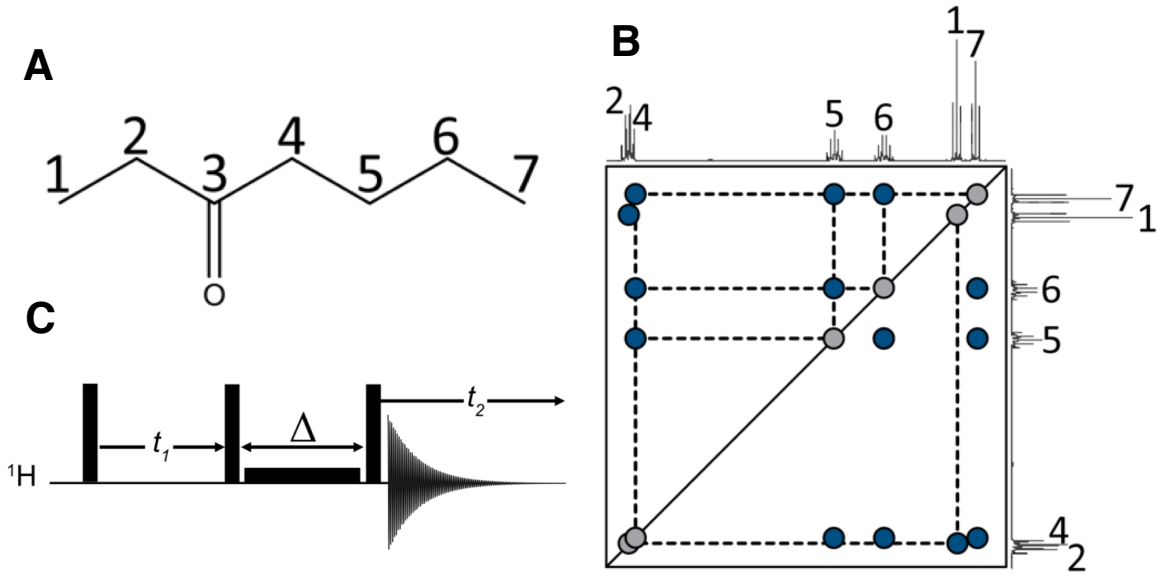

Figure 24 - 2D TOCSY Pulse Sequence. 2D TOCSY Pulse Sequence Schematic. A) Chemical Formula for 3-Heptanone, B) A Schematic of a TOCSY spectrum for 3-Heptanone with annotated peaks, C) TOCSY Pulse Sequence Schematic. [97]

3.8.3. HSQC

Heteronuclear single quantum correlation (HSQC), observed in Figure 25, correlates different nuclei such as ^{1}H, ^{13}C, and ^{15}N through their J -Coupling in a similar fashion to COSY (Figure 23), but this is heteronuclear instead of homonuclear like COSY.

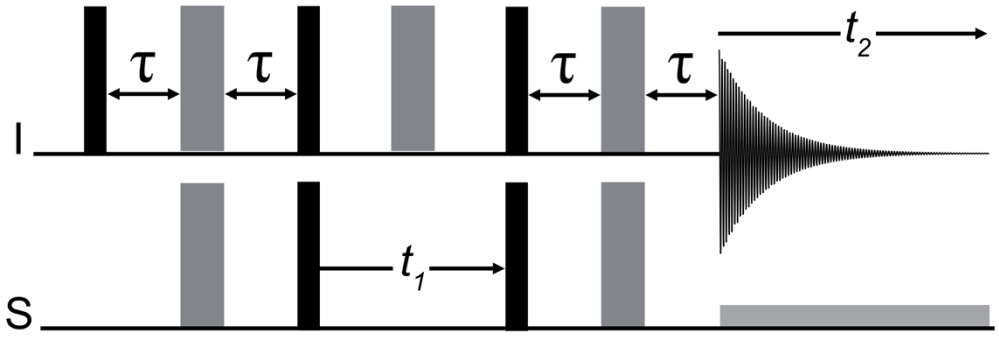

Figure 25 - HSQC 2D Pulse Sequence Schematic

The pulse sequence starts off with the insensitive nuclei enhanced by polarization transfer (INEPT) sequence.[97,164] This enhances weak signals from low γ nuclei such as ^{13}C and ^{15}N, by transferring polarization from a higher γ nuclei like ^{1}H.[98] After the initial polarization transfer, the S spin is allowed to evolve according to its chemical shift during the evolution period. During this time, the I spin is refocused using a 180˚ pulse to eliminate its chemical shift evolution, ensuring that only the chemical shift of the S spin is encoded. Finally, the magnetization is transferred back to the I spin for detection.[98]

3.8.4. HMQC

Heteronuclear multiple quantum correlation (HMQC), observed in Figure 26, also correlates different nuclei such as ^{1}H, ^{13}C, and ^{15}N through their J -Coupling like with the HSQC experiment.

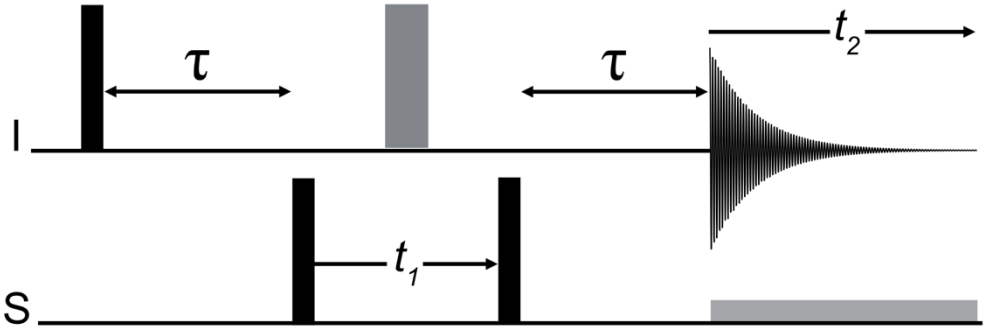

Figure 26 - HMQC 2D Pulse Sequence Schematic

The difference between the HMQC and HSQC pulse sequences is that during the evolution time, both the I and S spins are allowed to evolve in the HMQC experiment, whereas in HSQC, only the S spin evolves.168 Multiple quantum coherence is

transferred to heteronuclear nuclei by the 90° pulse. However, due to homonuclear proton J-coupling, this can lead to line or peak broadening in the S spin dimension, resulting in less resolution for the heteronuclear signals.[97]

Chapter 4 Experimental Methodology

The following chapter outlines the research methodology used in this study. The chapter is structured in chronological order according to the experimental methodology, providing a description, and explanation of the theory behind the methods. The specific methods used throughout this research are then outlined, with reasoning provided. Additional details about the research studies, such as sample type, collection, and cohort, will be provided in the subsequent results chapters.

4.1.1. Research Philosophy

Together this research aims to further expand on the potential utility of bNMR metabolomics, pushing the technology and building upon its strengths. To this end, this research will initially maximise the signal-to-noise ratio (within reason) of each sample at bNMR. Each experiment will be conducted for around 2 hours per sample. These studies were conducted gaining qualitative results as to maximise the number of scans. Sample preparation steps will also be minimised and kept simple to maintain NMR's minimal sample preparation strength.

4.2. Sample Preparation

For NMR analysis, each biofluid sample must be carefully prepared to ensure consistency and optimal conditions. This involves mechanical processes to remove unwanted materials that could interfere with sample relaxation, as well as chemical additives to prevent undesirable changes. These additives also aid in spectral alignment and quantification, ensuring accurate and reliable results.

4.2.1. Centrifuge

Particulate matter can interact with a sample often creating broader line widths, and is preferably removed in metabolomic sample preparation. Centrifugation is used to help precipitate sediment, proteins, and other unwanted cellular content from biological samples by separating particles based on their density and size.

During centrifugation, the samples are spun and high speeds, denser particles move away from the centre and conjugate at the bottom of the tube by centrifugal forces. Once the cycle has finished the supernatant can be transferred into a sterile 1.5mL microcentrifuge tube for storage until pipetted into the sample tube. If the rotations are too high (>10,000 g), then unwanted intracellular metabolites could be released due to cell breakage.

4.2.2. Internal Standard

An internal standard is often used in NMR to ensure the spectra are appropriately aligned. This standard can also often be used to calculate concentrations of metabolites present in spectra if the concertation of the internal standard is known and sufficient acquisition parameters are met. The standard chosen must not interfere with surrounding signals and possess a suitable solubility for the solvent of choice. In addition, quantitative experiments may need internal standards with suitable T_1 relaxation times, chemically inert and low volatility. There are three main internal standards that are used in NMR studies: Sodium trimethylsilylpropanesulfonate (DSS), Tetramethylsilane (TMS) and, Trimethylsilylpropanoic acid (TSP). Overall TSP was selected as the main internal standard during the projects due to its solubility with water, its signal far away from interfering signals and its low volatility. Formate is another internal standard that was also used in this research, as TSP can interact with proteins and other cellular content in blood. As a result, it is advised to use an alternate standard for this fluid. Although it does have the negative effect of a long T_1 for quantitative studies and can be in close proximity to surrounding signals.

4.2.3. Additives

Sodium azide is added to a sample to inhibit microbial contamination and growth. Deuterium is also commonly added as to lock the frequency (described in 4.3.4). As pH interferes with the chemical shifts, a suitable buffer needs to be added in order to correctly maintain the pH. A Sodium phosphate buffer allows for the control of the pH within a solution to ensure results obtained are accurate and reproducible.

4.3. Experiment setup procedure introduction

It is essential to ensure that experiments have been properly optimised to obtain accurate and reliable data. Failing to calibrate an experiment correctly could lead to incorrect excitation, increased noise, and wider line widths. To address these issues, optimisation of the magnetic environment and experiment setup is necessary. Depending on the hardware used, these tasks can be completed automatically and/or manually.

4.3.1. Pulse calibration

Before initiating a new experiment, a pulse calibration experiment must be conducted. The pulse calibration experiment arrays the length of the pulse until an estimated 360° pulse has been applied. When this pulse is applied there should be no signal after acquisition. The same 90° pulse length should be used for all samples in that given project. Changes could lead to improper excitations creating differences between spectra.

4.3.2. Tune and Match

Tunning and matching should be conducted on the nucelli and solvent of interest with a representative sample. The coil in the probe needs to be “tuned” so that the tuned circuit is resonant at the Larmor frequency. Matching the probe ensures maximal power transfer between the probe and the transmitter frequency. If matching is correctly optimised, then a sharp peak in observed in the NMR spectrum. If the spectrometer is incorrectly tuned and matched then this can lead to poor signal attenuation, peak broadening, and baseline disturbances.

4.3.3. Shimming

Shimming is the process where B^0 is made more homogenous by removing any small inhomogeneities present in the magnetic field. The term shim originates from when a small metal “shim” was added into a magnetic field to improve its homogeneity.[170,171] In modern spectrometers, this is now controlled with shim coils that surround the sample. The goal of shimming is to minimise the line width and produce a symmetrical peak.[170–172] A sample shim is completed for each sample

when placed into the spectrometer. This quicker shim is normally completed in a 1st order shim (x, y and, z) with higher order shimming (2nd, 3rd and 4th) that affects smaller-scale filed variations traditionally completed during routine maintenance.

4.3.4. Lock

The magnetic field is not perfect and is prone to drift over time.[173] In order to compensate for this, a spectrometer lock can be applied. This is accomplished by locking the frequency of the NMR spectrometer to the resonance frequency (field-frequency lock) of the sample being studied. When the lock is applied, the signal from the spectrometer is monitored for any changes in the resonance frequency. If the signal deviates from the set point, the lock will automatically adjust the frequency to bring the signal back to the set point. This ensures that the signal remains constant over time and allows for more accurate data acquisition. The lock uses the signal from a deuterated solvent, such as deuterium or deuterated chloroform, that is added to a sample during sample preparation. This is monitored through a continual wave experiment.[96,164]

4.3.5. Acquisition Delay

As temperature affects the chemical shifts of the protons in the sample, causing them to move to different positions in the spectrum, a delay of acquisition is applied to ensure the sample has reached the same temperature as the magnet. This also helps to decrease the line width of signals in a spectrum.

4.3.6. Sample-specific set-up parameters

For all sample acquisitions acquired on the bNMRs, a ten-minute delay was applied before shimming occurred to allow the probe temperature and sample temperature to become stable. After this time no chemical shift changes were observed. Both HF-NMR spectrometers were temperature controlled, so they did not require any delay. A sample-specific shim was applied to all samples to remove any small inhomogeneities which were present in the magnetic field. A deuterium lock is also applied to all samples during all experiments to avoid frequency shifts.

4.4. Acquisition Parameters

When running an experiment, the acquisition parameters need to be optimised. Depending on the metabolites of interest, or the solvent present, different acquisition parameters need optimising to ensure the desired output from the experiments is met.

4.4.1. Relaxation Delay

Nuclei must be allowed to relax before they are re-excited. This process is named relaxation delay often referred to as RD. As different signals relax at different rates it is important to use the longest $T1$ relaxation (slowest relaxing) signal of interest. For quantitative NMR this is normally set to $5 \times T1$, as magnetisation has nearly fully recovered (<99%) back to its equilibrium at B^0. To save time during acquisition, the relaxation delay can be reduced due in part to some signals of interest taking more than 30 seconds to relax and a middle ground is achieved between speed of acquisition and relaxation.

4.4.2. Number of Scans

To improve the signal-to-noise each experiment is repeated. The number of times the experiment is repeated is often called the number of scans. The spectra are then added together to achieve an improved signal. However, the improvement to the signal is not linear and instead is based on the inverse square rule, $\sqrt{N}$, where N is the number of scans. This means that to achieve double the signal-to-noise from an 8-scan experiment, a total of 64 scans will need to be completed. A total of 1024 scans was chosen throughout this research as minimal gains were observed beyond this point.

4.4.3. Number of Points

This parameter indicates the number of points recorded during the free induction decay (FID). The spacing between each point is calculated from the total number of points divided by the acquisition time. A sufficient number of points must be recorded to ensure that no signal resolution is lost.

4.4.4. Spectral Window

The spectral window refers to the range (often measured in frequency (Hz) or ppm) within which the spectrum is obtained. It's important to use a wide enough range to accurately capture the signals of interest. However, a wider spectral window will also increase the acquisition time. A broader spectral width can also aid in baseline corrections. As a general rule, it is recommended to leave a 10% gap on each side of the signals of interest to avoid interference from receiver filters.

4.5. NMR Spectrometers

The primary HF-NMR instrument used was the 400 MHz (9.4 Tesla) JEOL NMR Spectrometer at Nottingham Trent University, featuring the Delta software (JEOL, Tokyo, Japan). The use of this instrument allowed for a diverse range of experimental conditions and analyses such as 1D presaturation, WASTED and 2D TOCSY and COSY experiments.

Some experiments were also undertaken using an 800 MHz (18.8 Tesla) Bruker HF-NMR Spectrometer (Massachusetts, USA). This spectrometer, located at the University of Nottingham, was equipped with a 5mm cryoprobe and provided high-sensitivity and resolution NMR spectra for the chronic kidney disease study and preliminary results in the idiopathic epilepsy study.

Most bNMR experiments were conducted on the 60 MHz Oxford Instruments X-Pulse bNMR Spectrometer, utilising the Spin Flow 3.3 software (Oxford Instruments, Oxford, UK). The X-pulse was also equipped with a 25-slot autosampler. An additional 60 MHz Pulsar bNMR Spectrometer from Oxford Instruments (Oxford Instruments, Oxford, UK) (SpinFlow 3.0) was also used for the additional work on tube optimisation and the chronic kidney disease study (appendices 9.18 - 9.22).

4.6. Data Processing

After the spectra have been acquired, they need to be processed before statistical analysis can take place. This is completed through processing software such as

TopSpin and Mestrenova. Some software has been completed to automate this process; however, this is still in its early stages for bNMR.

4.6.1. Fourier Transformation

The first step of data processing is Fourier Transformation (FT). FT is the process of converting the FID from the time domain into the frequency domain. The spectra can appear noisy and so apodization can be applied.

4.6.2. Apodization

This is the process of applying a smoothing function to the FID to help improve the signal-to-noise and remove artefacts. Although there are many different functions which can be applied, the main techniques applied in one dimensional NMR include an exponential and Gaussian function. The decaying exponential is weighted so that the initial signal is multiplied by a larger factor and reduces the background noise towards the decaying signal. The Gaussian function applies a decaying bell-shaped curve allowing for improved visualization of low-concentration signals near the baseline. The goal of a smoothing function is to apply a factor that closely matches the decay of the signal.[97]

4.6.3. Zero Filling

As the name suggests, Zero-filling adds data points (of zero) at the end of an FID before being Fourier transformed (FT), to potentially improve the quality of the spectra due to the increased resolution in-between points and removal of noise at the end of the time domain acquisition. Typically, two to four times the number of acquired data points are selected for zero filling.

4.6.4. Phase Correction

The applied magnetisation may not correctly correspond with your receiver phase. To fix these issues a phase correction can be applied. To correct for this a zero-order phase correction (ϕ^0) the FID is rotated so that the absorption intensity is at its highest and the dispersion at its lowest. With first-order phase correction ($\phi 1$), this correction is applied diagonally across the spectrum.

4.6.5. Baseline correction

Distortions can be created during data acquisition that are not true. These can be removed manually or automatically though different baseline corrections. Close attention is important to ensure the true signal is recorded. All baseline corrections were completed manually through the peak pick Lorentzian fit function in Mestrenova.

4.6.6. Reference Alignment

TSP was used to align spectra to 0ppm. The spectrum was also then stacked and then smaller adjustments were made to ensure the chemical shifts stayed consistent. Although these problems are minimised through the sample preparations and experiment optimisations, small sample parameter differences such as pH, salinity or temperature can still need manual alignment to ensure optimum spectra and alignment.

4.6.7. Binning / Bucketing

Binning reduces the number of points in a spectrum by reducing the number of “bins” available. This allows for easier understanding of how different signals affect a spectra when analysing the data.

4.7. Data analysis

After the data was processed, analysis was conducted using two primary tools: Python and MetaboAnalyst. Python, a versatile programming language, offers a wide array of packages specifically designed for data analysis, making it a powerful tool for this purpose. On the other hand, MetaboAnalyst is an online platform tailored for metabolomics workflows, offering robust tools for single and multivariate statistical analyses, as well as pathway and biomarker analysis.

The analysis utilised two principal statistical approaches: univariate and multivariate statistics. Univariate statistics were applied to examine individual variables, while multivariate statistics were used to explore patterns and relationships across

multiple variables simultaneously. These methods provided comprehensive insights into the dataset, facilitating a deeper understanding of the underlying biological processes.

4.8. Univariate Statistics

Univariate analyses are often used in the initial stages of analysis to identify individual metabolites that are significantly altered in response to different conditions or treatments.[174] Univariate statistical analysis focuses on analysing one variable at a time.

4.8.1. ANOVA

An independent T-test is used to compare two independent groups, such as healthy as diseased. This can be further extended through one-way analysis of variance (ANOVA), which can assess if the means of two categories are significantly different across multiple groups such as the metabolite bins in an NMR spectra.

When analysing the distribution of samples for a particular metabolite bin or variable, box plots are commonly used. These plots allow for a visual analysis of how the samples are distributed between different groups. Any outliers present in the data are shown outside of the whiskers, which extend to 1.5 times the inter quartile range.

4.8.2. The Area Under the Receiver Operating Characteristic Curve

The area under the curve (AUC) is often used to evaluate the discrimination ability of a model by evaluating its predictive potential. These plots are generated from receiver operating characteristic (ROC) curve analysis, where sensitivity (true positive rate) is plotted against 1-specificity (false positive rate) for varying threshold values. The AUC represents the performance of a detection test or a predictive model. The AUC can range from 0 to 1 with the higher the value the better the discrimination the model holds against positive and negative cases. The true positive and true negative rate controls the sensitivity and specificity of a model. A trade-off between the two measurements is given in the model showing both the

highest sensitivity and specificity, shown by a red dot on the plot. This value has a false discovery rate (FDR), this is the expected proportion of false positives among all significant results.

4.8.3. Fold Change Analysis

Fold change is a simple yet powerful method for quantifying the relative difference in metabolite levels between two conditions. It can be calculated as a ratio, where a fold change greater than one indicates an increase, and a value less than one indicates a decrease. Fold change analysis is commonly used to identify metabolites that are increased or decreased in response to a treatment or condition. This information is then often used to interpret pathway analysis.

4.8.4. Volcano Plots

Volcano plots are often depicted as scatter plots, similar to fold change analysis. However, they combine the fold change on the X-axis with the statistical significance (p-value) on the Y-axis. To enhance clarity, the x-axis represents log2 fold change, while the y-axis represents the negative log10. Metabolites identified as significant will appear either in the upper left (indicating a relative decrease) or the upper right (indicating relative increase) of the plot.

4.9. Multivariate Statistics

Multivariate statistical analysis involves the simultaneous analysis of multiple variables (metabolites). This approach is crucial in metabolomics due to the complexity and high dimensionality of the data.

4.9.1. Principal Component Analysis

Principal Component Analysis (PCA) is an unsupervised statistical method used to reduce the dimensionality in data and is widely utilised in metabolomics due in part to its unbiased nature, leading to its highly advantageous implementation for non-targeted metabolomic studies.[174,175] Unlike some supervised methods, PCA calculates the maximum variation in the data set (X) without the influence from the

class labels (Y) and consequently not a classification method.[176] A PCA plot can take multidimensional data and represent it in a 2D plot, displaying variance and clustering among the data points. By displaying the eigenvectors, Principal Components (PC), across multiple axes, variance, clustering, and outliers can be observed. When potential outliers are identified, the weighting of the data set can be observed through a loading plot. The eigenvalue represents the amount of variance explained by each eigenvector. A higher eigenvalue means the associated PC explains a larger proportion of the variance in the data set.

4.9.2. Partial Least Squares Discriminant Analysis

Unlike PCA, Partial Least Squares Discriminant Analysis (PLS-DA) is a supervised test that maximises the covariance between the data set and the class labels, even in high-dimensional data. PLS-DA is highly advantageous in datasets that are highly collinear and have a noisy baseline, this is why this is frequently used in NMR analyses. Due to the extra supervision during this test, cross-validation needs to be completed to ensure the validity of the results. PLS-DA can be split into two parts: PLS where dimension reduction occurs, and DA, the prediction model.

Although PLS-DA is a supervised test, it does not assume a predefined fit to the distribution, unlike Orthogonal Projection to Latent Structures Discriminant Analysis (OPLS-DA). In principle, this means that correlations between non-class-based separation still impact distribution, which can be problematic when increasing the quantity of given classes. As with all supervised methods, small datasets allow for a higher likelihood of overfitting to be present.

To assess the significance of separation of the data set, a Variable Importance in Projection (VIP) score is produced. This is important to identify the most influential variable in the model, where a higher VIP score signifies a more important data set variable. Traditionally a score of above one is considered to have a significant impact on the class labels.

4.9.3. Orthogonal Projection to Latent Structures Discriminant Analysis

OPLS-DA can add further class separation through the orthogonal projection along by disregarding correlations not associated between the class labels. As a result, OPLS-DA is great at identifying potential biomarkers.

Due to the extra influence of the class variables, OPLS-DA is prone to overfitting and a permutation test can be completed to validate the reliability of the separation. During this test the class labels are randomly rearranged (permuted), creating a “shuffled” dataset where the OPLS-DA model is reperformed to compare against the original, non-permuted OPLS-DA model.

A histogram is then created to display the distribution of the models fit to the original data (R^2) and the consistency between the original and cross-validated predicted data (Q^2). A large difference observed between the original and permuted OPLS-DA models suggests a significant relationship between the variables and the classes. Often p-values (a metric that shows the likelihood of the data occurring under the null hypothesis) are also provided in association with the Q^2 and R^2 values.

Chapter 5 Metabolomic Analysis of Cerebrospinal Fluid: An Idiopathic Epilepsy Investigation

5.1. Introduction

The United Kingdom is home to over 13 million dogs, as of 2024, which represent 64.8% of the veterinary-visiting population, with emergency care and general check-ups being the most common reasons pet owners visit the vet.[177–180] However, veterinary costs have been steadily increasing to over £500 as of 2022.[9,178] This rise in costs is partly driven by advancements in veterinary medicine and an increased demand for comprehensive animal healthcare.[9] However, in 2022, 19% of dog and cat owners delayed vet visits due to these costs, with 20% of that group reporting they would no longer be able to afford their pets if faced with unexpected expenses.[178] Veterinarians have noted this impact, with 99% of vets reporting cases where animals should have been brought in sooner, and 1 in 5 pets not receiving timely treatment.[178] Financial limitations are a major factor, with 52% of vets observing that clients struggle to cover preventive care costs, while 70% report difficulties affording diagnostic care and treatment.[181]

The rising costs of veterinary care not only influence general healthcare accessibility for pets but also have significant implications for managing chronic conditions like epilepsy, which require extensive diagnostics and ongoing treatment. Epileptic seizures are a common neurological issue in veterinary medicine, characterised by abnormal and excessive neurological activity.[182] Epilepsy ranks among the top ten conditions for which pet insurance claims are most frequently filed, with costs for diagnosis and treatment ranging from $200 to $5,000, covering tests like bloodwork, magnetic resonance imaging (MRI), and spinal taps, as well as treatments that include anticonvulsants and surgery.[183] In 2013, over 5,000 dogs in Sweden were diagnosed with epilepsy, with more than half of the diagnosed dogs ultimately euthanised.[184] An estimated 91,000 dogs in the UK alone have epilepsy.[185] Idiopathic Epilepsy (IE) is the most common form of epilepsy (53% of all cases of epilepsy), clinically diagnosed from a process of elimination.[67,186] As a result, other forms of epilepsy such as reactive, where seizures are induced metabolically or from intoxication, and structural epilepsy, from a forebrain anomaly, are excluded from

affecting the seizure.[67] Previous diagnoses of IE have been caused by injury, developmental, metabolic and genetic origin. However, IE can be difficult to diagnose due to other conditions mimicking seizure activity, and its exact cause remains unclear.[23,67,182]

The International Veterinary Epilepsy Task Force (IVETF) has defined criteria which should be followed to meet a clinical diagnosis of IE.[23] This follows a three-tier system in order of confidence of diagnosis. To meet the tier 1 criteria, a history of two or more unprovoked seizures 24 hours apart needs to have occurred between the ages of six months and six years. There also needs to be an unremarkable interictal physical and neurological examination with no identified significant abnormalities on blood or urine analysis. Tier 2 follows on from tier 1 to include unremarkable: fasting and post-prandial bile acids; MRI of the brain; and Cerebrospinal fluid (CSF) analysis. Tier 3 adds the addition of the identification of electroencephalographic abnormalities characteristic of seizure disorders.[23]

CSF surrounds the brain and spinal cord and is commonly used in neurological and oncological disease detection.[187] Its main functions include providing protection, maintaining intracranial pressure, transporting nutrients, and removing waste from the brain and spinal cord. [187–189] The majority (70-80%) of CSF is produced by the choroid plexus which filters plasma and creates a blood-CSF barrier, that helps to maintain the composition of CSF.[190] The main composition of CSF is water (<99%), with additional constituents containing amino acids, glucose and electrolytes.[191] Some small amounts of blood cells and proteins like albumin, globulins, and enzymes, can also be present in the fluid.[191] However, abnormal concentrations of these components can suggest the presence of infection, inflammation or disruptions to the blood-brain barrier, all of which are associated with various neurological conditions.[189,190] CSF is frequently collected from the cerebellomedullary cistern at the back of the neck or the lumbar cistern in the lower back of dogs.[188,192] The invasive nature of CSF collection, along with the limited ethical availability of samples from healthy control animals, has resulted in fewer studies on CSF compared to blood or urine. Additionally, the limited sample volume can restrict analysis, especially after other clinical tests are completed.192 Despite these challenges, CSF remains a crucial biofluid for neurological biomarker research, as certain markers may not cross the blood-brain barrier.[193] Limited

research has focused on epilepsy biomarkers in CSF, with studies largely restricted to proteins[194–201], genetic information[197,202–204], and basic metabolites like lactate and glucose.[197,199,200]

With the difficulty of diagnosing IE, a low-cost rapid solution that is easily accessible to veterinarians should be explored, for suspected and routine check-ups on dogs.[21] Given the challenges of diagnosing IE, a low-cost, rapid, and accessible solution for both suspected and routine check-ups on dogs is essential. This study aims to identify which metabolites can be observed using bNMR, determine the optimum pulse sequence for analysing CSF samples, investigate significant metabolite differences (biomarkers) between dogs with IE and healthy dogs and evaluate if a panel of metabolites can be developed to collectively differentiate between dogs with IE and healthy dogs.

5.2. Materials and Methods

5.2.1. Ethical Approval

All samples were collected with informed consent from pet owners at the Dick White Referral Centre (DWR) with ethical approval for this study approved by the Nottingham Trent University (NTU) Ethical Comity Board ARE202139.

5.2.2. Sample Collection

All dogs in this study were client-owned, and informed consent was obtained from pet owners prior to sample collection and storage (-80°C) at DWR. After routine clinical investigations, any residual samples were stored at -80°C. The samples were then collected from DWR and delivered to Nottingham Trent University's Medical Technologies Innovation Facility on ice in freezer boxes before being stored at -80°C until analysed on the HF-NMR and bNMR.

5.2.3. NMR Sample Preparation

The samples were first placed on ice and gently mixed by inversion until partially thawed. They were then allowed to reach room temperature while continuing to mix carefully. Samples with visible contamination, i.e., blood, were removed from the sample cohort. The maximum sample volume (≥400 μL) was pipetted from the

sample tube into a 1.5 mL sterile microcentrifuge tube. 50 μL of a 0.5% trimethylsilylpropanoic acid (TSP) in D_2O (w/v) and 50 μL 0.2% sodium azide in D_2O (w/v) was added. A 0.1M phosphate buffer solution (7.2 pH) in D_2O (v/v) was then pipetted to fill the remaining volume (100 – 350 μL) to make a final volume of 550 μL. Samples were then gently mixed by inversion, pipetted into clean 5 mm NMR tubes, and then stored for up to two weeks at 4°C until analysed on the bNMR and HF-NMR.

5.2.4. Study Population

CSF samples (n = 225) for this study were collected from DWR. Samples were classified and filtered based on cohort criteria, with any sample below 200 μL being excluded (see Chapter 5.3.2 for more information). IE samples were classified by Linnaeus clinicians using the Tier II criteria established by the IVETF, as described in Chapter 5.1. Control samples, also classified by Linnaeus Clinicians, were selected based on the absence of neurological conditions, no seizure activity, and normal results in blood tests, MRI, and CSF examinations. Following sample triage, a total of 39 CSF samples were deemed suitable for this study, comprising 19 samples from dogs diagnosed with IE and 20 from controls.

Table 3 - Study Population of IE CSF samples and controls

Characteristic	IE (n = 19)	Controls (n = 20)	Total (n = 39)
Age (years)	3.75 ± 2.27	8.24 ± 3.72	6.05 ± 3.81
Sex (M:MN / F:FN)	6:6 / 2:5	7:6 / 2:5	13:12 / 4:10
Breed Groups	6 Cross, 1 Herding, 1 Hound, 2 Non-Sporting, 6 Sporting, 1 Terrier, 2 Toy,	2 Cross, 1 Herding, 3 Hound, 1 Non-Sporting, 8 Sporting, 3 Terrier, 2 Working,	8 Cross , 2 Herding, 4 Hound, 3 Non-Sporting, 14 Sporting, 4 Terrier, 2 Toy, 2 Working
CSF Protein	0.17 ± 0.05	0.29 ± 0.18	0.23 ± 0.14
Nucleated Cell Count	2.17 ± 1.47	94.54 ± 333.95	65.37 ± 276.22
Red Cell Count	20.38 ± 33.12	183.29 ± 363.35	104.33 ± 270.77

IE: Idiopathic Epilepsy. M: Male, MN: Male Neutered, F: Female, FM: Female Neutered

5.2.5. NMR Spectroscopy Acquisition Parameters

Initial NMR spectra of the CSF samples was conducted by staff at the University of Nottingham using an 800 MHz Bruker spectrometer equipped with a 5 mm cryoprobe. A 1D nuclear overhauser effect spectroscopy (NOESY) presaturation pulse sequence was used to acquire the spectra. The full parameter list is included below: scans: 256, receiver gain: 34, relaxation delay: 12 seconds, pulse width: 10.7 μs, presaturation frequency: 4.79 ppm, acquisition time: 3.1457 seconds, spectrometer frequency: 800.32 MHz, spectral width: 10416.7 Hz, acquisition size: 32768, temperature: 25˚C.

Samples were additionally analysed at NTU using a 400 MHz NMR Jeol ECX spectrometer. The parameters were as follows: Presaturation Periodic Refocusing of J Evolution by Coherence Transfer **(**PROJECT), temperature at 19˚C, number of scans: 128, receiver gain: 50, relaxation delay: 12 seconds, pulse width: 11.22 *μ*s, acquisition time: 2.186 seconds, Tau: 2500 *μ*s, 20 echoes, spectrometer frequency: 399.52 MHz, spectral width: 5995.2 Hz, and acquired size: 16384. All samples were shimmed, locked to deuterium and tuned and matched.

Additionally, bNMR data were acquired using a 60 MHz Oxford Instruments X-Pulse with an autosampler attached. The water suppression with a transverse relaxation filter that eliminates distortions (WASTED-II) pulse sequence parameters included: filter 5000 Hz, acquisition points 16384, temperature at 37˚C, number of scans 1024, relaxation delay of 2 seconds, Tau 2500 *μ*s, 20 echoes, P90 6.893 *μ*s, receiver attenuation 32, W5 water suppression 555 *μ*s, gradient ramp time 100 *μ*s, gradient duration 4000 *μ*s, and gradient recovery time 1000 *μ*s. All samples were shimmed and locked to deuterium. Tunning and matching occurred daily with no large deviations noted.

5.2.6. Data Processing

After acquisition, the data were processed in MestreNova (Version 14.1.1). Each sample was zero-filled, Fourier transformed, referenced to TSP at 0 ppm, and a 1 Hz weighted apodization function was applied. Manual phase and baseline corrections were also performed. Following processing, 0.01 ppm bucketing was applied to data from the 400 MHz and 60 MHz systems, while manual binning was

used for the 800 MHz spectra due to its higher operating frequency. More detailed information on these methods is provided in Chapter 4.6.7.

5.2.7. Data Analysis

Data analysis was conducted using Python (version 3.10) with packages including pandas (version 1.3.4)[205], numpy (version 1.21.4)[206], matplotlib (version 3.5.1)[207], scipy (version 1.8.0)[208], and statsmodels (version 0.13.2)[209], as well as the online metabolomics package MetaboAnalyst 6.0.[210] Prior to multivariate and univariate analyses, the distribution of all metabolite features was examined within MetaboAnalyst using density plots of normalized intensity values. The density maps indicated that the data were approximately normally distributed following normalization and scaling, with no evidence of skewness or outliers that could bias subsequent analyses. Establishing normal distribution is important as it ensures that statistical assumptions underlying parametric tests and multivariate models, such as OPLS-DA and linear regression, are met. This improves the interpretability and reliability of variance partitioning, correlation strength, and model performance metrics. The observed normal distribution therefore supports the validity of the subsequent statistical and multivariate analyses performed in this study.

5.3. Results

5.3.1. NOESY Pulse Sequence with Water Suppression Using ^{1}H NMR at 800 MHz

Exploratory analysis of the 225 CSF samples was first analysed to identify the metabolites present. Previous research has been divided on the most suitable pulse sequence to use for CSF acquisition in metabolomics, with the main pulse sequences used being between NOESY and a T2 filter experiment such as Carr-Purcell-Meiboom-Gill (CPMG) or PROJECT.[193,197] The NOESY Presaturation (noesypr1d.split) pulse sequence was initially used to identify metabolites on an 800MHz ^{1}H HF-NMR spectrometer. The 1D NOESY Presaturation pulse sequence is well suited for metabolomic analysis due to its robust ability to handle varying concentrations of water present in a sample.[161] The identification of metabolites were certified by screening the NMR spectra in the Human Metabolome Database

(HMDB)[211], as well as COSY (correlation spectroscopy) (Appendix 9.6). The identified metabolites were also compared with existing NMR literature exploring CSF metabolites. A total of 28 different metabolites were identified at 800MHz from dog CSF samples.[161] Figure 27 shows a representative spectrum of canine CSF with 24 metabolites, each number corresponding to a metabolite. Four metabolites that were identified but less frequently observed, are shown in appendix 9.9; the corresponding metabolites are 2-hydroxybutyric acid, 3-hydroxybutyric acid, acetone, and pyruvic acid. The most abundant metabolites across spectra were lactate, acetoacetic acid, glucose, and histamine.

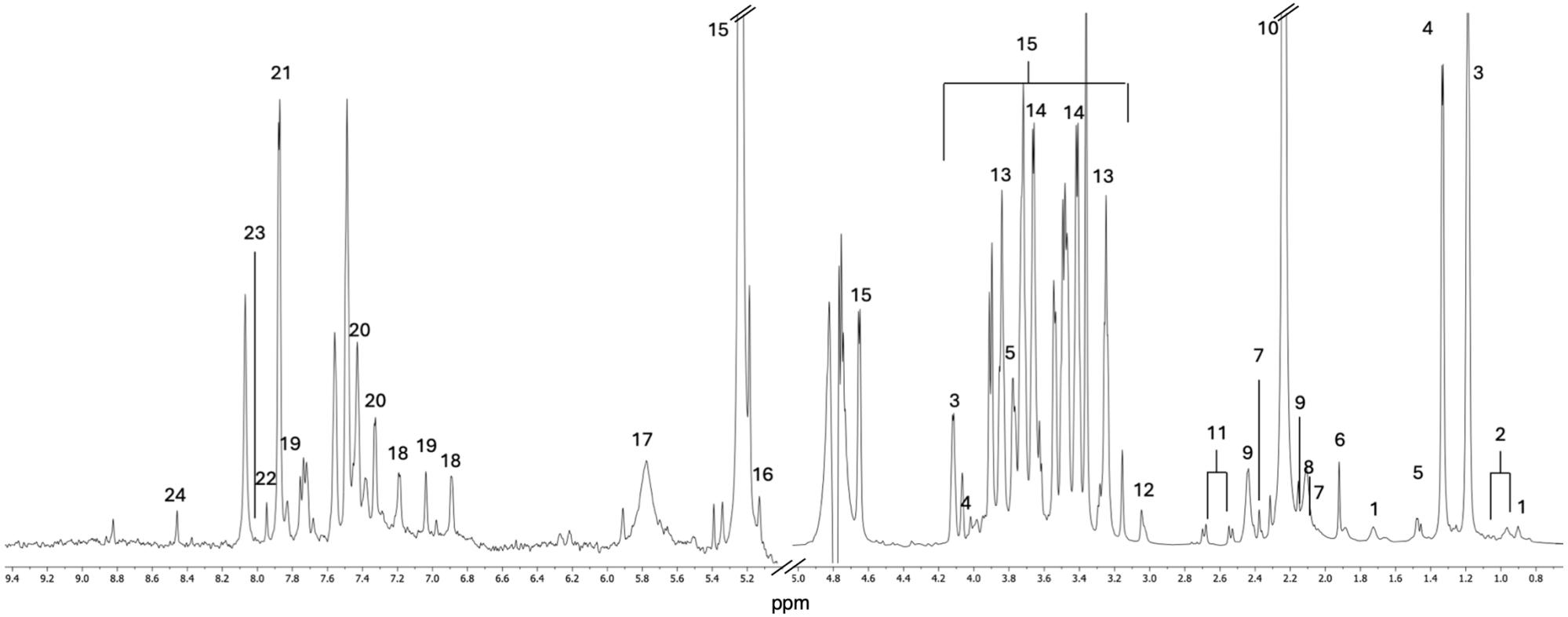

Figure 27 - Annotated 800 MHz ^{1}H NMR NOESY Presaturation spectrum of representative control canine CSF between 0.6 - 5 and 5.1 - 9.4 ppm. The numbers correspond to a metabolite: These metabolites were: 1) Leucine, 2) Isoleucine, 3) Ethanol, 4) Lactate, 5) Alanine, 6) Acetic Acid, 7) Glutamic Acid, 8) Butyric Acid, 9) Glutamine, 10) Acetoacetic Acid, 11) Citrate, 12) Creatine / Creatinine, 13) 1,5-Anhydrosorbitol, 14) Glycerol, and 15) Glucose, 16) Mannose, 17) Urea, 18) Tyrosine, 19) Histidine, 20) Phenylalanine, 21) Histamine, 22)1-Methylhistidine, 23) Adenine, and 24) Formate.

5.3.2. The Effect of the Volume of CSF on NMR Spectra

Further exploratory analysis on the 225 CSF samples was completed to observe if metrics about the samples, such as breed type, diseases, sex, and sample volume, affected spectra. A principal component analysis (PCA) plot was created to visualise the variance of sample volume between spectra. Initial observations (shown in Figure 28) revealed that samples with less than 200μL of CSF tended to cluster together. This clustering was likely due to certain metabolites not appearing in these low-volume samples, as their concentrations fell below the noise level of the spectra. Despite attempts to mitigate these issues through Pareto scaling and normalisation, the variability in sample volume continued to affect the spectral results. Consequently, all samples with volumes below 200μL were excluded from the cohort to ensure data quality and consistency for subsequent analysis. A total of 138 CSF samples were used for subsequent exploratory statistical analysis.

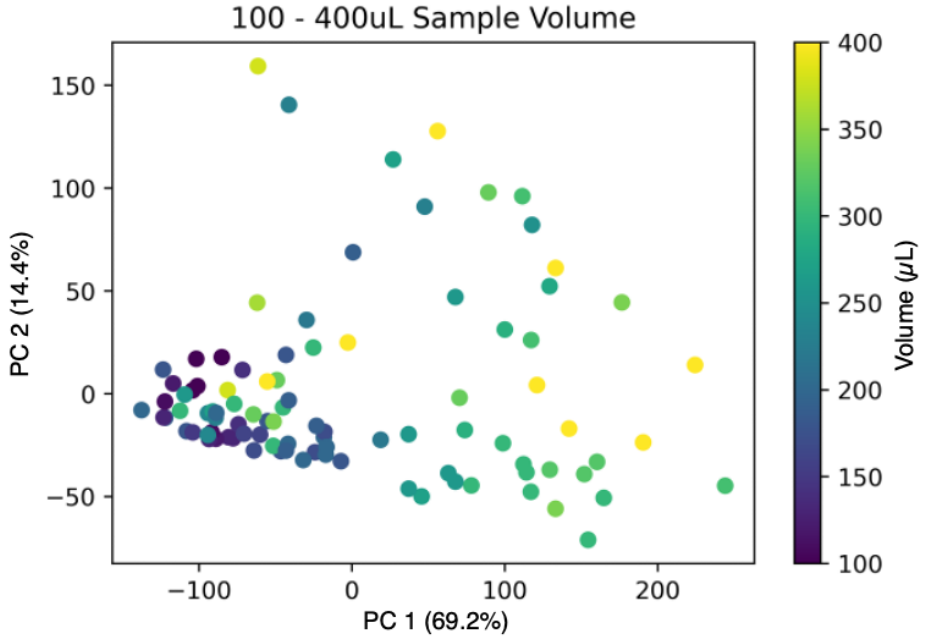

Figure 28 - Principal Component Analysis (PCA) plot of CSF samples with volumes ranging from 100μL to 400μL. PC1 and PC2 capture 69.2% and 14.4% of the variance, respectively. Sample volumes are indicated by a colour gradient: yellow represents samples with 400μL of CSF, green ~300 μL, blue ~200uL, and purple represents samples with 100μL or below. The clustering of low-volume samples (purple) suggests potential volume-related variability affecting spectral data.

5.3.3. The Effect of Protein Content in CSF Samples on NMR Spectra

Protein and other large macromolecules, like lipids and cells, can affect NMR relaxation rates from their influence on molecular motion and magnetic field fluctuations.[97] The influence from slower tumbling rates that closely match the NMR frequency range, enhances dipole-dipole (interaction of two nuclei magnetic field) interactions leading to faster relaxation and causing line broadening.[97]

Given the potential influence of proteins on NMR spectra, and in light of research by Albrecht *et al. (*2020) suggesting proteins may not significantly impact spectra, it was important to investigate this factor in detail.[212] 48 CSF samples, classified by clinical data from DWR, were selected based on protein content: 30 samples with high protein content and 18 with low protein content. To maximise separation and examine the metabolic differences associated with protein levels, an Orthogonal Partial Least Squares Discriminant Analysis (OPLS-DA) plot was used. The OPLS-DA plot (Figure 29a and b) depicts the separation of metabolomic profiles between a normal protein content sample (red) and a high protein content sample (green), as classified by DWR during routine CSF analysis. Each point on the plot represents an individual sample, and the distinct clustering indicates robust metabolic differences associated with the experimental conditions.

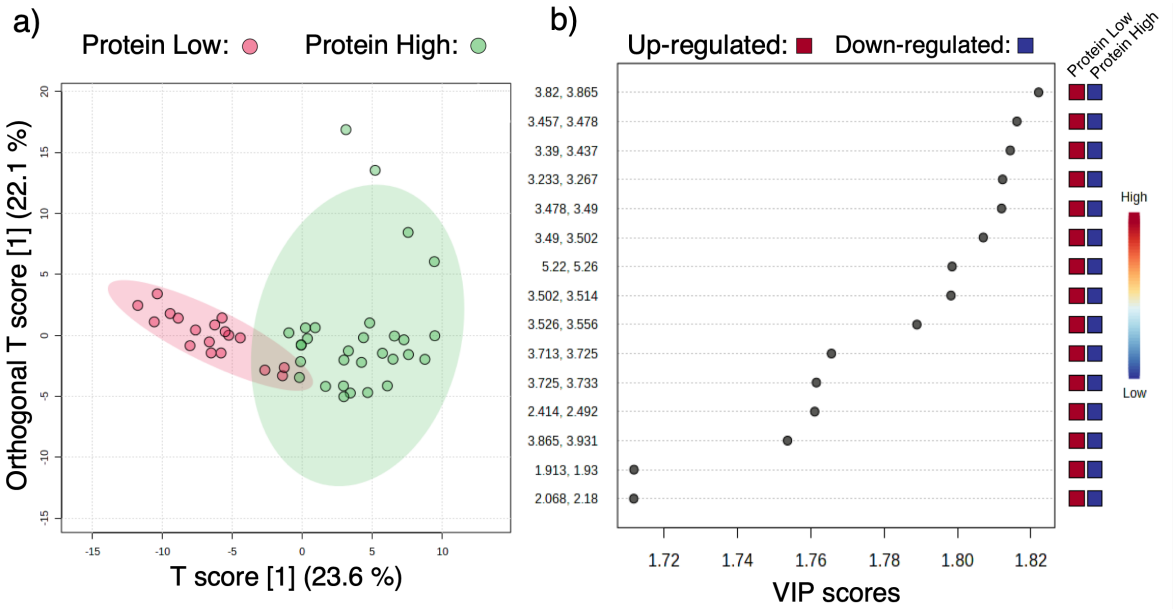

Figure 29 - OPLS-DA Plot with VIP scores showing the effects of protein content on spectra of CSF. a) OPLSA plot of Normal (red) and increased Protein (green) concentrations. High correlation (R^2 = 0.742, $p < 0.001$) and predictive ability (Q^2 = 0.578, $p < 0.001$) is observed. b) VIP scores plot showing the concentrations of smart metabolite bins with their significance. The Variable Importance for Projection (VIP) plot shows the metabolite bins (ppm) on the left, the VIP score on the bottom highlighting the contribution to the separation observed, and the relative increase or decrease of each bin compared to the two sample variables. Blue indicates a lower relative concentration with red indicating a higher relative abundance.

The OPLS-DA analysis revealed a strong correlation ($R^2 > 0.7$) and predictive ($Q^2 > 0.4$) potential between protein content. Two high-protein samples fell outside the 95% confidence region, indicating greater variability in samples rich in protein. High-protein samples showed decreased levels of metabolites across the top 15 VIP (Variable Importance in Projection) contributing bins, suggesting that the proteins acted as relaxation mechanisms, leading to decreased relative metabolite concentrations in spectra with elevated protein levels.

Due to the significant effect of high protein content on the spectra, these samples were excluded from the study cohort. A total of 30 high-protein samples were removed. These high-protein samples also contained elevated levels of cellular content; however, remaining cellular components, such as red blood cells (RBCs) and nucleated cell counts (NCCs), did not appear to affect the spectral data *via* OPLS-DA analysis after their exclusion. After the removal of high-protein and low-volume (< 200 μL) samples, 39 samples (with clinical category confirmation) remained that met the study criteria, as summarised in Table 3. Age did have an effect on the metabolome of the CSF samples (Appendix Figure 9.10), with differences observed between a puppy and a senior dog, however, none of the remaining samples were in these categories.

Since sample preparation was complete, alternative pulse sequences incorporating T_2 filters were explored to minimise protein influence on the spectra.

5.3.4. T2 filtered pulse sequences for CSF Analysis

A simple approach was adopted, similar to that used by Albrecht *et al.* (2020), which did not involve removing proteins or other macromolecules from the samples physically. However, as indicated by the data in Figure 29, the relaxation effects of these macromolecules on the spectra needed to be minimised. Although Ruiz-Cabello *et al.* (2022) demonstrated a sample processing technique where proteins in blood samples were filtered out, this would have increased analysis costs and added additional steps and time; complicating the initially intended straightforward approach.

One approach that would mitigate the need for extra sample preparation is manipulating the nuclei *via* different pulse sequences to reduce the impact of macromolecules on the sample. By incorporating delay periods between the excitation and acquisition of a signal, faster-decaying components from larger macromolecules are allowed to decrease by losing phase coherence. This component is named a T_2 filter, where chemical shift and field inhomogeneities can be refocused during a spin echo. More information on this topic can be found in Chapter 3.6. The CPMG pulse sequence, which uses a looped spin echo, was first applied to these samples to see if this pulse sequence was suitable. J modulation, highlighted in Figure 30, was observed with significant modulations between 4.65 and 3.65 ppm. Although the CPMG pulse sequence has shown a decrease in interfering macromolecule signals, only the chemical shift is refocused during the pulse sequence, with J allowed to evolve.

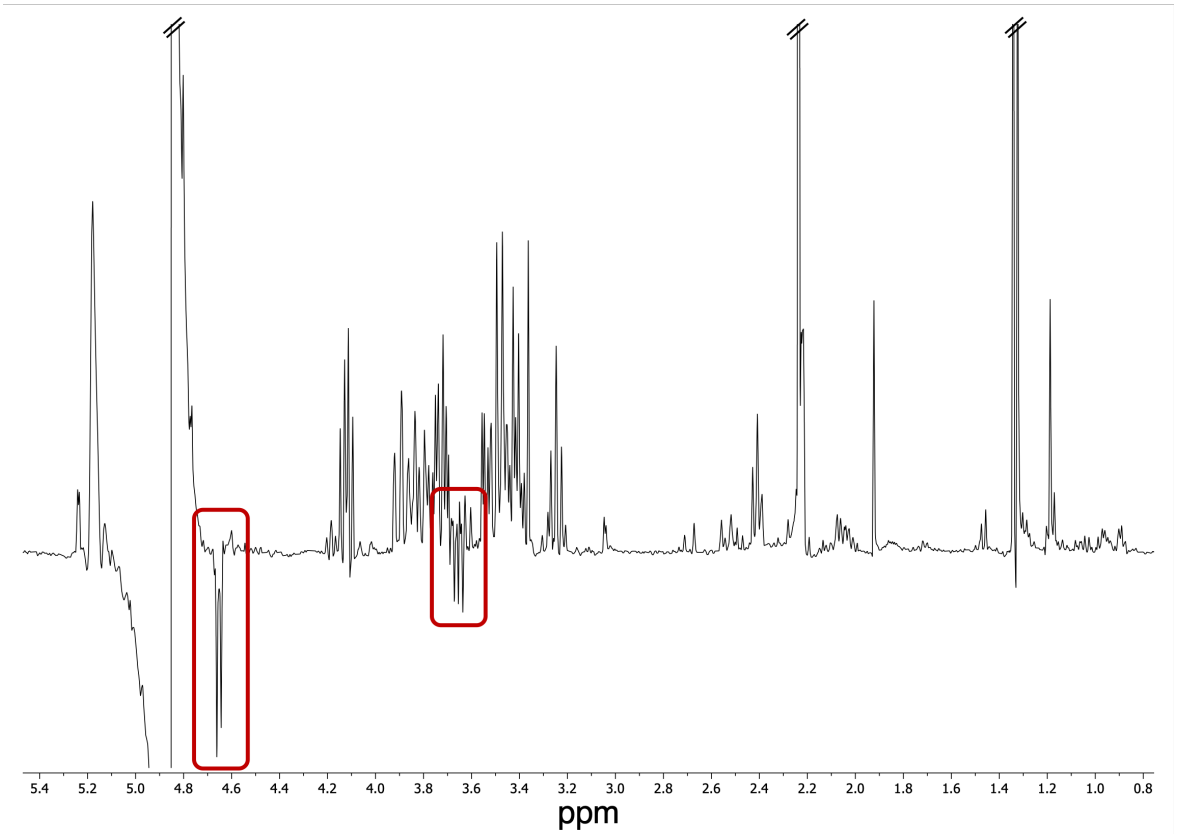

Figure 30 - A HF-NMR ^{1}H NMR 400 MHz spectra of a representative CSF sample acquired using the CPMG experiment. The Red boxes identify where significant J modulation has occurred in glucose. Smaller J modulations around lactate have also arisen. Double slashed lines (//) indicate where the spectra have been cut.

The PROJECT pulse sequence can be used to reduce J modulation while allowing macromolecules to dephase.[160] PROJECT is also averse to sample heating issues due to the longer τ delays compared to CPMG.[160] However, macromolecules were

not the only feature which needed to be supressed. Given the high-water content in CSF, an efficient solvent suppression method was required.

For solvent suppression, presaturation was applied on the HF-NMR spectrometer, while the WET (Water suppression enhanced through T_1 effects) pulse sequence with a PROJECT block was initially tested on the bNMR spectrometer. However, insufficient water suppression was observed on bNMR *via* this pulse sequence, potentially due to lock stability issues. As a result, the WAter Suppression with a Transverse relaxation filter that Eliminates Distortions (WASTED-II) pulse sequence was then used for bNMR analysis.[165,166]

WASTED-II, as shown in Figure 31, incorporates the PROJECT pulse sequence with Robust-5 for water suppression. The addition of a lock pre-focusing gradient and spin locks help to reduce inhomogeneities, radiation dampening and pulse miscalibrations.[165,166]

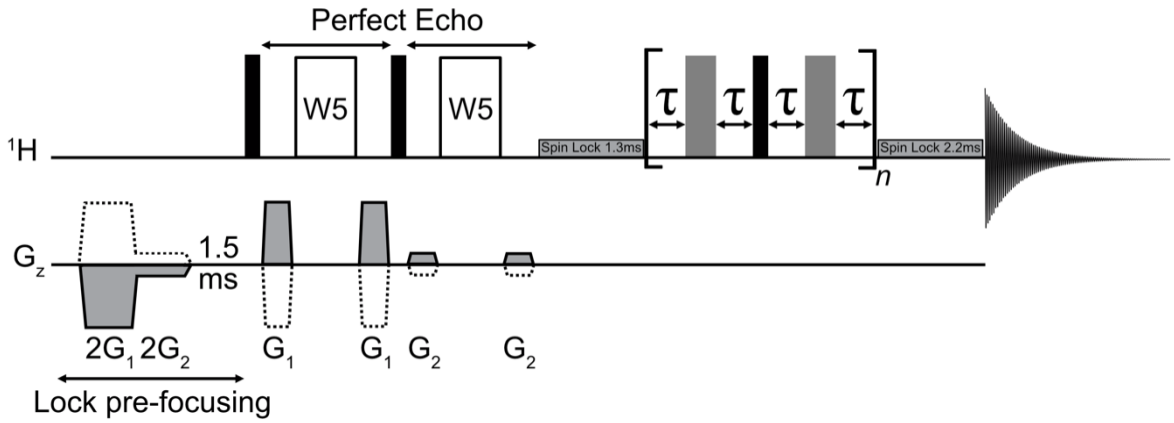

Figure 31 - WASTED-II pulse sequence schematic.

Robust-5 is shown in the left half of the diagram with the PROJECT pulse sequence in the right half. G_z is the gradient applied to the z axis. The dotted lines are to signify the reverse is used for every other pulse. W5 refers to the WATERGATE 5 hard pulses. τ is the delay length with n being the number of repeats PROJECT will complete. [165,166]

Using the WASTED-II pulse sequence on the bNMR spectrometer at 60 MHz, 16 metabolites were identified in a control CSF sample (Figure 32). For comparison, 20 metabolites were identified using the Presaturation PROJECT pulse sequence on the 400 MHz HF-NMR spectrometer (Figure 33). The additional metabolites observed on the HF-NMR (marked in the red box in Figure 33) included those in the aromatic region: histidine, phenylalanine, histamine, 1-methylhistidine, and formate.

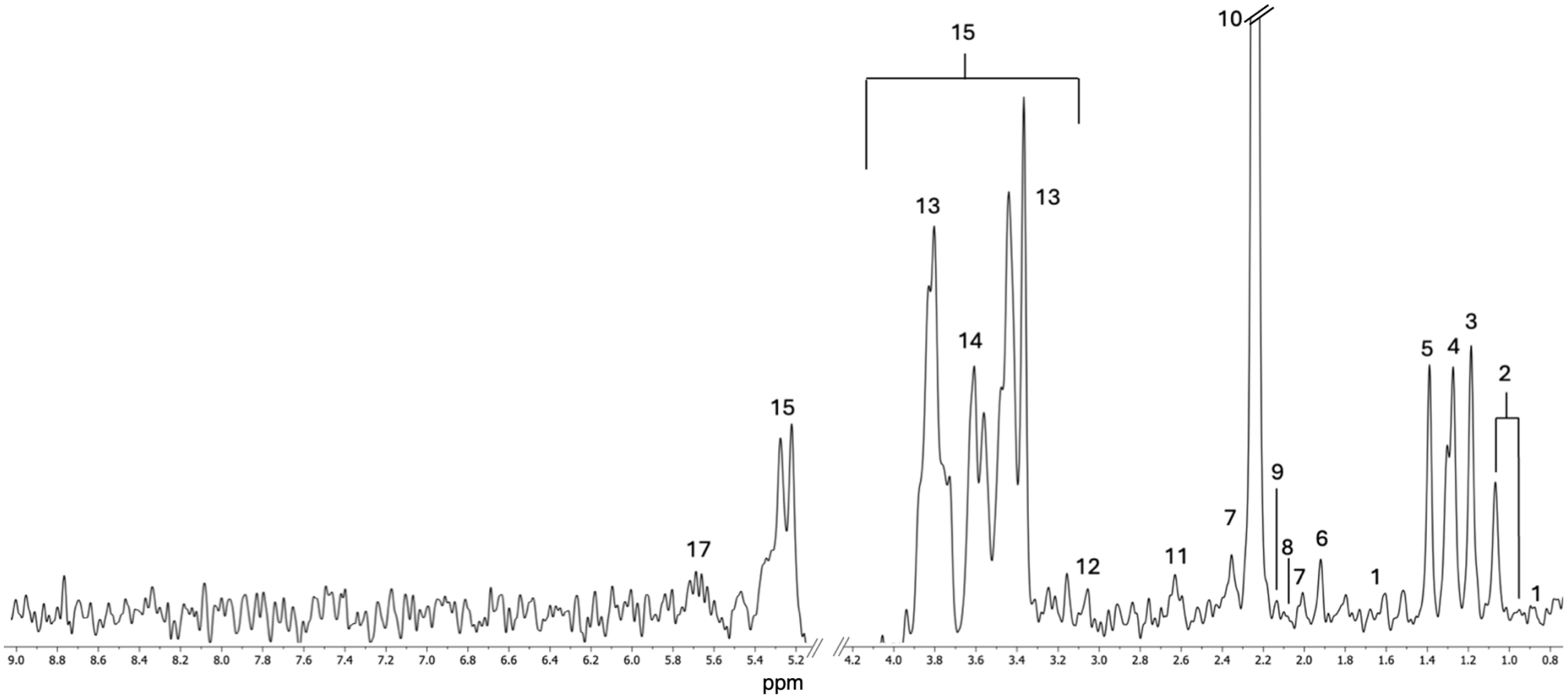

Figure 32 - bNMR spectrum between 0.8 – 4.2 ppm and 5.2 - 9.0 ppm of CSF, recorded using the WASTED-II pulse sequence.

The numbers correspond to metabolites, these metabolites were: 1) Leucine, 2) Isoleucine, 3) Ethanol, 4) Lactate, 5) Alanine, 6) Acetic Acid, 7) Glutamic Acid, 8) Butyric Acid, 9) Glutamine, 10) Acetoacetic Acid, 11) Citrate, 12) Creatine / Creatinine, 13) 1,5-Anhydrosorbitol, 14) Glycerol, 15) Glucose and 17) Urea.

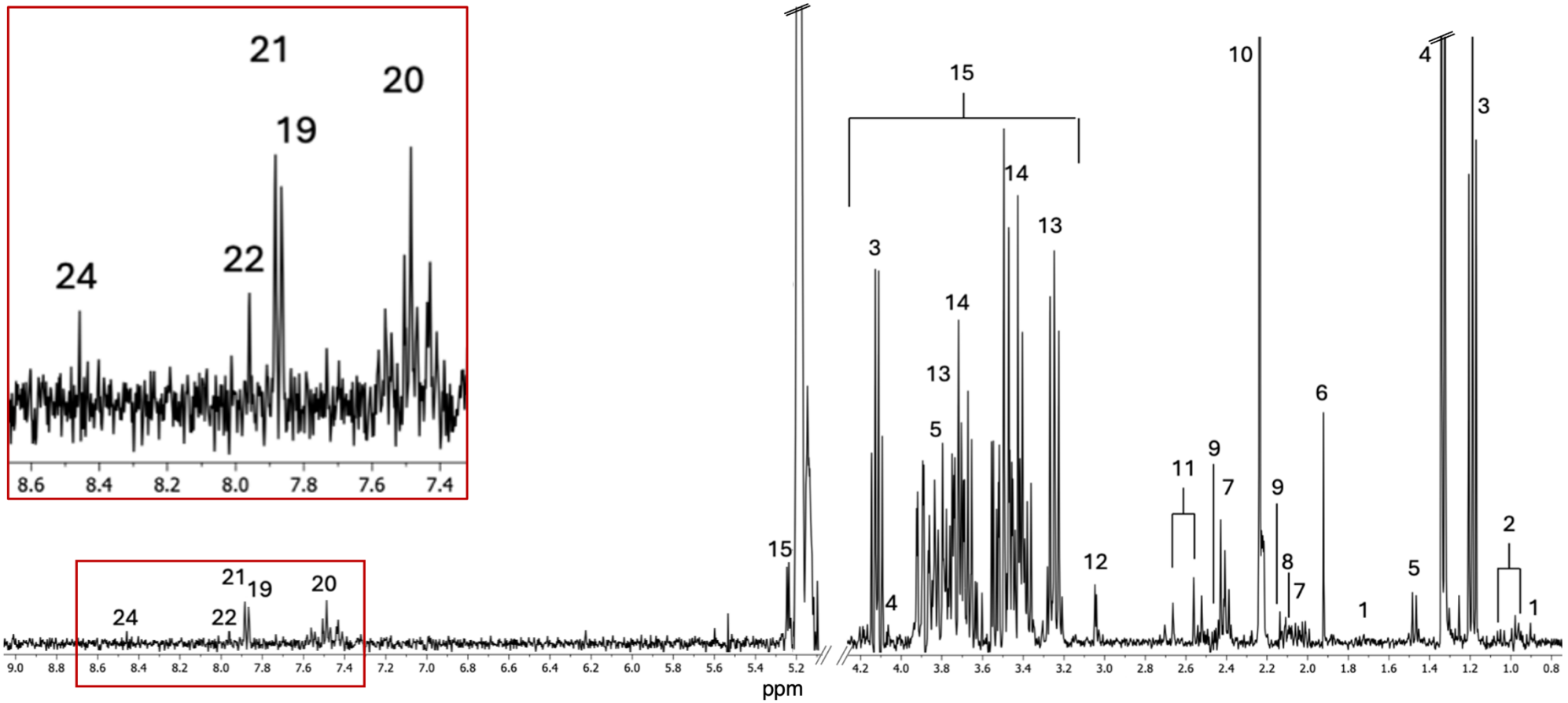

Figure 33 - 400MHz ^{1}H HF-NMR spectrum between 0.8 - 4.2 ppm and 5.2 – 9.0 ppm of CSF, recorded using the presaturation project pulse sequence. The numbers on the spectra correspond to metabolites, these metabolites are: 1) Leucine, 2) Isoleucine, 3) Ethanol, 4) Lactate, 5) Alanine, 6) Acetic Acid, 7) Glutamic Acid, 8) Butyric Acid, 9) Glutamine, 10) Acetoacetic Acid, 11) Citrate, 12) Creatine / Creatinine, 13) 1,5-Anhydrosorbitol, 14) Glycerol, 15) Glucose, 19) Histidine, 20) Phenylalanine, 21) Histamine, 22)1-Methylhistidine, and 24) Formate.

5.3.5. Univariate Analysis

Box plots and area under the curve (AUC) plots were generated to evaluate potential biomarkers in the metabolomic dataset. Following normalisation by sum and Pareto scaling (Figure *34*), distinct group separations were revealed, highlighting specific metabolites with potential biomarker relevance in the 400MHz HF-NMR dataset. The normalisation and scaling approaches helped to minimise inter-sample variability, enhancing the visibility of key metabolites contributing to group differentiation. Statistical significance is supported *via* a p-value below 0.05 and an AUC above 0.7.

5.3.5.1 Lactic Acid (1.32 ppm)

Lactic acid levels were significantly lower in abundance in CSF samples from dogs diagnosed with IE compared to controls (Figure *34*A and Figure *34*B), with statistical analysis confirming significant differences ($p < 0.001$). The AUC analysis indicated good discrimination (AUC = 0.758), and the interquartile range (IQR) between groups showed clear separation with no outliers outside the whiskers, supporting its potential as a biomarker. A high false discovery rate (FDR) was also observed.

5.3.5.2 Citric Acid (2.59 ppm)

Similarly, citric acid showed a decrease in CSF samples from IE dogs (Figure *34*C and Figure *34*D). The AUC analysis indicated strong group discrimination (AUC = 0.753) with significant differences ($p < 0.01$), high sensitivity (0.7), and specificity (0.9). However, the FDR was high at 0.344. Some overlap in the IQRs between groups was noted, with a few outliers (shown in the box plots) in both control and IE groups.

5.3.5.3 Urea (5.65 ppm)

Urea at 5.65 ppm was increased in IE samples, showing significant group differences ($p < 0.05$) (Figure *34*E and Figure *34*F). The AUC indicated good discrimination (AUC = 0.73) with a sensitivity of 0.8, specificity of 0.7, and a lower FDR (0.09) than the other metabolites analysed. The IE group displayed a smaller IQR, with some outliers in both groups.

5.3.5.4 Urea (5.86 ppm)

Unlike the previous urea signal, an alternative urea peak showed a lower abundance in IE samples compared to controls (Figure *34*G and Figure *34*H). Univariate analysis confirmed the significance ($p < 0.01$) of this difference, suggesting altered urea metabolism in IE. The AUC showed good discrimination (AUC = 0.743) despite a high FDR (0.641), with high sensitivity (0.9) and good selectivity (0.6). Extreme outliers were present in both groups, and both groups displayed a narrow IQR. The differences from the urea bins could be due to the sharper peak widths from a Lack of interfering macromolecules.

5.3.5.5 Tyrosine (6.52 ppm)

A tyrosine peak was increased in IE samples relative to controls (Figure *34*I and Figure *34*J). Although univariate analysis showed differences between groups, they did not reach statistical significance ($p > 0.05$). Outliers in this metabolite region caused narrow box plots. The FDR was moderate (-0.307), and both sensitivity and selectivity were at 0.7, with an AUC indicating modest discrimination (AUC = 0.685).

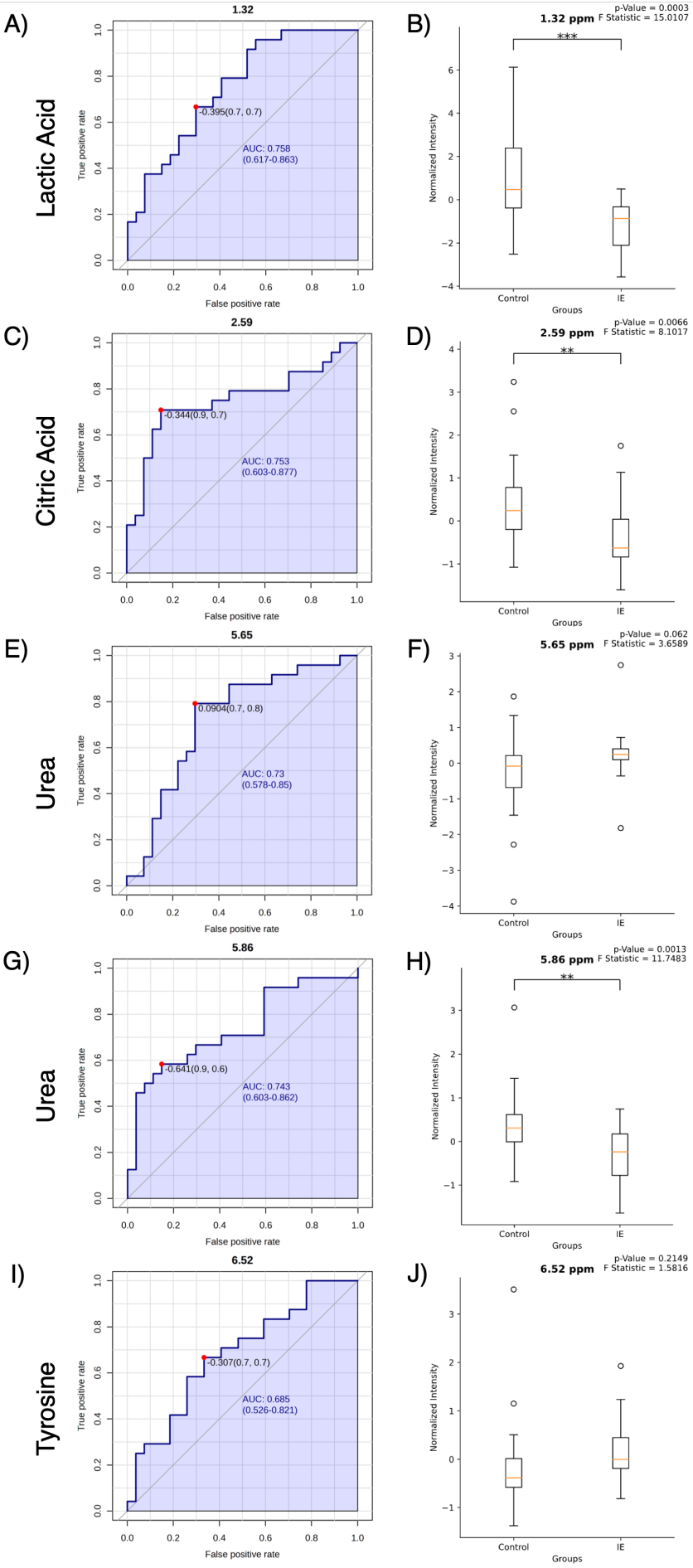
A)
Lactic Acid
1.32
-0.395(0.7, 0.7)
AUC: 0.758
(0.617-0.863)
True positive rate
False positive rate
B)
p-Value = 0.0003
1.32 ppm F Statistic = 15.0107
***
Normalized Intensity
Control
IE
Groups
C)
Citric Acid
2.59
-0.344(0.9, 0.7)
AUC: 0.753
(0.603-0.877)
True positive rate
False positive rate
D)
p-Value = 0.0066
2.59 ppm F Statistic = 8.1017
**
Normalized Intensity
Control
IE
Groups
E)
Urea
5.65
0.0904(0.7, 0.8)
AUC: 0.73
(0.578-0.85)
True positive rate
False positive rate
F)
p-Value = 0.062
5.65 ppm F Statistic = 3.6589
Normalized Intensity
Control
IE
Groups
G)
Urea
5.86
-0.641(0.9, 0.6)
AUC: 0.743
(0.603-0.862)
True positive rate
False positive rate
H)
p-Value = 0.0013
5.86 ppm F Statistic = 11.7483
**
Normalized Intensity
Control
IE
Groups
I)
Tyrosine
6.52
-0.307(0.7, 0.7)
AUC: 0.685
(0.526-0.821)
True positive rate
False positive rate
J)
p-Value = 0.2149
6.52 ppm F Statistic = 1.5816
Normalized Intensity
Control
IE
Groups

Figure 34 - AUC and box plots of lactic acid, citric acid, urea, and tyrosine. A) ROC curve for lactic acid (1.32 ppm) with a false discovery rate (FDR) threshold of 0.395, showing sensitivity and specificity at 70%. B) Box plot for lactic acid with strong significance ($p < 0.001$). C-D) AUC (0.753) and box plot for citric acid (2.59 ppm) with FDR of 0.344, sensitivity of 70%, and specificity of 90% ($p < 0.01$). E-F) AUC and box plot for urea (5.65 ppm) showing sensitivity of 80%, specificity of 70%, and non-significant p-value ($p > 0.05$). G-H) AUC (0.743) and box plot for urea at 5.86 ppm with sensitivity of 90%, specificity of 60%, and significant p-value ($p < 0.01$). I-J) AUC (0.685) and box plot for tyrosine (6.52 ppm), showing sensitivity and specificity of 70%, and non-significant p-value ($p > 0.05$). Outliers in the box plots are indicated by circles.

5.3.6. Cumulative ROC

To assess the collective discriminatory power of lactic acid, citric acid, urea, and tyrosine for distinguishing IE from control samples in CSF using HF-NMR, a cumulative receiver operating characteristic (ROC) test was performed. This test combines the metabolite signals into a single model, allowing the evaluation of the metabolite's combined performance (sensitivity, specificity, and AUC) and assessing their clinical utility as a multi-metabolite (bin) panel.

The cumulative AUC (Figure 35b) was determined to be 0.847 (95% CI: 0.684 - 0.986, $p = 0.008$), demonstrating a strong predictive performance of the combined metabolite panel. A total of eight samples, four from each category, were excluded from the data set to be used for testing the model (Figure 35a), with the remaining 43 samples used for the training of the model. The separation along the x-axis indicates how well the classifier distinguishes between the two groups. Samples closer to 1.0 on the probability axis are more confidently classified as IE, while those closer to 0.0 lean toward being classified as controls. A total of 13 samples were wrongly classified, however, given the confidence interval (0.684 - 0.986) and AUC value (0.847), this model suggests its potential for clinical utility.

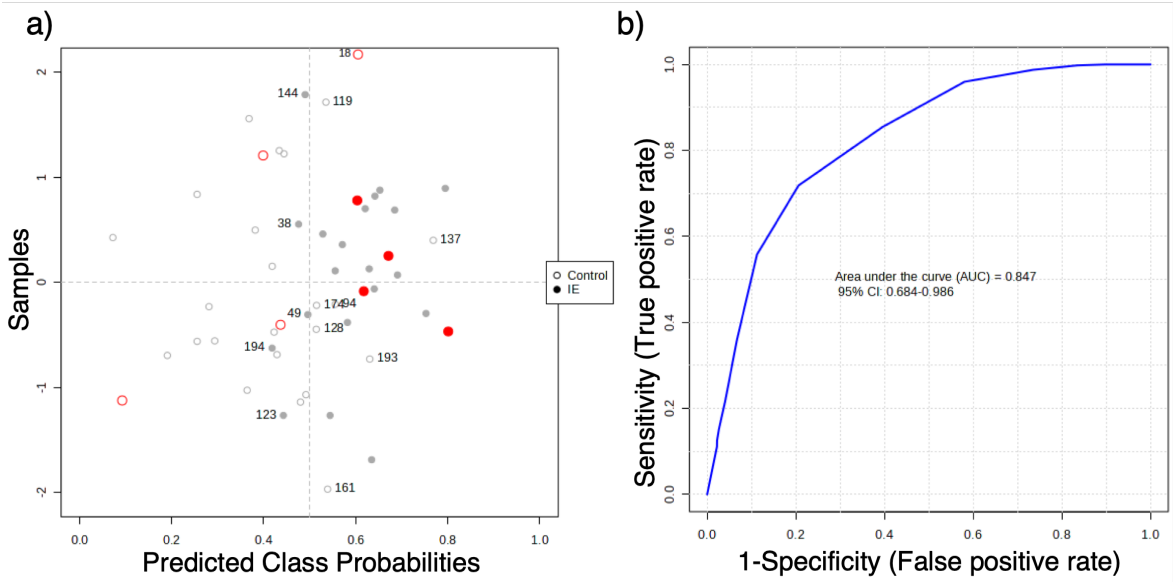

Figure 35 - Cumulative ROC Test and AUC Plot for Classifier Performance. a) shows predicted class probabilities for distinguishing IE samples from controls using a classifier based on selected metabolites: lactic acid, citric acid, urea, and tyrosine. Testing data are displayed in red, while training data are shown in grey, allowing visual assessment of model performance across both sets. Samples closer to the probability of 1.0 indicate a stronger classification as IE, while those near 0.0 suggest a control classification. b) displays the cumulative ROC curve for the classifier, with an AUC of 0.847 (95% CI: 0.684–0.986), indicating good discriminatory power.

5.3.7. Multivariate Analysis of Idiopathic Epilepsy and Healthy Controls

Multivariate analysis (MVA) for metabolomic data can help the complexity of high-dimensional datasets by considering multiple variables simultaneously to uncover intricate patterns among metabolites and groups. MVA can allow for dimension reduction, using techniques such as PCA.

5.3.7.1 Statistically Significant Bins Distinguishing Between IE and Control Samples

A Venn diagram (Figure 36) displays the overlap between statistically significant ($p < 0.05$) bins identified in bNMR and HF-NMR data. In total, 12 bins were found to be significant in both methods, while 54 bins were unique to the bNMR data and 36 were unique to the HF-NMR data.

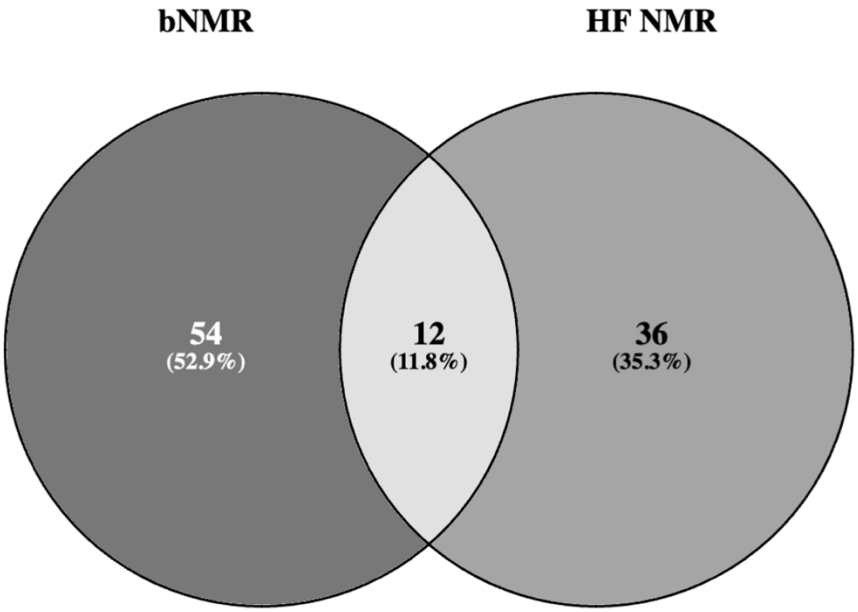

Figure 36 - Venn Diagram of the number of significant bins (non-FDR corrected) between spectrometers distinguishing IE from healthy controls.

Volcano plots were used to explore the significant fold change (FC) bins between IE and control CSF samples. The metabolite bins that are both statistically significant appear in either blue or red, depending on whether tere is a relative increase or decrease between healthy controls and IE samples (Figure 37).

To control for multiple comparisons, a FDR correction was applied to the data, as shown in Figures 33b) and d). Although no bins met the FDR threshold, the bNMR data were closer to this threshold, suggesting a stronger trend toward statistical significance.

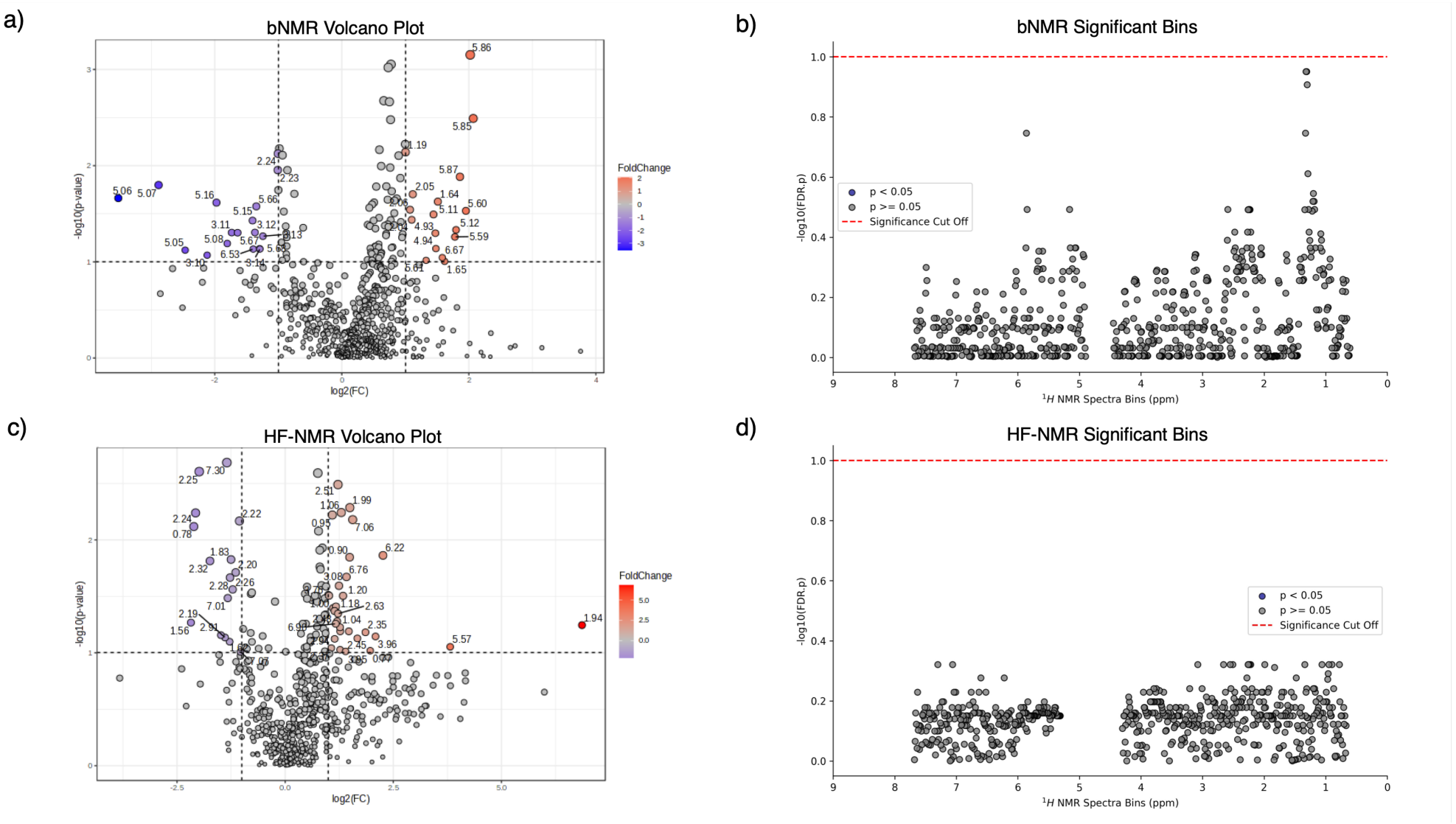

Figure caption on next page.

Figure 37 - Significant bins distinguishing IE from healthy controls across the bNMR and HF-NMR results. a) and b) correspond to bNMR results, with c) and d) corresponding to HF-NMR. Figures a) and c) correspond to volcano plots with those significantly increased and decreased appearing in the top right and left of the figures respectively. b) and d) show FDR-corrected significant bins spread across spectra.

5.3.7.2 Principal Component Analysis of IE and Control Samples

A PCA plot was used to observe any clusters within the samples. PCA reduces dimensionality and variables from a dataset. The IE samples from the bNMR data showed no distinct clusters between the control and IE samples (Figure 38). A total of 41.9% of the variance is explained by the PCA plot (PC1 = 27.3% and PC2 = 14.6%). The 95% confidence regions (the red and green ellipses) show two observable outliers, one control and one IE sample. The control and IE sample outliers had higher levels of lactic acid, which contributed to why they were outside their respective eclipse. Increased lactic acid is most likely caused by anaerobic metabolism, like that seen in infections and seizures.

The PCA plots, Figure 37a) and d) illustrate sample distribution based on metabolomic profiles of the control CSF samples against the IE group. The loadings plots, Figure 37b) ,c) ,e), and f), shows the correlation between metabolites and principal components (PCs). Metabolites with greater variability will appear further away from the baseline at 0.

The bNMR and HF-NMR PCA loadings plot, Figure 38b), c), d) and e), display a similar loading and weighing function, with metabolites between 0 and 5 ppm contributing considerably to the overall distribution across samples. Acetone at 2.22 ppm and lactic acid at 1.32 ppm showed a greater influence of variance across the samples. A lack of variance between the group types was also observed in the HF-NMR PCA plot (Figure 38d). This PCA plot did however have banding into two groups. This was caused by differences in the lactate concentrations, and where the maximum lactate signal was located between two different bins.

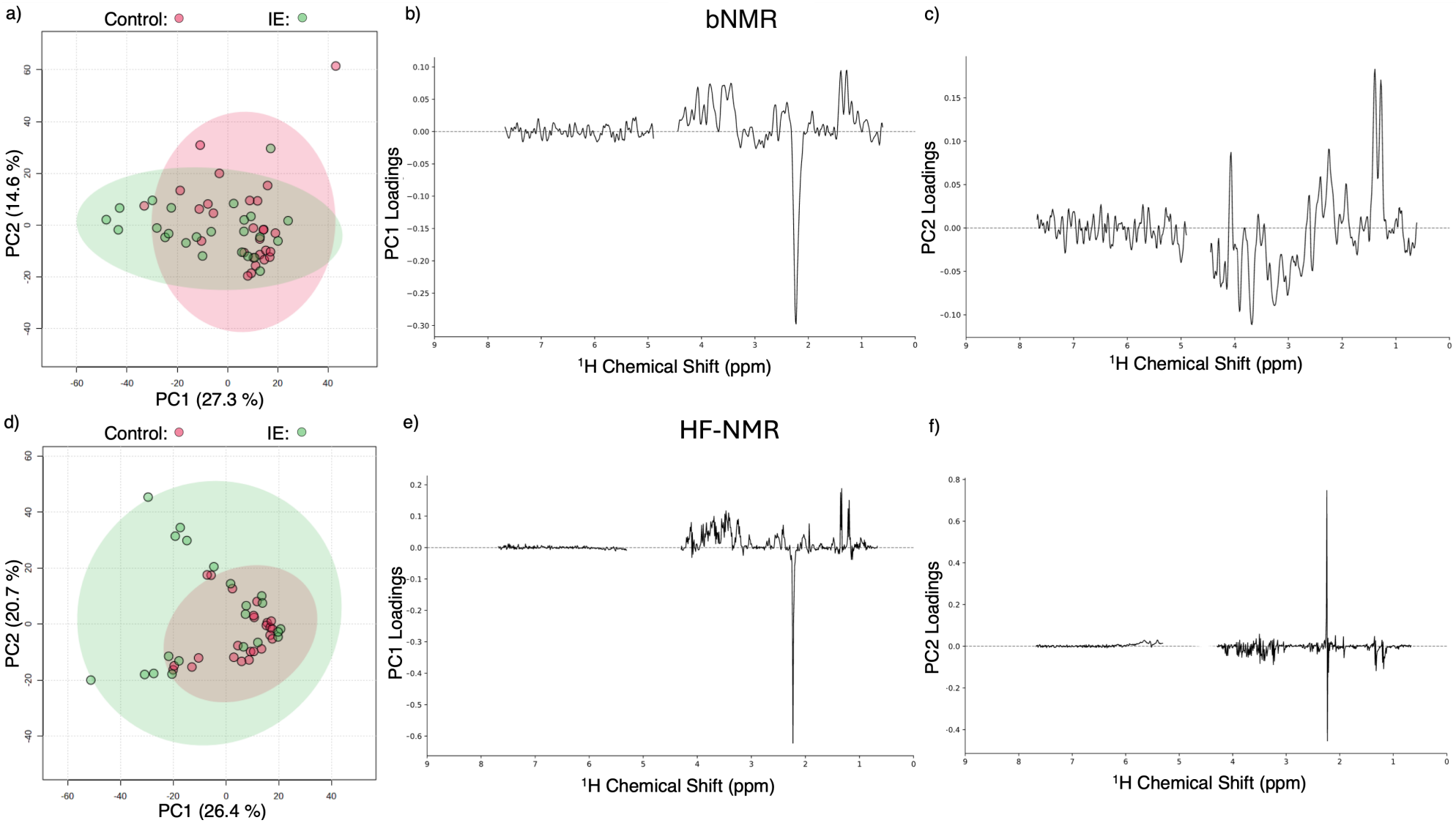

Figure caption on next page.

Figure 38 - PCA and Loading Plots for bNMR and HF-NMR Datasets. PCA plots, a) and d), display the distribution of control samples (red) and IE samples (green). The top row (a, b, c) shows bNMR data, while the bottom row (d, e, f) presents HF-NMR data. In the bNMR dataset, PC1 and PC2 account for 27.3% and 14.6% of the variance, respectively. In the HF-NMR dataset, PC1 and PC2 explain 26.4% and 20.7% of the variance, respectively.

5.3.7.3 OPLS-DA Between IE and Control Groups

OPLS-DA was employed to maximise the separation between CSF samples from dogs with IE and healthy controls. The bNMR OPLS-DA model was assessed using Q2 and R2 values, revealing a Q2 value of -0.128, indicating poor predictive ability, and an R2 value of 0.644, suggesting moderate goodness of fit. However, neither of the p-values associated with these metrics were statistically significant ($p = 0.3695$ for Q2 and $p = 0.1065$ for R2), indicating limited confidence in the model's performance. The OPLS-DA plot (Figure 35) further showed a poor distinction between IE and control samples, with an Orthogonal T score of 12.2% and a T score of 4.7%, underscoring the challenges in discriminating between the two groups using this approach. The outliers from the 95% confident regions were sample 132 (control) and sample 224 (IE). The HF-NMR OPLS-DA plot, Figure 35d, d), a). The model performed well with a great R2 value of 0.82 ($p<0.05$) with some predictive potential ($Q2 = 0.187$, $p< 0.05$).

The colour maps, c) and f), indicate the strength of the association between metabolites and the separation between the two classes. Peaks in the positive direction represent metabolites that are in higher abundance while negative peaks are related to a lower abundance. The plot provides insights into the metabolites contributing most to the discrimination between the two classes, aiding in interpreting biological differences and potential biomarkers. c) and f) show signals around 2.25 and 1.32 ppm having a large effect on the separation between IE and Control samples. This is also displayed by the VIP loading scores plot, with lactate (1.32 ppm) being decreased in IE samples and acetone (2.25 ppm) being increased in IE samples.

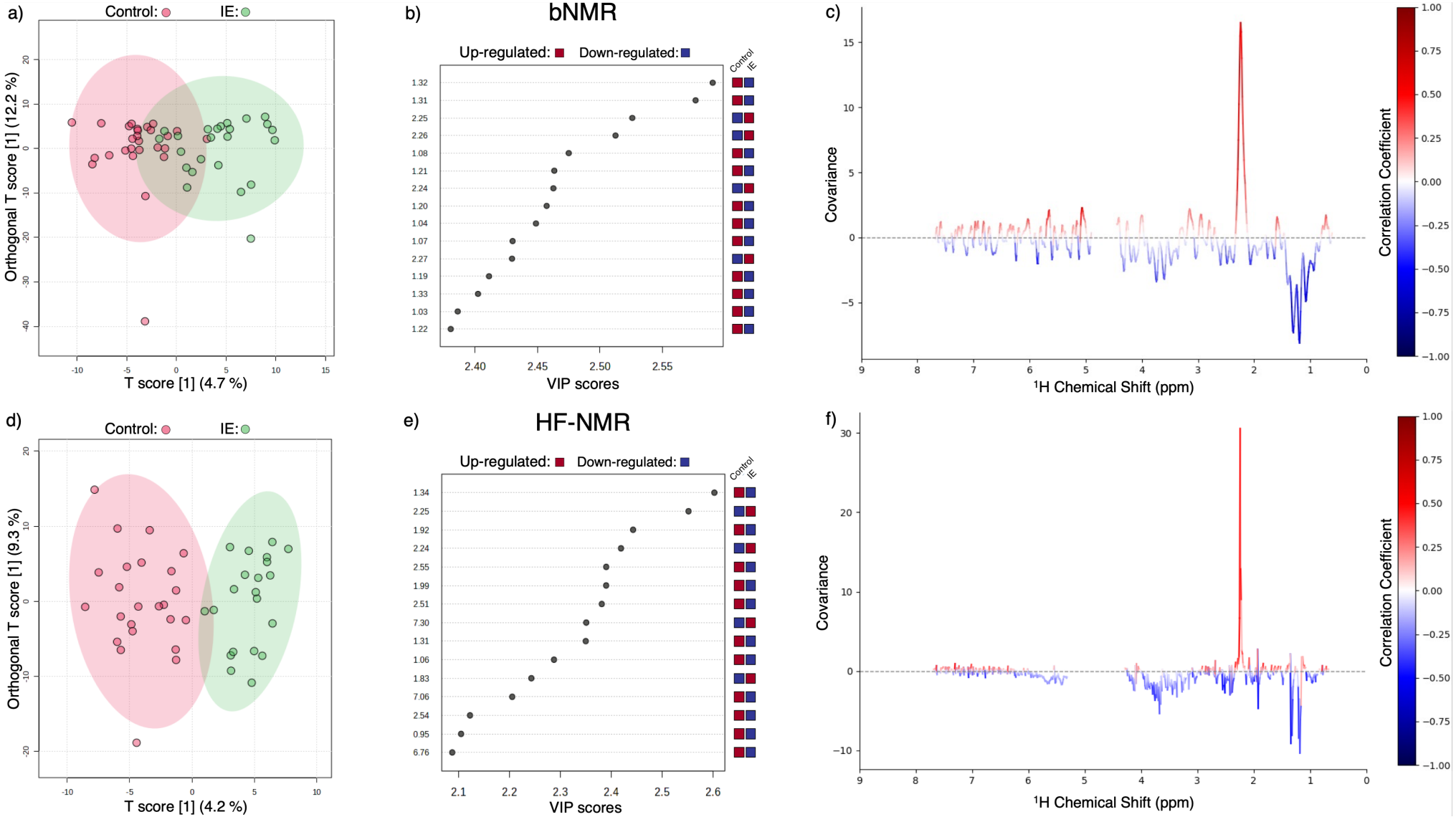

Figure caption on next page

Figure 39 - OPLS-DA Plots for bNMR and HF-NMR Data Comparing Controls and IE Samples in CSF. a) and d) show the OPLS-DA score plots, with control samples in red and IE samples in green. The variables significantly influencing the separation in the OPLS-DA models are highlighted in the corresponding VIP score plots (b for bNMR and e for HF-NMR) and the correlation coefficient/covariance plots across the spectra (c for bNMR and f for HF-NMR). bNMR Q^2 =0.128, p=0.3695, and R^2 = 0.644, p=0.1065. HF-NMR Q^2=0.187, p<0.05 and R^2=0.82, p<0.05.

5.3.8. A Comparison of the Univariate and Multivariate Analysis of Each Metabolite

A total of 20 metabolites were statistically evaluated using both the OPLS-DA algorithm and AUC analysis across the bNMR and HF-NMR data. From the HF-NMR statistical analysis, 18 of the metabolites had a VIP score higher than one, with only urea and D-alanine yielding a score of less than one. These suggest strong significance from these 18 metabolites in contributing to the separation observed in Figure 39 D. The AUC analysis yielded eight significant metabolites in HF-NMR analysis (2-hydroxybutyric acid, 3-hydroxybutyric acid, acetic acid, citric acid, creatinine, D-glucose, isoleucine, and leucine). 16 metabolites were decreased in association with IE and four were in higher abundance.

From the bNMR analysis ten metabolites had a VIP score above 1. The AUC analysis yielded six significant metabolites in bNMR analysis (3-hydroxybutyric acid, acetone, citric acid, lactic acid, pyruvic acid, and urea). 13 metabolites were decreased in association with IE and seven were increased in concentration.

Table 4 - Summary of bNMR CSF Metabolites from statistical analysis for discriminating IE from Healthy Controls.

	bNMR						HF-NMR					
Metabolite	IE trend	VIP	Sensitivity	Specificity	AUC	p -Value	IE trend	VIP	Sensitivity	Specificity	AUC	p - Value
1,5-Anhydrosorbitol	Up	0.381	0.5	0.8	0.580	0.268	Down	1.327	0.7	0.7	0.675	0.168
2-Hydroxybutyric acid	Down	0.707	0.8	0.4	0.529	0.687	Down	2.017	0.8	0.7	0.755	0.014 *
3-Hydroxybutyric acid	Down	2.457	0.6	0.8	0.698	0.006 **	Down	1.923	0.8	0.6	0.673	0.031 *
Acetic acid	Up	0.304	0.7	0.4	0.522	0.975	Down	2.440	0.4	0.9	0.623	0.025 *
Acetone	Up	2.526	0.7	0.6	0.690	0.011 *	Up	2.419	0.5	0.7	0.591	0.145
Citric acid	Down	1.766	0.9	0.7	0.753	0.007 **	Down	1.832	0.7	0.7	0.760	0.003 **
Creatine	Down	1.160	0.7	0.7	0.657	0.406	Down	1.338	0.6	0.7	0.641	0.106
Creatinine	Up	0.693	0.5	0.7	0.503	0.984	Down	1.649	0.7	0.7	0.671	0.026 *
D-Alanine	Up	0.314	0.4	0.8	0.509	0.819	Up	0.338	0.6	0.7	0.526	0.633
D-Fructose	Down	0.264	0.7	0.5	0.543	0.947	Down	1.676	0.5	0.8	0.641	0.111
D-Glucose	Down	1.702	0.7	0.7	0.657	0.069	Down	2.068	0.7	0.7	0.679	0.026 *
Glutamine	Down	0.643	0.8	0.5	0.631	0.086	Down	1.852	0.7	0.7	0.671	0.081
Glycerol	Up	0.130	0.8	0.5	0.511	0.961	Down	1.062	0.8	0.5	0.599	0.264
Histidine	Up	0.477	0.6	0.6	0.508	0.715	Up	1.179	0.6	0.6	0.559	0.209
Isoleucine	Down	1.804	0.5	0.8	0.631	0.142	Down	1.672	0.8	0.6	0.706	0.017 *
Lactic acid	Down	2.590	0.7	0.7	0.752	0.001 ***	Down	2.350	0.7	0.5	0.655	0.059
Leucine	Down	2.108	0.7	0.7	0.644	0.099	Down	2.105	0.6	0.8	0.696	0.006 **

Phenylalanine	Down	0.058	0.6	0.6	0.505	0.671	Up	1.080	0.6	0.6	0.567	0.339
Pyruvic acid	Down	1.539	0.7	0.6	0.665	0.042 *	Down	1.438	0.7	0.7	0.667	0.113

VIP: variable importance in projection, IE: Idiopathic Epilepsy, *: $p < 0.05$, **: $p < 0.01$, ***:$p < 0.001$.

5.3.9. ROC Curve-Based Model Creation on the Top Six bNMR Metabolites

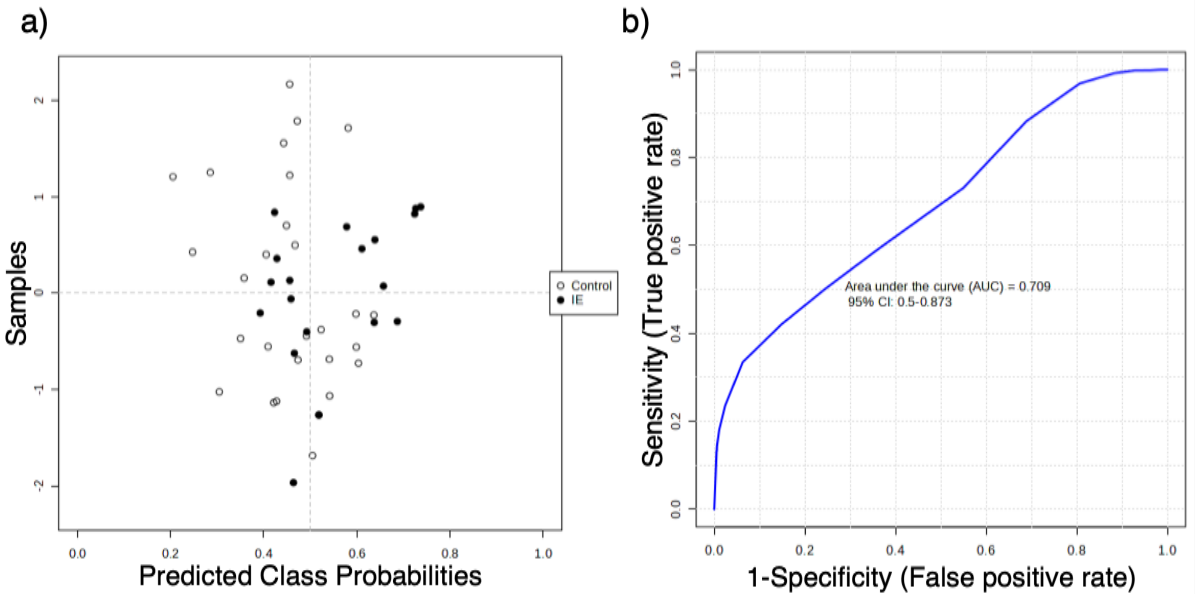

Figure 40 - Plot of ROC cumulative analysis for the biomarker model. b) ROC cumulative analysis AUC of 0.709, 95% CI (0.5-0.873) p = 0.05. Predictive accuracy of 0.622 p = 0.098. The predicted class probabilities for all samples based on the PLS-DA biomarker model are shown in panel a).

From comparing the two datasets, six metabolites (3-Hydroxybutyric acid, acetone, glutamate, lactic acid, isoleucine, and glucose) were chosen to be used in a ROC curve-based- model. This biomarker model used a PLS-DA algorithm. Eight samples were withheld from the model to be used for validation. These metabolites were chosen based on their AUC, VIP and p-value scores between both datasets. The model showed a good AUC value of 0.709, however, a low predictive potential with both stats showing it to not be statistically significant.

5.4. Discussion

The clinical diagnostic approach used for detecting and diagnosing IE has been a process of elimination by exhausting other causes of seizure activity, making it challenging to identify the disease.[67] The second tier of IVETFs IE diagnosis criteria currently includes routine CSF analysis but does not have a biomarker detection tool to diagnose the disease. However, using bNMR for detecting IE in dogs through CSF analysis could provide a low-cost detection method (< £2 consumable costs). This study aimed to identify detectable metabolites using bNMR, find an optimal pulse sequences for CSF analysis, and investigate significant metabolite differences between dogs with IE and healthy controls.

There is currently no published research on CSF analysis using bNMR. As such, it is important to identify which metabolites are detectable by bNMR. Despite facing challenges posed by the broad signals in bNMR CSF spectra, this study has identified 16 metabolites that could be used in future metabolomic studies. Although bNMR has a lower operating frequency than HF-NMR and the presence of proteins in the sample contributes to broad signals, this study has made progress in identifying metabolites at 60MHz for a CSF sample with minimal sample preparation.

Using different spectrometer fields (800MHz, 400MHz, and 60MHz), this study has exposed the limitations of the lower field spectrometers. The bNMR spectrometer was unable to identify five metabolites that the 400MHz spectrometer could, these were histidine, phenylalanine, histamine, 1-methylhistidine, and formate. However, the bNMR could identify urea, which was unidentifiable using the 400MHz; most likely due to the use of the presaturation pulse sequence that was used on the 400MHz spectrometer suppressing nearby signals to the water. The 400MHz and 60MHz spectrometers were also unable to detect mannose, tyrosine, and adenine. This is most likely due to the lower sensitivity of the spectrometers, the relatively low abundance of some metabolites, and the larger peak widths observed in the lower field spectrometers. Future work on sample preparation may help to improve the signal-to-noise ratio. However, these issues could also stem from suboptimal spectrometer setup or variations in the concentrations of CSF samples used for analysis. In future studies, increasing the amount of CSF used for NMR analysis could help detect/identify further metabolites at these lower magnetic field frequencies. However, it should be noted that in veterinarian diagnostics, especially where smaller animals are being tested, lower volume samples for diagnostic testing may be preferred.

After comparing the metabolite signals and their respective statistical values from the OPLS-DA and AUC analysis, Table 4, it was found that there were discrepancies in metabolite regulation between the spectrometers. For instance, 1,5 anhydrosorbitol and glycerol were increased in bNMR but decreased in the HF-NMR. However, the statistical significance of these results did not meet the minimum threshold ($p > 0.05$), which indicates that there is little or no evidence to

support the findings of significant differences between IE and controls of these metabolites. This helps to explain the deviation in the regulation of relative metabolite concentrations.

The regulation of acetic acid presented a discrepancy between the bNMR and HF-NMR data. While the bNMR data indicated an increase, the HF-NMR data showed a decrease. Interestingly, acetic acid met the evidence criteria for association in the HF-NMR data but not in the bNMR data. This disparity could be attributed to the difference in sensitivity between the two spectrometers, where the bNMR data was close to its limit of detection, hence the inability to accurately distinguish differences in this metabolite. The significance of acetic acid in IE detection, as observed in the HF-NMR data, was corroborated by a metabolomics study using gas chromatography-mass spectrometry (GC-MS).[213] Hasegawa *et al.* (2014) employed GC-MS to compare IE and control samples, identifying 16 metabolites that were statistically different between the two groups.[213] Notably, four of these metabolites were also identified in our study using HF-NMR and bNMR.[213] Hasegawa *et al.* (2014) reported an increase of isoleucine, acetic acid, and glutamine and a decrease of pyruvic acid in IE compared to the control group.[213] In contrast, the HF-NMR analysis suggested that all four of these metabolites were decreased, aligning with the literature only for pyruvic acid.[213] This discrepancy could be due to the overlap of nearby metabolites interfering with concentrations, which might also explain why bNMR could not distinguish this metabolite for IE detection. Glutamine is further reported to be disrupted in perturbed neurotransmitter cycling, astrocyte metabolism, or blood brain barrier function. Nevertheless, studies in canine IE and human epilepsy have found changes, though direction varies.

Several factors could contribute to the differences observed between our study and the GC-MS study: sample preparation, centrifugation, and analytical techniques.[213] The GC-MS study used a paper-based extraction method, which could alter the concentrations of metabolites present in their samples.[213] The GC-MS sample preparation involved centrifuging samples at forces up to 15,000g. Recent research has raised concerns about the impact of high-force centrifugation on CSF samples.[212] Albrecht *et al.* (2020) suggest that high forces can negatively affect the

presence of metabolites and cause cells to break, introducing new metabolites to the sample.[214,215]

In this study, centrifugation was avoided after the initial sample collection to mitigate these potential effects. The inherent differences between NMR and GC-MS techniques could contribute to variations in metabolite detection and quantification. These methodological differences highlight the importance of standardised protocols in metabolomics studies and the need for careful interpretation when comparing results across different analytical platforms. Future studies should aim to address these discrepancies and establish robust, reproducible methods for CSF metabolomics in IE detection.

The analysis of both HF and bNMR data revealed 3-hydroxybutyric acid as the most promising biomarker for IE. This metabolite showed a consistent decrease in both datasets, demonstrating statistical significance and high VIP scores. This is metabolite is biologically plausible as a biomarker for IE. Ketone bodies, which include 3-hydroxybutyric acid, have documented anticonvulsant effects and are central to the mechanism of ketogenic therapies.[216] The brain's main fuel is glucose. However, during periods of high energy demand or low glucose availability, such as that during a seizure, ketone bodies can instead be used as an alternative energy source. The ketogenic diet (high-fat and low-carbohydrate) is a well-established and effective treatment for epilepsy. This is due to the diet forcing the body to produce ketone bodies to shift the metabolism away from typically energy production. This shift is known to have powerful anti-convulsant effects, this further supports 3-hydroxybutyric acid as a key biomarker for IE diagnosis.[216] Reduced 3-hydroxybutyric acid may therefore reflect altered brain energy metabolism or a lack of protective ketosis, supporting its potential as a diagnostic or monitoring biomarker.[216] This finding underscores its potential as a robust indicator for IE diagnosis.

Examining the overall trends, the HF-NMR data predominantly indicated the decrease of metabolites in cases of IE, with the notable exceptions of acetone and alanine, which were increased. The bNMR data supported the increase of acetone, which was statistically significant ($p < 0.05$). Additionally, the bNMR analysis identified lactic acid, pyruvic acid, and urea as decreased metabolites with VIP

scores exceeding 1, indicating their high significance in distinguishing IE from controls. The increase of acetone, another ketone body, further supports a general shift in ketone metabolism. This finding provides a direct link between your metabolomic data and a known anti-epileptic therapeutic mechanism. Pyruvic acid and lactic acid further support a disruption to energy metabolism. Pyruvic acid is the end product of glycolysis and the gateway to the Krebs cycle, the main contributor to aerobic metabolism. Lactic acid is a biproduct produced from pyruvate during periods of high energy demand. Previously lactic acid has been identified as significant but traditionally this has been noted to be significantly increased.[217] In tonic-clonic seizures lactic acid is found with elevations found with in ~90% of cases within 30 minutes after seizure termination.[217]

However, the extraction of CSF of this cohort included in this study was taken much longer than 30 minutes after seizure activity. This could therefore be a return to normal energy production with a reduction in altering metabolism in an effort to regulate normal energy metabolism or a different pathway in which IE present over other seizure activity. The unknown nature of IE continues to make mechanistic understanding of the disease hard to understand, therefore more studies with larger cohort could further improve this study.

Discrepancies were observed between HF and bNMR data for five metabolites: 1,5-anhydrosorbitol, acetic acid, creatinine, phenylalanine, and glycerol. These metabolites exhibited opposite regulation patterns in the two datasets. Several factors could explain these discrepancies, including low metabolite abundance, differences in baseline correction techniques, or varying sensitivities between the two analytical instruments. It should be noted that these metabolites had low VIP scores, suggestive of little weighting significance in distinguishing between IE and healthy controls for the bNMR OPLS-DA model. In the bNMR data, lactic acid and urea emerged as strong discriminators between IE and control groups, demonstrated by high AUC values. However, it's worth noting that the observed differences in urea concentration might be influenced by the WATERGATE solvent suppression technique or baseline correction adjustments, warranting careful interpretation.

A further limitation of this study was the relatively low sample (n = 39) cohort. If a similar study is replicated in the future, the sample size should aim for more than 100 samples, including larger groups of breed types and diseases, to ensure proper identification of significance. This low sample number could have also skewed biased models like OPLS-DA to overcompensate and create an unwarranted correlation, though this was avoided as much as possible in this study *via* the use of permutation tests. Increasing the number of samples would also enhance the cumulative ROC tests, as only four samples (about 10%) from the healthy and IE groups were available for validation of the model. Despite the small size of the validation group, the combined ROC test was able to distinguish between IE and control samples with a relatively high degree of confidence, achieving an AUC of 0.847, which was statistically significant ($p < 0.01$).

From a methodological perspective, several considerations emerged. The peak widths in the CSF spectra remained broad, particularly in bNMR, due to its lower operating frequency and the presence of residual proteins. This suggests that further optimisation of sample preparation could potentially improve metabolite detection, especially for the targeted analysis of specific metabolites of interest. The application of baseline correction, while similar for both HF- and bNMR datasets, was performed in separate groups, potentially defining different baselines and affecting the results. It is also important to note that this study was qualitative rather than quantitative. Further analysis should be conducted on qualitative studies to ensure that the results can be reliably quantified with minimal sample preparation and using the WASTED-II pulse sequence.

The identified metabolites offer valuable markers for IE diagnosis. Moreover, these metabolite profiles could be instrumental in monitoring disease progression and treatment response, paving the way for more personalised veterinary care. However, to fully realise their diagnostic potential, it is essential to standardise protocols for CSF metabolomics studies, ensuring reproducibility and comparability across analytical platforms. Furthermore, conducting larger-scale validation studies will be essential to confirm the diagnostic accuracy of the identified biomarkers in diverse canine populations.

5.5. Future Work

From the identifiable metabolites present in this study, the tracking of other diseases may also be viable. CSF is a relatively rare biofluid in the field of metabolomic research. As such, there is a reduced number of studies on the biofluid completed using NMR compared to urinary analysis and blood analysis. The results obtained in Figure 29, inferred very strong evidence for being able to distinguish between high and normal protein content samples, with predictive capacity. Although outside the realm of this preliminary research into IE CSF analysis using bNMR, and were hence excluded from the sample cohort, protein content may be able to be ascertained using lower operating frequencies and even using bNMR. This could provide further use to bNMR, making it more viable for routine analysis if other diseases are found to be able to be distinguishable on the spectrometer as well.

Although CSF analysis is routine for IVETF tier 2 diagnosis of IE, it does add avoidable risk if a blood- or urine-based analysis could yield similar results. Therefore, further efforts could be made to identify biomarkers in biofluids which carry less risk to the patient. The IVETF identify that the “identification of causative genetic mutation of breed-specific movement disorders will significantly improve our ability to diagnose these conditions”. A wide genomic study into IE could greatly help to understand the cause of IE as well as guide metabolomic research. Further attention is also needed to fill the research gap of seizure severity and frequency on the metabolome. This not only could help with monitoring but also with diagnoses as well.

Though this study incorporated many breeds with a range of different ages, making the study more generic to a general population of dogs, breed-specific variables affecting a dog’s metabolome may have unknowingly skewed the data. A future study which could extend the sample cohort to enable breed-specific investigations could eliminate risks of breed-specific metabolome changes to IE.

Further limitations of this research, from the lack of sample volume from some samples, could have impacted the weighting of some results during normalisation. A future study where the sample cohort was more uniform with a higher concentration of CSF could help improve future studies.

5.6. Conclusion

The gap this study aimed to address lies in the analysis of IE and the potential for bNMR to detect biomarkers in CSF. Existing research by Hasegawa *et al.* (2014) identified significant differences between controls, IE and other forms of epilepsy. However, the capabilities of bNMR, a low-cost analytical technique, were untested for the application of CSF metabolomic studies. Therefore, this study was focused on evaluating whether a minimal sample preparation method could effectively reveal IE biomarkers, thereby demonstrating the potential of bNMR as a viable tool for IE diagnosis.

Despite the moderate correlation shown (R^2: 0.644) in the OPLS-DA model for the bNMR data, the predictive ability and statistical significance were insufficient for robust classification. Several factors may contribute to these limitations, including the inherently low sensitivity of bNMR and the considerable overlap in metabolite signals. In contrast, HF-NMR has demonstrated its ability to distinguish IE from the controls (R^2: 0.82) with statistical significance ($p < 0.05$) using an OPLS-DA model.

Currently, the sensitivity of untargeted CSF metabolomics using bNMR is insufficient for reliable diagnosis. However, a more targeted approach, as demonstrated in this study through the cumulative ROC test (AUC: > 0.7, $p > 0.05$), suggests that key metabolites such as 3-hydroxybutyric acid, could serve as a useful biomarker for clinicians in determining IE using bNMR. This study has shown that the metabolites identified in this study are capable of distinguishing IE using HF-NMR. However, further refinement and validation are necessary to improve the sensitivity and predictive power of bNMR for clinical CSF applications in IE diagnosis.

Chapter 6 Metabolomics Analysis of Blood Plasma: An Asthma Investigation

6.1. Introduction:

Asthma is a chronic respiratory disease that affects millions of people worldwide, characterised by an obstructed airflow in the lungs, increased sensitivity of the airways, and ongoing inflammation.[17,218,219] The UK has one of the highest prevalences of asthma in the world, with over 5.4 million of its population having the disease.[220]

Furthermore, the UK faces significant challenges in managing the disease, including the highest rate of severe asthma hospitalisations with insufficient respiratory specialists to meet the patient demand.[221,222] This has contributed to 46% of children who died from asthma receiving inadequate care.[222] Asthma imposes a significant burden on the UK, costing over £1.1 billion between 2011-12, with 14% of these costs arising from 6.3 million consultations.[222,223] Between 2008 to 2018 deaths from asthma in England and Wales increased by 33%.[224] The cost of asthma has since risen to an estimated £3 billion in 2019.[225,226] Notably, many asthma deaths and expenses are preventable with improved management and early interventions.[222] Without appropriate measures, the mortality rate due to asthma in some regions is expected to increase significantly in the coming years.[227]

Common asthma triggers include allergies (allergic asthma), pollution (non-allergic asthma), cold air (seasonal asthma), workplace (occupational asthma), and physical activity (exercise-induced asthma), leading to the disease being well managed with the correct prescriptions and plans in place.[17] However, there are tougher forms of the disease, like difficult-to-control (DTC) asthma, severe asthma (unresponsive to high-dose treatments) and eosinophilic asthma (infections), where more specialised treatment needs to be provided and managed in specialist clinics.

DTC asthma refers to asthma that remains uncontrolled despite high doses of drugs or inhaled and oral corticosteroids.[228] Around 1 in 5 adults (17%) have DTC asthma, which is likely to arise from alterable factors such as the incorrect technique of

inhaler usage (≤ 80%), non-compliance (≤ 75%), smoking, and comorbidities such as obesity and obstructive sleep apnoea.[17,220,228,229]

The NHS uses three main tests *via* breath analysis to help diagnose asthma cases: FeNo test (£25.13)[226], which measures levels of nitric oxide for signs of inflammation; spirometry (£17.37)[226], a measure of lung capacity and speed of deflation; and peak flow test (£9.87)[226], a speed of lung deflation recorded over multiple visits.[230] However, these tests are not always reliable or followed by clinicians. A systematic assessment of DTC asthma cases found that 12% did not have asthma, 20% were not correctly confirmed to have DTC asthma, and 7% had additional undiagnosed diseases.[13] This statistic is further exemplified by the estimated £1.5-7.5 million the NHS could save each year by reducing misdiagnoses of asthma alone.[13]

Traditional methods of monitoring asthma severity rely on patient-reported symptoms, medication usage, and interference with daily life activities.[16,231] However, these methods may not always accurately predict the severity of asthma, and an analytical-based method could help improve detection. The disease's variability, including its different characteristics and responses to treatment, presents challenges for healthcare professionals in monitoring and detecting asthma.[16] Therefore, monitoring systems are needed to track the condition to improve asthma prediction and detection effectively.[232]

Metabolomics offers a solution to this problem; however, the cost of analysis still holds back the field to be effectively used for widespread clinical use. One promising approach to enhance asthma prognosis and detection involves using bNMR. This method offers a cost-effective and portable solution for analysing biological samples and providing insights into disease progression. By comparing the results obtained from bNMR with those from HF-NMR, the suitability of bNMR for detecting asthma and the metabolites that can be detected at lower sensitivity can be assessed.

Despite extensive research into NMR-based metabolomic approaches to asthma detection, bNMR is yet to be employed. Existing research efforts have focused on a range of different biofluids, including exhaled breath condensate (EBC)[233,234] urine[235,236], blood plasma[237] and blood serum[219,238,239] to gain insights into the

metabolic alterations associated with asthma. These studies have provided valuable insights into the underlying pathophysiological mechanisms of asthma and have identified potential biomarkers for diagnosis and monitoring.

Most of the research efforts in NMR metabolomics for asthma have focused on EBC, as highlighted in a reviewed by Kelly *et al.* (2016). Of the 21 studies that had been conducted, only six had been completed by NMR, with four focused on EBC, one with urine and the other with blood plasma.237 However, previous studies have yet to address the application of detection models in more cost-effective solutions as they have all previously used HF-NMR.[241]

Jung *et al.* (2013) conducted a study using a 600 MHz HF-NMR spectrometer to observe the metabolic profile of asthma in healthy individuals from blood plasma.[238] The study successfully demonstrated that multivariate statistical analysis *via* partial least squares discriminant analysis (PLS-DA) and area under the curve (AUC) analysis, was able to distinguish asthmatic (90.9%) from healthy adults (100%), suggesting that proton NMR may be an effective tool for asthma diagnosis.[238] The study employed a minimal sample preparation approach, requiring only centrifugation and the addition of a buffer solution, and reduced the broad signals from proteins and lipids *via* the Carr Purcell Meiboom Gill (CPMG) pulse sequence.[238] Jung *et al.* (2013) identified 30 metabolites at 600 MHz using proton NMR with seven of which being classified as significant (formate, methanol, acetate, choline, O-phosphocholine, arginine, and glucose) for the association to identify between asthmatics and the control samples.[238]

This research will explore two different forms of asthma, DTC as well as well-managed asthma (MA), to collectively identify biomarkers between asthma phenotypes and healthy controls (HC) in plasma samples. No study has specifically compared the metabolic profiles of these phenotypes. However, existing literature indicates distinct metabolic signatures, with DTC asthma patients exhibiting higher levels of lactate, alanine, and pyruvate, suggesting increased anaerobic glycolysis and altered energy metabolism.[15,239]

In this chapter, a pilot study of blood plasma samples from patients with asthma is presented. The aim is to identify the metabolites in plasma and potential biomarkers

at both the HF-NMR and bNMR levels using minimal sample preparation. This exploration could lead to more personalised and effective management strategies for asthma patients, as well as highlight the potential of bNMR metabolomics in asthma detection and management.

6.2. Materials and Methods

6.2.1. Study Population

A total of 122 subjects were considered for this study, including 60 individuals with DTC asthma, 26 with MA, and 36 HC. The demographic and clinical characteristics of the study population are summarised in the table below.

Table 5 - Clinical characteristics of the asthmatic study population

Characteristic	DTC (n=60)	MA (n=26)	HC (n=36)	Overall (n=122)
Age (years)	51.03 ± 15.54	25.42 ± 7.48	27.75 ± 4.63	38.70 ± 16.87
Sex (M/F)	20/40	11/15	20/16	51/71
BMI (kg/m²)	29.87 ± 6.99	24.37 ± 2.84	23.66 ± 2.72	26.87 ± 6.04

M: Male, F: Female, BMI: Body Mass Index, DTC: Difficult-To-Control, MA: Well-Managed Asthma, HC: Healthy Controls

6.2.2. Ethical Approval

All samples were collected with informed consent in approval of the Nottingham Trent University (NTU) Ethical Comity Board (Ethics code: 689 and NCT03996590).

6.2.3. Sample Collection

The MA and HC samples were collected from participants at NTU. Participants completed a questionnaire and consent form covering ethnicity, sex, height, and weight. NTU participants needed to be non-smokers, with no serious symptoms of asthma over the past 12 months and no treatment of antibiotics of the past 3 months. Clinicians at Southampton University Hospital collected DTC samples. These were collected as a part of the Wessex AsThma CoHort of difficult asthma (WATCH) study. Samples were stored at -80°C until they were transferred to NTU on dry ice. All samples provided for this project were confirmed by GP for disease state. The

WATCH participants for DTC classification also needed to be on high dose therapies and/ or with continuous or frequent use of oral steroids.

Venous blood samples (8 mL) were drawn from the antecubital fossa region using a butterfly needle into Ethylenediaminetetraacetic acid (EDTA) plasma vacutainers. The tubes were gently inverted and then centrifuged immediately for 15 minutes at 1,500 relative centrifugal force (RCF) at 4°C. The supernatant plasma layer was aliquoted and stored at -80 °C until further analysis.

6.2.4. NMR Sample Preparation

Samples were thawed at room temperature and vortexed for 30 seconds. Subsequently, 300μL of plasma was transferred into a 1.5mL microcentrifuge tube. Then 300 μL of a 0.2 M phosphate buffer deuterium solution, containing 0.2% sodium azide and 0.218 mM calcium formate, was added. Calcium formate was added as an internal standard, more detail can be found in Chapter 4.2.2. The mixture was vortexed for 30 seconds and then centrifuged at 12,000 RPM for 10 minutes at 4°C. Finally, 550 μL of the supernatant was transferred into a 5mm Wilmad economy (600 MHz) NMR tube, achieving a final calcium formate concentration of 0.1 mM.

6.2.5. NMR Spectroscopy

Samples were analysed at NTU using a 400 MHz ^{1}H NMR Jeol ECX spectrometer. The WASTED-II parameters were as follows: temperature at 18.6˚C, number of scans 256, receiver gain 50dB, relaxation delay 5 seconds, pulse width 11.22 μs, acquisition time 2.7315 seconds, Tau 2500 μs, 20 echoes, spectrometer frequency 399.52 MHz, spectral width 12 ppm, and acquired size 16384 points. All samples were shimmed, locked to deuterium and tuned and matched.

The bNMR data was acquired using a 60 MHz Oxford Instruments X-Pulse with an autosampler attached. The WASTED-II pulse sequence parameters included: filter 5000 Hz, acquisition points 16384, temperature at 37˚C, number of scans 1024, relaxation delay 2 seconds, Tau 2500 μs, 20 echoes, pulse width 6.893 μs, receiver attenuation 32, W5 water suppression 555 μs, gradient ramp time 100 μs, gradient

duration 4000 μs, and gradient recovery time 1000 μs. All samples were shimmed and locked to deuterium. Samples were tuned and matched every day, with no observable difference observed.

6.2.6. Data Processing

After acquisition, the data was processed through MestreNova (14.1.1). All samples were zero-filled, Fourier transformed, referenced to calcium formate (8.44 ppm), and had a Gaussian apodization at 1 Hz weighting function applied. Manual corrections were made for phase and baseline. Following data processing, 0.01 ppm bucketing was applied and exported as a .csv file. Data was normalised by sum and Pareto data scaling applied *via* MetaboAnalyst6.0.36 Prior to multivariate and univariate analyses, the distribution of all metabolite features was examined within MetaboAnalyst using density plots of normalized intensity values. The density maps indicated that the data were approximately normally distributed following normalization and scaling, with no evidence of skewness or outliers that could bias subsequent analyses. Establishing normal distribution is important as it ensures that statistical assumptions underlying parametric tests and multivariate models, such as OPLS-DA and linear regression, are met. This improves the interpretability and reliability of variance partitioning, correlation strength, and model performance metrics. The observed normal distribution therefore supports the validity of the subsequent statistical and multivariate analyses performed in this study.

6.2.7. Data Analysis

Data analysis was conducted using Python (version 3.10) with packages including pandas (version 1.3.4)[205], numpy (version 1.21.4)[206], matplotlib (version 3.5.1)[207], scipy (version 1.8.0)207, and statsmodels (version 0.13.2)[209], as well as the online metabolomics package MetaboAnalyst 6.0.209

6.3. Results

This chapter represents the results of the bNMR analysis conducted to compare three groups: patients with DTC asthma, HC and people with MA. The primary

objective of this study is to identify significant differences in bNMR biomarkers among asthmatic groups, as well as identify the metabolites that are detectable using bNMR. This results chapter will be divided into sub-chapters to help answer questions relating to bNMR's potential utility in metabolomics using blood plasma.

6.3.1. Blood Plasma Assignment

The use of databases such as the HMDB and chenomix, were used to assign 1H NMR spectra of blood plasma. Assignment confirmation was obtained through COSY spectra (Appendix 2-4). In total 20 metabolites from the bNMR spectra (*Figure 41*) and 22 metabolites from the HF-NMR spectra (Figure 42) were identified. Similar concentrations of metabolites were observed across both spectrometer fields with lipids, EDTA and formate being the most abundant. The latter two of which was added to the sample for anticoagulation and spectral alignment. Other metabolites which were in relatively large abundance include proline, dimethyl amine, glucose and lactate. The red boxes found in *Figure 41* and Figure 42 display a zoomed-in section of the spectra to help better show these lower concentration metabolites.

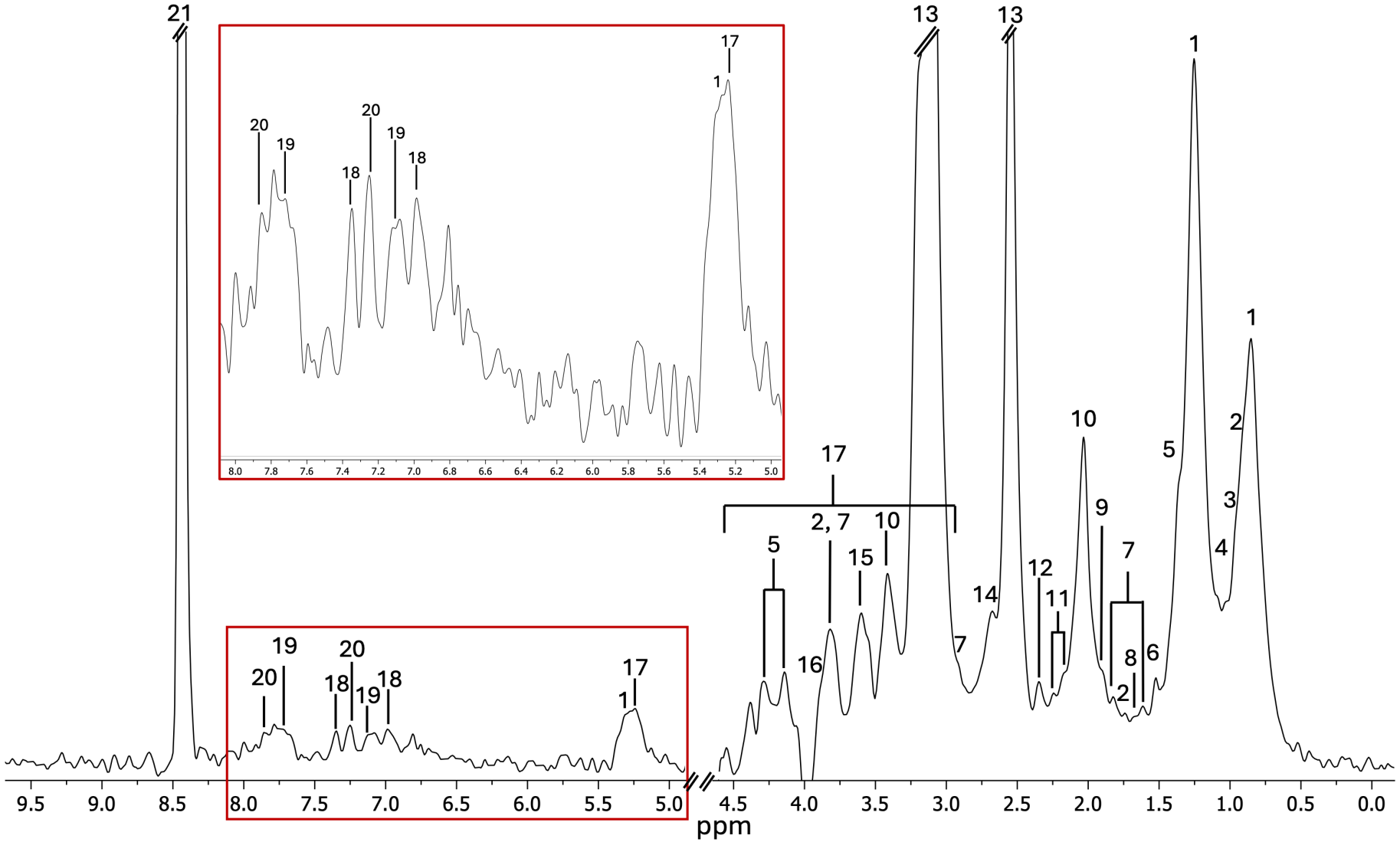

Figure 41 - bNMR representable assigned spectra of blood plasma. 1 Lipids; 2 Leucine; 3 Valine; 4 Isoleucine; 5 Lactate; 6 Alanine; 7 Lysine; 8 Arginine; 9 Acetate; 10 Proline; 11 Glutamine; 12 Glutamate; 13 EDTA; 14 Dimethylamine; 15 Glycine; 16 Creatine; 17 Glucose; 18 Tyrosine; 19 Histamine; 20 Histidine; and 21 Formate.

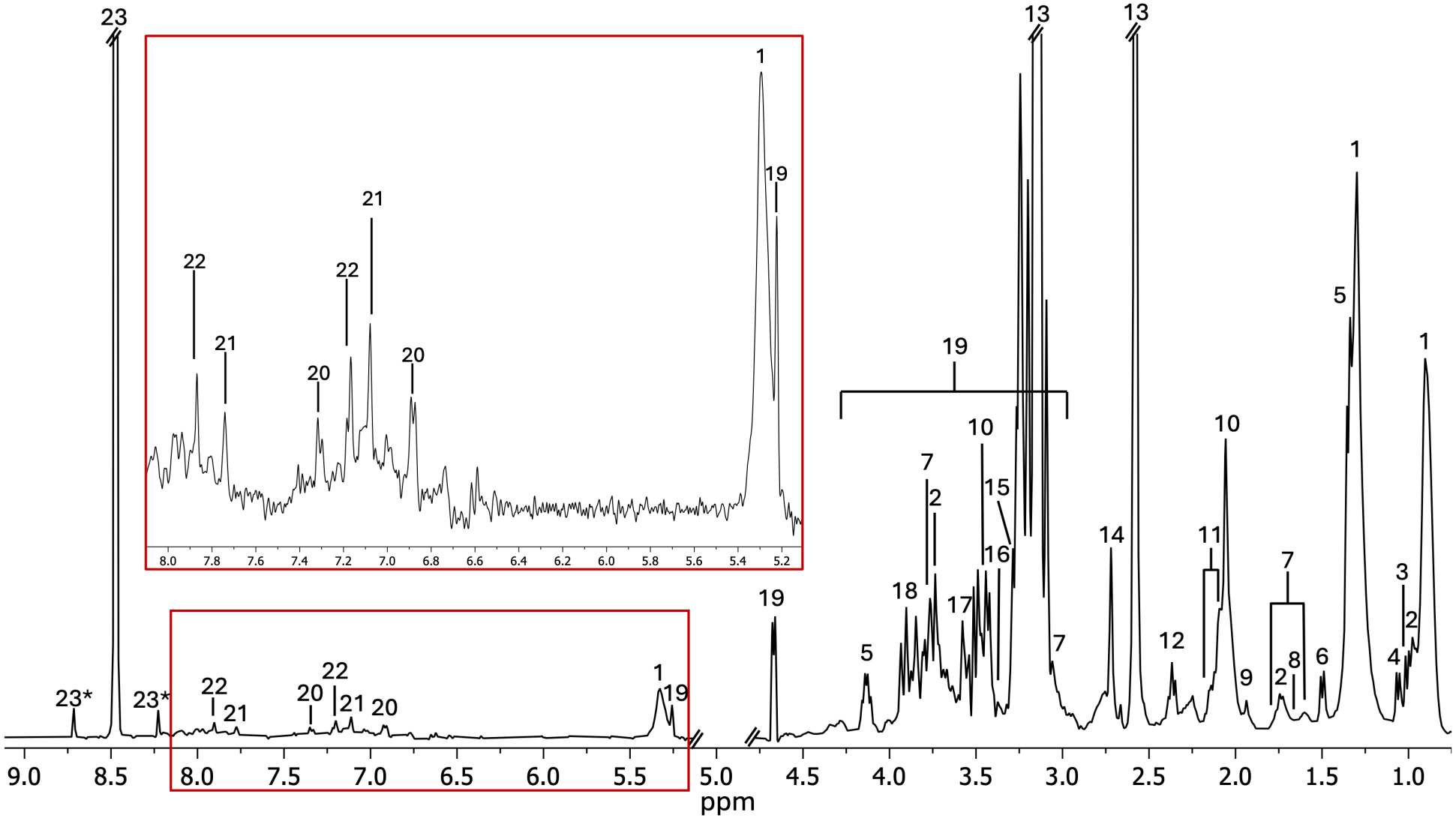

Figure 42 - HF-NMR representable assigned *spectra of blood plasma. 1 Lipids; 2 Leucine; 3 Valine; 4 Isoleucine; 5 Lactate; 6 Alanine; 7 Lysine; 8 Arginine; 9 Acetate; 10 Proline; 11 Glutamine; 12 Glutamate; 13 EDTA; 14 Dimethylamine; 15 TMAO; 16 Methanol; 17 Glycine; 18 Creatine; 19 Glucose; 20 Tyrosine; 21 Histamine; 22 Histidine; 23 Formate, * ^{13}C satellite.*

6.3.2. Multivariate Metabolite Analysis

The bNMR and HF-NMR spectroscopy analysis revealed significant metabolite differences between the three groups. Key metabolites that showed significant variations are presented below along with the general trend of the data between the spectrometers.

6.3.3. Comparison Between Well Managed Asthma, Difficult-to-Control Asthma, and Healthy Controls

6.3.3.1 Principal Component Analysis

Principal component analysis (PCA) was conducted to observe and compare variances between bNMR and HF-NMR data (Figure 43) across the three groups: MA n = 26 (Blue), DTC Asthma n = 60 (Red), and HC n = 36 (Green). The bNMR data explained 60.9% of the total variance (Figure 43a), while HF-NMR explained 50.4% (Figure 43d). There was little separation between the groups, although the controls showed slightly more separation in the bNMR PCA plot. Both datasets noted outliers, with similar regions contributing to the main variance. The loadings plots (Figure 43 b, c, e and f) show the main variance is explained from branched chain amino acids (BCAA's) and the sugars found between 3 and 4 ppm. Regions where EDTA were present were removed.

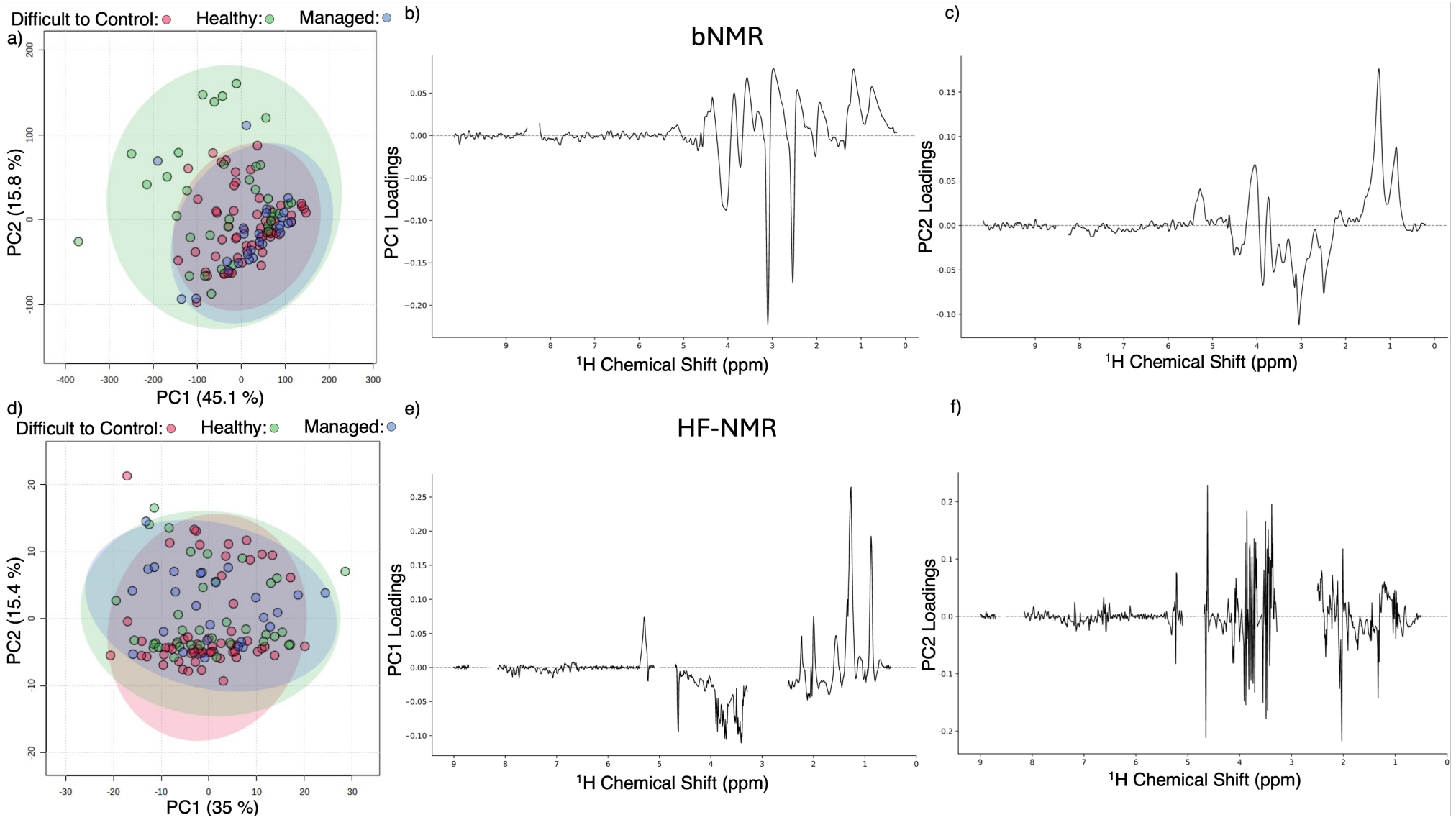

Figure caption on the next page.

Figure 43 - PCA plot of asthmatic and healthy samples illustrating the distribution of samples across two principal components (PC1 and PC2). Each point represents a sample, colour-coded by group: Healthy Controls (HC) n = 36 in green, Managed Asthma (MA) n = 26 in blue, and Difficult-to-Control Asthma (DTC) n = 60 in red. The ellipses represent the 95% confidence intervals for each group, indicating the spread and central tendency of the samples within each group. Loadings plot for the PCA illustrating the contribution of individual bins to the variance in the data (b,c,e,f). The x-axis shows the chemical shift (ppm), and the y-axis represents the loading values for PC1 (middle plots) and PC2 (the two right plots). The top columns relate to bNMR (a,b,c), while the bottom figures (d,e,f) relate to HF-NMR analysis.

6.3.3.2 SPLS-DA

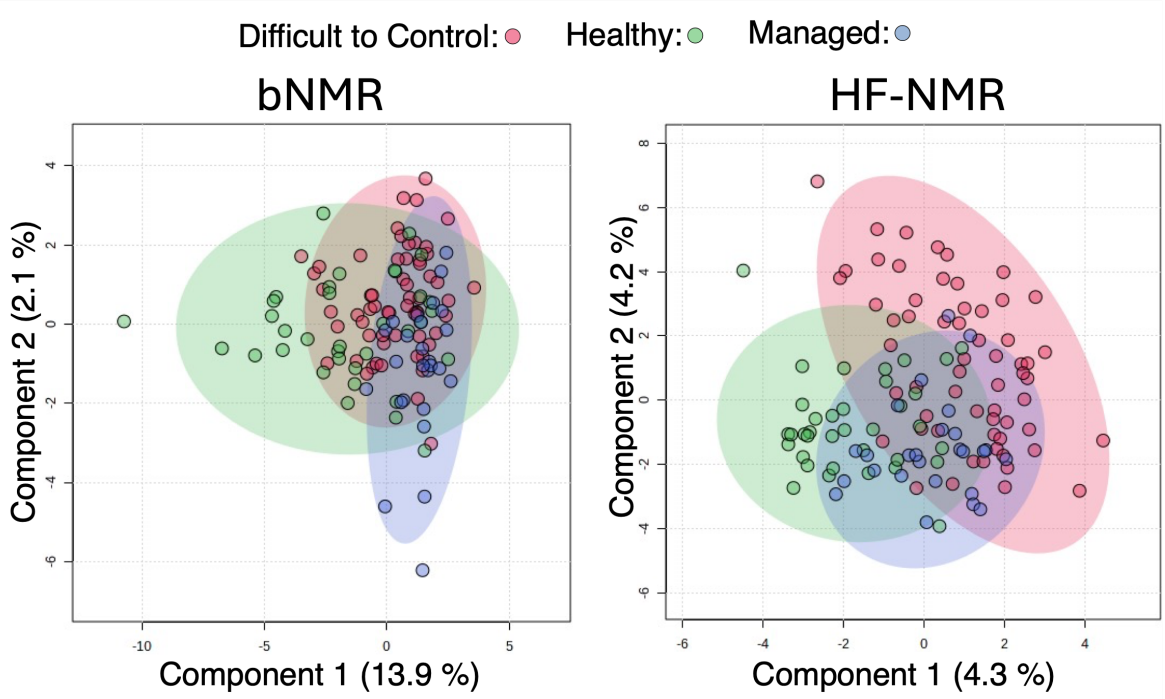

Figure 44 - SPLS-DA plot illustrating the separation of samples into different groups : HC in green, MA in blue, and DTC in red. Each point represents a sample colour-coded by group. Each colour corresponding ellipse marks the 95% confidence regions. The bNMR data is located to the left, while the HF-NMR SPLS-DA plot is located on the right. The bNMR SPLS-DA plot explained 16% of the data, while only 8.5% is explained in the HF-NMR SPLS-DA plot.

Sparse – partial least squares discrimination analysis (SPLS-DA) was used to supervise data to maximise separation between the three variables. Similar to the PCA figures, there are outliers present in the bNMR and HF-NMR SPLS-DA plot (Figure 44). The bNMR SPLS-DA plot explained 16% of the total variance, whereas the HF-NMR SPLS-DA plot only explained 8.5%. Neither spectrometer showed good separation between the groups, however, the HF-NMR data shows a slightly stronger separation between groups, especially the DTC group. The controls in the bNMR data show the best separation.

6.3.3.3 Significant Bins Between the Asthma Groups and Controls

In total, there were 183 significant false discovery rate (FDR) corrected bins in the bNMR data and 108 bins that were significant in the HF-NMR data (Figure 45a and c). The HF-NMR identified a larger number of FDR-corrected bins. The bNMR data did not identify any bins that were significant when distinguishing DTC from MA. Similar bins were also identified in the bNMR data that were significant to distinguish between the asthmatic types making up 74.9% of the total significant bins in the bNMR data.

The HF-NMR data (Figure 45c). showed a more even spread across the different data types and could distinguish between groups with more bins, as well as a wider variety of bins (Figure 45d) that can be used to explain the data types. The disparity between the spectrometer types is most likely because of peak widths resulting in more overlap of signals in the bNMR data and a reduction of significant bins in the aromatic region (6-9 ppm), due to the higher sensitivity of the HF-NMR. More significant bins are located between 0-5ppm in the bNMR data.

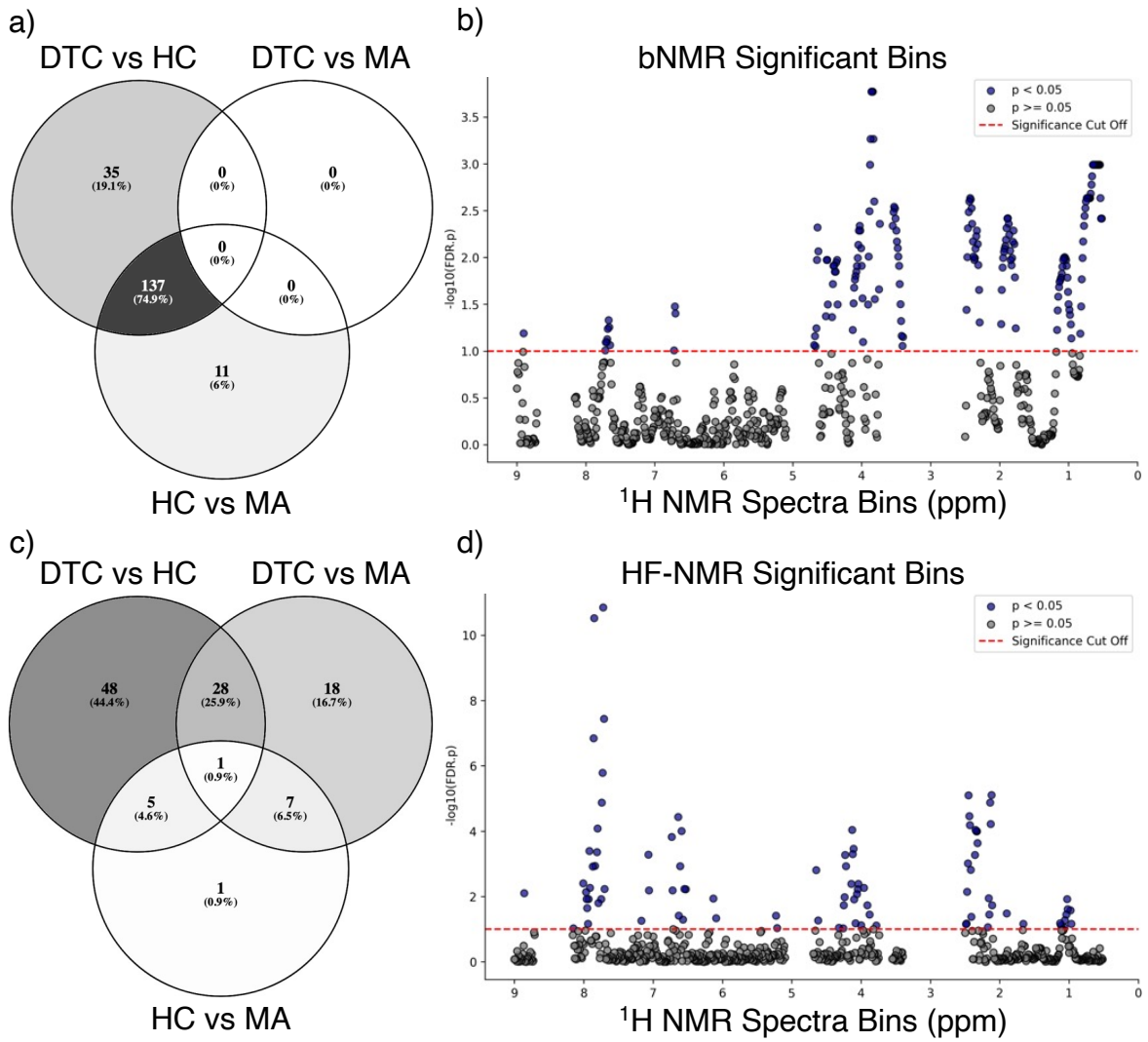

Figure 45 - Significant (< 0.05) FDR corrected associations between DTC, MA and the HC are shown in Venn diagrams A and C for bNMR and HF-NMR respectively. . The overlap of matching bins are located in between group types that can distinguish group types. Plots B (bNMR) and D (HF-NMR) show the FDR significant bins, highlighted in blue, that appear above the threshold identified by the red line. The x-axis represents the chemical shift (ppm), and the y-axis shows the -log10 adjusted p-value, with significant bins highlighted. The water peak and EDTA signals were removed from the spectra explaining for the gaps.

6.3.4. Comparison between Difficult-To-Control Asthma and Healthy Controls

In this section, individuals diagnosed with DTC asthma n = 60 will be compared against the healthy controls n = 36. The significant bins will first be explored before moving on to exploring PCA, orthogonal partial least squares discrimination analysis (OPLS-DA) and area under the curve (AUC) plots, to explore biomarkers to distinguish between the two disease states.

6.3.4.1 Significant Bins Comparing Difficult-To-Control Asthma with Healthy Controls.

Volcano plots are used to identify metabolites that show significant differences between two given groups. It combines the fold change (FC) as well as the FDR-corrected statistically significant (< 0.05) bins. Significant bins are located in the top right and left sides of the volcano plot, with the left side indicating a decrease in the metabolite and the right side indicating an increase. The bNMR volcano plot (Figure 47a) shows DTC bins around 4.42ppm are significantly decreased compared to the HC, whereas the HF-NMR DTC bins (Figure 47b) around 4.78ppm are significantly increased compared to the HC group.

The significant bins (identified by T-test) are also plotted (Figure 47b and d) in relation to their ppm value. Similar regions of HF-NMR and bNMR spectra are identified in both plots, with more statistically significant bins present around 8 ppm in the HF-NMR data compared to the bNMR spectra. The Venn diagram (Figure 46) shows the cross-over of significant bins that were observed in the HF-NMR and bNMR data as well as those which were only seen in their respective data cohort. The bNMR showed more significant independent bins (132) than the HF-NMR data (42). There were 40 bins where that were significant in both bNMR and HF-NMR spectrometers. Therefore, a total of 172 bins in the bNMR and 82 bins in the HF-NMR. This discrepancy is most likely due to the different operating temperatures of the spectrometers and the lower operating frequency of bNMR with wider peak widths and lower sensitivity.

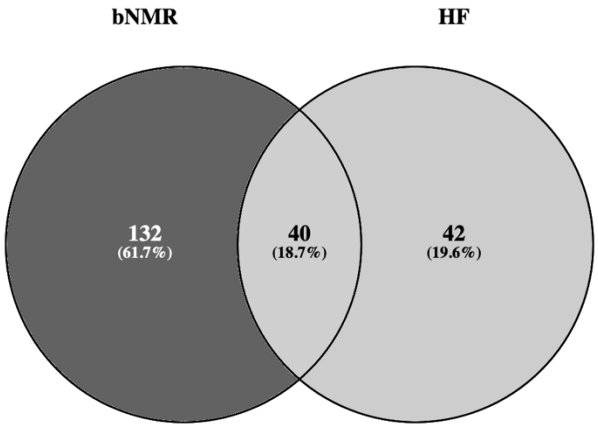

Figure 46 - Significant (< 0.05) FDR corrected associations between DTC and the HC for the bNMR and HF-NMR data respectively.

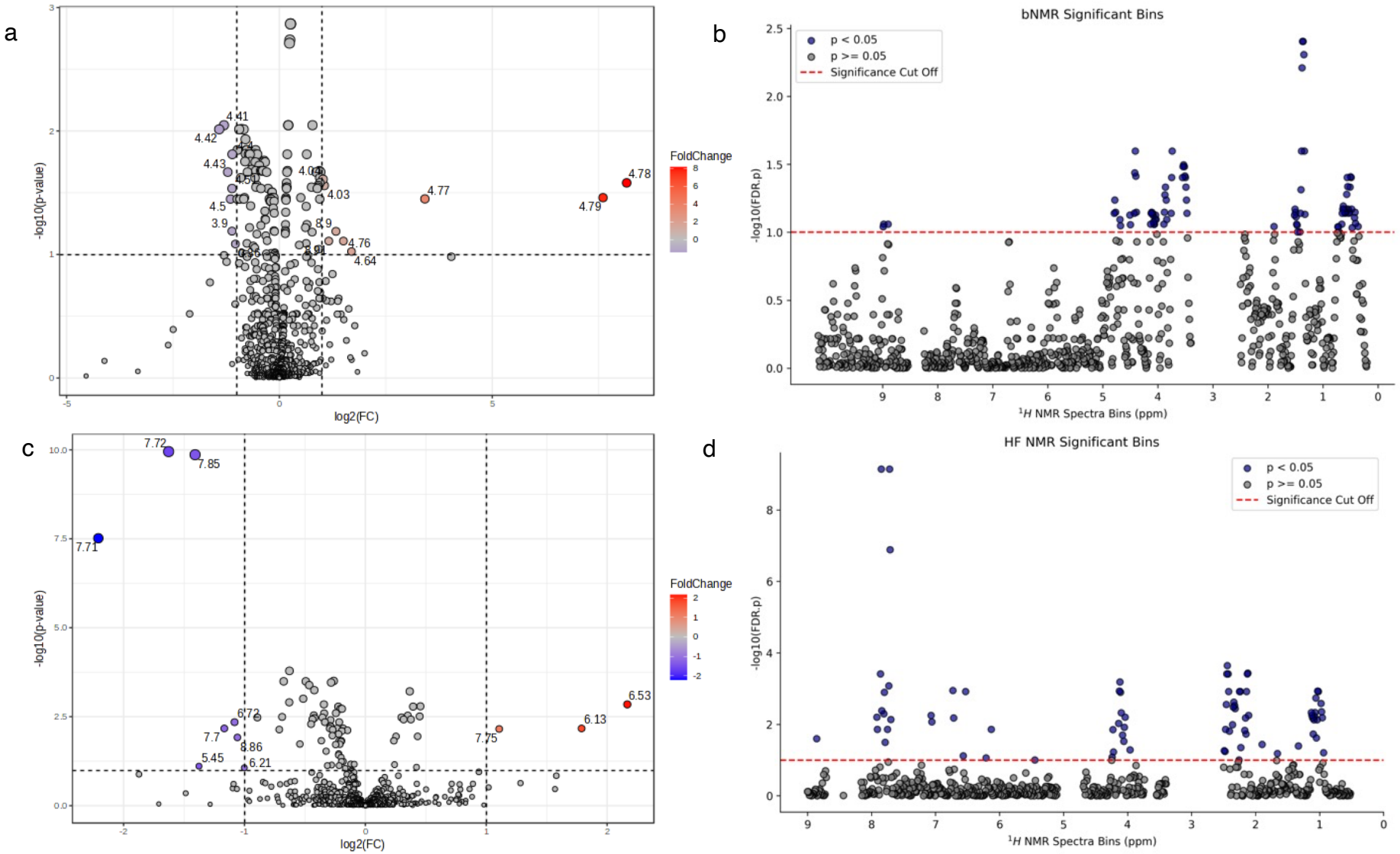

Figure caption on the next page.

Figure 47 - Volcano and scatter plots of significant bins distinguishing DTC and HCs. The volcano plots (A and C) show the log2 fold change on the x-axis and the -log10 p-value on the y-axis. Metabolites with significant changes are highlighted in red (increased) and blue (decreased). Scatter plots (B and D) display significant bins across the spectrum. The x-axis represents the bins, and the y-axis represents the -log10 FDR adjusted p-value. Significant bins (FDR adjusted p-value < 0.05) are highlighted, indicating their statistical significance in differentiating between groups. The top plots correspond to the bNMR data, while the bottom two plots relate to HF-NMR.

6.3.4.2 PCA Analysis: Principal Component Analysis of Difficult-To-Control Asthma and Healthy Controls

PCA was used to explore the general variance and group separation between the two groups. The PCA plots (Figure 48a and d) illustrate a distinct lack of clustering of the HC, and DTC groups. The HC samples (green) are slightly more separated from the DTC samples (red) in the bNMR PCA plot (Figure 48a), while no separation is observed in the HF-NMR PCA plot (Figure 48b). The 95% confidence ellipses indicate the variability within each group, with the HC group showing the largest spread, suggesting greater heterogeneity in this group. The bNMR PCA plot (Figure 48a) explains a similar amount of the total variance (43.5%) compared to the HF-NMR PCA plot (Figure 48b) explaining 50.1% of the total variance. PC 2 explains a similar variation, however, PC 1 of the bNMR is considerably different around 4 ppm compared to the HF-NMR data.

.

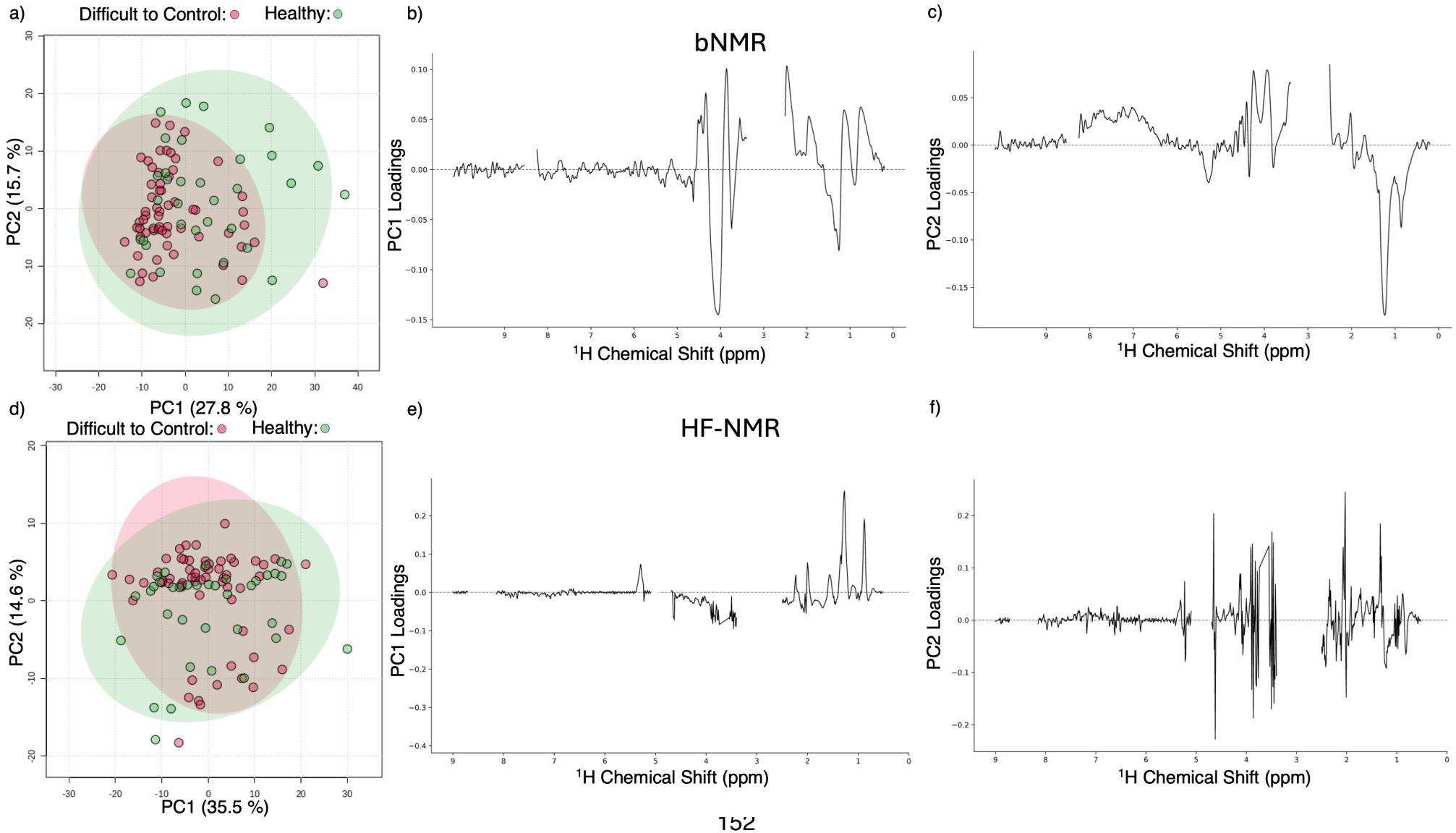

Figure caption on the next page.

Figure *48* - PCA plots (a and d) illustrating the distribution of samples across two principal components (PC1 and PC2) for the bNMR and HF-NMR data respectively.

Each point represents a sample, colour-coded by group: HC n = 36 in green, and DTC n = 60 in red. The ellipses represent the 95% confidence intervals for each group, indicating the spread and central tendency of the samples within each group. The axes show the percentage of variance explained by PC1 and PC2, providing insight into the data's dimensionality and group separation. The loadings plots for PC1 (b and e) and PC2 (c and f) are shown against the ppm axis. Gaps in the figures are the water signal and EDTA signal locations, removed to eliminate their influence on the data. The bNMR data is shows in the top three figures and the bottom three figures are for the HF-NMR data.

6.3.4.3 OPLS-DA Analysis: Discriminating Difficult-To-Control Asthma from Healthy Controls

To enhance group separation and identify the metabolites contributing most to the differences between groups, OPLS-DA was conducted. The OPLS-DA plot in Figure 49a and d illustrate the separation of samples based on their respective groups. The plots clearly show a distinct separation between the HC (green) and DTC (red) groups for the HF-NMR data, with 95% confidence ellipses further confirming the clustering. Notably, there was no overlap observed in the HF-NMR OPLS-DA plot, and minimal overlap observed in the bNMR OPLS-DA plot. Permutation testing with 2,000 permutations revealed significant differences between the observed Q^2 value of 0.614 ($p<0.001$) and R^2 value of 0.916 ($p<0.001$) for the HF-NMR data. Conversely, the bNMR data exhibited results lacking in predictive power (Q^2: 0.0756, $p = 0.0025$), with insufficient separation between the two groups (R^2: 0.56, $p = 0.1705$) and a high p-value above the threshold. The VIP and scores plots show some similarities between spectrometer types, especially between 3 and 0 ppm. However significant bins around 7.7ppm were not identified in the bNMR data.

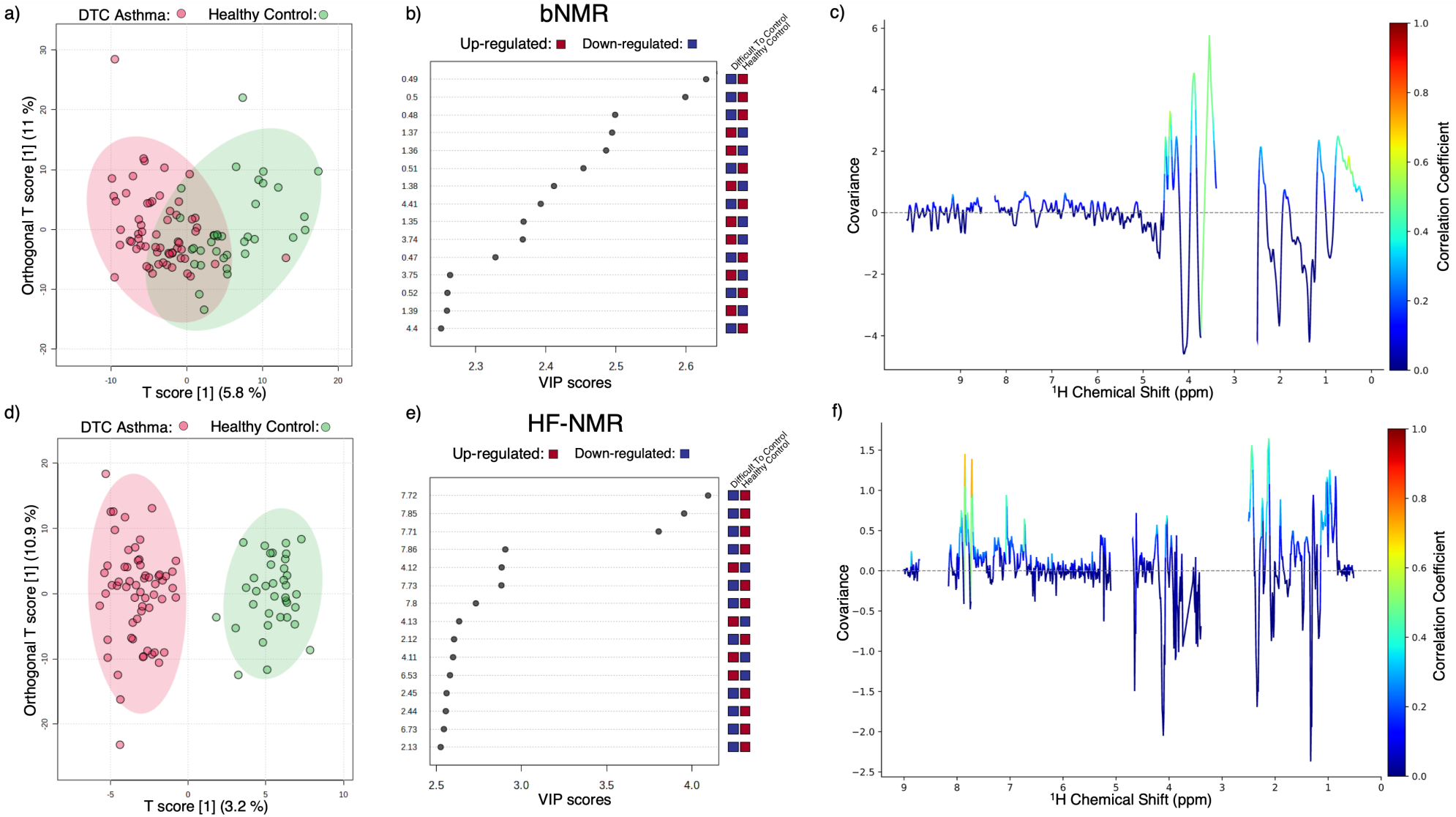

Figure caption on the next page.

Figure 49 - OPLS-DA plots (a and d) illustrating the differentiation of samples from HC's shown in green, and DTC asthma represented in red. Each data point corresponds to a sample and is color-coded by group. The plot effectively distinguishes groups based on class membership and orthogonal variation, with the ellipses denoting the 95% confidence intervals for each group. Loadings plot for the OPLS-DA (c and f) showing the contribution of individual metabolites to the group separation. The x-axis shows the chemical shift (ppm), and the y-axis represents the loading values. The VIP scores for the top 15 bins are shown in plots b and e.

6.3.4.4 ROC Curve Analysis: Evaluating Biomarker Performance in Difficult-To-Control Asthma versus Healthy Controls

The diagnostic performance of the bins was evaluated using receiver operating characteristic (ROC) curves. The ROC curve for distinguishing between HC and DTC (Figure 50) was generated, and the AUC was calculated to assess the accuracy of the biomarkers. Both the HF-NMR and bNMR AUC plots show that the models with 100 variables has the best performance. Notably, the HF-NMR data performed very well, exhibiting an AUC of 0.906 (95% confidence interval: 0.8-0.984) with a predictive accuracy of 82.5%. Conversely, the bNMR data yielded a lower AUC of 0.668 (95% confidence interval: 0.455-0.863), falling below the customary AUC threshold of 0.7, with a predictive accuracy of 62.2%. The predicted class probabilities using the 100 variable model show a higher number of incorrectly predicted classes were identified from the bNMR data (Figure 50c) compared to the HF-NMR data (Figure 50d).

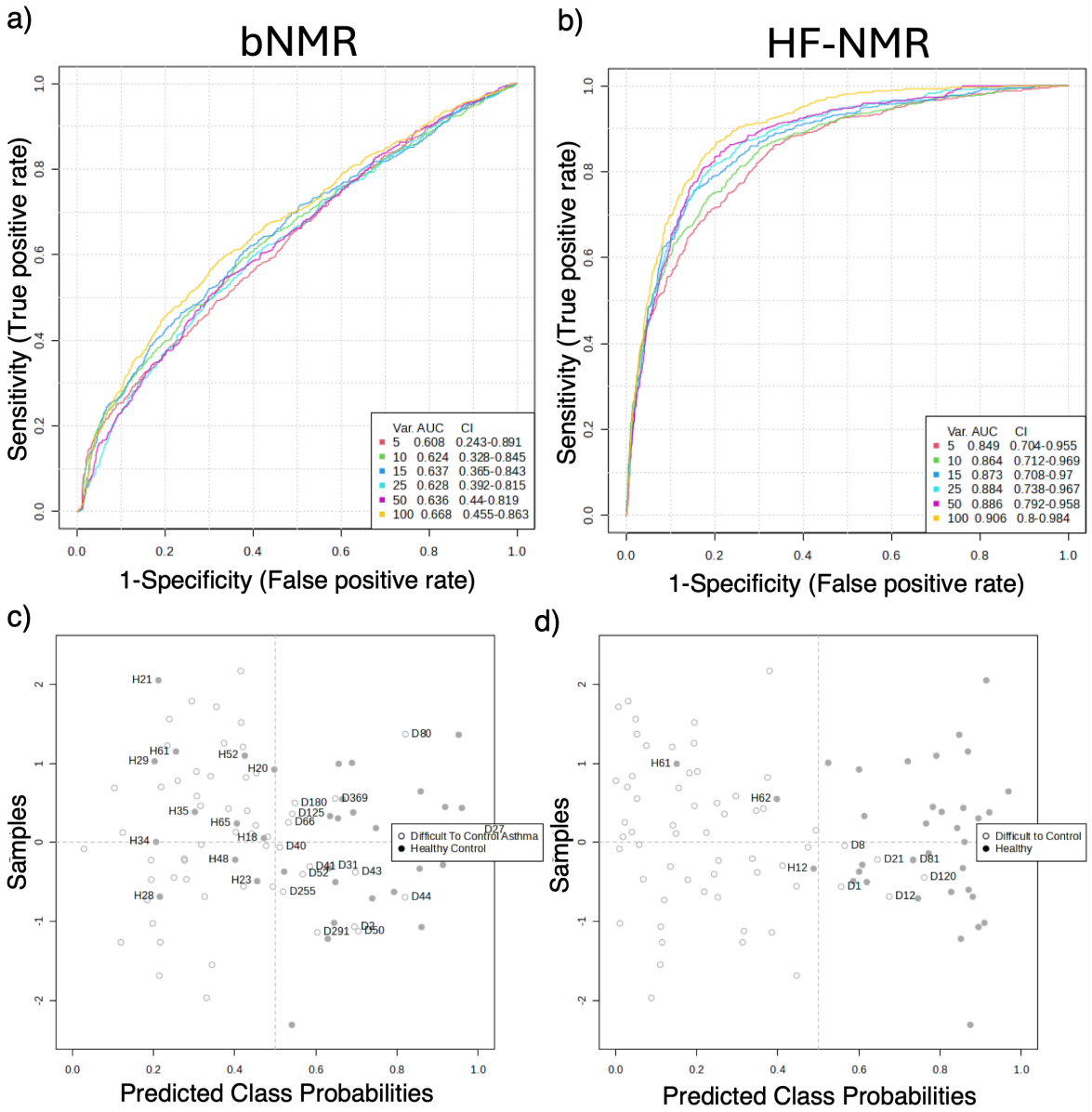

Figure 50 - ROC curve (a and b) showing the performance of biomarker models for distinguishing between HC's and DTC. The AUC indicates the accuracy of the biomarkers, with values closer to 1.0 indicating excellent discrimination. The plot includes sensitivity (true positive rate) on the y-axis and 1-specificity (false positive rate) on the x-axis. Plots c and d show the predicted class probabilities for all samples using a single biomarker model.

Table 6 - Metabolites summarising the data from the bNMR and HF-NMR spectra comparing Difficult-to-Control Asthma against Healthy Controls.

	bNMR							HF-NMR						
Metabolite	Regulation	VIP score	AUC	Sensitivity	Specificity	p-Value	FDR	Regulation	VIP score	AUC	Sensitivity	Specificity	p-Value	FDR
Acetate	Down	0.48	0.67	0.7	0.6	0.122	0.404	Up	0.67	0.58	0.5	0.7	0.250	0.612
Alanine	Up	2.10	0.67	0.6	0.7	0.008	0.087	Up	1.19	0.63	0.6	0.7	0.029	0.189
Creatine	Down	1.94	0.59	0.8	0.5	0.026	0.167	Up	1.08	0.59	0.6	0.6	0.064	0.309
Glucose	Up	0.22	0.55	0.8	0.4	0.417	0.767	Up	1.04	0.54	0.6	0.5	0.055	0.936
Glutamate	Down	0.80	0.65	0.6	0.7	0.052	0.256	Up	2.46	0.72	0.6	0.7	0.000	0.003
Glutamine	Down	1.27	0.68	0.7	0.6	0.014	0.115	Down	1.54	0.68	0.5	0.8	0.001	0.016
Glycine	Down	2.08	0.85	0.8	0.8	0.001	0.040	Up	0.13	0.51	0.6	0.5	0.793	0.936
Histamine	Up	0.58	0.55	0.5	0.7	0.552	0.852	Down	2.73	0.75	0.7	0.7	0.000	0.001
Histidine	Up	1.27	0.66	0.7	0.6	0.025	0.081	Down	0.17	0.54	0.5	0.7	0.905	0.982
Isoleucine	Down	0.25	0.57	0.7	0.5	0.307	0.864	Down	0.94	0.71	0.8	0.6	0.028	0.188
Lactate	Up	1.56	0.74	0.8	0.6	0.000	0.025	Up	1.57	0.67	0.8	0.6	0.004	0.040
Leucine	Up	1.23	0.56	0.7	0.5	0.235	0.598	Down	0.51	0.56	0.7	0.5	0.291	0.643
Lysine	Down	0.80	0.71	0.7	0.7	0.014	0.091	Down	1.68	0.63	0.6	0.6	0.004	0.037
Methanol	-	-	-	-	-	-	-	Up	0.13	0.56	0.6	0.5	0.080	0.461
Phenylalanine	Up	0.60	0.51	0.5	0.5	0.543	0.850	Down	0.61	0.64	0.6	0.7	0.490	0.791
Tyrosine	Down	0.20	0.58	0.6	0.6	0.289	0.633	Down	1.55	0.64	0.7	0.7	0.073	0.331
Valine	Down	1.12	0.67	0.6	0.7	0.042	0.233	Down	1.34	0.67	0.6	0.7	0.002	0.024

ROC: receiver operating curve, FDR: false discovery rate, VIP: variable importance in projection

6.3.5. Comparison between Difficult-To-Control Asthma and Well Managed Asthma

Distinguishing between similar disease types can be vital to ensure diseases are being correctly detected and characterised. In this subchapter, the two asthma groups DTC (n = 60) and MA (n = 26) are investigated. The same statistical techniques used to distinguish between DTC and HC will be applied here to identify possible biomarkers that can be used to distinguish between the groups as well as compare the two spectrometers, to identify the differences between them.

6.3.5.1 Significant bins between Difficult-To-Control Asthma and Well Manged Asthma

The volcano plot analysis (Figure 52a and c) revealed that there were more significant bins in the HF-NMR data compared to the bNMR data. A noticeable decrease in fold change was observed in the bNMR data around the 4 ppm region, while the HF-NMR data showed an increase in metabolite bins at 6.64 ppm and 6.67 ppm. In these figures, the scatter plots (Figure 52b and d) indicate that there are no significant bins in the bNMR data, while some significant bins remain in the HF-NMR data, primarily around the 8 ppm region. The Venn diagram (Figure 51) further highlights that 54 FDR-adjusted significant bins were identified in the HF-NMR data but not in the bNMR data. This suggests that bNMR may not effectively distinguish between the DTC and MA groups.

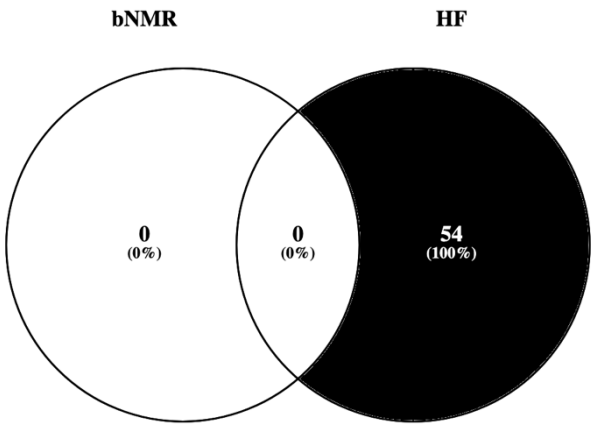

Figure 51 - Significant (< 0.05) FDR corrected associations between DTC and MA for the bNMR and HF-NMR data respectively.

a)

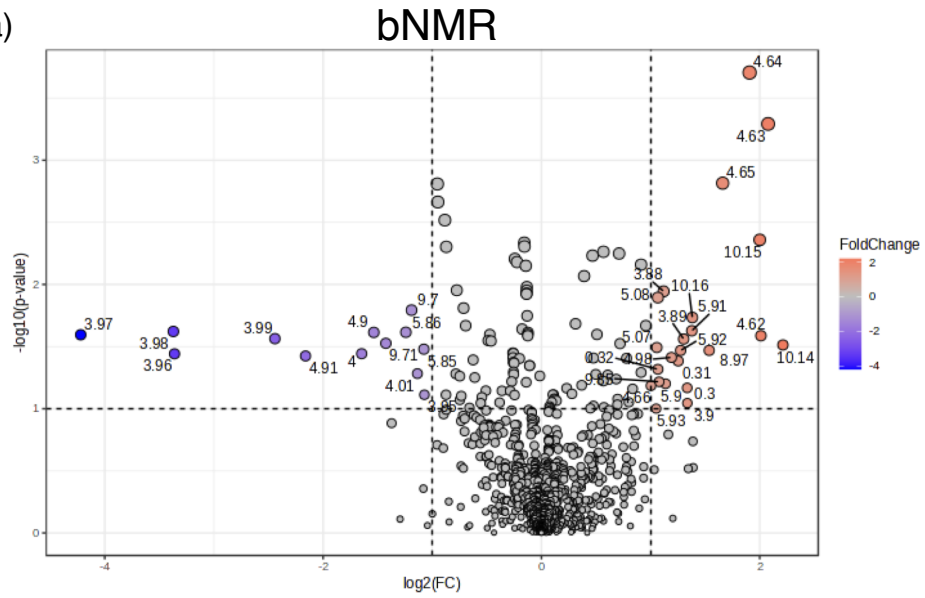
bNMR
-log10(p-value)
log2(FC)
FoldChange

b)

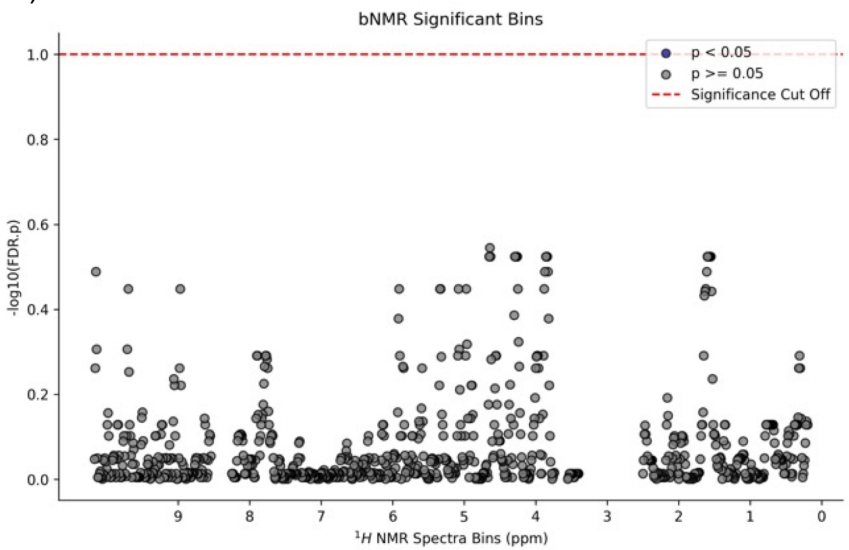
bNMR Significant Bins
p < 0.05
p >= 0.05
Significance Cut Off
-log10(FDR,p)
¹H NMR Spectra Bins (ppm)

c)

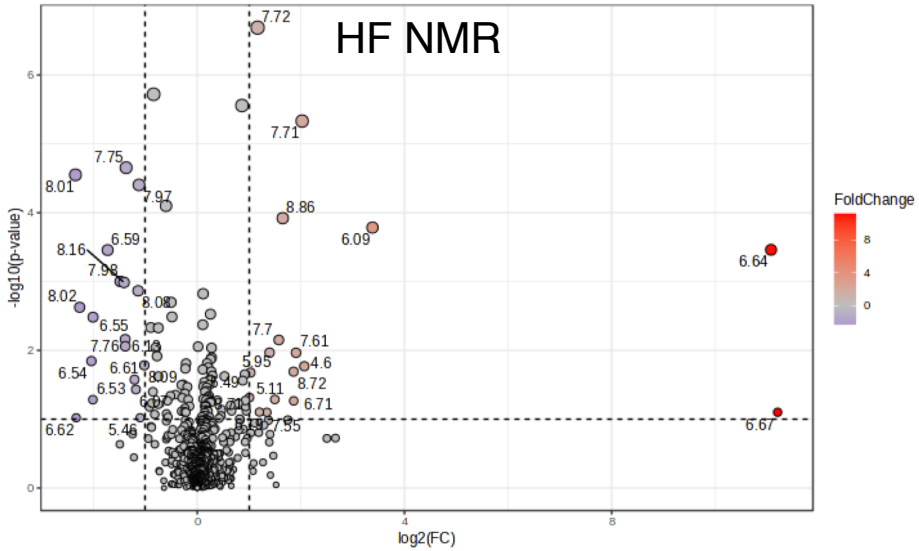
HF NMR
-log10(p-value)
log2(FC)
FoldChange

d)

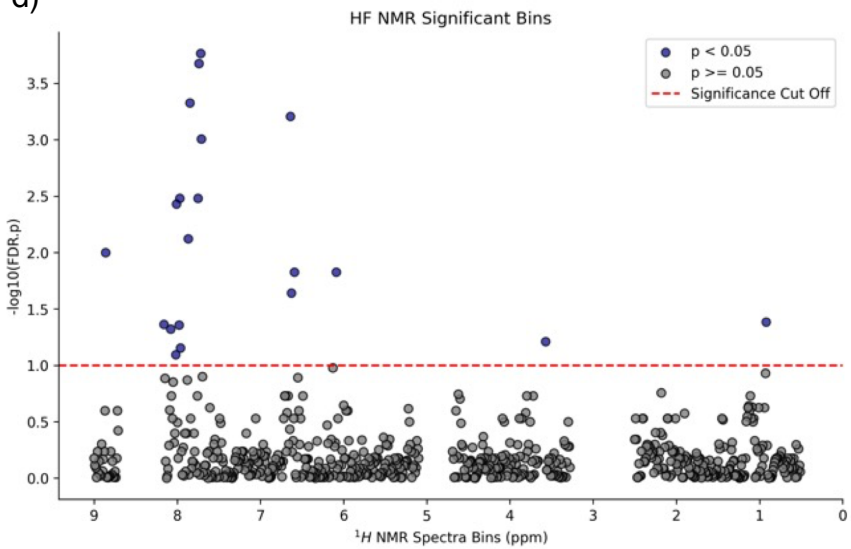
HF NMR Significant Bins
p < 0.05
p >= 0.05
Significance Cut Off
-log10(FDR,p)
¹H NMR Spectra Bins (ppm)

Figure 52 - Volcano and scatter plots of significant bins distinguishing asthma types.

The volcano plots (a and c) show the log2 fold change on the x-axis and the -log10 p-value on the y-axis. Metabolites with significant changes are highlighted in red (increased) and blue (decreased). Scatter plots (b and d) display significant bins across the spectrum. The x-axis represents the bins, and the y-axis represents the -log10 FDR adjusted p-value. Significant bins (FDR adjusted p-value < 0.05) are highlighted, indicating their statistical significance in differentiating between groups. The top plots correspond to the bNMR data (a and b), while the bottom two relate to HF-NMR (c and d).

6.3.5.2 PCA: Principal Component Analysis of Difficult-To-Control Asthma and Well Managed Asthma

PCA plots (Figure 53a and d) reveal minimal variation between the two groups in either the HF-NMR or bNMR data. Additionally, a total of four outliers were detected outside the 95% confidence regions in the bNMR data, with only two outliers observed in the HF-NMR data. The bNMR data accounts for 41.6% of the total variance, whereas the HF-NMR data explains a higher percentage at 55.9%. The main variance in the data observed from PC1 (Figure 53b and e) and PC2 (Figure 53c and f) is attributed to signals ranging between 0 and 5 ppm in both the HF-NMR and bNMR.

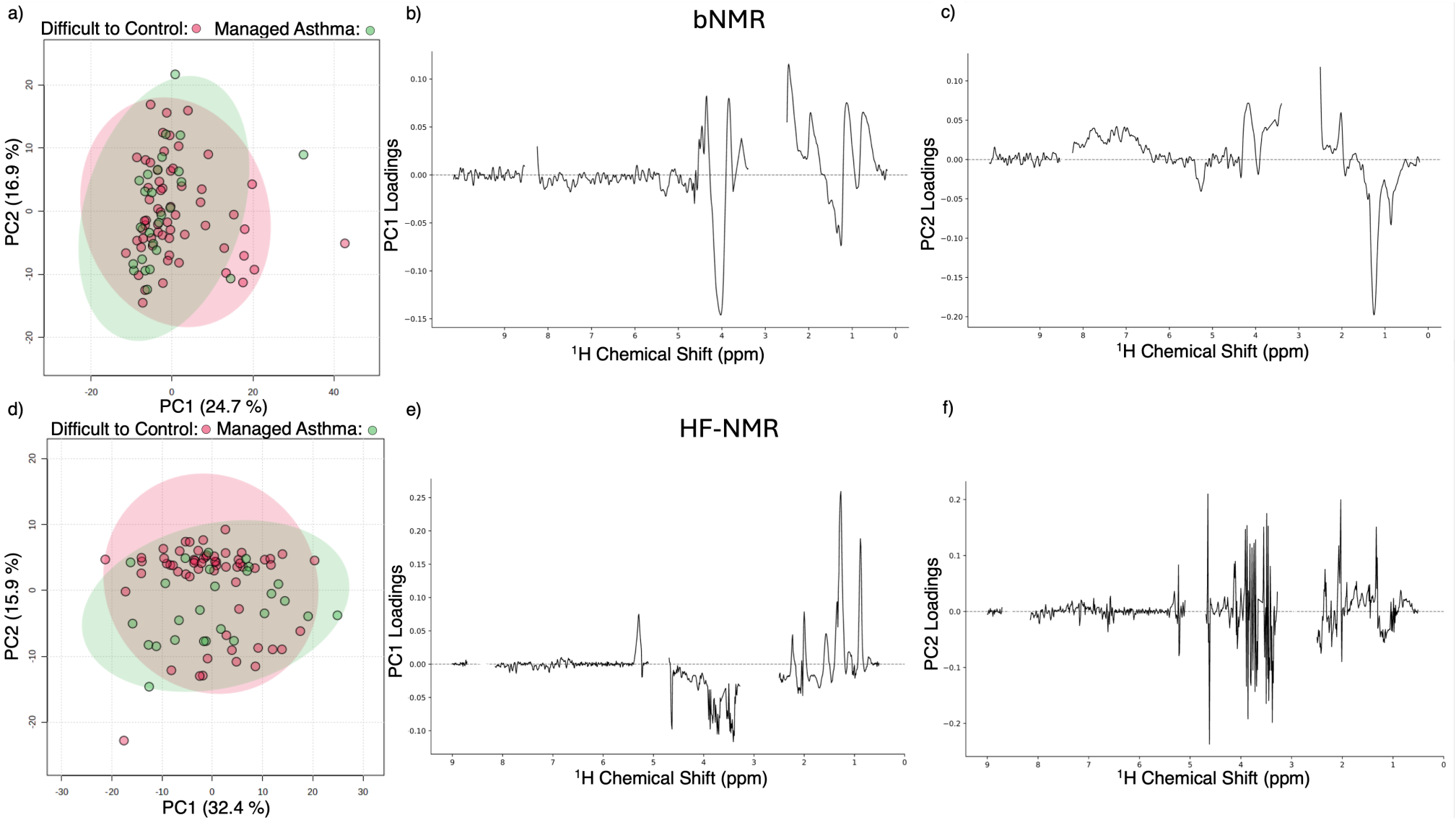

Figure caption on the next page.

Figure 53 - PCA plots (a and d) illustrating the distribution of samples across two principal components (PC1 and PC2) for the bNMR and HF-NMR data respectively.

Each point represents a sample, colour-coded by group: MA in green (n = 26), and DTC in red (n = 60). The ellipses represent the 95% confidence intervals for each group, indicating the variance of the samples within each group. The axes show the percentage of variance explained by PC1 and PC2, providing insight into the data's dimensionality and group separation. The loadings plots for PC1 (b and e) and PC2 (c and f) are shown against the ppm axis. Gaps in the figures are the water signal and EDTA signal locations, removed to eliminate their influence on the data. The bNMR data (a, b, and c) is shows in the top three figures and the bottom three figures are for the HF-NMR data (d, e, and f).

6.3.5.3 OPLS-DA: Discriminating Difficult-To-Control Asthma from Well Managed Asthma

To enhance group separation and identify the metabolites contributing most to the differences between groups, OPLS-DA was conducted. The OPLS-DA plot in *Figure 54*a and d illustrate the separation of samples based on their respective groups. The plots clearly show a distinct separation between the MA (green) and DTC (red) groups for the HF-NMR data, with 95% confidence ellipses further confirming the clustering. Notably, there was no overlap observed in the HF-NMR OPLS-DA plot, and minimal overlap was observed in the bNMR OPLS-DA plot. Permutation testing with 2,000 permutations revealed significant differences between the observed Q2 value of 0.495 ($p<0.001$) and R2 value of 0.762 ($p<0.001$) for the HF-NMR data. Conversely, the bNMR data exhibited results lacking in predictive power (Q2: 0.339, $p<0.001$), but sufficient separation between the two groups (R2: 0.907, $p = 0.023$). The VIP and scores plots show some similarities between spectrometer types, especially between 4 - 5 ppm.

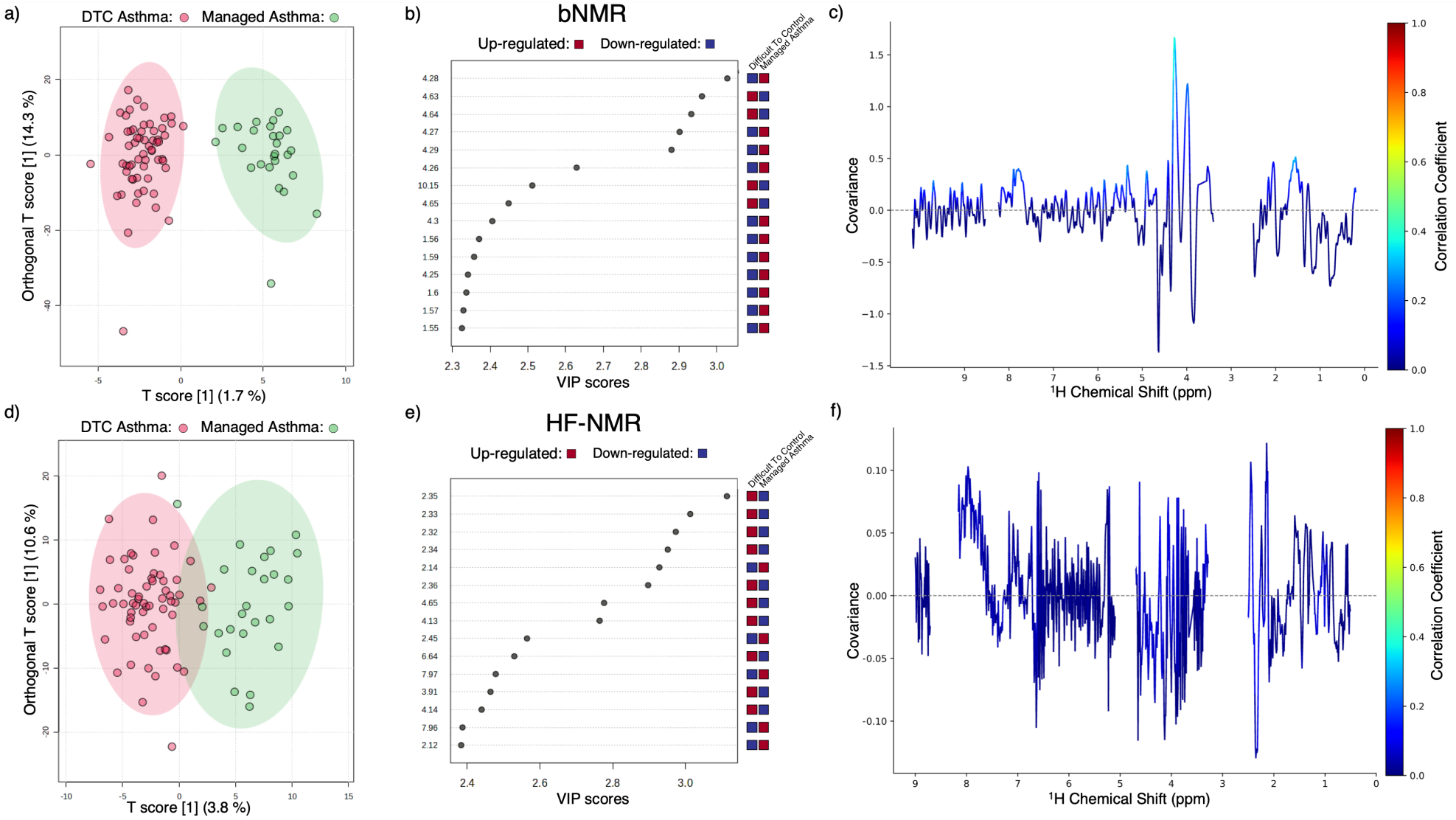

Figure caption on the next page.

Figure 54 - OPLS-DA plots (a and d) illustrating the differentiation of samples from MA shown in green, and DTC represented in red. Each data point corresponds to a sample and is colour-coded by group. The HF-NMR OPLS-DA (d) plot effectively distinguishes groups based on class membership and orthogonal variation, with the ellipses denoting the 95% confidence intervals for each group. Loadings plot for the OPLS-DA models (c and f) showing the contribution of individual metabolites to the group separation. The x-axis shows the chemical shift (ppm), and the y-axis represents the loading values. The top 15 bins and their VIP score are shown in b and e.

6.3.5.4 Univariate Receiver Operating Characteristic Biomarker Analysis

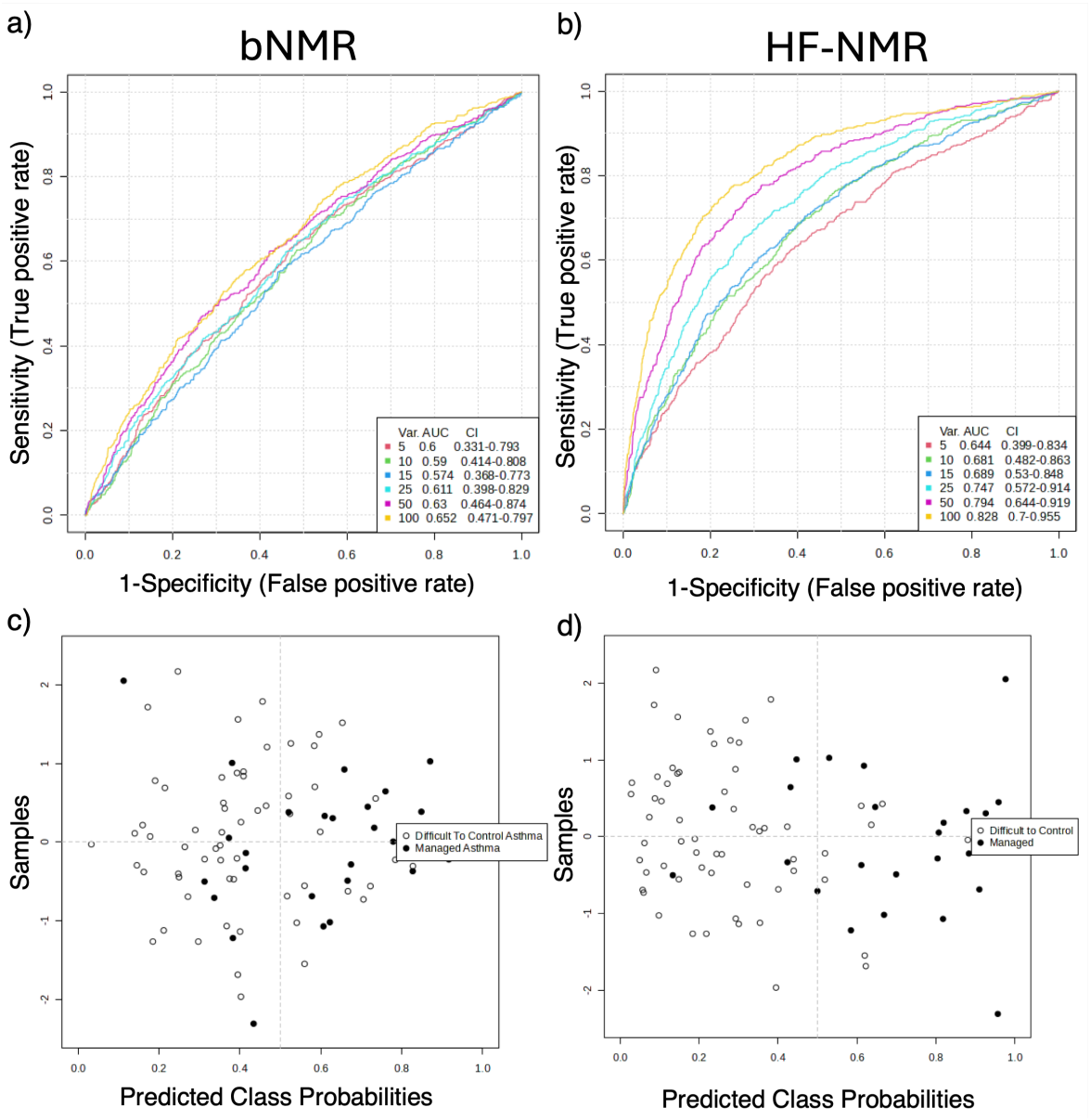

Figure 55 - ROC curves (a and b) showing the performance of biomarker models for distinguishing between Managed Asthma (MA) and Difficult-to-Control Asthma (DTC). The bNMR figures are displayed in a) and c) with the HF-NMR plots b) and d) on the right. The Area Under the Curve (AUC) indicates the accuracy of the biomarkers, with values closer to 1.0 indicating excellent discrimination. The plot includes sensitivity (true positive rate) on the y-axis and 1-specificity (false positive rate) on the x-axis. Plots c) and d) show the predicted class probabilities for all samples using a single biomarker model.

Multivariate exploratory ROC analysis indicates that using 100 variables yields the best AUC value of 0.652 (CI: 0.471–0.797), with a predictive accuracy of 61% for the bNMR data (Figure 55). In contrast, the same analysis for the HF-NMR set of 100 variables shows an AUC above 0.828 (CI: 0.7–0.955), achieving a predictive accuracy of 78%. The predicted class probabilities support these findings, with more samples incorrectly identified in the bNMR plot compared to the HF-NMR plot. These results support the findings observed in the OPLS-DA plots that the HF-NMR data is better at predicting between the disease states than the bNMR data.

Table 7 - Metabolites summarising the data from the bNMR and HF-NMR spectra comparing Difficult-to-control Asthma against Well Managed Asthma.

	bNMR							HF-NMR						
Metabolite	Regulation	VIP score	AUC	Sensitivity	Specificity	p-Value	FDR	Regulation	VIP score	AUC	Sensitivity	Specificity	p-Value	FDR
Acetate	Up	1.29	0.57	0.8	0.4	0.217	0.814	Up	0.58	0.57	0.6	0.6	0.928	0.981
Alanine	Down	1.33	0.60	0.7	0.5	0.238	0.829	Up	0.29	0.56	0.5	0.7	0.092	0.547
Creatine	Up	1.05	0.65	0.6	0.7	0.268	0.879	Up	2.46	0.70	0.8	0.7	0.101	0.505
Glucose	Down	0.42	0.56	0.6	0.7	0.695	0.970	Down	1.80	0.73	0.7	0.7	0.017	0.241
Glutamate	Up	0.70	0.52	0.7	0.4	0.755	0.979	Up	3.11	0.80	0.7	0.9	0.098	0.503
Glutamine	Up	0.63	0.55	0.5	0.7	0.410	0.903	Down	0.33	0.53	0.7	0.5	0.030	0.295
Glycine	Down	0.35	0.57	0.5	0.7	0.986	0.999	Down	0.20	0.55	0.5	0.6	0.002	0.062
Histamine	Down	1.76	0.63	0.5	0.7	0.052	0.595	Down	1.28	0.62	0.5	0.7	0.058	0.399
Histidine	Down	1.55	0.74	0.8	0.7	0.063	0.643	Up	1.02	0.57	0.6	0.5	0.250	0.665
Isoleucine	Down	0.67	0.52	0.6	0.5	0.817	0.990	Up	0.58	0.53	0.5	0.6	0.016	0.237
Lactate	Down	0.58	0.52	0.6	0.5	0.538	0.960	Up	0.53	0.61	0.7	0.5	0.082	0.480
Leucine	Up	0.14	0.50	0.7	0.5	0.635	0.970	Up	0.21	0.56	0.6	0.6	0.001	0.041
Lysine	Up	1.17	0.54	0.4	0.6	0.778	0.985	Up	0.49	0.55	0.6	0.6	0.023	0.266
Methanol	-	-	-	-	-	-	-	Down	0.13	0.57	0.5	0.7	0.079	0.467
Phenylalanine	Up	1.23	0.58	0.6	0.5	0.218	0.814	Up	0.66	0.55	0.6	0.6	0.211	0.652
Tyrosine	Down	0.09	0.51	0.4	0.5	0.925	0.990	Down	0.10	0.57	0.5	0.7	0.164	0.581
Valine	Up	0.69	0.53	0.5	0.5	0.898	0.990	Down	1.02	0.62	0.6	0.7	0.035	0.984

ROC: receiver operating curve, FDR: false discovery rate, VIP: variable importance in projection

6.3.6. Comparison between Well Managed Asthma and Healthy Controls

The volcano plots (Figure 57a and c) reveal similar regions in both the HF-NMR and bNMR data sets when comparing MA (n = 26) and HC (n = 36). However, the bNMR data displays a larger number of significant FDR-modified bins compared to the HF-NMR data as shown in the Venn diagram in Figure 56. Specifically, the bNMR data shows more significant metabolites between 0-5 ppm, while the HF-NMR data only identified two significant metabolites in this range. In total, 148 bins were identified as significant in the bNMR data, whereas only 14 bins were identified as significant in the HF-NMR data. Notably, no matching bins were observed between the two data sets. This is despite similar bins around 8.00 ppm in bNMR and HF-NMR datasets both showing significant bins.

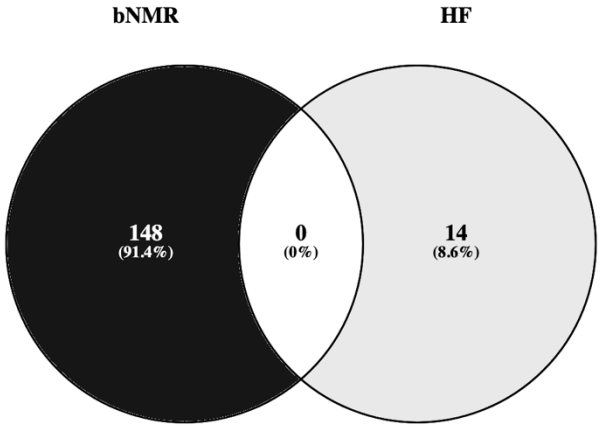

Figure 56 - Significant (< 0.05) false discovery rate (FDR) corrected associations between Healthy Controls and Managed Asthma for the bNMR and HF-NMR data, respectively.

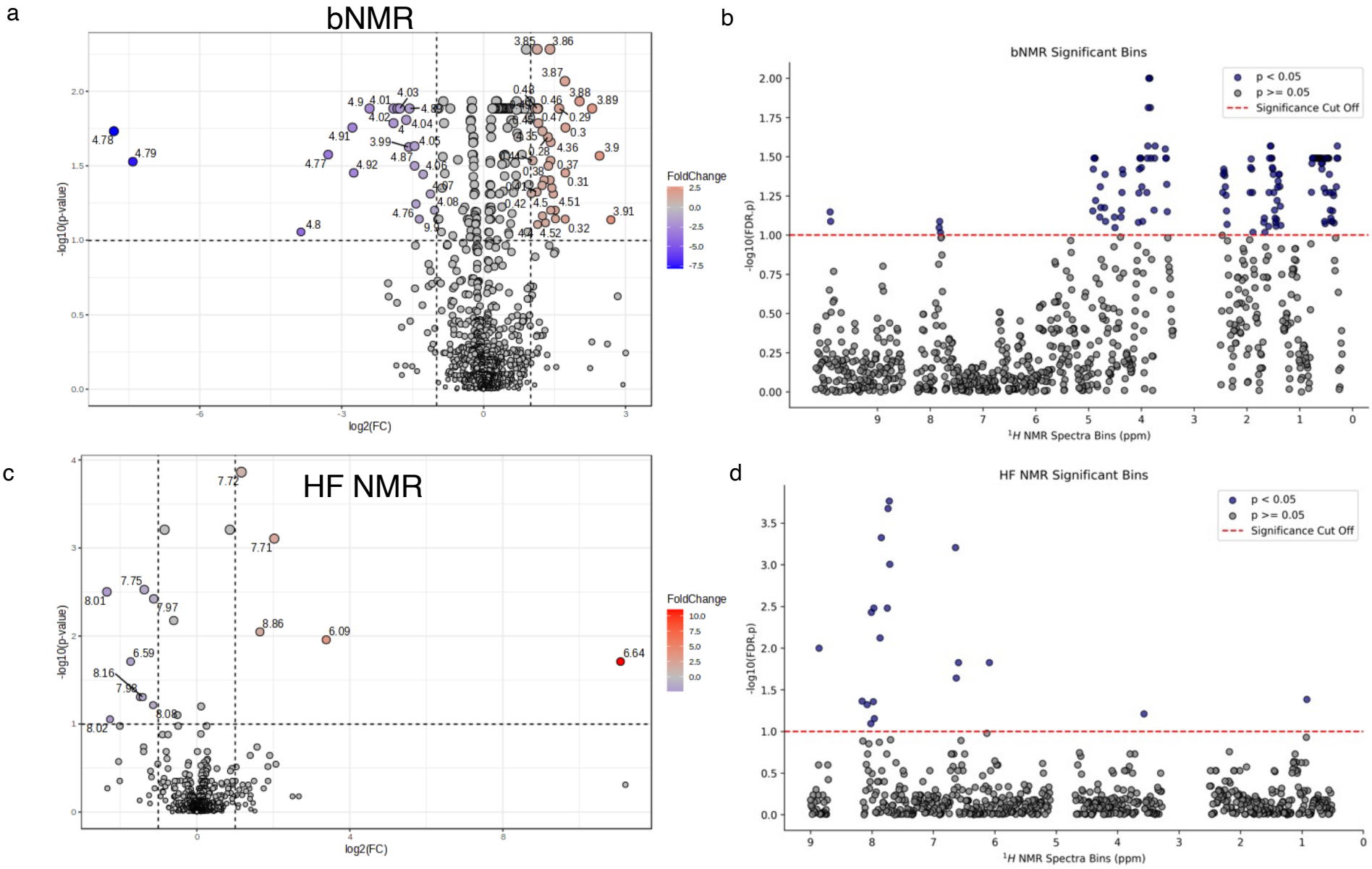

Figure caption on the next page

Figure *57* - Volcano and scatter plots of significant bins distinguishing between HCs and MA.

The volcano plots (a and c) show the log2 fold change on the x-axis and the -log10 p-value on the y-axis. Metabolites with significant changes are highlighted in red (increased) and blue (decreased). Scatter plots (b and d) display significant bins across the spectrum. The x-axis represents the bins, and the y-axis represents the -log10 FDR adjusted p-value. Significant bins (FDR adjusted p-value < 0.05) are highlighted, indicating their statistical significance in differentiating between groups. The top plots correspond to the bNMR data, while the bottom two plots relate to HF-NMR.

6.3.6.1 PCA: Principal Component Analysis of Healthy Controls Asthma and Well-Managed Asthma

The PCA plots (*Figure 58*) indicate that there is no significant overlap between the two groups. The Healthy group shows a larger variance than the MA group, with two principal components explaining 45.2% of the variance. In contrast, the HF-NMR PCA plot shows no separation between the groups, with PC1 and PC2 explaining a total of 55.9% of the variance. Furthermore, four outliers were observed in the bNMR group, whereas only two outliers were identified in the HF-NMR group.

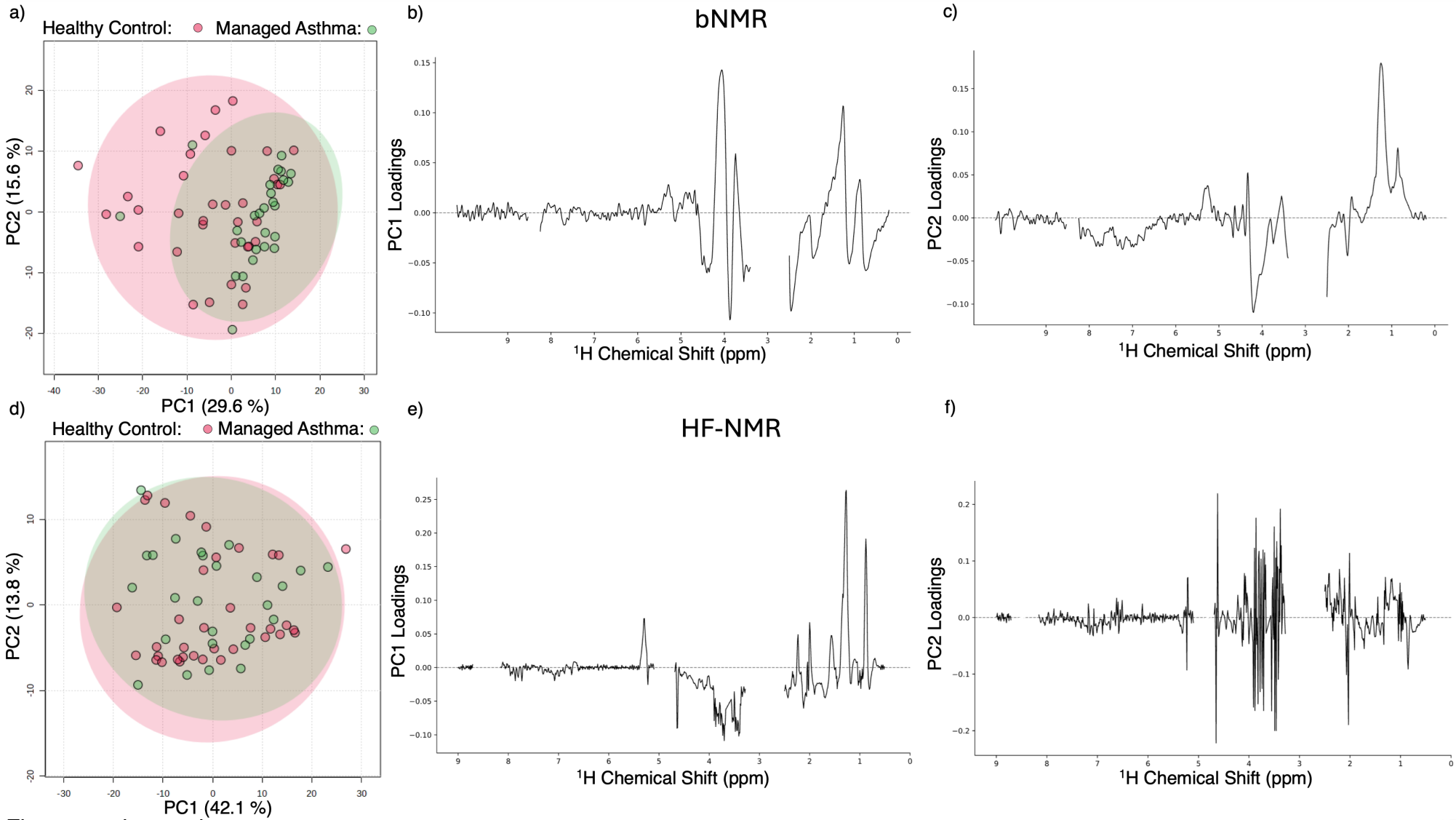

Figure caption on the next page.

Figure *58* - Principal Component Analysis (PCA) plots (a and d) illustrating the distribution of samples across two principal components (PC1 and PC2) for the bNMR and HF-NMR data respectively.

Each point represents a sample, colour-coded by group: MA in green (n = 26), and HC in red (n = 60). The ellipses represent the 95% confidence intervals for each group, indicating the spread and central tendency of the samples within each group. The axes show the percentage of variance explained by PC1 and PC2, providing insight into the data's dimensionality and group separation. The loadings plots for PC1 (b and e) and PC2 (c and f) are shown against the ppm axis. Gaps in the figures are the water signal and EDTA signal locations, removed to eliminate their influence on the data. The bNMR data is shows in the top three figures and the bottom three figures are for the HF-NMR data.

6.3.6.2 OPLS-DA: Discriminating Managed Asthma from the Healthy Controls

The OPLS-DA analysis shows excellent separation for both the bNMR and HF-NMR data sets. For the bNMR data, the R^2 value is 0.906 ($p < 0.001$), with a Q^2 value of 0.288 ($p < 0.001$). In the case of the HF-NMR data, similar results are observed, with only a few outliers detected in the healthy cohort and just one sample outside the 95% confidence region in the MA group. The distinction between groups is primarily driven by metabolites between 6-9 ppm, which include aromatic metabolites such as tyrosine, histamine and histidine. The R^2 value for the HF-NMR analysis is 0.921 ($p < 0.01$), and the Q^2 value is 0.532 ($p < 0.001$).

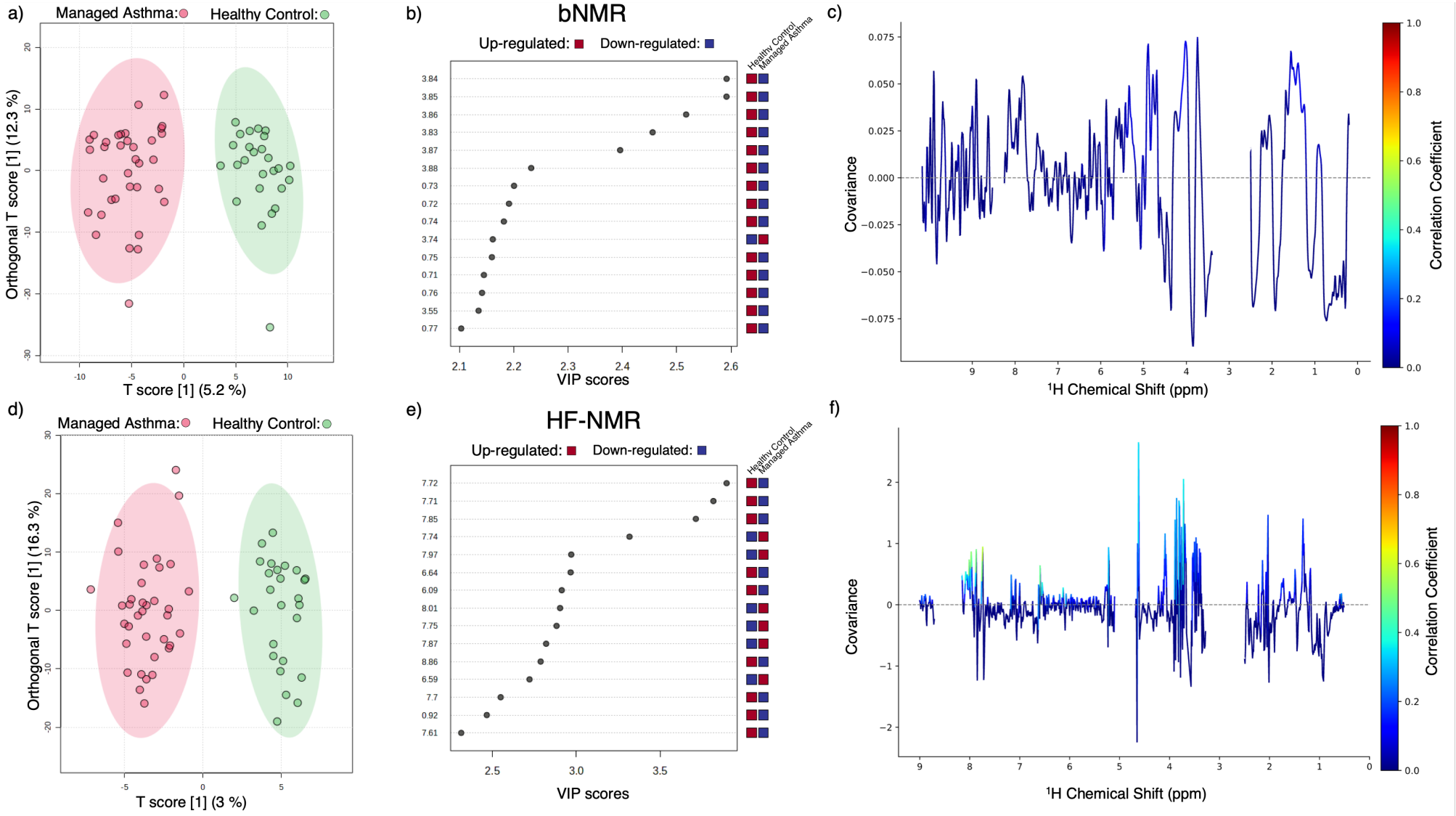

Caption on the next page.

Figure 59 - OPLS-DA plots (a and d) illustrating the differentiation of samples from MA shown in green, and HC represented in red. Each data point corresponds to a sample and is colour-coded by group. The plot effectively distinguishes groups based on class membership and orthogonal variation, with the ellipses denoting the 95% confidence intervals for each group. Loadings plots (c and f) for the OPLS-DA showing the contribution of individual metabolites to the group separation. The x-axis shows the chemical shift (ppm), and the y-axis represents the loading values. The top 15 bin and thier VIP score are shown in b and e corresponding to bNMR and HF-NMR respectively.

6.3.6.3 ROC Univariate Biomarker Analysis

The SVM classification method identified 100 variables with the highest AUC value at 0.774 (CI: 0.538-0.918) for the bNMR data, resulting in a predictive accuracy of 69%. The HF-NMR data, ROC analysis also demonstrates that the AUC value strengthens with an increase in the number of variables. Using 100 variables, the AUC reached 0.834 (CI: 0.743-0.947). The predictive accuracy of these two classification methods was the closest matched than previously seen for the other categories compared.

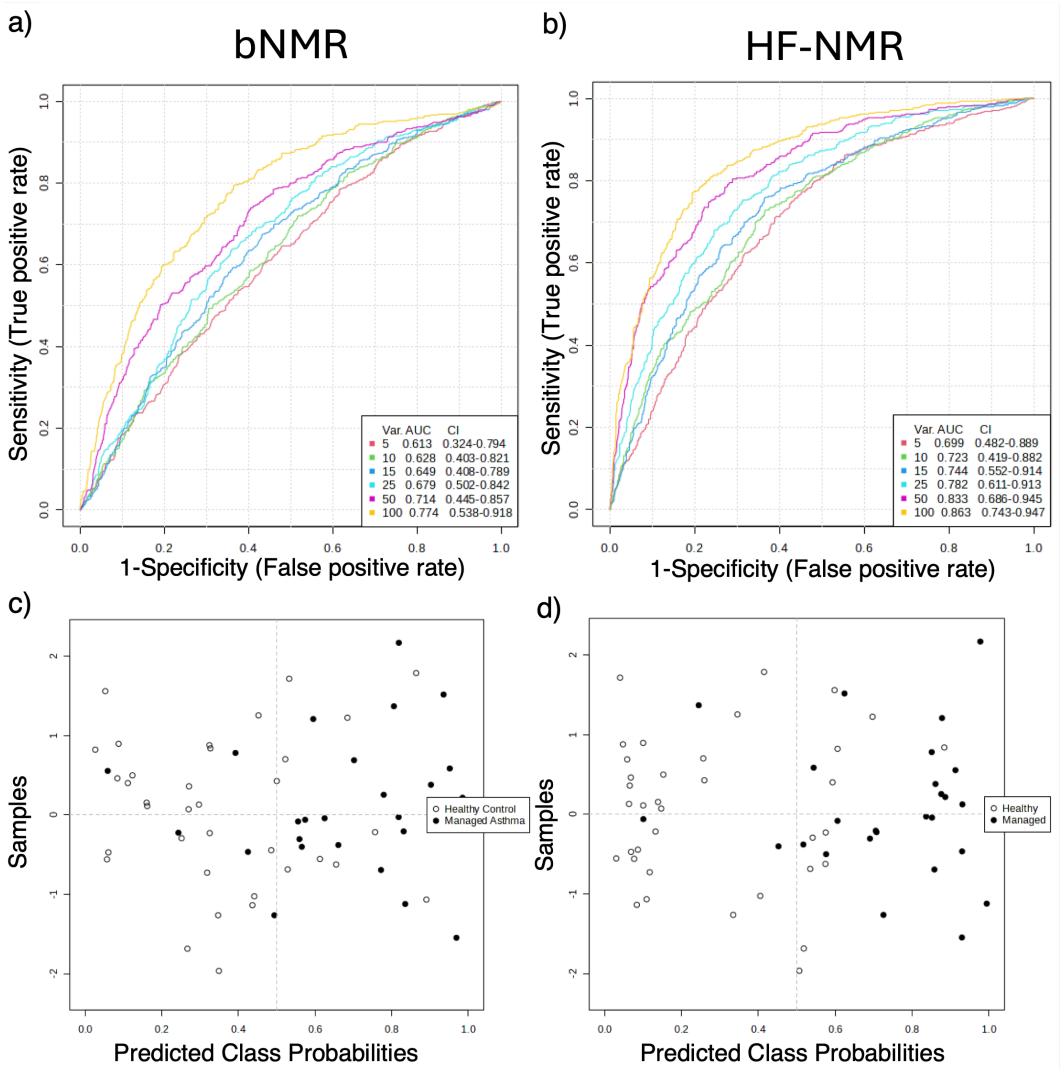

Figure 60 - ROC curve (a and b) showing the performance of biomarker models for distinguishing between MA and HC. The bNMR figures are displayed on the left (a and c) and the HF-NMR plots are on the right (b and d). The AUC indicates the accuracy of the biomarkers, with values closer to 1.0 indicating excellent discrimination. The plot includes sensitivity (true positive rate) on the y-axis and 1-specificity (false positive rate) on the x-axis. Plots c and d: Plot of predicted class probabilities for all samples using a single biomarker model.

.

Table 8 - Metabolites summarising the data from the bNMR and HF-NMR spectra comparing Healthy Controls against Well Managed Asthma.

	bNMR							HF-NMR						
Metabolite	Regulation	VIP score	ROC	Sensitivity	Specificity	p-Value	FDR	Regulation	VIP score	ROC	Sensitivity	Specificity	p-Value	FDR
Acetate	Up	2.02	0.73	0.7	0.7	0.003	0.037	Up	0.11	0.51	0.5	0.6	0.928	0.981
Alanine	Down	1.58	0.70	0.8	0.6	0.009	0.069	Down	0.69	0.59	0.6	0.7	0.129	0.547
Creatine	Up	1.44	0.62	0.6	0.7	0.005	0.032	Up	1.21	0.62	0.7	0.6	0.101	0.505
Glucose	Down	0.41	0.59	0.5	0.7	0.293	0.582	Down	1.81	0.69	0.6	0.7	0.017	0.241
Glutamate	Up	1.46	0.68	0.7	0.7	0.041	0.180	Up	1.56	0.63	0.6	0.7	0.098	0.503
Glutamine	Up	1.89	0.73	0.7	0.7	0.005	0.049	Up	1.23	0.64	0.8	0.5	0.030	0.295
Glycine	Up	2.14	0.81	0.9	0.7	0.000	0.028	Up	2.10	0.71	0.6	0.8	0.002	0.062
Histamine	Down	1.48	0.71	0.6	0.9	0.018	0.082	Up	1.82	0.65	0.6	0.8	0.058	0.399
Histidine	Down	2.09	0.83	0.8	0.7	0.002	0.032	Up	0.98	0.61	0.7	0.5	0.250	0.665
Isoleucine	Up	0.97	0.60	0.5	0.7	0.339	0.628	Up	1.64	0.67	0.6	0.7	0.016	0.237
Lactate	Down	1.19	0.64	0.6	0.7	0.040	0.272	Down	1.00	0.59	0.7	0.5	0.082	0.480
Leucine	Down	0.51	0.54	0.7	0.4	0.233	0.502	Up	1.33	0.61	0.7	0.6	0.001	0.041
Lysine	Up	1.83	0.75	0.7	0.7	0.006	0.038	Up	1.35	0.66	0.8	0.6	0.023	0.266
Methanol	-	-	-	-	-	-	-	Up	1.58	0.65	0.7	0.7	0.079	0.467
Phenylalanine	Down	0.43	0.56	0.7	0.5	0.500	0.748	Up	1.17	0.64	0.7	0.6	0.211	0.652
Tyrosine	Up	0.42	0.57	0.6	0.5	0.422	0.695	Up	1.01	0.60	0.7	0.5	0.164	0.581
Valine	Up	1.40	0.69	0.7	0.7	0.043	0.185	Up	1.78	0.51	0.5	0.7	0.076	0.295

ROC: receiver operating curve, FDR: false discovery rate, VIP: variable importance in projection

6.4. Discussion:

Traditional asthma monitoring methods rely heavily on patient-reported symptoms, medication use, and daily activity interference, however, these approaches often fail to provide an accurate assessment of asthma severity.224,228,229 This study aimed to explore the potential of bNMR spectroscopy as a cost-effective solution for analysing biological samples and detecting phenotypes of asthma. By comparing bNMR results with HF-NMR, this research aims to evaluate the effectiveness of bNMR in detecting asthma and identifying relevant metabolites at this lower sensitivity.

6.4.1. Metabolite Changes Between Well-Managed Asthma and Healthy Controls

In a comparison between healthy individuals and those with well-managed asthma, it was discovered that the concentrations of glutamine, glycine, and lysine were lower in the latter group. These three metabolites were considered the most significant and were consistent with both the bNMR and HF-NMR datasets. However, glutamine and glycine did not meet the FDR threshold (FDR<0.05) in the HF-NMR dataset in contrast to the bNMR dataset. Therefore, lysine was the only bin that was FDR significant across datasets. Additionally, five other metabolites, namely acetate, creatine, glutamine, glycine, and histidine, were deemed significant in the bNMR data.

The most comparable study, conducted by Jung *et al.* (2013), analysed healthy individuals and those with asthma using HF-NMR.[238] They identified asthmatic patients to be characterised by increased levels of methionine, glutamine, and histidine and by decreased levels of formate, methanol, acetate, choline, O-phosphocholine, arginine, and glucose. This aligns with the findings present in this study with glutamine, methanol, acetate and glucose aligning with disease regulation and histidine aligning with the HF-NMR results.[238] However, Jung *et al.* (2013) emphasised the need for further investigation due to their relatively small sample size (n = 65) compared to the larger cohort presented in this chapter (n = 122).[238]

Although histamines' high bNMR VIP score suggests a significant contribution, the regulation of this bin was the opposite between datasets. However, the bin was not significant in the HF-NMR dataset although this correlates with Jung et al. (2013) study. This could be a result of overfitting of the model in this bin, but it could also be a result of overlap of nearby proteins and lipids, which are known to have an effect on spectra.

Three other metabolites did not correlate between datasets, these were phenylalanine, leucine, and histidine.[239] Phenylalanine did not meet the significance threshold and had no significant statistics pointing towards its significance in the bNMR data, even though its metabolite regulation matched the literature. The HF-NMR data showed some significance from the VIP (1.17) and ROC (0.6) scores with an increase in healthy controls. However, this contrasts with studies that used GC-MS and NMR, which reported phenylalanine as higher in asthmatic patients, although, these findings were observed in a urine study and not a plasma-based study. study.[238,242]

Leucine was also identified in these papers as having a low concentration in asthmatics. This result agrees with the bNMR data, even though the data suggests a lack of importance for this metabolite from other metrics such as the VIP score and ROC value. This was significant in the HF-NMR data but reported that leucine is higher in asthmatics, conflicting with existing research. Due to the lack of sample preparation taken in this study, lipids acting as relaxation mechanisms could have affected the intensity of the metabolite.[237]

Histidine has been reported as decreased in asthmatics, which agrees with the bNMR results but not the HF-NMR results which were insignificant.[238,242] Moreover, the metabolites creatine, glucose, isoleucine, lactate, and valine were all significant in the bNMR and HF-NMR datasets, with the results aligning with existing research. This suggests that asthma can be detected through both bNMR and HF-NMR.

6.4.2. Metabolite Changes Between Difficult-To-Control and Healthy Controls

Six metabolites, namely alanine, glutamine, isoleucine, lactate, lysine, and valine, displayed consistent regulation patterns across both datasets (bNMR and HF-NMR), suggesting their potential as robust biomarkers for discriminating between the DTC and HC groups. However, discrepancies were observed for several metabolites which have been previously reported in asthma pathogenesis. Notably, histamine, emerged as the most promising candidate in the HF-NMR data, based on its high VIP and ROC score, although it failed to reach statistical significance in the bNMR dataset. This discrepancy could be attributed to the lower sensitivity of bNMR spectrometers compared to their HF-NMR counterparts, leading to potential signal overlap or a relatively low abundance of the metabolite.

Three metabolites, glycine from the bNMR dataset and glutamine and histamine from the HF-NMR dataset, displayed significant AUC values, indicating their potential as diagnostic biomarkers.[237,242] However, their significance levels did not align between the two datasets, possibly due to variations in signal resolution or peak overlap. After applying an FDR correction, only two metabolites, glycine and lactate, retained statistical significance in the bNMR dataset. While lactate was also FDR corrected and significant in the HF-NMR data, glycine did not reach significance, potentially due to signal overlap with glucose or other nearby metabolites. These findings suggest that a subset of metabolites, including glycine and lactate, could serve as valuable biomarkers for detecting and differentiating DTC asthma from HCs.

6.4.3. Metabolic Changes Between Asthma Phenotypes

The comparison between the DTC and MA groups revealed several notable findings. In the bNMR data, no individual metabolite bins reached statistical significance after an FDR correction was applied. This lack of significant results could be attributed to the lower sensitivity of benchtop spectrometers compared to their HF counterparts, but may also be bNMR struggling to distinguish between closely related phenotypes.

Despite this limitation, histamine emerged as the most promising candidate for distinguishing between DTC and MA in both bNMR and HF-NMR datasets. Histamine exhibited high VIP scores (1.76 in bNMR and 1.28 in HF-NMR) and moderate ROC values (0.63 in bNMR and 0.62 in HF-NMR), indicating its potential as a biomarker for discriminating between the two asthma phenotypes. Glucose and glutamate also showed promise as potential biomarkers, with glucose displaying a high VIP score (1.80) and ROC value (0.73) in the HF-NMR data, and glutamate exhibiting a high VIP score (3.11) and ROC value (0.80) in the same dataset. The HF-NMR data showed that leucine was the only metabolite with FDR-corrected statistical significance yet lacked power in discriminating between the disease types as seen in the VIP (0.21) and ROC (0.56) scores.

The variations observed between the bNMR and HF-NMR datasets can be attributed to several factors. Differences in peak widths and signal resolution between the two spectrometer types can lead to the potential overlap of closely located metabolite signals, resulting in signal suppression or masking especially in bNMR. Additionally, the closely matched metabolomic profiles of the DTC and MA groups suggest that the subtle differences between these asthma phenotypes may require higher sensitivity and resolution to be accurately distinguished.

6.4.4. Biomarkers and their Asthma Phenotypes

Histamine is a well-established mediator of allergic inflammation and asthma pathogenesis, released from mast cells and basophils upon exposure to allergens or irritants.[243] In this study, histamine emerged as a key biomarker distinguishing not only MA from healthy controls but also DTC from MA. This finding is biologically coherent: poorer disease control is typically associated with heightened airway inflammation and mast cell activation, both of which increase histamine release.[243] Lysine, another key metabolite identified, plays a critical role in regulating inflammatory gene expression through lysine acetylation, a post-translational modification that modulates chromatin accessibility and cytokine transcription in activated immune cells.[244]

Several amino acids identified in this study, including glycine, glutamine, and glutamate, are known mediators of immunological activity and antioxidant defence in asthma.[245] Phenylalanine, conversely, has been reported to exert adverse pro-inflammatory effects when elevated. These observations are consistent with the metabolite profiles reported here.[245] Changes in lactate levels further support metabolic reprogramming within the asthmatic airway.[246] Increased lactate production reflects a shift from oxidative phosphorylation to aerobic glycolysis, akin to the “Warburg effect” observed in cancer cells, suggesting that immune and epithelial cells in inflamed airways may adopt similar metabolic strategies.[246] Given this overlap, future studies should ensure that biomarker panels can discriminate asthma-related metabolic reprogramming from cancer-associated signatures. The observed alterations in glucose metabolism also support the notion of energy pathway remodelling, with the direction and magnitude of change dependent on disease severity and inflammatory burden.[247]

The relative decreases in lysine, glutamine, and glycine observed among asthmatic patients align with multiple independent studies implicating amino acid pathway perturbations as central features of asthma.[245] Glutamine, in particular, is consumed by activated immune cells at rates comparable to or exceeding glucose.[245,247] Its depletion reflects the high metabolic demands of chronic inflammation, while supplementation has been shown to attenuate allergic airway inflammation *via* increase of MAPK phosphatase-1.[248] These findings suggest that reduced glutamine availability may contribute to persistent inflammatory signalling in asthma.

Glycine serves as a key precursor for glutathione synthesis, the principal antioxidant in the respiratory tract. Its depletion likely reflects increased oxidative stress, a defining feature of chronic asthma.[245] Similarly, lysine’s role in post-translational acetylation links its metabolism to transcriptional regulation of immune responses, underscoring its relevance to the inflammatory phenotype observed.[244]

The elevation of lactate in asthmatic patients is particularly noteworthy. It represents a fundamental shift in cellular energy metabolism, wherein activated immune and structural cells rely more heavily on glycolysis even under oxygen-rich conditions.[246,248] This metabolic reprogramming supports rapid cellular proliferation, cytokine production, and tissue remodelling. Moreover, chronic airway remodelling and mucus plugging can create localized hypoxic environments that further promote lactate accumulation, making it both a marker and potential driver of disease progression.

Histamine also emerged as the strongest discriminator between DTC and MA phenotypes in the HF-NMR dataset. As a principal mediator released during mast cell degranulation, histamine induces bronchoconstriction, increases vascular permeability, and amplifies local inflammation.[243] Its higher levels in DTC asthma suggest enhanced mast cell activity and more severe allergic inflammation in this phenotype.[243] The absence of histamine as a significant feature in the bNMR dataset likely reflects its relatively low abundance and the spectral resolution limits of lower-field instrumentation, emphasising the importance of analytical sensitivity when detecting low-concentration metabolites.

Overall, the metabolic signatures identified in this study demonstrate strong biological plausibility and align closely with prior metabolomics literature on asthma. A recent systematic review of 21 asthma metabolomics studies reported that amino acids (notably glycine, glutamine, and alanine), lactate, acetate, and metabolites related to oxidative stress and immune function are consistently associated with asthma across populations, biospecimens, and analytical platforms. This convergence supports the robustness of the findings presented here and strengthens confidence that the biomarkers identified reflect genuine metabolic perturbations in asthma pathophysiology rather than analytical artefacts or random variation.

6.5. Conclusion

This study highlights the potential for bNMR to be used as a cost-effective screening tool for asthma. Through the comparison of OPLS-DA and AUC results with HF-NMR data, this research has identified key metabolites, such as lysine, glutamine, glycine, and lactate, as consistent biomarkers to distinguish between MA and control samples. Additionally, histamine and glucose emerged as potential candidates for differentiating between managed asthma (MA) and difficult-to-control (DTC) asthma, though their significance was only validated in the HF-NMR data, suggesting difficulty in the ability of bNMR to distinguish between disease phenotypes.

Further optimisation of minimal sample preparation and data acquisition protocols, as well as the utilisation of complementary analytical techniques and larger cohorts, are warranted to validate and characterise these potential biomarkers for their diagnostic and prognostic utility in asthma management.

In conclusion, this research demonstrates that bNMR can reliably detect metabolic changes in asthma, supporting its role as a complementary tool to HF-NMR. However, the differentiation of disease phenotypes may require the higher sensitivity and resolution offered by advanced analytical platforms. By addressing these limitations and continuing to refine methodologies, bNMR could play a pivotal role in expanding the accessibility of metabolomics and its prognostic utility for asthma diagnostics.

Chapter 7 Type II Diabetes Monitoring, Detection, and Bariatric Surgery Outcome Prediction

7.1. Introduction

Diabetes mellitus (DM) is a non-communicable disease characterised by impaired insulin production or sensitivity, which pertains to periods of hyperglycaemia and hypoglycaemia.[249–251]The micro- and macrovascular complications arising from DM were identified in 2019 as the primary cause of approximately 100,000 cases of heart failure, 27,000 cases of myocardial infarctions and a minimum of 10,300 cases of end-stage renal disease annually.[252–257]

Further complications for patients with DM include preventable sight loss and a risk of limb amputation that is 20 times greater than their healthy counterparts.[252–257] However, serious complications can be mitigated through tight glycaemic control, achieved primarily *via* continual monitoring of blood glucose (BG) levels and frequent medical interventions.[255,258–260] DM is a broad term that includes type 1 diabetes mellitus (T1DM) and type 2 diabetes mellitus (T2DM). T1DM is defined by the destruction of insulin-producing β cells of the pancreas, often as part of an autoimmune response.[252,257,261,262] As a result, BG levels need to be monitored and appropriately managed by routine injections of insulin into adipose tissue.[263][264] Although the aetiology of T1DM is not fully understood, genetic predispositions contribute to an increased risk of β cell destruction. This destruction can also be induced by infections which affect immunoregulation.[255,265,266]

Approximately 4.4 million people in the UK live with diabetes, with an additional 1.2 million living with T2DM who are undiagnosed.[267] T2DM presents as one of the most prevalent chronic metabolic disorders of the 21st century (~90% of all UK diabetes cases), despite its progression being largely preventable.[250][249,261] Unlike T1DM, the defining characteristics of T2DM include both progressive development of insulin resistance and chronic hyperglycaemia.[268,269] Insulin resistance in a clinical setting, is associated with elevated insulin due to compensation by the pancreas to attain normoglycemia; as a result, the pancreas is overworked to meet the required insulin levels. Over time, the pancreas becomes less effective and

unable to produce sufficient insulin, leading to chronic hyperglycaemia. Although the exact pathology of insulin resistance is complex, the majority of causal factors include advanced age, genetic predispositions, and lifestyle factors such as lack of activity and poor diet leading to obesity.[262] A combination of any of these factors and the infrequency of regular DM screening could support a high persistence of T2DM in older populations.[262] The vast majority (97.5%) of T2DM cases are associated with at least one co-morbidity, whilst 88.5% of patients suffer from at least two co-morbidities, which are often linked in their pathology.[261] Health complications can begin to develop 5-6 years before a patient is diagnosed with T2DM and these complications could be avoided by identifying potential biomarkers associated with early-stage T2DM and implementing different monitoring techniques.[268,269]

High BG levels are a primary manifestation of DM, however despite hyperglycaemia having a complex etiological process, elevated plasma glucose levels and glycated haemoglobin are currently the sole biomarkers for diabetes diagnosis.[268] There are two direct methods of BG testing for DM diagnosis: the fasted plasma glucose test (FPG) or the oral glucose tolerance test (OGTT).[270,271] An indirect method (HbA1c) is based on measuring glucose by the percentage of glycated haemoglobin, which can have a strong positive correlation with chronic hyperglycaemia.[272,273] A diagnostic guide for diabetes and prediabetes is shown in Table 9. DM is often determined after two positive tests at different time points to mitigate the effects of daily perturbations. However, such techniques lack predictive capacity.

Table 9 - Diagnostic criteria for diabetes and pre-diabetes.

	Normal/ Non-diabetic	**Pre-diabetes**	**Diabetes**
FPG (mmol/L)	< 5.5	5.5 – 7.0	> 7.0
OGTT (mmol/L)	< 7.8	7.8 – 11.1	> 11.1
HbA1c (mmol/L)	< 42	42 – 47	> 47

The HbA1c test assesses chronically elevated BG and can be used to complement other tests for diagnosing the development of T2DM. Although factors such as age and ethnicity can impact haemoglobin glycation, measuring the percentage of

HbA1c can provide a representation of BG level for the previous 8 -12 weeks.[273–276]

Compared to the FPG and OGTT tests, the HbA1c test is not affected by fasting status or perturbations caused by stress or illness.[273,277] Despite these advantages, the accuracy of the test has been questioned.[277–279] The technique relies on the glycation of haemoglobin, a process that occurs over the lifespan of erythrocytes (red blood cells), which typically live for around 120 days.[277] Any variation in the rate of erythrocyte turnover, such as increased production or destruction, can affect the HbA1c reading, potentially leading to inaccurate results.[277] For example, individuals who are pregnant, suffer from sickle cell anaemia, or have experienced a large volume of blood loss often have altered erythrocyte turnover. In cases of blood loss, this is due to accelerated production of new erythrocytes to compensate for the loss, while in sickle cell anaemia, abnormal erythrocyte destruction shortens their lifespan.[277] These factors compromise the reliability of the HbA1c test in such cohorts. As a result, BG is traditionally measured *via* the FPG or OGTT in these cohorts.[280]

Unlike the HbA1c test, the FPG test can diagnose DM without having to account for patient-specific variables such as age or sex, which makes its application straightforward in comparison to the HbA1c test. However, patient adherence to the minimum 8-hour fasting period can be challenging to control. Moreover, the presentation of intercurrent diseases and conditions such as infection, stress medication, recent dietary intake and dehydration has the potential to affect the test results; thus, is a limitation of the FPG test's effectiveness.[271,281–283] Another factor to consider is that without the presence of clear clinical symptoms, such a test needs to be repeated or confirmed by another test such as the OGTT to provide a more stable and reliable measure of BG regulation.[271,281–283]

The OGTT has been recommended as an early diagnostic test for T2DM in patients who are gaining weight and have HbA1c within a pre-diabetes range. This test measures blood glucose levels before, and at regular intervals after, consuming a glucose drink to monitor the body's ability to process sugars.[281] Similar to FPG, the OGTT is considered a low-risk test that can be used for pregnant women and other patients who are unable to receive accurate results with HbA1c

testing.[256,281,284] However, in order to obtain reliable results analysis needs to be completed over multiple days, with at least 8 hours of fasting before sample collection takes place.

The global increasing prevalence of obesity and its related comorbidities, notably T2DM, represents, an escalating global public health crisis.[147] With the International Diabetes Federation predicting a T2DM prevalence at 10.5%, innovative approaches to management and treatment are crucial.[147] Bariatric surgery has emerged as a powerful tool for achieving effective and long-lasting weight loss, significantly impacting T2DM remission and glycaemic control.[285] Over 50,000 bariatric surgeries took place from 2012 – 2022 in the UK.[286–288] Although mortality rates associated with bariatric surgery remain low at 0.13%, surgical outcomes remain variable with 15% of cases unable to achieve weight loss.[288–290] Factors contributing to this include non-adherence to post-surgery guidelines, psychological challenges, and metabolic differences. Bariatric surgery also comes at a huge cost, with procedures ranging between $12,000 to $30,000 in America.[291]

The ability to predict the outcomes of bariatric surgery is a pivotal goal of this field, allowing for the risks associated with surgery to be minimised, along with cost benefits to healthcare providers to be better managed.[292] Several predictive models have been developed, including the DiaRem score, which considers factors such as age, HbA1c levels, and medication usage.[293–295] The ABCD model incorporates additional patient-specific characteristics (age, body mass index, C-peptide, and diabetes duration).[294] Despite their potential, the complexity of these models may limit their widespread implementation. While these models have shown promise, their reliance on static, predefined variables limit their adaptability to individual patients that might not capture subtle variations influencing surgical success.

Alternatively, metabolites could be used as predictors from non-invasive biofluids such as urine or saliva. Recent advancements in the application of metabolomics, specifically NMR spectroscopy, have offered a promising avenue toward achieving this goal.[296] Metabolomics enables the comprehensive analysis of small-molecule metabolites within biological systems, providing an in-depth understanding of the biochemical changes associated with obesity, T2DM, and a patient's response to surgical intervention.[296] While high-field NMR (HF-NMR) has limited clinical

applications due to its costly maintenance and operation, benchtop NMR (bNMR) is emerging as a cost-effective solution for investigating T2DM and other metabolic conditions.[108,297–302] This cost reduction comes at the expense of sensitivity and as such studies need to be undertaken in conjunction with HF-NMR to fully understand its utility for healthcare applications.[297]

Three diabetes studies using bNMR have been conducted to date, where diabetes is able to be detected from healthy individuals, however further work on pre-diabetes and other factors affecting the metabolome such as surgery have not yet been explored.[108,297–302] Unlike static predictive models, bNMR can identify real-time biomarkers to provide a comprehensive view of the biochemical landscape pre- and post-surgery. This approach allows for identifying subtle metabolite variations linked to weight loss, glycaemic control, and overall surgical outcomes, potentially improving prediction accuracy. Additionally, bNMR's ability to generate reproducible, high-throughput data could make it a more scalable solution for healthcare systems, enabling dynamic, data-driven adjustments to patient care. These advantages highlight the potential of metabolomics to address the limitations of traditional models, paving the way for more effective and personalised bariatric surgery planning.[297]

As well as testing the detection capabilities of bNMR, this study investigated three different bariatric surgery methods: biliopancreatic diversion (BPD), laparoscopic greater curvature plication (LGCP), and laparoscopic adjustable gastric banding (LAGB). Although all three methods reduce stomach capacity, they function through distinctly different mechanisms, with some involving more drastic surgical procedures. BPD involves removing a large portion of the stomach and bypassing the majority of the small intestine. This surgery can often lead to significant weight loss through restriction and malabsorption, as well as nutritional deficiencies that can require long-term vitamin and mineral supplementation. LAGB is less invasive and involves placing an adjustable band around the stomach to restrict the intake and size of the stomach. This procedure often leads to less weight loss than BPD and is subject to complications like band slippage or erosion. LGCP also reduces the stomach size by folding the stomach in on itself and suturing the greater curvature without removing any stomach tissue or bypassing the intestine. Like the

LAGB surgery, LGCP is less invasive but typically results in less weight loss than other procedures.

Limited research has been conducted on these surgery types with BPD being updated with Roux-en-Y gastric bypass, often called RYGB for short. RYGB is another type of bariatric surgery that is more commonly used than BPD for a more drastic change in weight loss. RYGB creates a smaller stomach pouch and reroutes the small intestine to limit food intake and nutrient absorption. Much like BPD, it can also lead to nutritional deficiencies. Figure 61 shown below, includes these four types of surgery and how they differ. It is unknown how BPD, LAGB, LGCP change the metabolome and if these changes are detectable by bNMR.

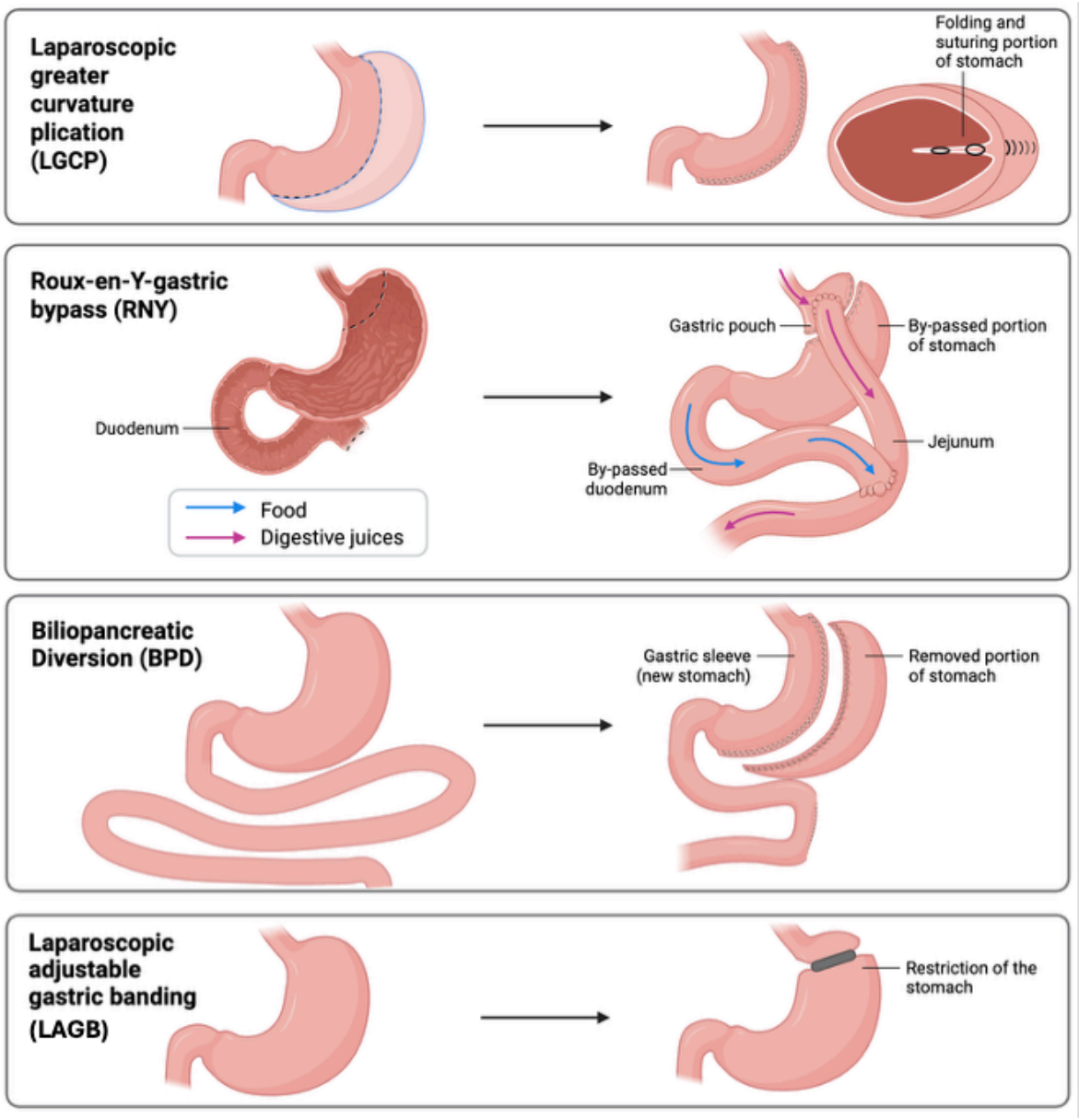

Figure 61 - Different types of bariatric surgery and their medical procedure.294

This chapter will address three main questions. Firstly, can bNMR technology monitor diabetes progression (healthy, pre-diabetic and diabetic) through a patient's urine sample. Secondly, can bNMR distinguish differences in metabolome among patients who have undergone gastric surgery. Finally, can it be used as a predictor of outcomes. The bNMR analysis will be compared against HF-NMR for validation. This study focuses on using urine as a non-invasive biofluid and bNMR technology to develop better tools for monitoring and predicting outcomes in bariatric surgery and managing T2DM. This research through the evidence-based demonstration of utility could have significant implications for personalised treatment strategies and improved patient care in the field of bariatric surgery.

7.2. Materials and Methods

7.2.1. Ethics Declaration

This study was approved by the Ethics Committee of the Institute of Endocrinology (EC: 19/5/2009, Prague, Czech Republic) and Nottingham Trent University (integrated research application system (IRAS) code 81368). All study participants provided written and informed consent per the Declaration of Helsinki.[304]

7.2.2. Pre- and Post-Bariatric Surgery Samples

In total 54 patients were recruited for this study, with 41 Caucasian women providing urine. These participants are morbidly obese (BMI>35 Kg/m2) and T2DM. The mean age of this group was 52.79 with a standard deviation of 8.28. In total, three different bariatric surgery types were investigated: BPD; n = 13, LGCP; n=17, LAGB; n=11. The participants were recruited at the OB clinic, Prague, Czech Republic.

Table 10, below shows the characteristics of the sample cohort n = 84, including body mass index (BMI) scores along with common diabetes scores which can be used to diagnose the diseases. Measurements were taken three times throughout the study. Once before the surgery (pre-surgery), one-month post-surgery, and six months post-surgery. Although samples were acquired one-month post-surgery many of the analytical metrics from this time point were not recorded, so have been excluded from comparisons where data is not available. 17 samples were recorded as pre-diabetic, 5 as non-diabetic, and 62 as diabetic.

Table 10 - Sample cohort characteristics for bariatric surgery patients. The average and standard deviation of each result are provided for each collection time where available. The average is first provided along with the standard deviation.

Characteristic	Pre-Surgery n = 35	One Month Post-Surgery n = 12	6-months Post-Surgery n = 37
BMI (kg/m²)	44.13 ± 7.03	43.74 ± 7.28	38.45 ± 6.4
HbA1c (mmol/mol)	54.43 ± 9.98	N/A	44.54 ± 9.19
Glucose (mmol/L)	8.94 ± 2.41	N/A	7.16 ± 1.58
HOMA-IR (mmol/L)	11.12 ± 5.35	N/A	7.66 ± 3.53

7.2.3. Clinical Laboratory Data

Following a ten-hour overnight fast, venous blood was sampled in all patients, collected in chilled EDTA-containing tubes with and without aprotinin (for glucose and insulin measurements), aliquoted and frozen at -80°C until assayed. Aprotinin is a protease inhibitor that prevents the degradation of certain proteins and peptides in blood samples. Fasted blood samples and anthropometric assessments were performed at two distinct time points: before the surgical procedure (baseline) and 6-months after the surgery. During these assessments, biopsies of abdominal subcutaneous white adipose tissue were also conducted. Serum glucose, HbA1c and lipids were determined using the Cobas 6000 analyser. Insulin resistance was assessed using the homeostatic model assessment of insulin resistance (HOMA-IR). Body weight was measured to the nearest 0.5 Kg and height to the nearest 1 cm. All clinical metrics were obtained by the OB Clinic. One further time point, one-month post-surgery, was also sampled. Not all samples from this time point had a HOMA-IR and HbA1c assessment completed.

7.2.4. Urine Samples

A total of 120 urine samples were collected following a ten-hour overnight fast. These samples were aliquoted, frozen at -80°C, and later delivered to Nottingham

Trent University. Of the samples, 40 were collected before surgery, 36 one-month post-surgery, and 44 six-months post-surgery. The samples were categorised as follows: 5 were identified as healthy, 23 as pre-diabetic, 67 as diabetic, and 25 as unknown. The samples were received on dry ice, in freezer boxes. Samples were stored at -80˚C until preparation for NMR analysis. For sample preparation, the samples were first placed on ice and gently mixed by inversion until partially thawed. They were then allowed to reach room temperature while continuing to mix carefully. Samples were subsequently vortexed for ten seconds. The sample volume (500μL) was pipetted from the sample tube into a 1.5 mL sterile microcentrifuge tube. Then, both 50μL of 0.07% TSP in D_2O (w/v) and 50μL of 0.4% sodium azide in D_2O (w/v) solutions were added to the microcentrifuge tube. A 7.2 pH 0.5M phosphate buffer solution in D_2O (v/v) was then pipetted (100μL) into the microcentrifuge tube. Samples were then gently mixed by inversion and pipetted (650μL) into a newly purchased 5mm NMR tube. Prepared samples were stored at 4°C until they were analysed on the bNMR and HF-NMR spectrometers.

7.2.5. Materials and Reagents

The 5-mm diameter borosilicate NMR tubes were purchased from Wilmad (Z565229). The microcentrifuge tubes and pipette tips were obtained through Nottingham Trent University Stores. All other materials were purchased from Sigma-Aldrich Ltd. (Gillingham, UK).

7.2.6. NMR Acquisition

The HF-NMR spectra were acquired on a 400 MHz JEOL spectrometer (School of Science and Technology, Nottingham Trent University) operating at a frequency of 399.52 Hz. The samples were acquired using a presaturation pulse sequence with 32,768 acquisition points, 256 scans, an acquisition time of 3.277s, and a relaxation delay of 6s. All samples were automatically tuned, matched, and shimmed with a deuterium lock to avoid drifting spectra.

The bNMR spectra were acquired on a 60 MHz Oxford Instruments X-pulse spectrometer operating at 59.69 Hz. The samples were acquired using a WET-180-Auto pulse sequence with 16,384 acquisition points, 1024 scans, an acquisition time

of 4.096s, and a relaxation delay of 2s. All samples were shimmed with a deuterium lock to avoid drifting spectra. Tuning and matching were undertaken manually every day during sample acquisition. No large deviation was observed from the tuning and matching between analysis days.

7.2.7. Data Analysis

After the spectra had been acquired, they were processed through Mnova (version 14.3.1). All samples were zero-filled, Fourier transformed, and TSP referenced (0ppm), with an apodization weighting function applied (1 Hz Exponential, 1 Hz Gaussian). All phase and baseline corrections were completed manually. After data processing had been completed, 0.01ppm bucketing was then applied. The water signal region was removed from both HF-NMR and bNMR data.

Statistical analysis was performed using MetaboAnalyst (version 6.0).[210] This included all multivariate analyses such as principal component analysis (PCA), partial least squares discriminant analysis (PLS-DA) and orthogonal partial least squares discriminant analysis (OPLS-DA), as well as pathway analysis.174 PCA is a model used to observe clustering in a given data set, which can allow for the identification of outliers from a sample cohort. PLS-DA and OPLS-DA are supervised techniques that further support identifying metabolites presenting the maximum variation between classes. The data was normalised in MetaboAnalyst by median and Pareto scaling was applied. Prior to multivariate and univariate analyses, the distribution of all metabolite features was examined within MetaboAnalyst using density plots of normalized intensity values. The density maps indicated that the data were approximately normally distributed following normalization and scaling, with no evidence of skewness or outliers that could bias subsequent analyses. Establishing normal distribution is important as it ensures that statistical assumptions underlying parametric tests and multivariate models, such as OPLS-DA and linear regression, are met. This improves the interpretability and reliability of variance partitioning, correlation strength, and model performance metrics. The observed normal distribution therefore supports the validity of the subsequent statistical and multivariate analyses performed in this study.

More information on the statistical models can be found in the methodology chapter (Chapter 4).

7.3. Results

7.3.1. ^{1}H NMR Analysis of Urine Samples

The water signal located between δ 4.70 – 5.10 ppm was removed from the spectra. The metabolites were identified using the Human Metabolome Database (HMDB)210, 2D HSQC and COSY spectra (Appendix 10–13). Figure 62 and Figure 63 (see below) show the identified metabolites at both HF-NMR (Figure 62) and bNMR (Figure 63). In total 21 metabolites were identified at HF-NMR, with 19 being identified at bNMR. The acquisition parameters for the spectra are listed in Chapter 7.2.6. The slashes in the spectra represent where cuts in the spectra have been made by removing the water signal, and where the concentration of signals is too high.

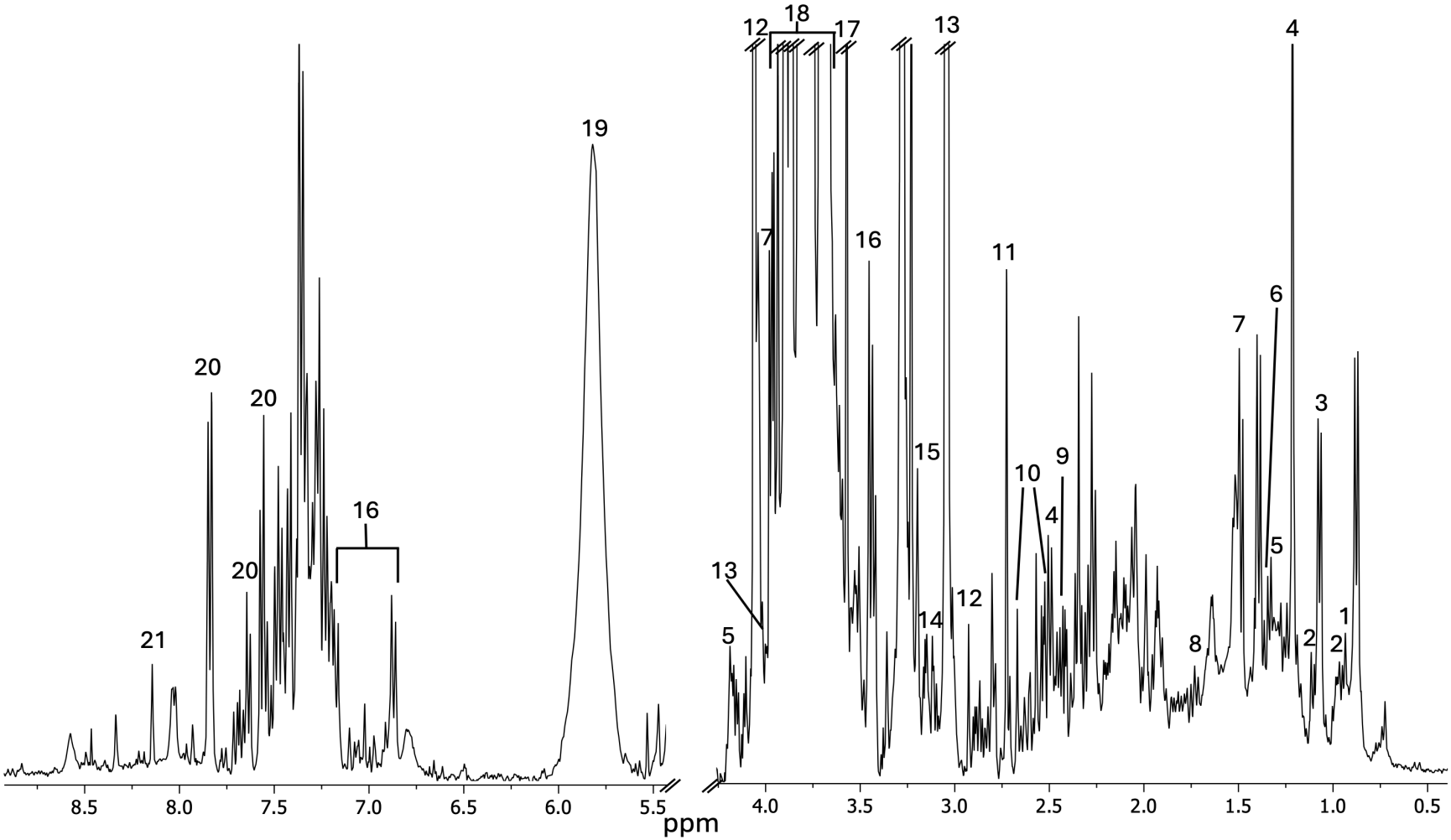

Figure 62 - [1]H 400Mhz HF-NMR Identified Urine Metabolites from 0.4 - 9ppm. Each number represent a metabolite: 1) α-ketoisocaproic acid, 2) valine, 3) 3-hydroxy isobutyrate, 4) 3-hydroxy isovaleric acid, 5) lactate, 6) 2-hydroxy isobutyrate, 7) alanine, 8) arginine, 9) acetone, 10) citrate, 11) dimethylamine, 12) creatinine, 13) creatine, 14) choline, 15) trimethylamine-N-oxide (TMAO), 16) 4-hydroxy phenylacetate, 17) glycine, 18) glucose 19) urea, 20) hippuric acid, and 21) formate and its [13]C satellites.

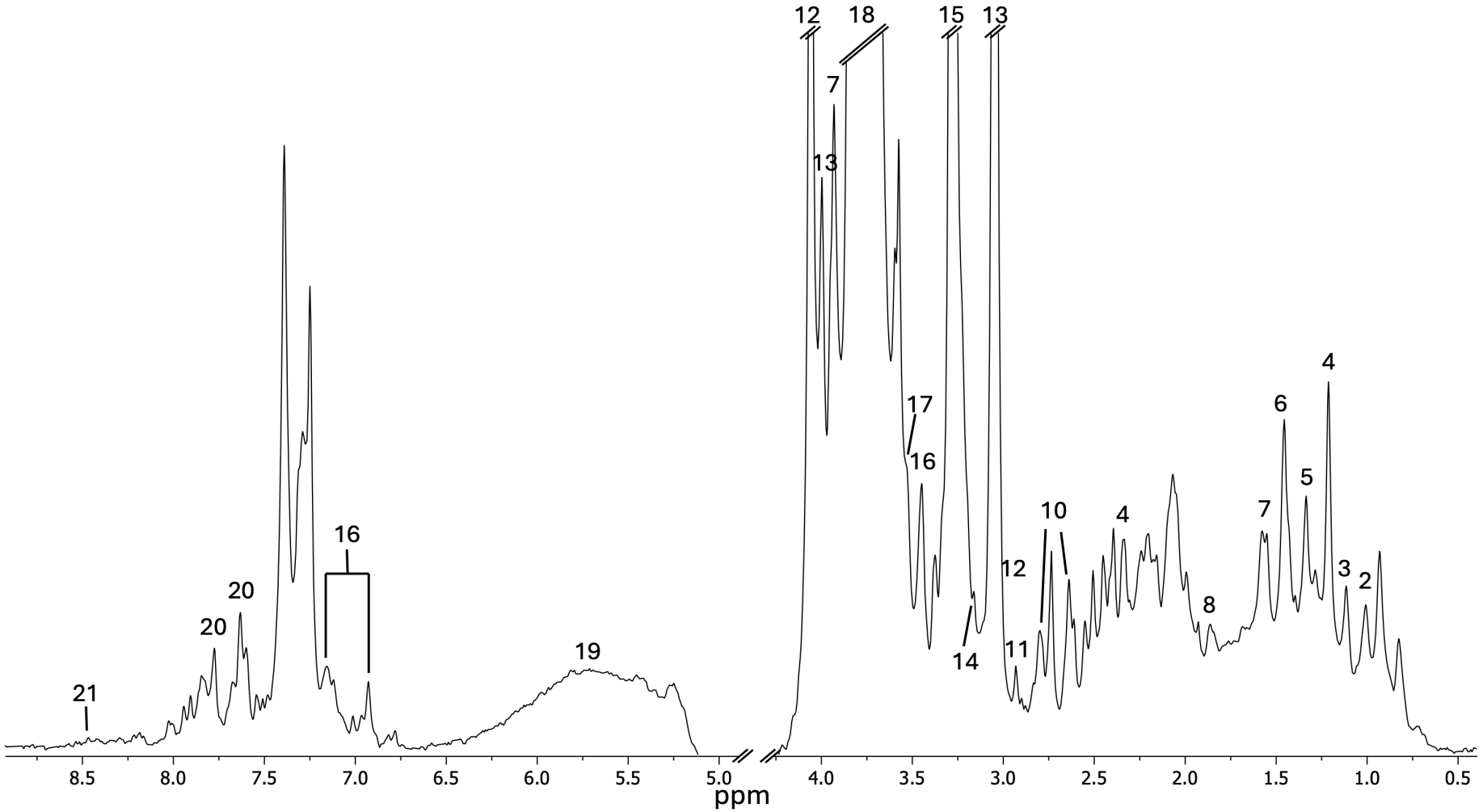

Figure 63 - ^{1}H 60Mhz HF-NMR Identified Urine Metabolites from 0.4 -9ppm.

Each number represent a metabolite: 2) valine, 3) 3-hydroxy isobutyrate, 4) 3-hydroxy isovaleric acid, 5) lactate, 6) 2-hydroxy isobutyrate, 7) alanine, 8) arginine, 10) citrate, 11) dimethylamine, 12) creatinine, 13) creatine, 14) choline, 15) trimethylamine-N-oxide (TMAO), 16) 4-hydroxy phenylacetate, 17) glycine, and 18) glucose., 19) urea, 20) hippuric acid, and 21) formate and its ^{13}C satellites.

7.3.2. Diabetes Disease Classification Before Bariatric Surgery

The following sub-chapter presents the results associated with diabetes disease classification according to the HbA1c categories of healthy (42 mmol/mol), pre-diabetic (42 to 47 mmol/mol) and diabetic (48 mmol/mol). To further explore the variance in the data, different statistical approaches, namely PCA, PLS-DA, sparse PLS-DA (sPLS-DA) and OPLS-DA, were applied in MetaboAnalyst (6.0).209 No data filtering was applied during pre-processing; however, sample normalization by median, and Pareto scaling was applied to the dataset before statistical analysis was undertaken as described in Chapter 7.2.7.

7.3.2.1 Multivariate Statistical Analysis of Diabetic, Pre-diabetic and Non-diabetic Samples *via* PCA

A PCA plot was used to identify any outliers (n = 84) and initial variance in the data obtained (904 metabolite bins) on the HF-NMR and bNMR (Figure 64). Overlap from all three clusters (diabetic, pre-diabetic and non-diabetic) was observed in Figure 64a) and 5d), with no definable attribute contributing to group distribution. Of the clusters shown, the non-diabetic group has the smallest confidence region, with the diabetic group having the largest variance as exemplified by the largest 95% ellipse. Five samples were outside of their 95% confidence regions in the bNMR data: namely three diabetic and two pre-diabetic samples. Eight samples were outside of their 95% confidence regions in the HF-NMR data: namely six diabetic and two pre-diabetic samples. The outlier sample spectra were individually inspected and after a comparison with the general samples were subsequently removed from the dataset. These samples were outside of their categorical ellipses due to abnormal levels of creatine and lactic acid compared to the other metabolites in their spectra. Statistical analysis shown from chapter 7.3.2.3 onwards was subsequently performed on 79 bNMR samples, and 76 HF-NMR samples.

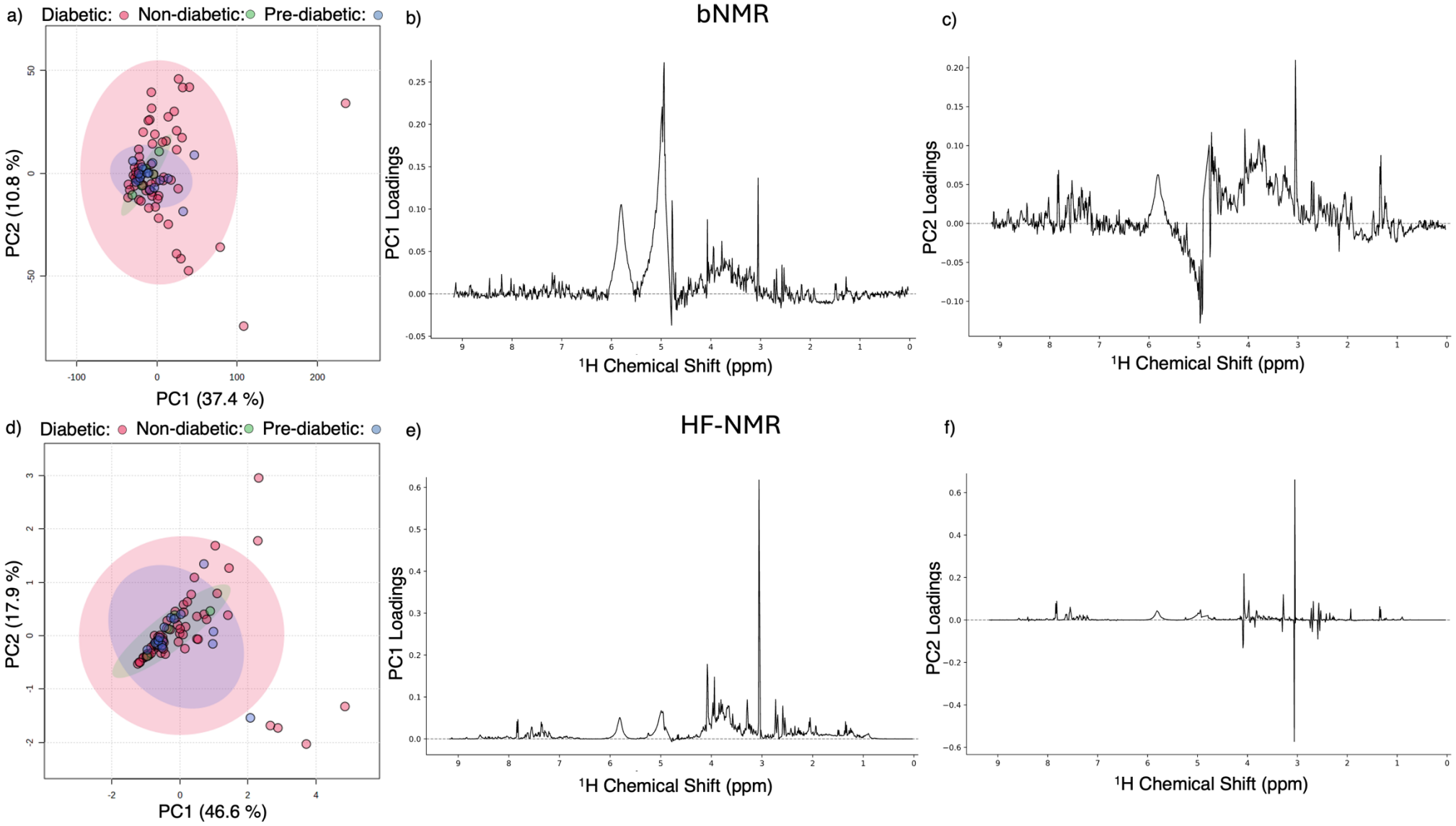

Caption on the next page.

Figure *64* - PCA plots of diabetic, pre-diabetic and healthy urine samples in bNMR and HF-NMR. Figures a), b), and c) are associated with bNMR data, whereas d), e), and f) are associated with the HF-NMR data. Figures b) and e) show the principal component 1 and how it is weighted across the spectra, and Figures c) and f) are for the principal component 2. Figures a) and d) show the diabetic samples in red, healthy in green and pre-diabetic samples in blue.

7.3.2.2 Multivariate Statistical Analysis of Diabetic, Pre-diabetic and Healthy Samples *via* sPLS-DA

A sPLS-DA plot was selected as a supervised model to show the variance between all HbA1c levels classified as non-diabetic, pre-diabetic and diabetic samples. As shown in Figure 65, there were no healthy sample outliers. At both HF-NMR and bNMR, the diabetic and pre-diabetic samples had smaller confidence regions than the non-diabetic samples. The classification error rates in the bNMR and HF-NMR sPLS-DA plots suggest a high error rate with limited ability to distinguish between classes.

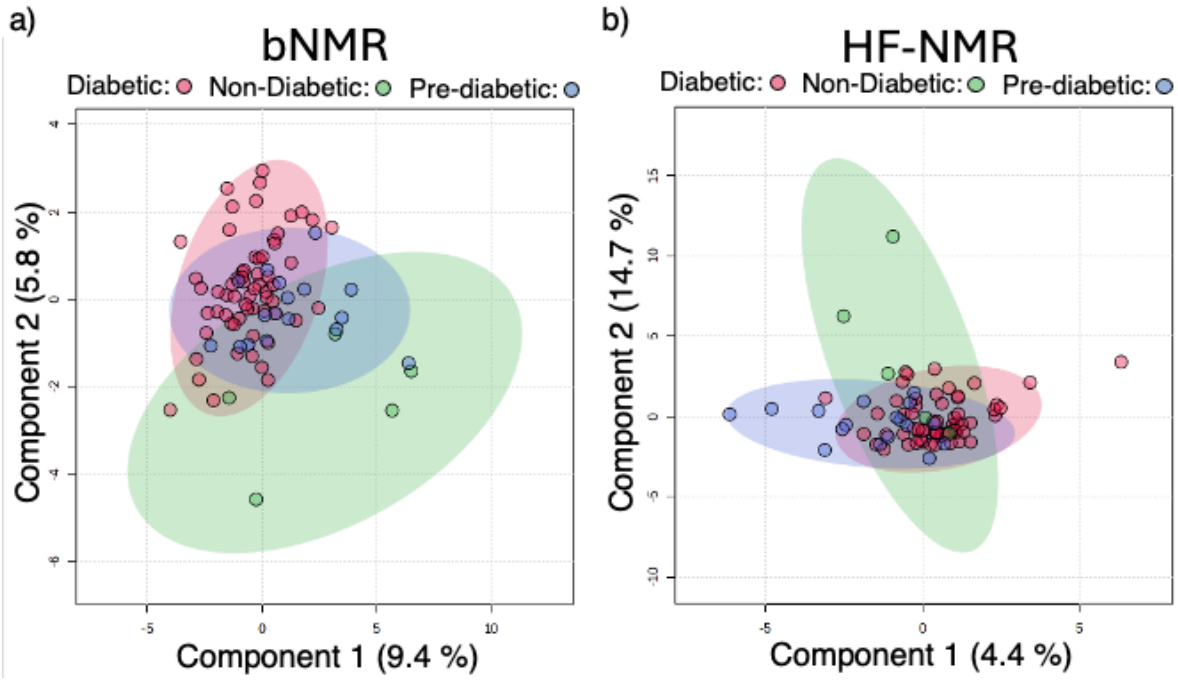

Figure *65* - sPLS-DA of bNMR and HF-NMR comparing HbA1c categories.

a) bNMR 47.6% classification error rate shown on the left. b) HF-NMR 53.6% classification error rate. Diabetic samples are shown in red, pre-diabetic samples are shown in blue and non-diabetic samples are shown in green. Ellipses represent the 95% confidence regions.

7.3.2.3 OPLS-DA of Diabetes and Pre-diabetes Before Bariatric Surgery

As there were no observable differences between health categories by sPLS-DA, the more supervised technique, OPLS-DA, was used. Due to the low number of healthy pre-surgery samples (n = 5), the healthy cohort was not included to be

analysed *via* OPLS-DA to avoid bias. OPLS-DA results of both diabetic (n = 21 for bNMR and n = 20 HF-NMR) and pre-diabetic (n = 8 for bNMR and n = 5 for HF-NMR) conditions are shown in Figure 66a) and 62d) for the bNMR and HF-NMR data, respectively. Both Figure 66a) and 62d) show overlap between the diabetic and pre-diabetic cohorts. The R^2 values for both OPLS-DA plots also were above the significance threshold of $p < 0.05$. However, the R^2 values for the bNMR and HF-NMR plots were 0.524, and 0.653 respectively, below the 0.7 thresholds set out for OPLS-DA.

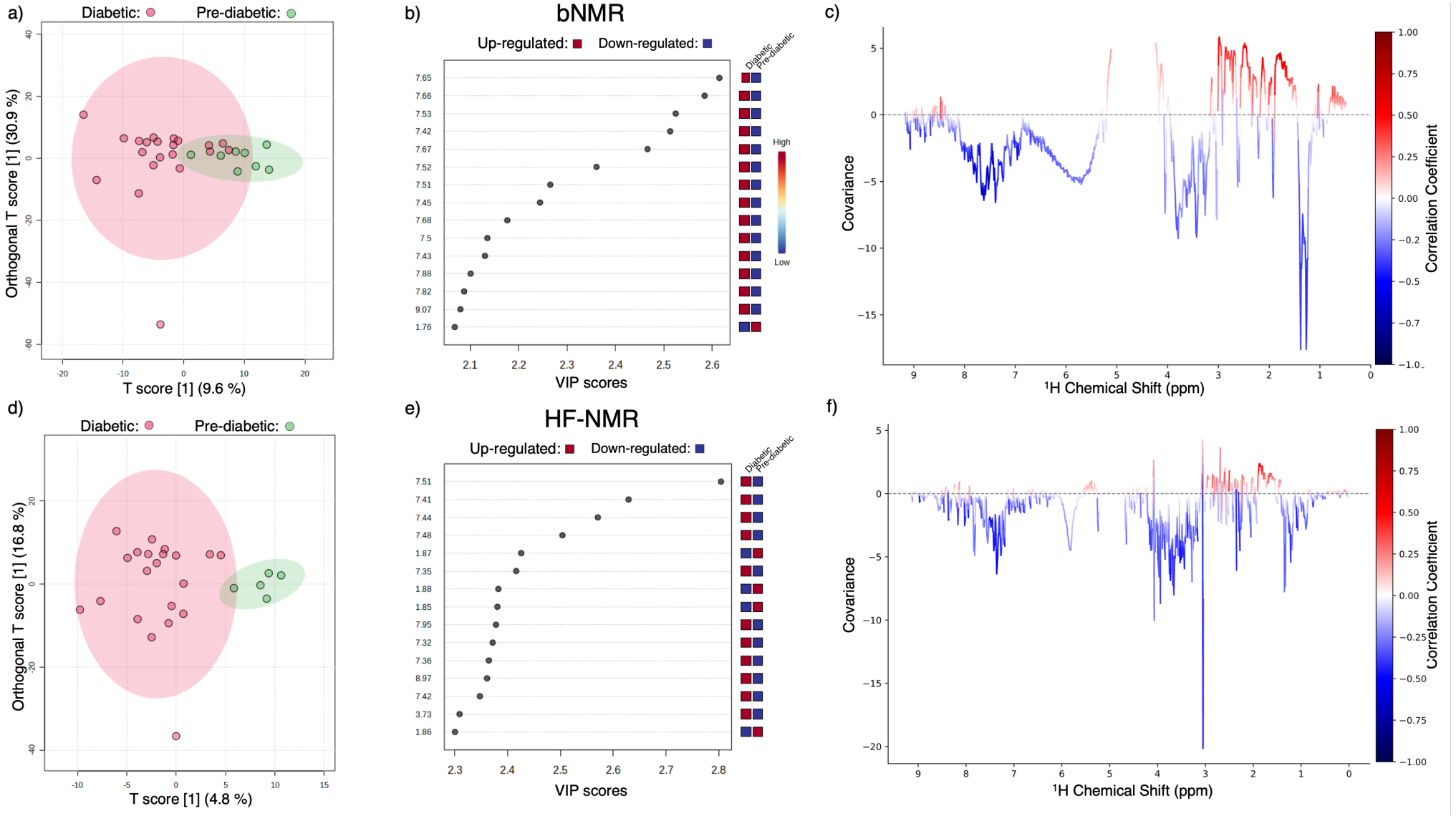

Caption on the next page.

Figure *66* - OPLS-DA score plots and corresponding loading plots for pre-surgery diabetic and pre-diabetic samples analysed using bNMR and HF-NMR.
(a) bNMR OPLS-DA score plot ($Q^2 = 0.176$, $p < 0.05$; $R^2Y = 0.524$, $p > 0.05$) showing partial separation between diabetic (red) and pre-diabetic (green) samples. (b) and (c) represent the PC1 and PC2 loading plots for the bNMR analysis, respectively. (d) HF-NMR OPLS-DA score plot ($Q^2 = -0.415$, $p > 0.05$; $R^2Y = 0.653$, $p > 0.05$) illustrating limited separation between diabetic and pre-diabetic groups. (e) and (f) correspond to the PC1 and PC2 loading plots for the HF-NMR analysis, respectively. Data ellipses in the score plots represent 95% confidence intervals.

7.3.3. Bariatric Surgery's Influence on the Metabolome

Due to the potential influence of bariatric surgery on the metabolome, the samples were further split into three categories based on their time of sample collection: before surgery, one-month post-surgery and 6-months post-surgery. The one-month post-surgery samples and the 6-month post-surgery samples were subsequently removed from the following dataset to compare diabetes and pre-diabetes without a potential influence of the surgery.

An OPLS-DA model (Figure 67) was applied to observe differences between the pre-surgery (n = 36 for bNMR and n = 35 HF-NMR) and 6-month post-surgery (n = 39 for bNMR and n = 41 for HF-NMR) samples. A small separation between the pre- and post-bariatric surgery is observed in Figure 67. The bNMR plot (Figure 67a) exhibits a higher T score (7.3%) compared to 4.1% that shown in the HF-NMR plot (Figure 67b). This is further observed by the orthogonal T score, where the bNMR plot shows a value of 26.3%, while the HF-NMR plot shows 9.1%. Overall low R^2 and Q^2 values were observed across both plots and are suggestive of no significant differences between the two sample cohorts.

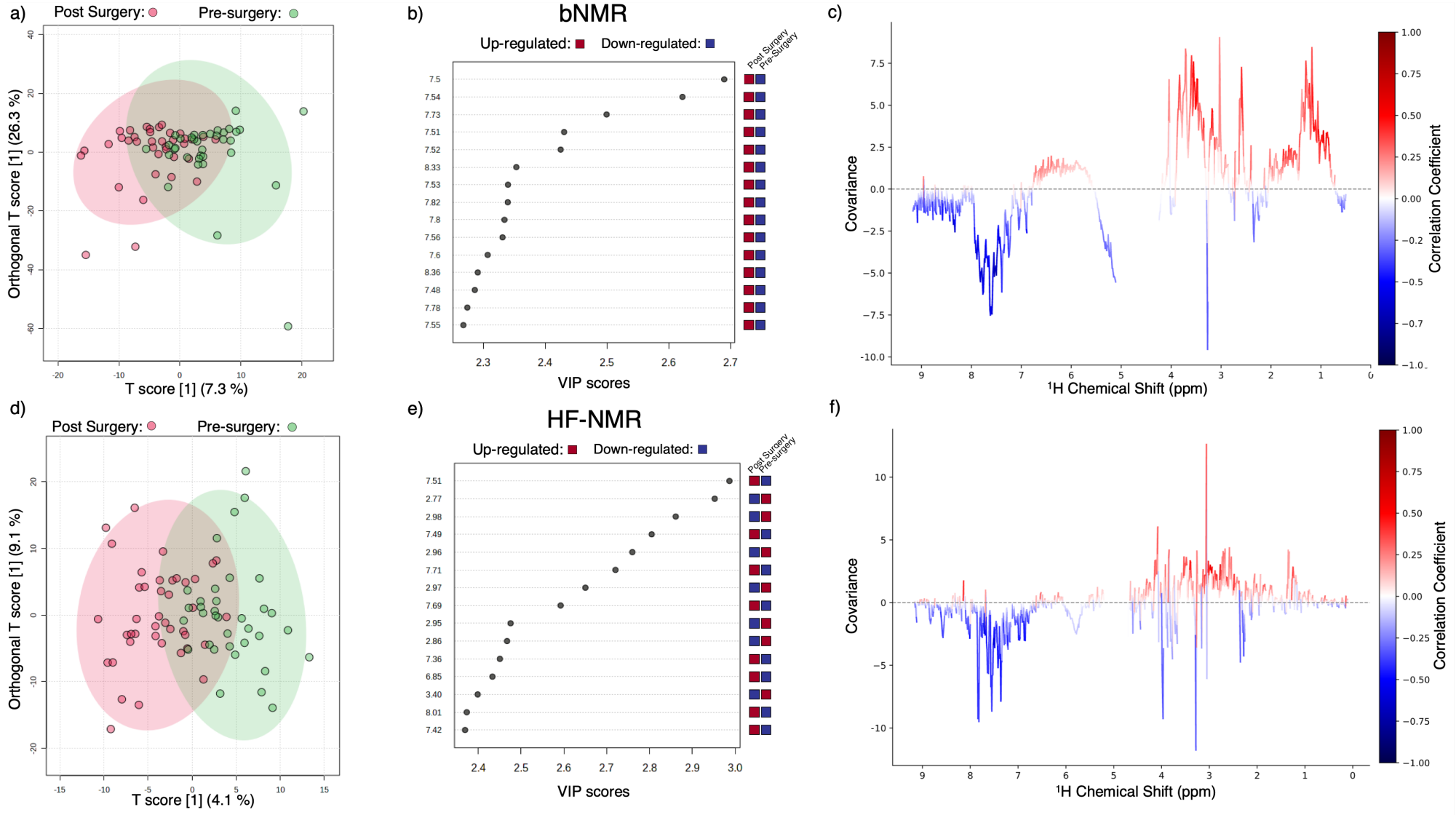

Figure caption on the next page.

Figure 67 - OPLS-DA plots of pre- and post-surgery samples from bNMR and HF-NMR samples. a) bNMR OPLS-DA plot Q^2:0.2, $p < 0.05$, R^2:0.426, $p < 0.05$. d) HF-NMR OPLS-DA plot of Q^2:0.133, $p < 0.01$, R^2 0.581, $p < 0.05$. In Figure 67, a), b), and c) are from the bNMR data and d), e), and f) are from the HF-NMR data. Red represents post-operative samples in the OPLS-DA plot, with green representing pre-surgery samples.

7.3.3.1 PLS-DA of Bariatric Surgery Types Compared with Pre-Surgery Samples

The 6-month post-surgery data cohort was further split into the surgery types. A PLS-DA plot (Figure 68) was used to show the variance between pre-surgery (n = 36 for bNMR and n = 35 for HF-NMR) and post-bariatric surgeries (bNMR: n = 12 BPD, n = 12 LGCP, n = 10 LAGB, and HF-NMR n = 12 BPD, n = 15 LGCP, n = 9 LGGB) in the HF-NMR and bNMR datasets. Limited variance is observed between LGCP, LAGB, and pre-surgery samples compared to BPD surgery in Figure 68a. This observation is more apparent in the HF-NMR PLS-DA plot (Figure 68b). The outliers observed across both PLS-DA plots were due to abnormal creatine levels and TMAO. Both PLS-DA plots were statistically significant with a $p < 0.001$.

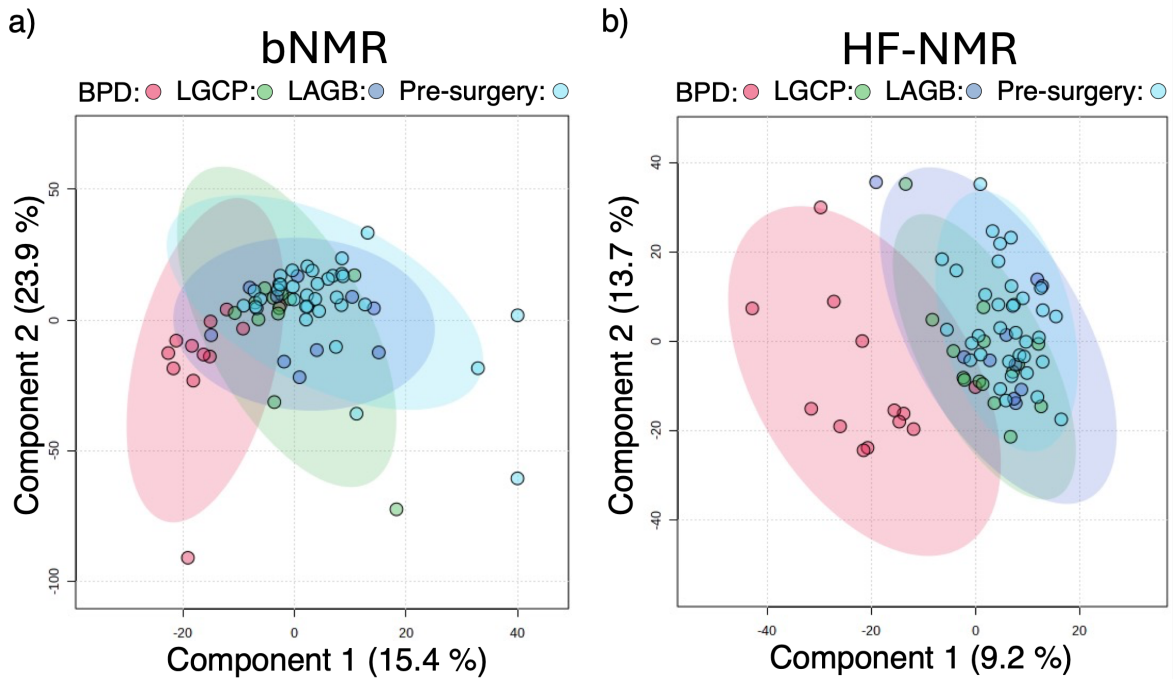

Figure 68 - PLS-DA plot showing pre-surgery samples and 6-month post-surgery samples split by surgery type. Red represents BPD, green, LGCP, purple LAGB, and light blue are pre-surgery samples. Each ellipse represents the 95% confidence region.

7.3.3.2 Surgery Type Separation by PLS-DA

After removing pre-surgery samples, variability and confounders influencing the metabolome from different surgery types were observed. Through PLS-DA, two

distinct clusters were detected in the HF-NMR data between the surgery types (Figure 69b). The clustering also showed a large overlap between LGCP and LAGB surgery types; however, BPD was largely separate from the laparoscopic adjustable surgeries. Separation is also observed in the bNMR data (Figure 69a); however, it is not as prominent as that in the HF-NMR PLS-DA plot. Both plots were also statistically significant with a $p < 0.01$.

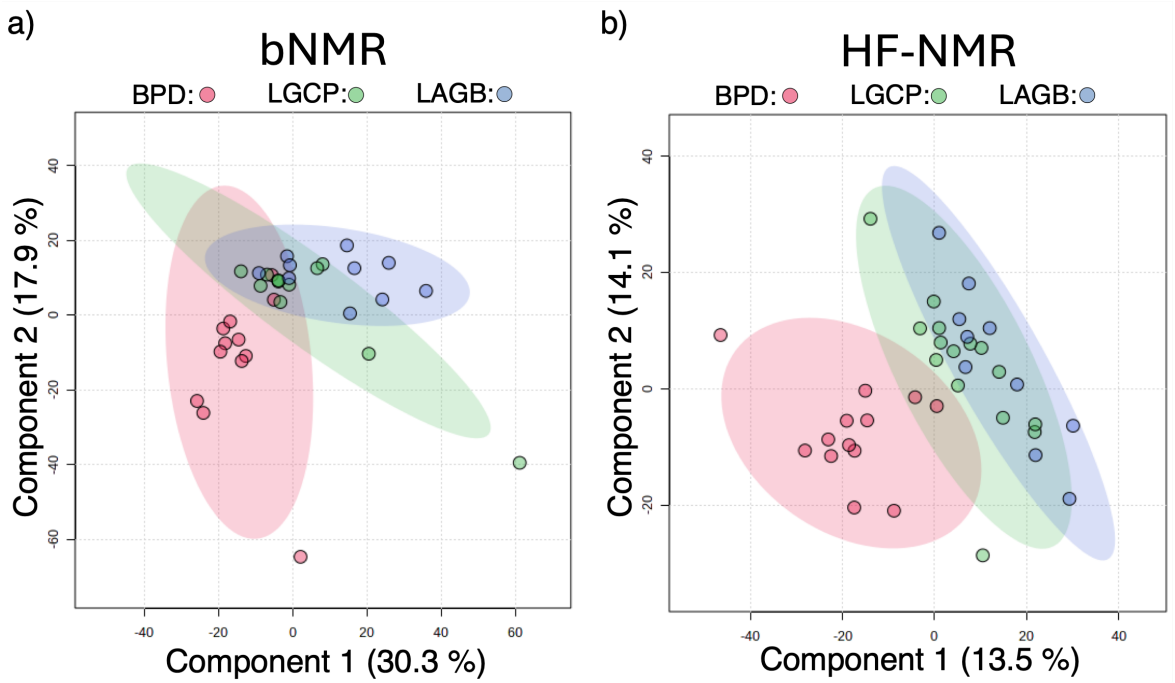

Figure 69 - PLS-DA plots separating surgery types. a) bNMR plot ($p < 0.01$) and b) HF-NMR plot ($p < 0.01$). Red colour represents BPD surgery (bNMR: n = 12, HF-NMR n = 13), green is LGCP (bNMR n = 12, HF-NMR n = 15), and blue is LAGB (bNMR: n = 10, HF-NMR: n = 10). bNMR explains 48.2% of the variance, while HF-NMR explains for 27.6% of the variance.

7.3.4. The Difference of BPD Surgery and Gastric Restriction Surgery

When clustering the surgery types into gastric restriction (LAGB and LGCP) against the BPD surgery, two clear groups with minimal samples outside the 95% confident regions are observed. Figure 70 shows both the bNMR and HF-NMR data have a strong positive correlation ($R^2 > 0.7$) with good predictive potential ($Q^2 > 0.4$). Volcano plot analysis and False Discovery Rate (FDR) were applied to minimise errors as described in Section 3. The HF-NMR data did not have any significant bins after FDR correction; however, the bNMR data shows many metabolite bins of significance (Figure 70).

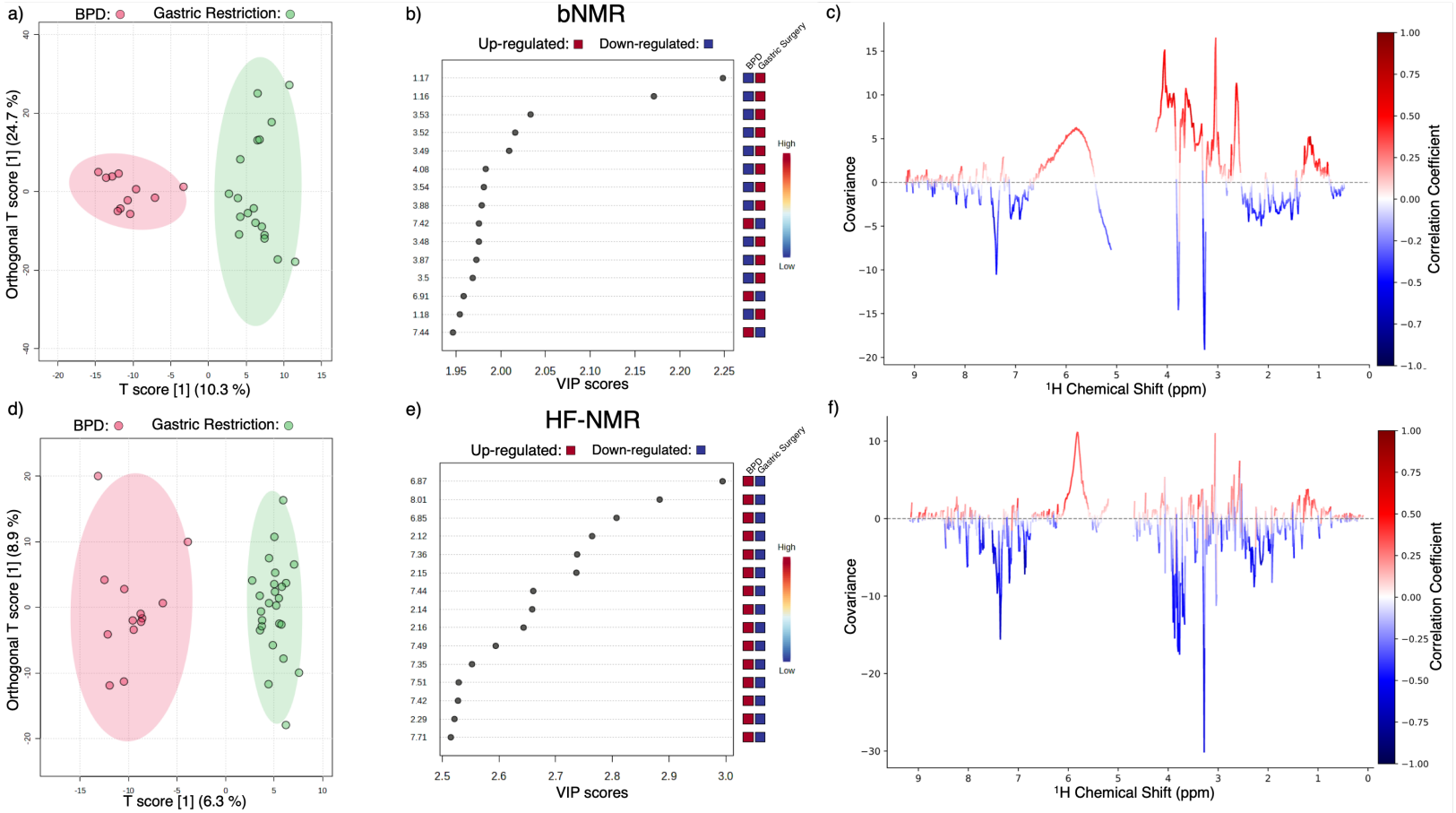

Figure 70 - OPLS-DA plot of BPD compared with gastric restriction surgery of bNMR and HF-NMR urine spectra. bNMR (a) has a Q^2 of 0.582, $p<0.001$, R^2 of 0.912, $p=0.052$ (BPD: n = 12 and Gastric Restriction: n = 22). b) HF-NMR Q^2 is 0.696, $p < 0.001$, R^2 is 0.943, $p < 0.001$ (BPD: n = 13 and Gastric Restriction: n = 25). An OPLS-DA loadings plot of the bNMR data from Figure 70a) shows the correlation between the bins (ppm) and the class separation. Each point in the plot represents a different ppm value (metabolite). The metabolites that are most strongly associated with the class separation have the highest and lowest loading scores. Data in red in the OPLS-DA plot is the BPD surgery, whilst gastric restriction surgery shown in green.

Figure caption on the next page.

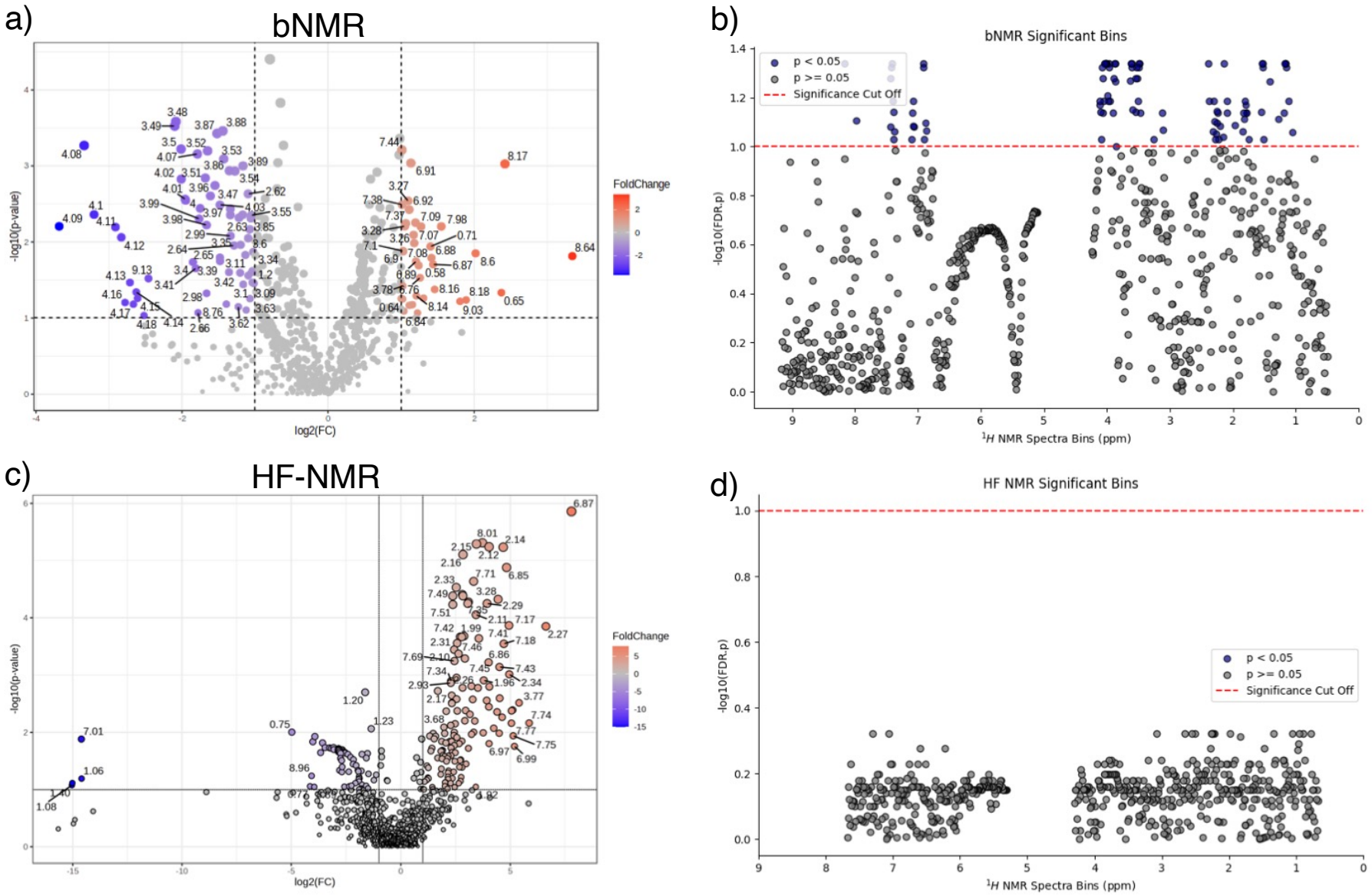

Figure caption on the next page.

Figure 71 - Volcano and significance plots of metabolites bins between BPD and gastric restriction surgery. Figure 71a) and b) represent bNMR data, whilst Figure 71c) and d) represent HF-NMR data. Plots a) and c) are volcano plots; b) and d) are FDR corrected significant bins.

A summary of each identified metabolite from Figure 62 and Figure 63, along with the corresponding VIP score and AUC value is presented in Table 11. The metabolites analysed show trends in their relative concentrations, VIP scores, sensitivities, specificities, AUC (Area Under the Curve) values, and p-values, indicating their significance in differentiating between BPD and gastric restriction surgery groups. The variation of metabolic dysregulation was observed at HF-NMR and bNMR, with some metabolites exhibiting contrasting trends between techniques, as shown in Table 11.

For instance, 2-Hydroxyisobutyrate metabolite showed divergent trends between techniques (increase in bNMR, decrease in HF-NMR) but with limited discriminatory power (AUC ≈ 0.5). In contrast, 3-Hydroxyisobutyrate was consistently decrease in both analyses, with moderate discriminatory power (AUC: 0.667-0.757, p = 0.083). 3-Hydroxyisovaleric acid demonstrated significant decrease, particularly in HF-NMR (VIP = 1.981, AUC = 0.803, p = 0.002). Furthermore, 4-Hydroxyphenyl Acetate showed decrease in bNMR but increased in HF-NMR, with high VIP scores (1.469 and 1.592, respectively) and significant p-values in both analyses. Acetone and alanine were consistently increased, with alanine showing particularly high significance in HF-NMR (VIP = 1.903, p = 0.005). Arginine also displayed an increasing trend in both techniques, with higher discriminatory power in HF-NMR (p = 0.004). Moreover, citrate and creatine showed decrease in bNMR but variability in HF-NMR, with citrate yielding significant results in bNMR (AUC = 0.813, p = 0.007). Dimethylamine and formate exhibited varying trends, while Glucose was consistently increase with high significance in HF-NMR (VIP = 2.211, p = 0.002). Urea and valine were consistently decreased, with valine showing particularly strong discriminatory power in both analyses (bNMR: AUC = 0.864, p = 0.002; HF-NMR: AUC = 0.818, p = 0.021). In conclusion, the reduced absorption of BPD surgeries seems to play a role on the metabolic landscape of these patients. The consistency of certain metabolites, such as valine and 3-hydroxyisovaleric acid, across both platforms strengthens their potential as biomarkers for differentiating these surgical outcomes.

Table 11 - Summary of bNMR and HF-NMR urinary metabolites from the OPLS-DA and ROC analysis comparing BPD and gastric restriction surgery.

	bNMR						HF-NMR					
Metabolite	BPD Trend	VIP	Sensitivity	Specificity	AUC	p - value	BPD Trend	VIP	Sensitivity	Specificity	AUC	p - value
2 - Hydroxyisobutyrate	Up	0.722	0.5	0.7	0.561	0.914	Down	0.512	0.6	0.6	0.572	0.507
3 - Hydroxyisobutyrate	Down	1.123	1	0.5	0.667	0.083	Down	0.906	0.8	0.7	0.757	0.083
3 - Hydroxyisovaleric acid	Down	1.371	0.6	0.8	0.813	0.024	Down	1.981	0.8	0.8	0.803	0.002
4 - Hydroxyphenyl Acetate	Down	1.469	0.8	0.7	0.773	0.010	Up	1.592	0.8	0.5	0.680	0.029
Acetone	Up	1.365	0.7	0.8	0.727	0.026	Up	1.281	0.8	0.6	0.686	0.038
Alanine	Up	0.997	0.6	0.7	0.662	0.098	Up	1.903	0.8	0.6	0.729	0.005
Arginine	Up	1.074	0.7	0.6	0.667	0.092	Up	0.283	0.7	0.8	0.732	0.004
Choline	Down	1.107	0.5	1	0.682	0.068	Down	1.113	0.5	0.6	0.551	0.846
Citrate	Down	1.799	0.8	0.8	0.813	0.007	Down	0.564	0.6	0.6	0.569	0.537
Creatine	Down	1.134	0.6	0.9	0.768	0.044	Up	1.076	0.5	0.6	0.542	0.228
Creatinine	Down	1.492	0.5	0.8	0.712	0.030	Up	0.799	0.7	0.6	0.640	0.175
Dimethylamine	Down	1.410	0.6	0.8	0.763	0.021	Down	0.903	0.7	0.6	0.637	0.155
Formate	Up	0.544	0.7	0.7	0.636	0.282	Up	0.305	0.6	0.5	0.511	0.992
Glycine	Down	1.793	0.7	0.9	0.818	0.009	Down	0.945	0.6	0.6	0.569	0.914
Hippuric Acid	Up	0.388	0.6	0.7	0.631	0.657	Up	0.403	0.5	0.8	0.572	0.676
Lactate	Up	0.437	0.6	0.6	0.510	0.539	Up	1.312	0.8	0.6	0.698	0.061
Glucose	Up	1.007	0.5	0.8	0.611	0.038	Up	2.211	0.6	0.8	0.738	0.002
Trimethylamine-N-Oxide	Down	0.047	0.5	0.8	0.561	0.872	Down	0.918	0.5	0.7	0.502	0.206
Urea	Down	1.131	0.7	0.6	0.636	0.075	Down	1.309	0.7	0.7	0.705	0.038

Valine	Down	1.851	0.7	0.9	0.864	0.002	Down	1.403	0.8	0.8	0.818	0.021
α - Ketoisocaproic acid	Down	1.029	0.7	0.6	0.657	0.163	Down	0.231	0.8	0.6	0.698	0.686

7.3.5. Post-surgery HbA1c Health Categories

After 6-months post-surgery, the patients had their HbA1c levels re-analysed. Many patients had regressed to either a pre-diabetic or non-diabetic HbA1c classified health status. Therefore, the statistical analysis comparing HbA1c classified health status was investigated for the post-surgery sample cohort.

7.3.5.1 OPLS-DA of Pre-Diabetes and Diabetes Samples After the Surgery

The OPLS-DA, presented in *Figure 72*, show a clear separation between pre-diabetes and diabetes, with no samples overlapping in each respective confidence region. The bNMR OPLS-DA plot (*Figure 72*a) shows a weaker distinction compared to the HF-NMR OPLS-DA plot (*Figure 72*d). Both plots exhibit weak to no predictive potential ($Q^2 < 0.4$), but there is a correlation between the study groups in the bNMR and HF-NMR plots with R^2 values of 0.79 and 0.995, respectively. However, both plots have significance levels above the 0.05 threshold, indicating a possible overfitting of the data. *Figure 72*c) and f) display similar regions contributing to their separation, with bins from 1-4ppm and 6.5-8ppm being significantly decreased and increased in pre-diabetics, respectively.

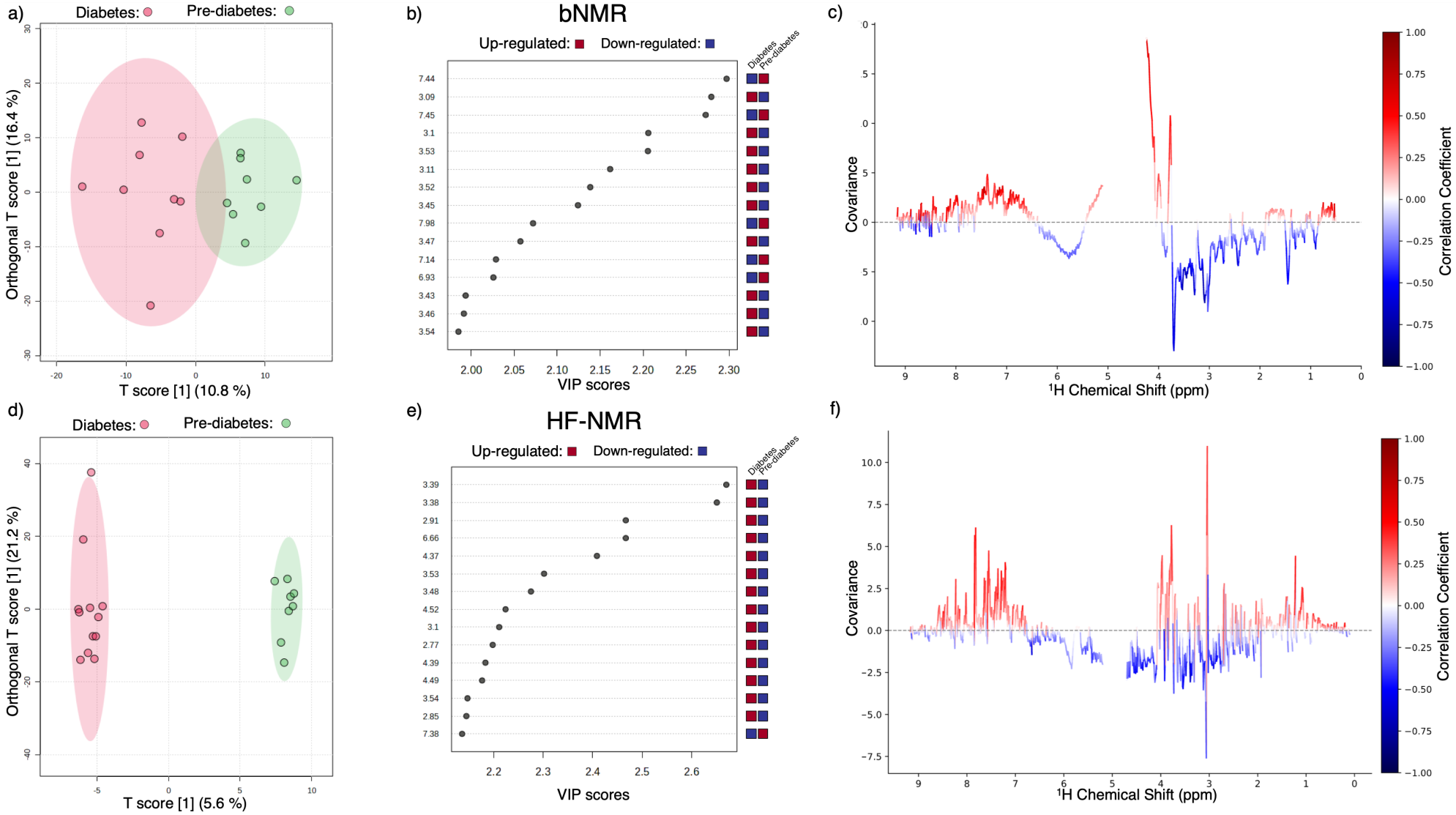
a)
Diabetes:
Pre-diabetes:
Orthogonal T score [1] (16.4 %)
T score [1] (10.8 %)
b)
bNMR
Up-regulated:
Down-regulated:
Diabetes
Pre-diabetes
7.44
3.09
7.45
3.1
3.53
3.11
3.52
3.45
7.98
3.47
7.14
6.93
3.43
3.46
3.54
VIP scores
c)
Covariance
¹H Chemical Shift (ppm)
Correlation Coefficient
d)
Diabetes:
Pre-diabetes:
Orthogonal T score [1] (21.2 %)
T score [1] (5.6 %)
e)
HF-NMR
Up-regulated:
Down-regulated:
Diabetes
Pre-diabetes
3.39
3.38
2.91
6.66
4.37
3.53
3.48
4.52
3.1
2.77
4.39
4.49
3.54
2.85
7.38
VIP scores
f)
Covariance
¹H Chemical Shift (ppm)
Correlation Coefficient

Figure 72 - OPLS-DA analysis of post-surgery diabetic and pre-diabetic samples using bNMR and HF-NMR. a) OPLS-DA score plot for bNMR analysis (Q^2 = 0.00168, $p > 0.05$; R^2 = 0.79, $p > 0.05$) (diabetes: n = 9, pre-diabetes n. = 8), showing limited separation between diabetic (red) and pre-diabetic (green) groups. b) VIP scores from bNMR analysis highlight significant metabolites contributing to group separation, with an increase (red) and decrease (blue) features. c) S-line plot for bNMR, displaying covariance and correlation of metabolites with class discrimination. d) OPLS-DA score plot for HF-NMR analysis (Q^2 = 0.244, $p > 0.05$; R^2 = 0.995, $p > 0.05$) (diabetes: n = 12, pre-diabetes: n = 8), indicating partial separation between diabetic and pre-diabetic groups. e) VIP scores for HF-NMR, showing key discriminatory metabolites. f) S-line plot for HF-NMR, illustrating metabolite covariance and correlation. Data ellipses in the score plots represent 95% confidence intervals.

7.3.5.2 OPLS-DA of Non-diabetic and Pre-diabetic Samples After Bariatric Surgery

The OPLS-DA model between pre-diabetic (n = 8) and non-diabetic (n = 15) samples presented in *Figure 73* shows a clear separation between the groups. However, there is some overlap in the bNMR OPLS-DA plot (*Figure 73*a) compared to the HF-NMR OPLS-DA plot in *Figure 73*d. Similar to the OPLS-DA plot mentioned earlier (*Figure 72*), the Q^2 values in *Figure 73* are lower, with insignificant p-values. The corresponding R^2 values are also weaker, with insignificant p-values. *Figure 73*c) and f) show similar weightings and directions of regulation of concentrations for metabolite bins. The exception was a region between 5.5 – 6.5ppm in *Figure 73*c), where urea appears to be higher in pre-diabetics compared to healthy individuals in the bNMR data.

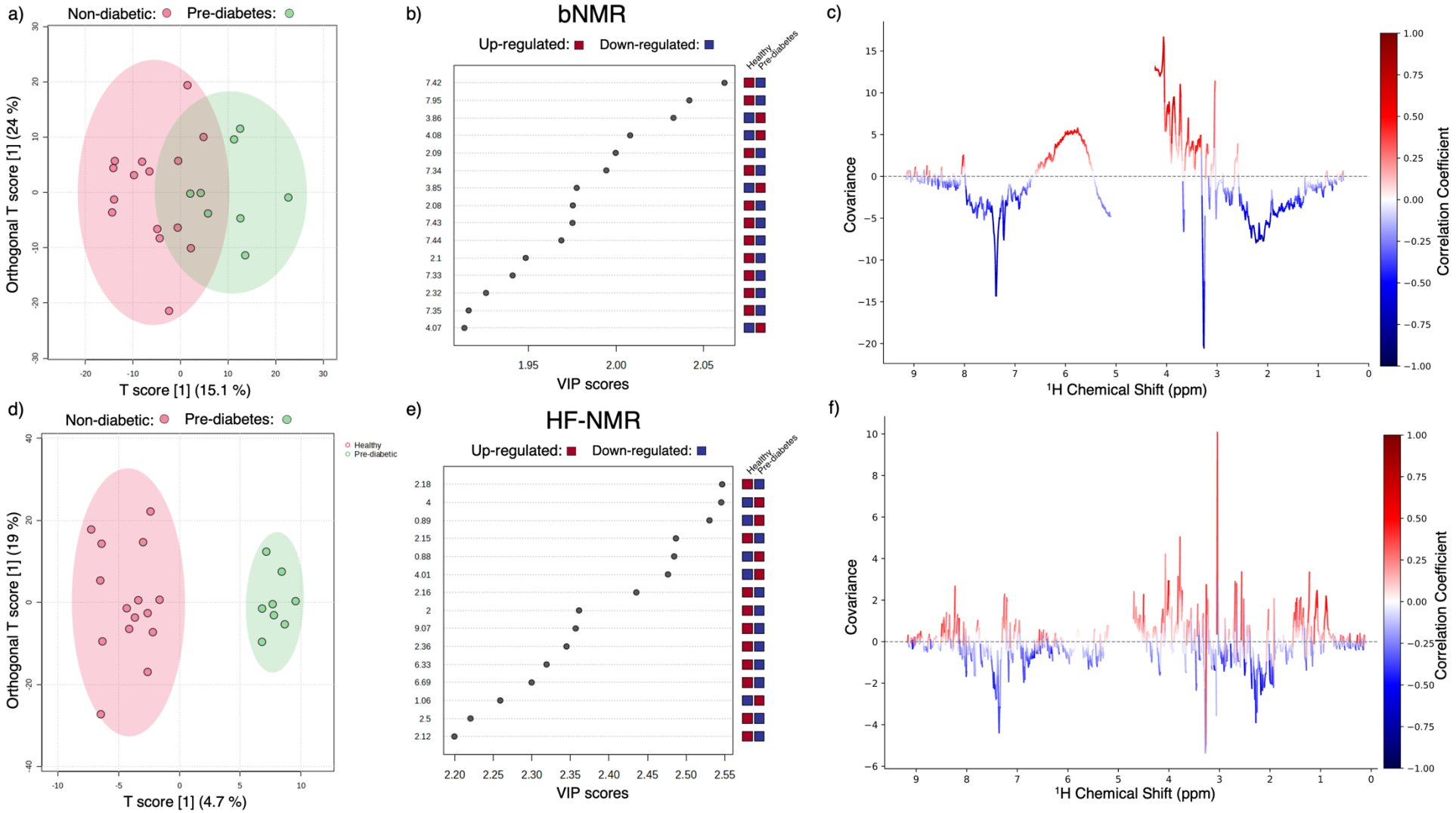
a)
Non-diabetic:
Pre-diabetes:
Orthogonal T score [1] (24 %)
T score [1] (15.1 %)
b)
bNMR
Up-regulated:
Down-regulated:
Healthy
Pre-diabetes
7.42
7.95
3.86
4.08
2.09
7.34
3.85
2.08
7.43
7.44
2.1
7.33
2.32
7.35
4.07
1.95
2.00
2.05
VIP scores
c)
Covariance
¹H Chemical Shift (ppm)
Correlation Coefficient
d)
Non-diabetic:
Pre-diabetes:
Healthy
Pre-diabetic
Orthogonal T score [1] (19 %)
T score [1] (4.7 %)
e)
HF-NMR
Up-regulated:
Down-regulated:
Healthy
Pre-diabetes
2.18
4
0.89
2.15
0.88
4.01
2.16
2
9.07
2.36
6.33
6.69
1.06
2.5
2.12
VIP scores
f)
Covariance
¹H Chemical Shift (ppm)
Correlation Coefficient

Figure *73* - OPLS-DA analysis of post-surgery non-diabetic and pre-diabetic samples using bNMR and HF-NMR.

a) OPLS-DA score plot for bNMR analysis (Q^2 = -0.146, $p > 0.05$; R^2 = 0.607, $p > 0.05$), showing overlap between non-diabetic (red) and pre-diabetic (green) groups. b) VIP scores from bNMR analysis highlighting metabolites contributing to group discrimination, with an increase (red) and decrease (blue) features. c) S-line plot for bNMR, displaying covariance and correlation of metabolites associated with group separation. d) OPLS-DA score plot for HF-NMR analysis (Q^2 = -0.457, $p > 0.05$; R^2 = 0.93, $p > 0.05$), showing limited separation between healthy and pre-diabetic groups. e) VIP scores for HF-NMR analysis, indicating discriminatory metabolites. f) S-line plot for HF-NMR, illustrating metabolite covariance and correlation. Data ellipses in the score plots represent 95% confidence intervals.

7.3.5.3 Post-Surgery Non-diabetic and Diabetic Cohorts

The OPLS-DA compared 6-month post-surgery non-diabetic (n = 15) with diabetic cohorts (bNMR: n = 9 and HF-NMR: n = 12), showing a strong correlation ($R^2 > 0.99$) in Figure 74. The statistical significance was confirmed in the bNMR OPLS-DA plot (Figure 74a) with $p < 0.01$, but not in the HF-NMR OPLS-DA plot (Figure 74d). The predictive potential was also observed, with Q^2 values of 0.657 and 0.357 in the bNMR and HF-NMR OPLS-DA plots, respectively. Figure 74c) and 16f) display the spectral regions weighted in the OPLS-DA model.

Similar results to Figure 74c) and f) were also observed in the volcano plots (Figure 75). The volcano plots (Figure 75a and c) showed statistically significant metabolite bins, but only the bNMR metabolite bins (Figure 75b) remained significant after FDR correction.

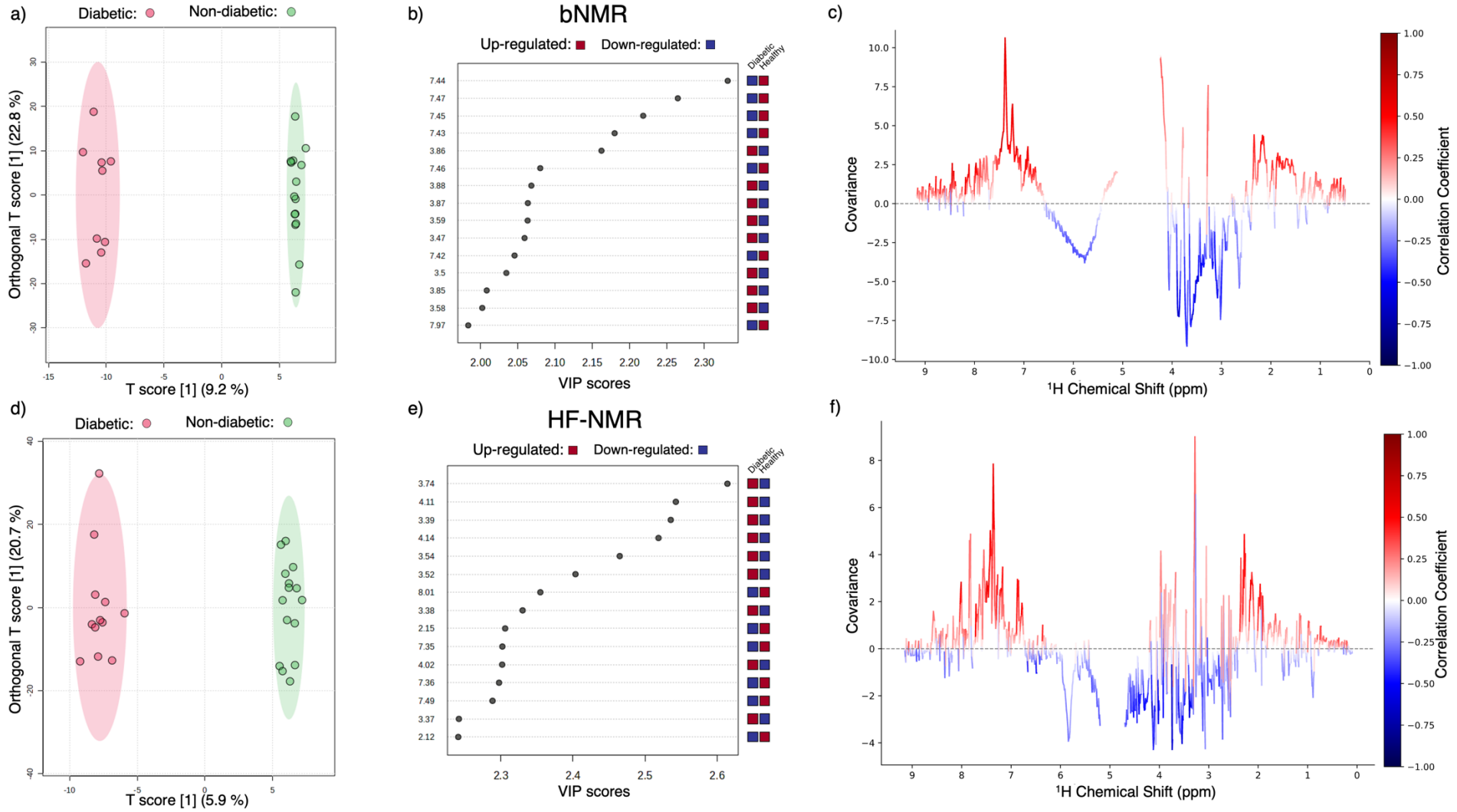

Figure 74 - OPLS-DA analysis of post-surgery non-diabetic (green) and diabetic (red) samples using bNMR and HF-NMR. a) bNMR score plot ($Q^2 = 0.657$, $p < 0.01$; $R^2 = 0.996$, $p < 0.05$) shows clear group separation. b) VIP scores highlight key discriminatory metabolites, and c) the S-line plot reveals metabolite covariance and correlation. d) HF-NMR score plot ($Q^2 = 0.357$, $p < 0.05$; $R^2 = 0.9923$, $p > 0.05$) shows partial group separation, with e) VIP scores and f) S-line plot identifying relevant metabolites. Ellipses indicate 95% confidence intervals.

a)

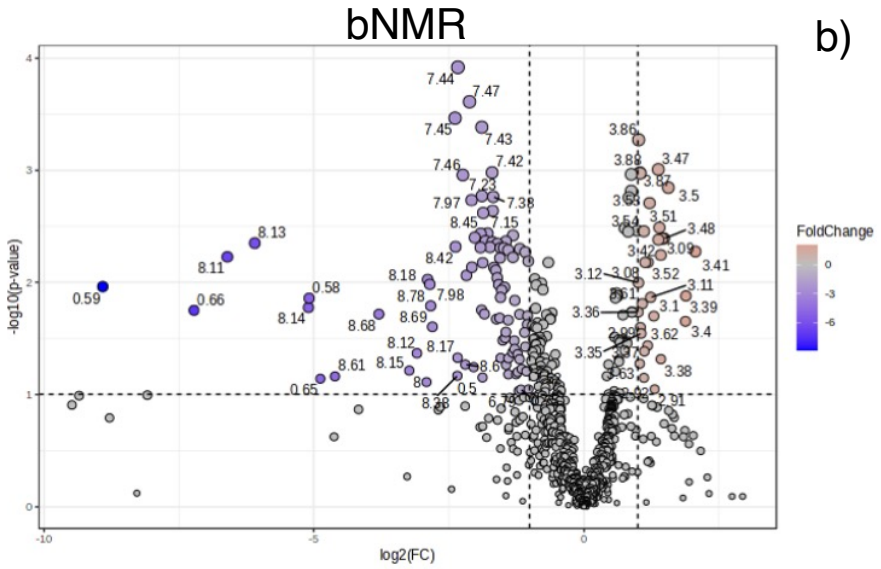
bNMR
-log10(p-value)
log2(FC)
FoldChange

b)

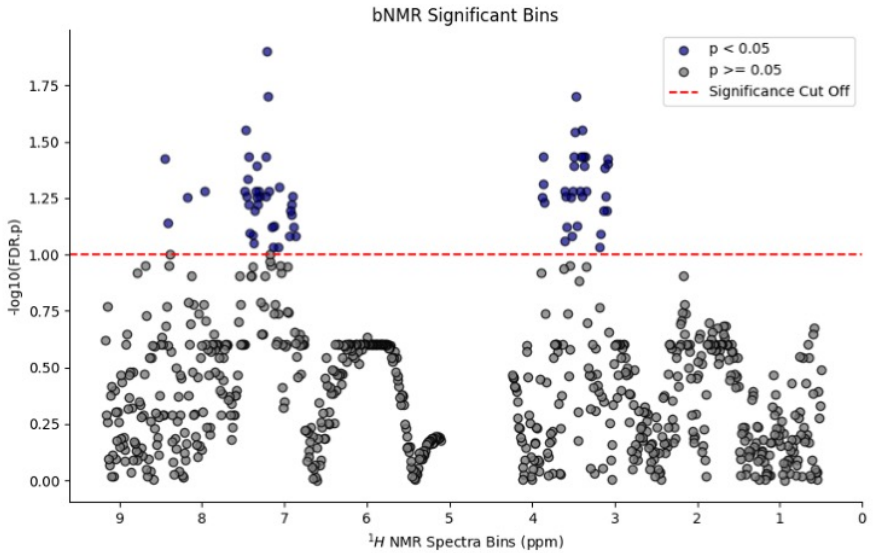
bNMR Significant Bins
p < 0.05
p >= 0.05
Significance Cut Off
-log10(FDR.p)
¹H NMR Spectra Bins (ppm)

c)

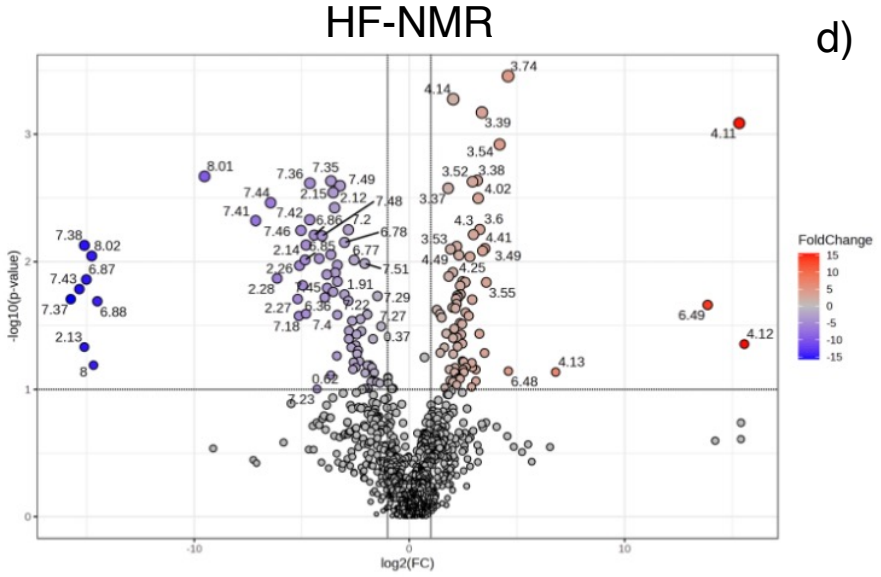
HF-NMR
-log10(p-value)
log2(FC)
FoldChange

d)

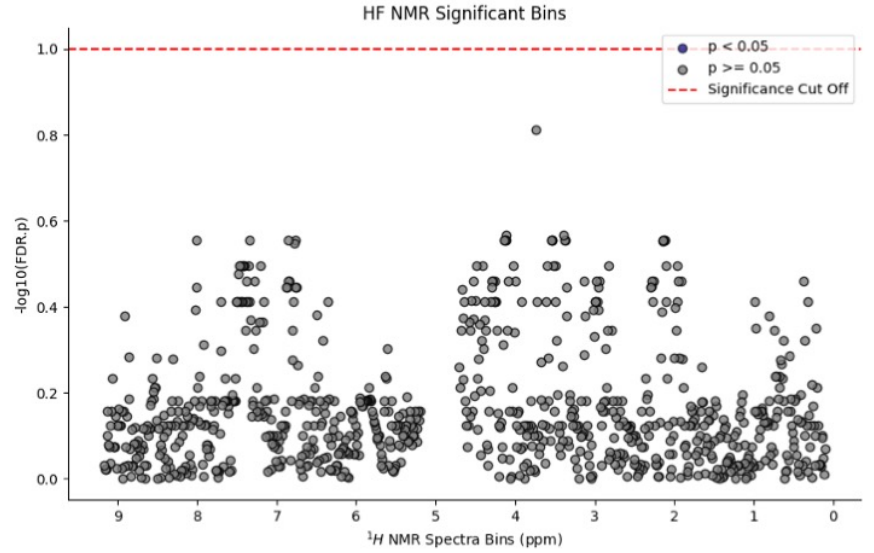
HF NMR Significant Bins
p < 0.05
p >= 0.05
Significance Cut Off
-log10(FDR.p)
¹H NMR Spectra Bins (ppm)

Figure 75 - Volcano and significance plots of metabolites bins between Diabetic and Non-diabetic Patients. a) and c) are volcano plots, with b) and d) showing FDR significant bins. a) and b) show bNMR data with c) and d) showing the HF-NMR data. FDR significant bins are shown in blue above the red dotted line in b) and d).

Table 2 summarised the metabolites with their VIP and ROC values, indicating that four metabolites were above the significance threshold: arginine, creatinine, formate, and glycine. The latter three also showed strong VIP values, with all four matching the diabetic trend, where arginine and formate decreased, and creatinine and glycine increased. ROC analysis revealed that no HF-NMR metabolites achieved an AUC above 0.7, whereas six bNMR metabolites did: arginine, creatinine, formate, glycine, hippuric acid, and TMAO. Additionally, bNMR data shows more metabolites with higher sensitivity and specificity compared to HF-NMR data. bNMR outperforms HF-NMR in identifying key metabolites and providing significant group separations. Metabolites like creatinine, formate, and glycine stand out as strong biomarkers in bNMR.

Table 12 - Summary of bNMR and HF-NMR urinary metabolites from the OPLS-DA and ROC analysis comparing non-diabetic and diabetic cohorts.

	bNMR						HF-NMR					
Metabolite	Diabetic Trend	VIP	Sensitivity	Specificity	AUC	p - value	Diabetic Trend	VIP	Sensitivity	Specificity	AUC	p - value
2 - Hydroxyisobutyrate	Down	0.210	0.8	0.5	0.533	0.760	Up	0.596	0.6	0.7	0.594	0.392
3 - Hydroxyisobutyrate	Down	1.125	0.6	0.9	0.644	0.099	Up	0.262	0.6	0.7	0.533	0.777
3 - Hydroxyisovaleric acid	Up	0.574	0.6	0.5	0.541	0.415	Up	0.477	0.7	0.6	0.628	0.537
4 - Hydroxyphenyl Acetate	Up	1.426	0.6	0.8	0.659	0.494	Down	0.884	0.8	0.4	0.594	0.275
Acetone	Down	1.100	0.8	0.7	0.674	0.154	Down	0.310	0.7	0.7	0.544	0.746
Alanine	Down	0.633	0.6	0.7	0.585	0.653	Down	0.285	0.7	0.5	0.544	0.852
Arginine	Down	1.390	0.8	0.7	0.741	0.039	Down	0.486	0.7	0.6	0.572	0.570
Choline	Up	1.322	0.8	0.5	0.644	0.382	Up	0.147	0.6	0.6	0.511	0.855
Citrate	Up	0.848	0.9	0.5	0.630	0.195	Up	0.282	0.5	0.7	0.517	0.752
Creatine	Down	0.291	0.6	0.7	0.504	0.672	Up	0.363	0.5	0.6	0.517	0.666
Creatinine	Up	1.418	0.7	0.9	0.726	0.034	Up	1.021	0.7	0.8	0.639	0.224
Dimethylamine	Up	0.364	0.6	0.7	0.556	0.606	Up	0.770	0.6	0.7	0.661	0.376
Formate	Down	1.966	0.7	0.7	0.711	0.047	Down	0.994	0.5	0.6	0.533	0.267
Glycine	Up	1.401	1	0.7	0.793	0.033	Up	1.014	0.8	0.5	0.650	0.222
Hippuric Acid	Down	0.963	0.7	0.7	0.741	0.175	Down	1.094	0.8	0.5	0.594	0.203
Lactate	Down	0.946	0.6	0.7	0.637	0.170	Down	0.337	0.6	0.7	0.578	0.663
Glucose	Up	0.251	0.7	0.7	0.630	0.687	Down	0.455	0.7	0.5	0.522	0.529
Trimethylamine-N-Oxide	Up	1.100	0.8	0.7	0.741	0.110	Up	0.017	0.7	0.5	0.600	0.935
Urea	Up	1.053	0.6	0.7	0.644	0.131	Up	0.758	0.8	0.7	0.667	0.341
Valine	Up	0.188	0.8	0.5	0.600	0.813	Up	0.417	0.7	0.6	0.578	0.533
α - Ketoisocaproic acid	Up	0.163	0.6	0.6	0.511	0.801	Up	0.675	0.6	0.5	0.506	0.402

7.3.6. Bariatric Surgery Outcome Prediction

A prediction model based on the HbA1c scores, using OPLS-DA, was applied to the outcome of bariatric surgery. The models used the cohort of pre-surgery samples and their respective HbA1c outcome health status from 6-months post-surgery. The study participants were categorised into groups based on their HbA1c improvement scores following bariatric surgery. The data was approximately split in half. A large improvement in a patient's HbA1c score was observed. Patients with a score of less than 11% were classified as the "small to no improvement" group, while individuals with scores exceeding 11% were placed in the "improvement" group.

The OPLS-DA plots presented in Figure 76 reveal contrasting outcomes between the bNMR and HF-NMR analyses. The bNMR results demonstrate insignificant low predictive ability and only moderate levels of explained variance. In contrast, the HF-NMR data exhibits a more predictive ability that is statistically significant. A high level of variance was explained too; however, this was above the significance threshold similar to the bNMR plot. Furthermore, the weighting of VIP scores differs notably between the bNMR and HF-NMR data, as illustrated in Figure 76c) and Figure 76f) in the region at around 3 ppm and 6 ppm. The volcano plots (Figure 77a and c) identify various metabolite bins as significant. However, it is important to note that the features depicted in Figure 77b) and 19d) lost their significance when an FDR correction was applied. Ultimately, no metabolite bins retained their significance after this correction. An analysis of the VIP and AUC levels, summarised in Table 13, highlights hippuric acid as a significant metabolite. This compound demonstrates a strong VIP score in both the bNMR and HF-NMR datasets. Hippuric acid appears to be increased in samples that exhibit an improvement trend following bariatric surgery. A few other metabolites were significant across both fields: creatine and glycine. bNMR also identified urea and α-Ketoisocaproic acid as significant, while HF identified citrate, dimethylamine, glycine, hippuric acid, and TMAO.

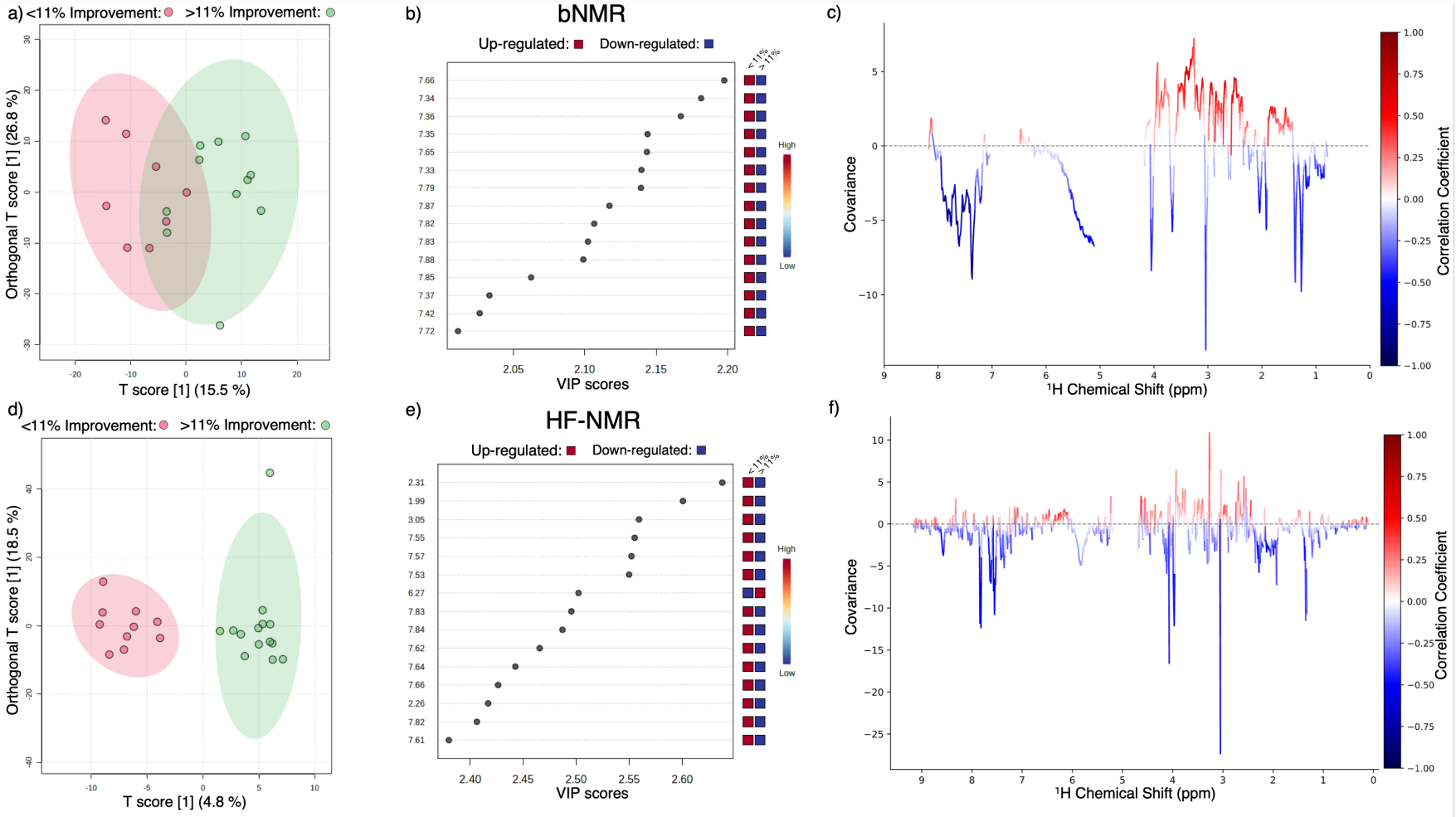

Figure 76 - OPLS-DA score plots for bNMR and HF-NMR comparing samples with <11% improvement (red) and >11% improvement (green). (a) bNMR: $Q^2 = 0.135$, $R^2 = 0.619$, $p > 0.05$ (<11%: n = 8, >11% n = 11), indicating limited predictivity and no statistically significant separation. (b) HF-NMR: $Q^2 = 0.291$, $R^2 = 0.706$, $p < 0.05$ (<11%: n = 10, >11% n = 11%), demonstrating moderate predictivity and significant group separation.

a)

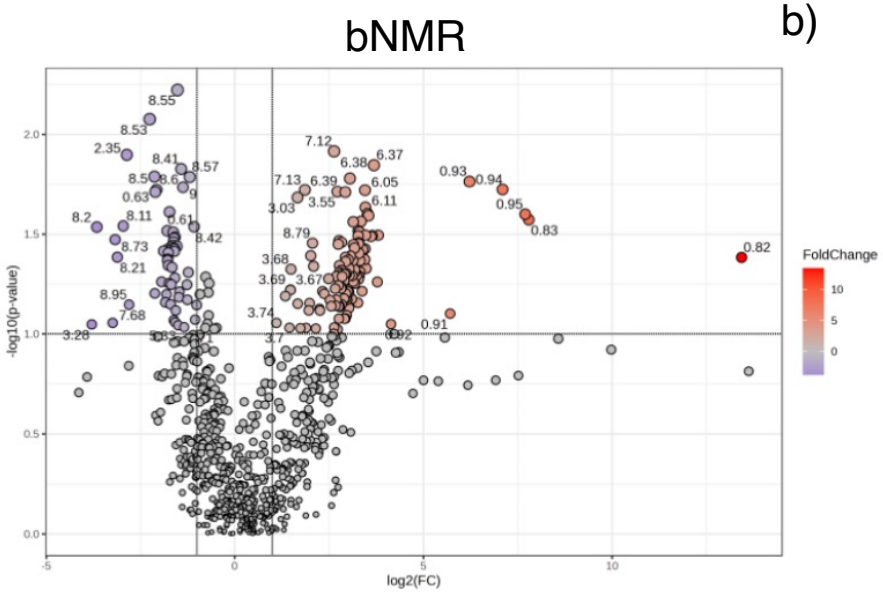
bNMR
-log10(p-value)
log2(FC)
FoldChange

b)

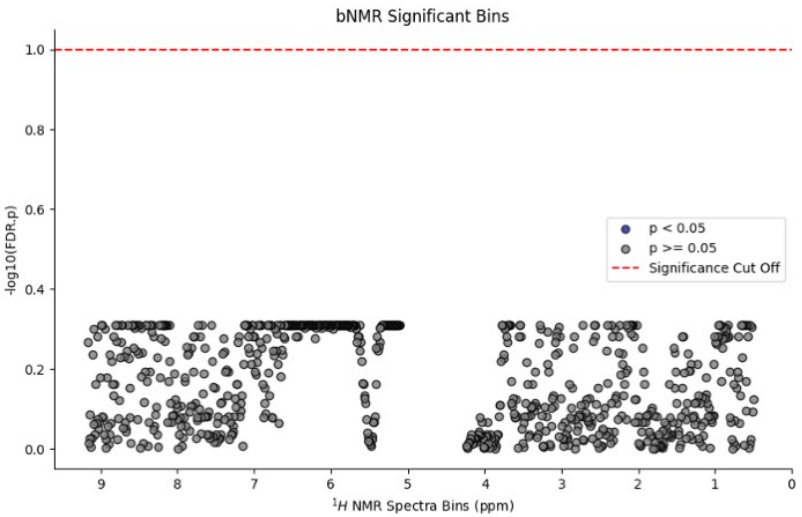
bNMR Significant Bins
-log10(FDR.p)
p < 0.05
p >= 0.05
Significance Cut Off
¹H NMR Spectra Bins (ppm)

c)

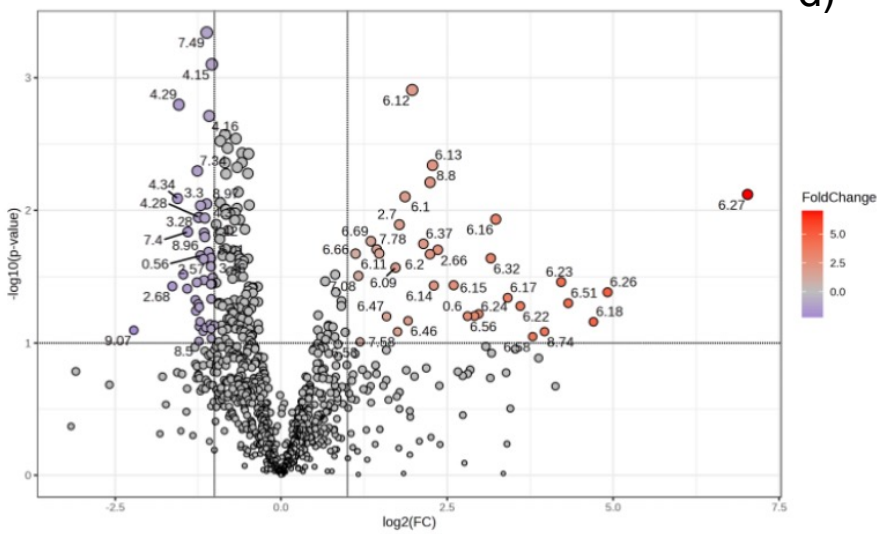
HF-NMR
-log10(p-value)
log2(FC)
FoldChange

d)

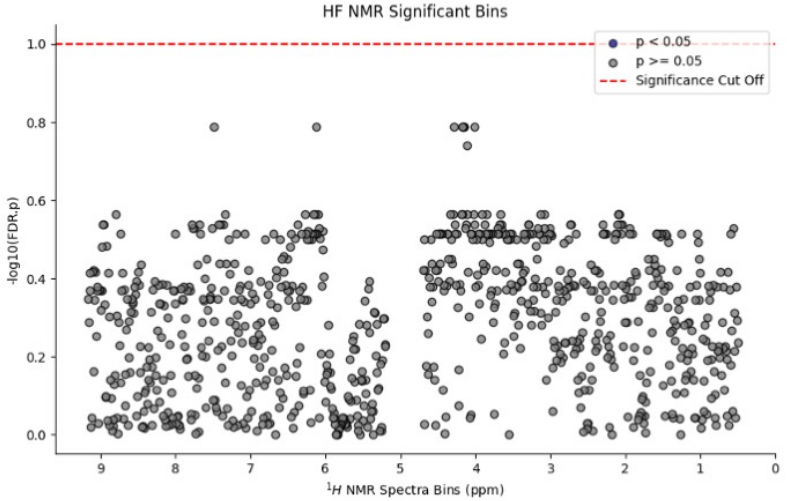
HF NMR Significant Bins
-log10(FDR.p)
p < 0.05
p >= 0.05
Significance Cut Off
¹H NMR Spectra Bins (ppm)

Figure 77 - Volcano and significance plots of metabolites bins between small to no improvement and improvement cohorts. a) and c) are volcano plots, with b) and d) showing FDR significant bins. a) and b) show bNMR data with c) and d) showing the HF-NMR data. The red line shown in Figures b) and d) is the significance cut-off line, where metabolite bins above this were below p of 0.05.

Ultimately, no metabolite bins retained their significance after this correction. An analysis of the VIP and AUC levels, summarised in Table 13, highlights hippuric acid as a significant metabolite. This compound demonstrates a strong VIP score in both the bNMR and HF-NMR datasets. Hippuric acid appears to be increased in samples that exhibit an improvement trend following bariatric surgery. A few other metabolites were significant across both fields: creatine and glycine. bNMR also identified urea and α-Ketoisocaproic acid as significant, while HF identified citrate, dimethylamine, glycine, hippuric acid, and TMAO. These results suggest that while HF-NMR has shown stronger predictive potential and correlation, bNMR could still be applicable if a model of particular metabolites is built.

Table 13 - Summary of bNMR and HF-NMR Urinary metabolites from the OPLS-DA and ROC analysis comparing improvement (>11% improvement) and small to no improvement (<11% improvement) sample cohorts.

	bNMR						HF-NMR					
Metabolite	Improvement Trend	VIP	Sensitivity	Specificity	AUC	p - Value	Improvement Trend	VIP	Sensitivity	Specificity	AUC	p - Value
2 - Hydroxyisobutyrate	Down	1.64	0.7	0.9	0.67	0.179	Down	1.05	0.6	0.6	0.57	0.497
3 - Hydroxyisobutyrate	Down	1.22	0.6	0.5	0.58	0.124	Up	0.84	0.9	0.5	0.60	0.580
3 - Hydroxyisovaleric acid	Down	1.37	0.6	0.5	0.63	0.150	Up	0.56	0.8	0.5	0.52	0.695
4 - Hydroxyphenyl Acetate	Up	0.64	0.7	0.6	0.57	0.499	Up	1.6	0.8	0.5	0.61	0.317
Acetone	Up	0.44	0.6	1	0.72	0.068	Up	0.44	0.8	0.5	0.58	0.661
Alanine	Down	1.44	0.8	0.7	0.67	0.194	Down	1.08	0.8	0.6	0.68	0.111
Arginine	Up	0.51	0.4	0.7	0.55	0.486	Down	1.42	0.8	0.5	0.64	0.090
Choline	Down	1.24	0.8	0.9	0.73	0.207	Up	1.81	0.9	0.5	0.69	0.110
Citrate	Up	1.72	0.6	0.8	0.71	0.249	Up	0.50	0.7	0.9	0.81	0.037
Creatine	Down	0.75	0.9	0.7	0.79	0.021	Up	1.77	0.7	0.7	0.71	0.043
Creatinine	Down	1.29	0.7	0.8	0.73	0.346	Up	1.60	0.7	0.6	0.72	0.047
Dimethylamine	Up	0.93	0.7	0.8	0.68	0.113	Up	1.67	0.9	0.9	0.85	0.005
Formate	Up	1.78	0.9	0.7	0.74	0.063	Up	1.05	0.6	0.7	0.64	0.493
Glycine	Up	1.7	0.6	0.9	0.71	0.019	Up	1.59	0.7	0.9	0.81	0.020
Hippuric Acid	Up	1.02	0.7	0.7	0.69	0.088	Up	1.71	0.8	0.9	0.79	0.036
Lactate	Down	1.64	0.8	0.6	0.67	0.068	Up	1.05	0.8	0.7	0.73	0.197
Glucose	Down	1.01	0.8	0.6	0.72	0.194	Up	1.68	0.8	0.8	0.75	0.167
Trimethylamine-N-Oxide	Up	0.91	0.8	0.7	0.77	0.090	Up	1.51	0.7	0.7	0.71	0.049
Urea	Down	1.25	0.6	0.8	0.70	0.041	Up	0.26	0.4	0.6	0.5	0.989
Valine	Down	2.07	0.7	0.7	0.70	0.104	Up	1.05	1	0.6	0.70	0.196
α - Ketoisocaproic acid	Down	2.05	0.7	0.9	0.70	0.017	Up	1.201	0.8	0.6	0.635	0.845

7.4. Discussion

7.4.1. Bariatric Surgery

Bariatric surgery has emerged as a viable intervention for managing obesity and its associated comorbidities, including insulin resistance and T2DM.[305] With the number of bariatric surgeries increasing by over 66% from 2011 to 2021 in America alone [305], this study aimed to investigate three key aspects: (1) whether bNMR can predict bariatric surgery outcomes, (2) if there are changes to the metabolome between different types of bariatric surgery, and (3) whether bNMR can distinguish between non-diabetic, pre-diabetic, and diabetic samples.[305] The results reveal distinct metabolic profiles from bariatric procedures, HbA1c health status and the potential of NMR as a surgery outcome predictor.

The PLS-DA plots in Figure 69 demonstrated significant differences ($p < 0.05$) in the metabolic profiles among the three bariatric surgery types (BPD, LGCP, and LAGB) and pre-surgery samples. Notably, the metabolic signature of BPD was distinct from that of gastric restriction-specific surgeries (LGCP and LAGB), as seen in Figure 70. This suggests that the type of bariatric surgery plays a crucial role in shaping the postoperative metabolic landscape. Previous studies comparing metabolomic profiles of RYGB, LAGB, LGCP and BPD have supported these differences; however, these studies focused on blood plasma and serum rather than urine.[306–309]

In a study by Kayser *et al.* (2017), metabolite differences between surgery types were reportedly less prominent 12 months post-surgery, with gastric restriction surgeries showing a return to baseline values after 3 months, unlike RYGB surgery.[310] This recovery pattern for LAGB, a type of gastric restrictive surgery, agrees with the findings in this research and could explain the lack of changes observed in the metabolomes seen in Figure 68 and Figure 69.

BPD surgery results in complex alterations to the metabolites due to the modifications in multiple factors such as gastric emptying, intestinal nutrient exposure, and energy expenditure.[311] Notable metabolites identified by this study include 3-hydroxyisovaleric acid, 4-hydroxyphenylacetate, acetone, Glucose, urea

and valine. These were statistically significant ($p < 0.05$), had a high VIP score (indicating strong contributions to the OPLS-DA model), and had high AUC value as summarised in Table 11. Low glycine levels were observed, these findings support the current literature, which indicates that bariatric surgery induces metabolic changes that are associated with alterations in amino acid and branched-chain amino acid concentrations. [307–309] These results suggest that these metabolites have a potential role in mediating the metabolic effects of BPD, warranting further investigation into their specific contributions to insulin resistant improvement.

7.4.2. Prediction of Surgery Outcome

The application of OPLS-DA to assess the correlation between metabolic changes and HbA1c improvement revealed promising predictive power (Figure 76). The separation plots (Figure 76a and d) indicate a distinction between patients with varying HbA1c improvement, suggesting a potential association between specific metabolic alterations and improvements in glycaemic control post-surgery. The HF-NMR (Figure 76a) and bNMR (Figure 76d) showed strong predictive potential and correlation. However, while the HF-NMR OPLS-DA model was classified as significant, the bNMR model did not meet the significance threshold of $p < 0.05$. Although Figure 76c) and f) suggest similar weighting, the differences are most likely due to lower sensitivity and signal overlap observed in bNMR spectra.

It is important to note that the OPLS-DA models experience a high likelihood of overfitting, underscoring the need for validation in larger independent cohorts. This caution is further supported by the results observed after applying an FDR correction in Figure 77b) and d), where no metabolite bin remained significant. Similarly, in the area under the curve of the receiver operating characteristic (AUCROC) models (Table 13), only glycine met the significance threshold, (had an AUC above 0.7, and a VIP score above 1) in both the bNMR and HF-NMR data. This metabolite demonstrates the most potential to be used as a predictor, as patients with higher glycine concentrations showed an 11% improvement in their HbA1c score. However, some metabolites were significant in their respective cohort. This was urea and α - Ketoisocaproic acid in the bNMR data and TMAO, hippuric acid, creatine, creatinine and dimethylamine. It is unclear why metabolites between spectrometer fields did not correlate clearly. Some metabolites such as

dimethylamine, hippuric acid, TMAO did correlate between the spectroemters, however, creatine, creatinine, urea and α - Ketoisocaproic acid were not consistent, potentially due to differences of magnet size, or from different excitations between presatureation and WET pulse sequences.

It is worth noting that while this study focused on urine samples using bNMR, other research efforts in T2DM prediction have employed more sensitive techniques, such as mass spectrometry and liquid chromatography, and have primarily focused on other biological samples, such as blood plasma and serum. [312–314] Additionally, these studies have utilised alternative predictive models to the HbA1c scores, such as DiaRem, ABCD, and IMS. [312–314] This difference in approach highlights the novelty of this study in exploring urine-based metabolomics for predicting bariatric surgery outcomes. This is especially advantageous as there are less requirements for sample collection and preparation.

7.4.3. Health Types and Detection

Diabetes and pre-diabetes detection and monitoring rely on several diagnostic methods, including fasting plasma glucose, oral glucose tolerance test and HbA1c, with HbA1c being one of the most widely used.[315] While this classification system has improved health monitoring of diabetes and glucose control, it has limited utility by only diagnosing pre-diabetes and diabetes. This research explored if bNMR could distinguish between healthy, diabetic and pre-diabetic individuals, differing from existing research by including a pre-diabetic sample cohort and an HbA1c-classified healthy group that is largely morbidly obese and have been through bariatric surgery.

Initial analysis using PCA and SPLS-DA models (Figure 64Figure 65) revealed they were unable to resolve between groups. However, the more supervised OPLS-DA model identified a correlation between HbA1c-identified healthy and diabetic samples with strong predictive potential. Both bNMR (Figure 74a) and HF-NMR (Figure 74d) demonstrated strong predictive potential (0.657 and 0.357, respectively) with statistical significance ($p < 0.01$ and $p < 0.05$, respectively) in distinguishing urine from non-diabetic and diabetic patients. A strong correlation between models was observed with both R^2 exceeding 0.99. Notably, only the

bNMR OPLS-DA plot showed a statistically significant R^2 value (R^2: 0.996, $p < 0.05$), differing from the HF-NMR model (R^2: 0.9923, $p > 0.05$). These results align with comparable bNMR and HF-NMR diabetes research, differing only in the HF-NMR R^2 value threshold for significance.[59,109,298,299,316,317]

The covariance observed in Figure 74c) and Figure 74f) shows similarities in the trends of significant metabolite regulation across the spectra. Table 12 further supports these findings, with the diabetic trends in metabolites such as creatinine, glycine, and hippuric acid matching metabolite regulation. These metabolites also exhibited strong VIP values (> 1) and were consistent with previous research summarised by Long *et al*. (2020), showing a significant association with diabetes. 309 By contrast, pre-diabetes could not be distinguished between non-diabetic or diabetic groups in both pre-surgery (Figure 66) and 6-month post-surgery for the bNMR samples, it could however be distinguished by HF-NMR for the post surgery data.

This contradicts previous research that identified glycine as a biomarker for pre-diabetes.[319] However, the disparity may be explained by different classification metrics; Wang-Sattler *et al.* (2012) classified pre-diabetes based on impaired glucose tolerance or impaired fasting glucose, rather than on HbA1c levels as used in this study. Previous research into pre-diabetes biomarkers has identified 32 metabolites, four of which (alanine, 3-hydroxy isovaleric acid, valine and glycine) were also identified in this study.[318] Differences in the identified metabolites may arise from inherent sample differences, with this study using urine samples instead of blood samples used in previous research.

The HF-NMR OPLS-DA models comparing diabetes and pre-diabetes (*Figure 72*d) , showed greater predictive potential (Q^2 = 0.244, and Q^2 = 0.457) and strong correlation (R^2 0.995 and R^2 0.93), respectively. However, these results should be interpreted cautiously as they did not meet the significance threshold ($p < 0.05$). The superior predictive ability and correlation of the HF-NMR model over the bNMR model could be attributed to the improved sensitivity of the HF-NMR spectrometer. This suggests that smaller biochemical fluctuations between these groups are detectable on HF-NMR spectrometers.

One factor that can cause differences in results is the unique characteristics of the group being studied, compared to similar studies.[319] While the patients' history before the study was unavailable, it is highly likely that these subjects had been struggling with weight control for some time to meet the criteria for bariatric surgery. Consequently, covariances such as insulin resistance may have affected results without being recorded.[320] Therefore, further longitudinal studies are needed to address metabolome changes associated with fluctuating HbA1c levels. Such research could lead to a better understanding of permanent changes in metabolism due to weight gain, insulin resistance, and diabetes treatment.

7.4.4. Metabolites

The emergence of glycine as the strongest predictor of HbA1c improvement (11% improvement in patients with higher glycine) is particularly noteworthy and aligns with extensive literature demonstrating reduced glycine levels as a hallmark of T2DM and metabolic dysfunction.[321] Glycine's roles, including potentiation of glucose-induced insulin secretion, anti-inflammatory effects, and serving as a precursor for glutathione synthesis, position it as a central mediator of metabolic recovery post-bariatric surgery.[321,322] The consistency of this finding across both bNMR and HF-NMR datasets strengthens confidence in its prognostic utility and suggests potential for clinical translation as a pre-operative screening tool to identify patients most likely to achieve diabetes remission.

The identification of valine, 3-hydroxyisovaleric acid, and α-ketoisocaproic acid as significant biomarkers reflects the well-established role of BCAA dysregulation in insulin resistance and T2DM pathogenesis.[322–324] Elevated BCAAs activate mTOR signalling, impair insulin signalling cascades, and reflect mitochondrial dysfunction in BCAA catabolism, all central features of diabetic metabolism.[324,325] Bariatric surgery, particularly BPD with its malabsorptive component, normalises BCAA levels through multiple mechanisms including reduced absorption, altered gut microbiome composition, and improved mitochondrial function.[326,327] The detection of α-ketoisocaproic acid, a BCAA catabolism intermediate, in the bNMR data is particularly valuable as it captures metabolic pathway activity rather than just static metabolite concentrations, potentially providing greater mechanistic insight.

The identification of hippuric acid, TMAO, dimethylamine, and 4-hydroxyphenylacetate reflects the profound restructuring of the gut microbiome following bariatric surgery.[326,328] Bariatric procedures, especially those with malabsorptive components like BPD, fundamentally alter nutrient flow through the gastrointestinal tract, leading to shifts in microbial populations and their metabolic outputs.[326,327] Hippuric acid, derived from microbial metabolism of dietary polyphenols, and TMAO, produced from choline and carnitine metabolism, serve as windows into this microbial reprogramming.[329] The association of decreased hippuric acid with T2DM remission aligns with literature demonstrating that specific microbiome configurations favour metabolic health.[326] The complex relationship observed with TMAO, where its directional change rather than absolute level may be predictive warrants further investigation but likely reflects individual variation in gut microbiome responses to surgery.

The distinct metabolic profile of BPD compared to restrictive procedures (LAGB, LGCP) has strong biological justification. BPD creates significant malabsorption through biliopancreatic diversion, leading to: (1) increased fat oxidation and ketogenesis (evidenced by elevated acetone), (2) altered amino acid absorption and metabolism (reflected in BCAA metabolites), and (3) dramatic shifts in gut microbiome ecology (captured by aromatic amino acid metabolites like 4-hydroxyphenylacetate).[321–329] The absence of detectable changes in LAGB metabolomes at 6 months aligns with Kayser et al. (2017), who reported that restrictive surgeries show metabolic recovery toward baseline by 3 months, unlike malabsorptive procedures which maintain distinct metabolic signatures long-term.[310] This suggests that BPD's metabolic benefits derive partly from sustained alterations in nutrient handling rather than solely from weight loss.

The identification of creatinine and urea as discriminators between diabetic and non-diabetic groups reflects the intimate connection between diabetes and renal function. Diabetic nephropathy is a leading cause of kidney disease, and alterations in creatinine clearance and urea metabolism serve as sensitive indicators of renal health.[272] Bariatric surgery improves renal function through multiple mechanisms including weight loss, improved glycaemic control, and reduced inflammation, all of which are captured in the normalisation of these metabolites. The concordance

between bNMR and HF-NMR for these markers strengthens their validity as clinical indicators.

The comparison of metabolites identified in the bNMR and HF-NMR spectra, Figure 62 and Figure 63, reveals fewer identifiable metabolites in the bNMR data. This observation is consistent with expectations, given the lower sensitivity and increased peak widths associated with bNMR technology. The number and types of identifiable metabolites are comparable to those reported in similar published research.59,108 However, it is important to note that certain key metabolites, specifically α and β glucose signals surrounding the water signal, which were identified in previous bNMR studies, were not detected in this research.108,289,290 This disparity between identifiable metabolites could be due to the different operating temperatures of the Oxford Instrument bNMR spectrometer used in this study (40°C) compared to the Magreteck spectrometer (25°C) employed in previous bNMR diabetes studies.

Another significant difference in this research is the use of the WET-180 pulse sequence, as opposed to the presaturation sequence commonly employed in previous bNMR diabetes studies.[109,298,299] While both pulse sequences are designed to reduce the water signal, the presaturation sequence can potentially yield better results and offer more selectivity than the WET pulse sequence.[330] The pre-sat pulse sequence was initially tested during parameter exploration and optimisation for this study, but it produced less optimal results compared to the WET-180 sequence in bNMR analysis.

The absence of glucose peaks in the spectra may also be influenced by the fact that many patients in this study were reportedly taking medication or the water suppression pulse sequence used (Appendix 14). These medications are known to manage and alter glucose concentrations, potentially affecting the detectability of glucose in the urine samples. For example, Metformin, a common medication for treating T2DM, works by decreasing glucose production in the liver and improving glucose uptake by cells.[331–333] Sulfonylureas, another class of T2DM medications, stimulate the pancreas to produce more insulin, which helps regulate insulin and reduce blood sugar levels.[334–338] This could also help to explain why differences between disease states are not as pronounced.

7.5. Future Work

While this study has provided valuable insights into the metabolic changes associated with bariatric surgery and diabetes progression, several limitations must be acknowledged and addressed in future research. The relatively small sample size (120 samples) in this study may limit the generalisability of the findings. Future research should aim to incorporate larger and more diverse cohorts to enhance the statistical power and external validity of the results. This could include patients from various ethnic backgrounds, age groups, and geographical locations to account for potential genetic and environmental influences on metabolic profiles.

Potential confounding factors such as dietary habits, physical activity levels, and medication use were not comprehensively addressed in this analysis. Future studies should implement more rigorous controls for these variables, possibly including detailed dietary logs, physical activity trackers, and comprehensive medication histories. This would allow for a more nuanced understanding of how these factors interact with metabolic changes post-surgery and at the bNMR scale.

A key limitation of this study is the lack of comparison with healthy individuals who have never been diagnosed with diabetes or classified as clinically overweight. Including such a control group in future research could reveal potentially irreversible metabolic pathway changes that might be distinguishable from the current dataset. This comparison could provide insights into the long-term metabolic consequences of obesity and diabetes, even after successful interventions.

The cross-sectional nature of this study limits the ability to establish causality between metabolic changes and surgical interventions. Future research should prioritise longitudinal studies that track patients over extended periods post-surgery, ideally for several years. This approach would provide a more robust understanding of the dynamic nature of metabolic alterations and could reveal long-term trends and potential relapses.

While this study focused on metabolomics using NMR spectroscopy, future research could benefit from integrating multiple omics approaches. Combining metabolomics with genomics, transcriptomics, and proteomics could provide a more

comprehensive picture of the molecular mechanisms underlying metabolic changes post-bariatric surgery. Given the differences observed between bNMR and HF-NMR results, future studies should work towards standardising NMR protocols for metabolomic analysis in diabetes and obesity research. This could include comparative studies of different pulse sequences, sample preparation methods, and data analysis techniques to establish best practices in the field.

The identification of key metabolites such as hippuric acid warrants further investigation into specific metabolic pathways affected by bariatric surgery and diabetes progression. Future studies could focus on targeted analyses of these pathways to elucidate their roles in metabolic improvements post-surgery. As this research progresses, efforts should be made to translate these findings into clinical applications. This could include the development of predictive models for surgical outcomes based on pre-operative metabolic profiles or the creation of non-invasive monitoring tools for post-surgical metabolic health.

By addressing these limitations and pursuing these future directions, researchers can build upon the foundation laid by this study to further understanding of the complex metabolic changes associated with bariatric surgery and diabetes progression. This knowledge will be crucial in developing more personalised and effective interventions for obesity and diabetes management.

Chapter 8 Final Discussion

This study has explored a range of biofluids, and pulse sequences to evaluate the potential of bNMR spectroscopy for disease detection. While prior bNMR research has primarily focused on diabetes and tuberculosis, this work has significantly expanded the scope by investigating additional diseases and challenging the technology with closely related disease phenotypes.

8.1. Disease Detection, Monitoring and Prediction

A key finding of this research was bNMR's ability to differentiate between various health states. For instance, the technology successfully distinguished HbA1c-defined healthy individuals from diabetic patients who had undergone bariatric surgery using urine samples (as discussed in Chapter 7). These findings are consistent with existing bNMR and HF-NMR research on diabetes detection. This study builds on previous work by including patients classified as pre-diabetic based on HbA1c levels, as suggested by Edgar *et al.* (2021). Interestingly, in this study, presented in this research, neither bNMR nor HF-NMR could distinguish this pre-diabetic state from healthy or diabetic patients, highlighting a potential limitation in detecting subtle metabolic changes. Previous research has successfully detected these changes using HF-NMR, though this was conducted using blood samples instead of urine. [339,340] Future research could investigate whether biofluid differences may influence pre-diabetes detection. In developing an action plan to combat diseases such as T2DM, health practitioners need to consider cost-effective solutions and ensure that the plan is suitable for the patient.

While the primary goal of healthcare is to provide the best possible care, it is equally important that the implemented plan yields meaningful results. Consequently, this research also determined the potential to use bNMR in predicting significant improvements in HbA1c results following bariatric surgery. While bNMR demonstrated promising predictive potential (Q^2: 0.135) and correlation (R^2: 0.619), it lacked statistical significance ($p > 0.05$) when compared to HF-NMR (Q2: 0.291, $p < 0.05$). These results suggest that predicting the outcomes of bariatric surgery may require a higher sensitivity of instruments, such as that of the 400 MHz HF-

NMR, than bNMR currently offers. Further exploration of pulse sequences, sample preparation, and a targeted approach could enhance the viability of bNMR for predicting surgical outcomes.

Contrastingly, in the asthma study analysing blood plasma (explored in Chapter 6), bNMR successfully differentiated between MA, DTC asthma, and HCs. Although HF-NMR showed stronger correlation and predictive potential between disease states, bNMR still met the statistical significance threshold, highlighting its potential as a valuable tool in disease detection and distinction. It also shows that bNMR has the ability to differentiate disease phenotypes, opening the possibilities for other diseases and comorbidities like chronic obstructive pulmonary disease (COPD), chronic kidney disease (CKD), and coronary heart disease (CHD).

Ruiz-Cabello *et al.* (2022) were among the first to explore the detection of closely related diseases and health states using blood plasma with bNMR. Although they claimed "perfect discrimination" between tuberculosis (TB) and paratuberculosis (PTB) using PCA, their conclusion is questionable as the 95% confidence regions necessary to support this claim were not presented. Similarly, their conclusion that cows could be differentiated based on vaccination status lacked data as evidence, with the confidence regions crucially missing. In contrast, this asthma study has, for the first time, shown the ability to distinguish between groups in a predictive model that is supported by data statistically. However, the limitations of bNMR revealed by this study need to be acknowledged. The technology struggled to distinguish between DTC and HCs, although these results were close to the significance threshold.

Similarly, in the IE study using canine CSF samples (Chapter 5), bNMR showed a lack of correlation and predictive potential for distinguishing IE from HCs. These observations emphasise the importance of understanding bNMR's role within the broader context of metabolomics research and clinical diagnostics. This study was also not without its limitations. Ethical considerations prevented the inclusion of true HCs in the sample cohort, as only animals visiting the vet for potential ailments were included. Future work should investigate whether this was a contributing factor and incorporate other diseases into the model.

While bNMR may not be suitable for in-depth characterisation of metabolic pathways, where HF-NMR analysis remains preferable, it shows considerable promise in developing detection models for conditions involving larger metabolic changes. In addition to bNMR's ability to distinguish between certain health states, it is also able to do this at a lower cost than HF-NMR analysis, making it an attractive option for large-scale screening and monitoring programs.

8.2. Metabolites and Future Detection and Monitoring of Diseases

Identifying disease-associated metabolites using bNMR presents significant implications for diagnostic and monitoring capabilities in a clinical setting. This research has unveiled the detectable metabolites in human blood plasma and urine, as well as the CSF analysis of dogs through bNMR analysis. Additional work, detailed in the appendices, has shown similar metabolites identified in cat urine (CKD) (Appendix 17-20), human blood serum (Appendix 22 and 23), and broth media obtained from bacterial culture cultivation (Appendix 21 and 22). However, it is important to provide support for research efforts going forward. To support future research efforts, enrichment analysis via MetaboAnalyst (version 6.0) revealed specific metabolite hits across various pathways.

In the blood plasma study on asthma, 21 metabolites were identified in the bNMR spectra, while HF-NMR detected 23 metabolites. The difference in the number of identified metabolites can be attributed to variations in sensitivity and peak widths between the two analytical platforms. This was an anticipated result based on previous research between spectrometer frequencies. Previous research has also shown similar observations, such as post-bariatric surgery urine analysis and the CSF study on IE in dogs.

The incomplete identification of all spectral peaks highlights current limitations in metabolomics database completeness. Most publicly available databases lack (such as the HMDB) comprehensive coverage above 1,000 MHz and below 100 MHz, which is not solely a limitation of bNMR but reflects a broader challenge for emerging analytical technologies. For instance, while Chenomx claims the capacity to identify 338 small molecules across various sample types, this technology

remains in its infancy, and the identification accuracy does not yet match that achievable with high-field NMR data.

The HMDB reports over 2,500 identified metabolites in biofluids; however, both benchtop and high-field NMR demonstrate limited coverage compared to mass spectrometry approaches, primarily due to lower instrumental sensitivity. Nevertheless, no single analytical platform can comprehensively identify all metabolites present in complex biological samples, given their diverse chemical properties and concentration ranges. As discussed in Chapter 1.6.5, gas chromatography-mass spectrometry (GC-MS) typically covers approximately 200 metabolites, while liquid chromatography-mass spectrometry (LC-MS) extends coverage to over 1,000 metabolites. This inherent complementarity among analytical platforms underscores that unidentified peaks represent both technical limitations and potentially novel or low-abundance compounds not yet catalogued in existing databases.

It is important to note that the goal of this research was not to identify all metabolites present in the samples, but rather to determine which metabolites are detectable using the lower sensitivity benchtop NMR technique. From the identified range of metabolites observed across urine, saliva, and blood, enrichment analysis on potential diseases that could be detectable was subsequently completed.

Enrichment analysis (Appendix 9.5) of the bNMR metabolites identified in blood plasma indicated 110 diseases that could be explored with the simplistic sample preparation of the EDTA tubes. These findings suggest that the identified metabolites could serve as reliable biomarkers for detecting and monitoring many other diseases. For instance, colorectal cancer, early preeclampsia, and pancreatic cancer all shared metabolites with those identified in Appendix 5 during this study (14, 12, and 10 metabolite hits respectively during enrichment analysis). bNMR could, therefore, be well suited to support the health objectives of healthcare providers like the NHS. Furthermore, bNMR could be used to improve cancer detection and monitoring and help reduce maternity-related deaths.

The early identification of diseases through metabolic profiling could enhance treatment efficacy and patient outcomes. Both early and late-onset preeclampsia

showed notable metabolites hits during enrichment analysis (12 and 11, respectively), indicating that metabolic changes could be instrumental in predicting and managing preeclampsia, potentially reducing adverse outcomes in pregnancies. Diseases such as schizophrenia and Alzheimer's disease also displayed significant metabolite hits, suggesting that metabolic profiling could aid in understanding the biochemical underpinnings of these complex disorders, possibly leading to improved diagnostic and therapeutic strategies.

For the bNMR analysis of CSF, the broad signals and low signal-to-noise ratio (SNR) made interpreting different amino acids, such as leucine and isoleucine, challenging. Nevertheless, out of the 16 metabolites that could be detected, 26 diseases identified from enrichment analysis (detailed in Appendix 9) were linked to CSF-related diseases and deficiencies. However, the lack of current research into bNMR CSF-related studies highlights the need for further research efforts to be undertaken to fully utilise the potential of bNMR in metabolomic studies. The list includes important and hard-to-diagnose neurological diseases that have the potential to be detected including Alzheimer’s disease, schizophrenia, and dementia. Routine diagnostics for Alzheimer’s and dementia are achieved *via* psychological examination. The implementation of analytical techniques for detection such as bNMR could improve accessibility for target populations most at risk such as individuals in care homes. This would additionally relieve the burden on practitioners and free up their time for other responsibilities.

From the bariatric surgery urine study, a total of 20 metabolites were detectable by bNMR when compared to HF-NMR, the only undetected metabolite was α-Ketoisocaproic acid. This correlates to 38 significant diseases (identified from enrichment analysis in Appendix 15) that have the potential to be detected and monitored by bNMR and much like with the CSF (Appendix 9) and blood plasma asthma (Appendix 5) studies, enrichment analysis includes cancers and neurological diseases. This highlights a potential starting point for future research, initially targeting well-understood diseases. However, these results should be interpreted cautiously due to the unknown capabilities of bNMR in detecting many of the suggested diseases. The associations between metabolites and diseases are important, but this research cannot conclude whether bNMR has the sensitivity required to differentiate potential small changes in the metabolome in diseases not

yet studied. Instead, they provide a foundation from which bNMR could be trialled for certain diseases, detection models, prognosis, and tracking.

8.3. Sample Preparation and Pulse Sequence Recommendations

A significant limitation of this research that warrants further investigation is the time required for sample analysis. With an average of two hours per sample for shimming, locking, and acquisition, future work could focus on optimising these processes to reduce analysis times without compromising detection accuracy. This optimisation will be crucial for the technology's practical implementation in clinical settings.

Throughout this investigation, several limitations were encountered. To maintain the cost and time benefits associated with bNMR, minimal sample preparation was undertaken. While advantageous in terms of practicality, this approach presented challenges when analysing complex biofluids such as CSF and blood serum/ plasma. In these cases, it was necessary to adopt pulse sequences capable of suppressing both water and macromolecule signals. Despite these challenges, bNMR demonstrates the capability to detect numerous metabolites, even in the presence of these additional relaxation mechanisms, highlighting its potential utility in clinical applications. A small preliminary study on the effects of NMR tube parameters on bNMR spectra was conducted, as shown in Appendix 16. The results demonstrated that more economical tubes perform just as well as those recommended for higher-field spectrometers. Consequently, significant cost reductions can be achieved by selecting the most affordable, suitable tubes for analysis.

The sample preparation and data acquisition methods employed in the blood plasma asthma study may have limited the separation observed between health types. The use of EDTA tubes for blood collection and the relatively minimal sample preparation protocol led to spectra with several unwanted signals. Additionally, the use of formate as an internal standard may have introduced an inherent limitation,

as blood can naturally contain small concentrations of formate. By adding formate, it could limit its use as a biomarker in asthma detection and prognosis.[341]

In a previous study, Ruiz-Cabello *et al.* (2022) also used plasma, although undertook the approach of completing further sample preparation to study bovine tuberculosis (TB). Ruiz-Cabello *et al.* (2022) used a centrifugal filter with a 3 kDa molecular weight cutoff to remove protein and lipid components from the sample**.** This costs between £3.34 - 6.36 on the filters alone per sample. This allowed the researchers to use the PRESAT pulse sequence without the need for a T2 filter. However, Ruiz-Cabello *et al.* (2022) failed to report the metabolites that they were able to identify using bNMR. With the cost of analysis completed throughout this research costing less than £2 per sample, the added filters add a large additional cost. With no spectra provided by Ruiz-Cabello *et al.* (2022) in their study, it is hard to compare the cost-to-value ratio of these additional sample preparation steps. However, future studies could be conducted to replicate the study completed by Ruiz-Cabello *et al.* (2022) and identify all metabolites present.

This research explored a range of pulse sequences, including WET-180-NOESY, WET-180, WET-CP, Presaturation, WET-180-CPMG, WET-180-Project, WASTED-II, and Robust-5. For bNMR urine analysis, WET-180 or WET-CP are recommended based on their superior performance of water suppression and the limited effect of the far-away solvent signal. Traditional water suppression techniques such as WATERGATE or presaturation, used more commonly in HF-NMR studies, provided insufficient SNR and water suppression, respectively.

The WASTED-II sequence, incorporating a T2 filter, showed promising results for water and protein suppression for plasma, serum and CSF. While WET-180-CPMG and WET-180-PROJECT were also tested, the results obtained were poor, potentially suggesting stability problems with the lock, which the WASTED-II pulse sequence was able to overcome. Previous research in CSF analysis using NMR has predominantly focused on two pulse sequences: Presat-NOESY and CPMG. Presat-NOESY is widely adopted due to its simplicity and apparent enhancement of small molecule signals. However, in cases where CSF samples contain high protein content, some studies opt for T2-filtered sequences like CPMG. The research findings indicate that WASTED-II outperformed all other tested pulse sequences,

(for samples with macromolecules present) including WET-180, WET-180-NOESY, Presaturation, WET-CPMG, and WET-PROJECT. The research also revealed that, because of the minimal sample preparation, a T2 filter was necessary to prevent interference from proteins. The T2 filter is capable of efficiently reducing protein signals without requiring complex sample preparation or pulse sequence optimisation. Considering the straightforward sample preparation protocol used in this study, there is considerable potential for implementing this approach in clinical settings.

With only one previous study completed using bNMR for saliva, future research efforts should explore this non-invasive biofluid further. Despite the lower abundance of metabolites in saliva, its less invasive nature combined with the cost-effectiveness of bNMR analysis presents an intriguing avenue for future research. For instance, routine dental check-ups could incorporate saliva monitoring at 6-month to 1-year intervals to track oral health-related diseases. HF-NMR has been previously used to detect periodontitis, cavities, and oral squamous cell carcinoma. It would also be interesting to investigate the best pulse sequence to use too, as findings may show WET-CP or WET-180 to be better suited for bNMR analysis than presaturation.

Another aspect of this research that warrants further investigation is the implementation of quantitative studies. The current research prioritised maximising SNR to enhance disease detection and metabolite identification. While quantitative studies could be implemented if required, it is worth considering whether disease detection alone might be sufficient before expanding into more detailed analyses for quantification.

8.4. Conclusion

While bNMR is not yet fully equipped for immediate implementation in healthcare settings, the research presented in this thesis, along with previous research in the field, strongly supports its potential as a valuable tool for disease detection and monitoring. Future research should prioritise larger population studies, potentially leveraging initiatives like the “Our Future Health” study, to investigate a broader

range of diseases and explore bNMR's capacity to monitor multiple conditions including comorbidities.

This research has shown that while bNMR cannot yet monitor diabetes progression or reliably predict outcomes like those following bariatric surgery, it can distinguish between healthy and diabetic states, demonstrating promising diagnostic capabilities. However, there are limitations with this study. Results obtained were not inherently quantitative, and some disease-specific biofluids, such as saliva, have yet to be thoroughly explored. Cancer detection, in particular, represents a key future target where bNMR could make a significant impact.Early cancer detection remains a critical clinical challenge, and current screening methods are often invasive, expensive, or limited to specific cancer types. The ability of bNMR to analyse multiple biofluids with minimal sample preparation could provide a rapid, cost-effective screening tool capable of detecting metabolic signatures across various cancer types, potentially enabling earlier intervention when treatment is most effective.

The addition of new disease studies in this research, including asthma, further highlights bNMR’s potential in metabolomics. Commonly studied biofluids like urine and blood plasma present a clear opportunity to reduce false positives and false negatives in disease detection while enabling more widespread use of metabolomics due to the low-cost analysis. Modern pulse sequences and bNMR hardware allow for simplified sample preparation, making this method advantageous for rapid, affordable analysis. Further research is needed to fully explore where bNMR lacks the specificity to fully distinguish between similar disease phenotypes. Nevertheless, its ability to highlight metabolic markers of interest could help guide healthcare providers in earlier disease intervention.

To optimise bNMR for healthcare applications, future research should consider two approaches: (1) employing bNMR as an initial screening tool to broadly identify potential diseases, followed by more targeted and expensive methods for confirmation, or (2) enhancing sample preparation and analytical complexity for cases requiring precise phenotype differentiation. Comparative studies using both simple and complex sample preparation could help identify the best strategies for bNMR deployment.

Modern pulse sequences and bNMR hardware support the ability for reduced sample preparation while still obtaining a wide range of metabolites. As such qualitative studies using water suppression pulse sequences that benefit from a shorter acquisition time, like WET and WATERGATE, could enable optimum signal is gained in the shortest period.

By leveraging the straightforward methodologies detailed in this research, along with the potential disease markers identified through enrichment analysis, this work can help pave the way for advancements in personalised medicine and public health. bNMR offers a promising tool to support the transition from reactive to proactive healthcare by enabling earlier diagnosis and timely intervention. Its scalability and versatility make it ideal for broad population screening initiatives, which could significantly enhance public health efforts. Additionally, this research has introduced a novel approach for the identification of idiopathic epilepsy markers, a condition that currently requires prolonged and complex diagnostic procedures. Future studies should investigate how bNMR could be integrated into early screening programs to facilitate intervention before clinical symptoms arise.

Chapter 9 Appendices

9.1. Comparison of 2D COSY and TOCSY NMR Spectra

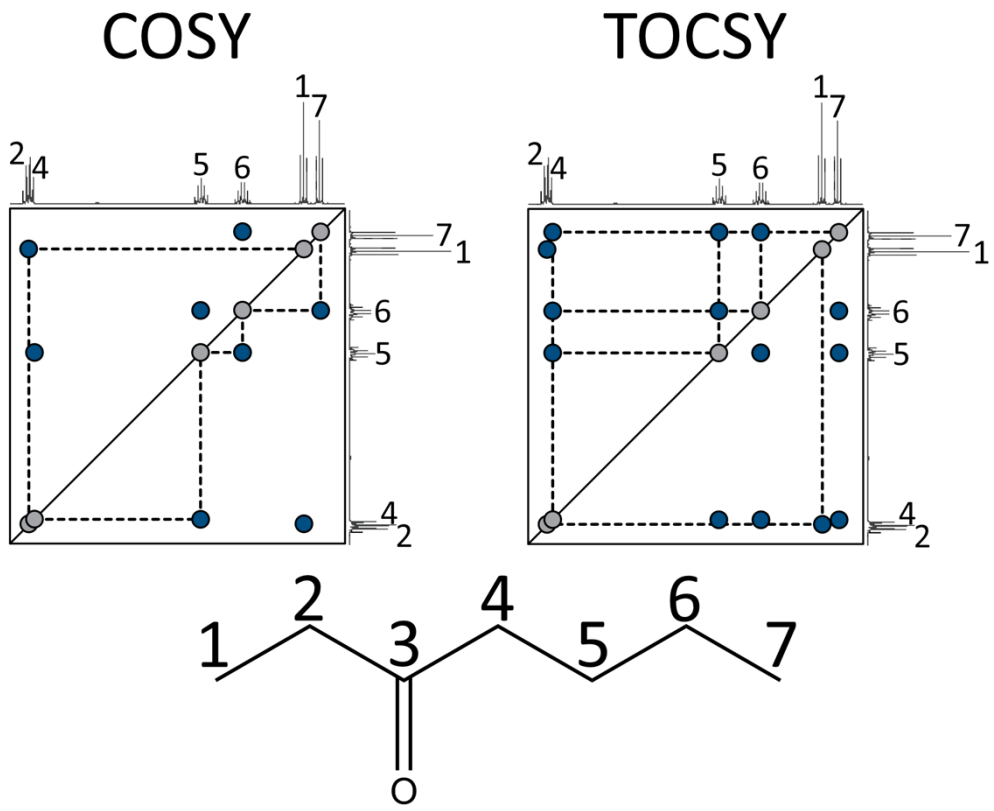

Figure 78 - A comparison of 3-Heptanone using COSY and TOCSY. This figure illustrates the differences between the COSY (left) and TOCSY (right) spectra.

9.2. 2D COSY NMR Spectrum of Blood Plasma Metabolites

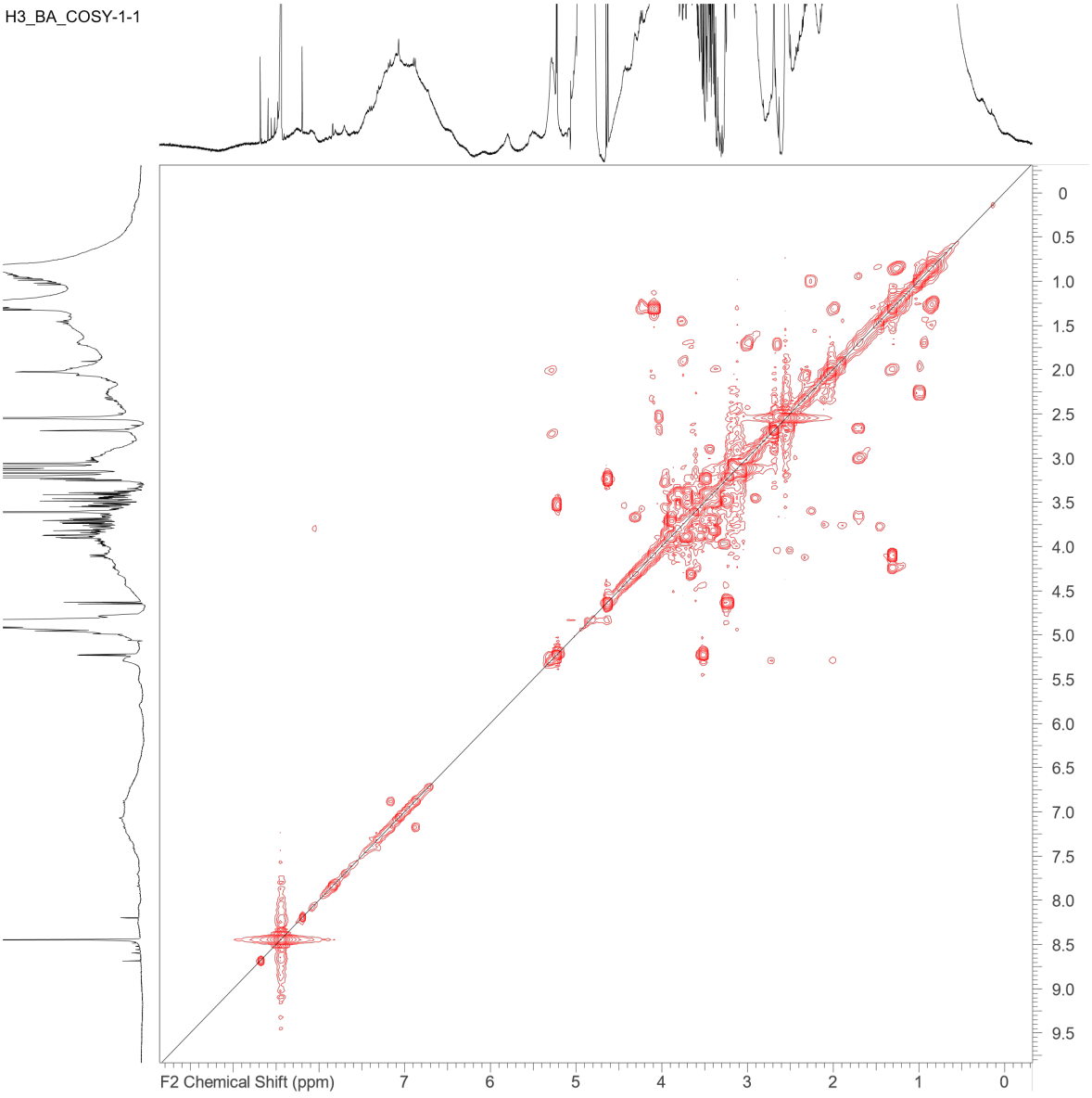

Figure 79 – COSY NMR Spectrum of Blood Plasma. The full 2D COSY spectrum shows cross-peaks representing scalar couplings between protons in blood plasma metabolites. Diagonal signals correspond to auto-correlations, while off-diagonal cross-peaks indicate correlations between coupled proton pairs, providing insight into the structure and connectivity of metabolites in the sample.

9.3. Expanded COSY NMR Spectrum of Blood Plasma (0 – 5ppm)

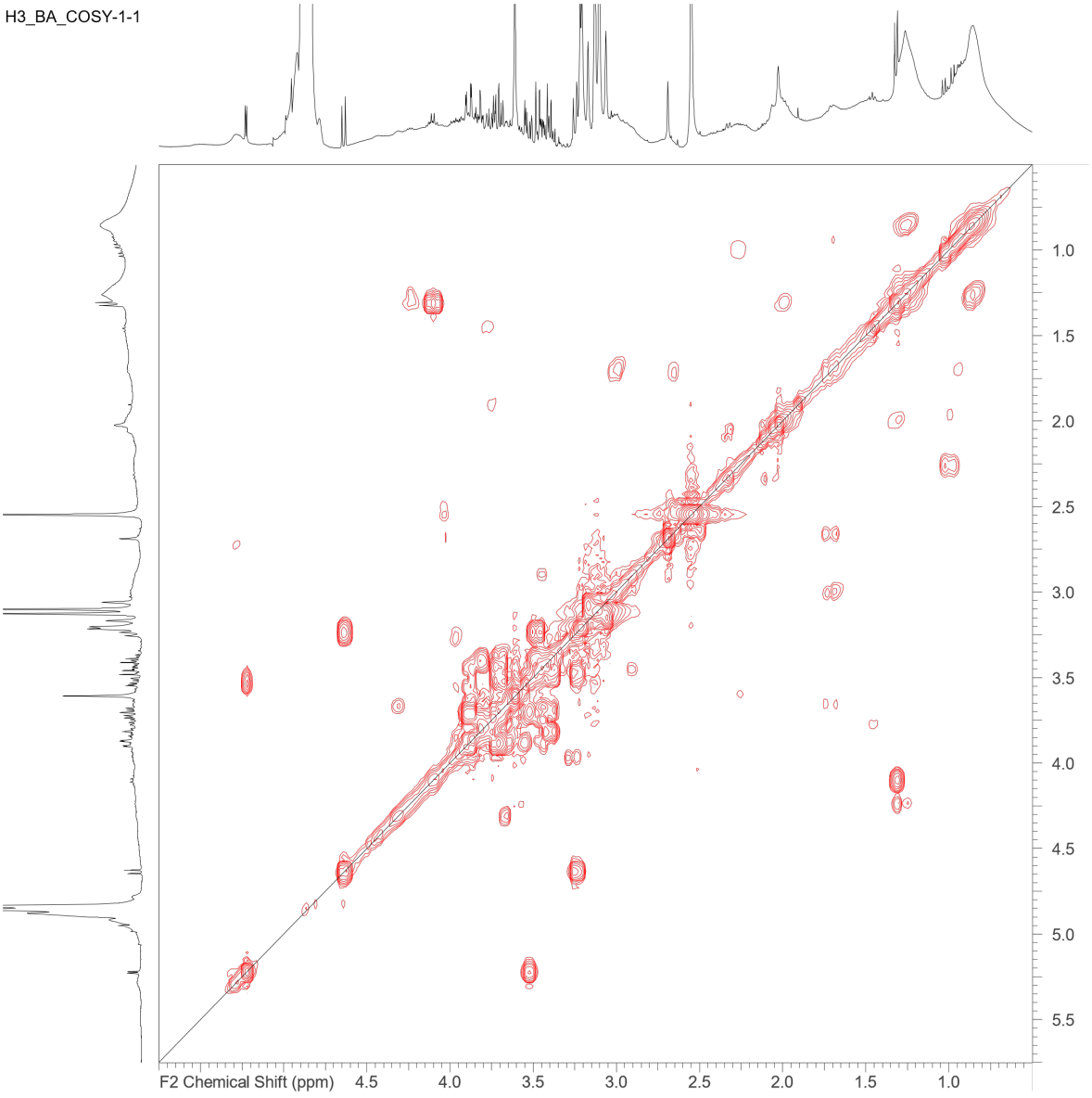

Figure 80 - 0-5ppm COSY NMR Spectrum of Blood Plasma.

9.4. Expanded COSY NMR Spectrum of Blood Plasma (3 – 9ppm)

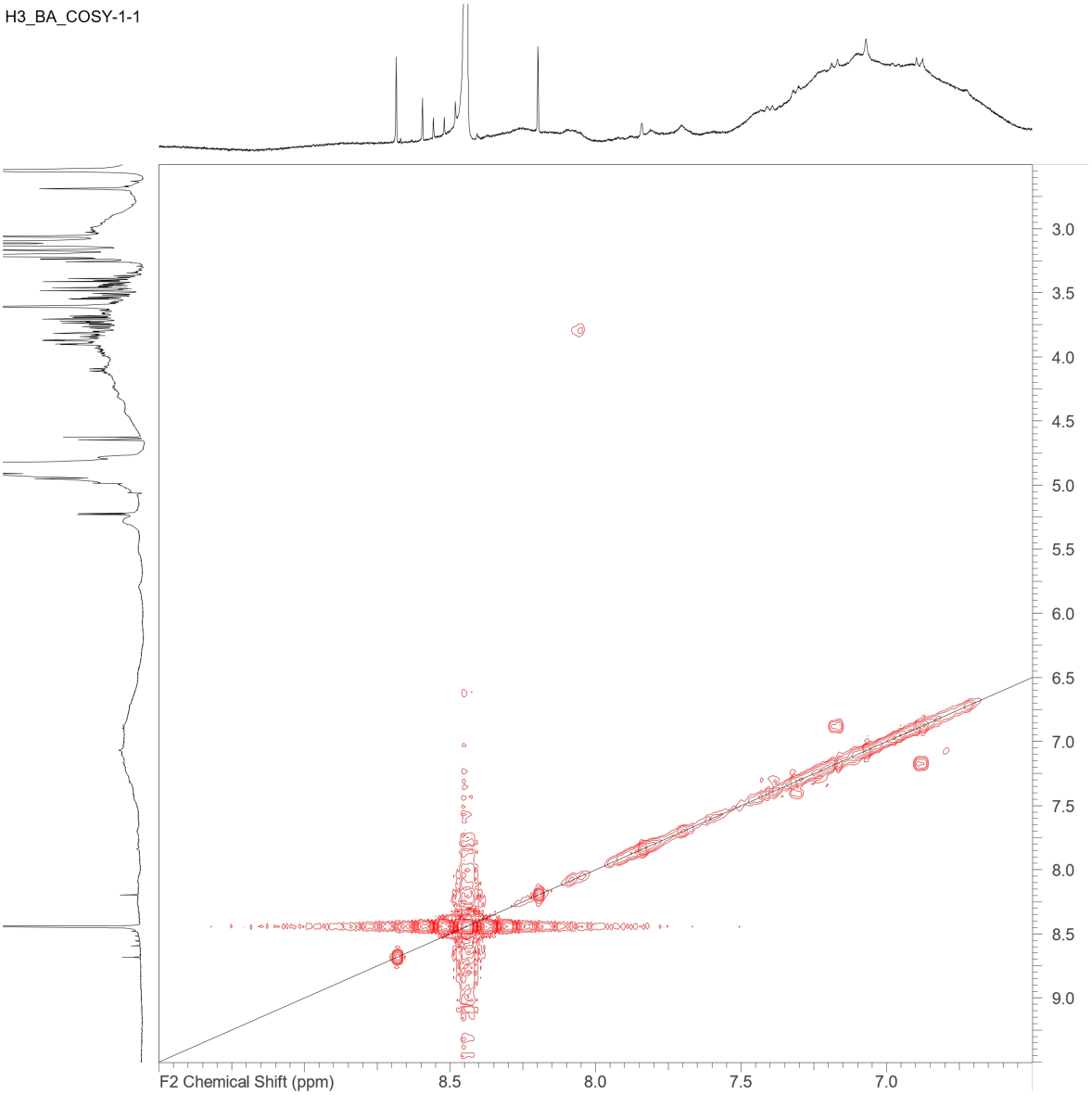

Figure 81 - 3-9ppm COSY NMR Spectrum of Blood Plasma.

9.5. bNMR Blood Plasma Enrichment Analysis

In this study, a broad spectrum of metabolites identified by bNMR was analysed to explore their association with various other diseases and health conditions. The table below presents the diseases that have the potential to be detected by bNMR in blood plasma samples. The total number of metabolites in each disease pathway, the number of metabolite hits, and their corresponding p-values and FDR values are also provided. In total 110 (HMDB identified studies) diseases/health conditions were recognised from the identified bNMR metabolites.

Table 14 - Summary of Identified bNMR Blood Plasma Metabolite Associations with Various Diseases. This table presents the total number of metabolites in each disease/ health condition, along with their significance (p-value) and corrected significance (False Discovery Rate).

Diseases/ health conditions	Total metabolites in pathway	Metabolite hits	p-value	FDR
Colorectal cancer	54	14	***	***
Early preeclampsia	45	12	***	***
Pancreatic cancer	21	10	***	***
Schizophrenia	101	13	***	***
Late-onset preeclampsia	40	11	***	***
Lipoyltransferase 1 Deficiency	12	8	***	***
Epilepsy	15	8	***	***
Alzheimer's disease	59	9	***	***
Pregnancy	766	13	***	***
Fumarase deficiency	13	5	***	***
Dihydrolipoamide Dehydrogenase Deficiency	8	4	***	***
Maple syrup urine disease	11	4	***	***
Histidinemia	4	3	***	***
Sepsis	23	4	***	***
Branched-chain Keto Acid Dehydrogenase Kinase Deficiency	6	3	***	***
Phosphoenolpyruvate Carboxykinase Deficiency 1, Cytosolic	7	3	***	***
N-acetylglutamate synthetase deficiency	9	3	***	***
Phenylketonuria	9	3	***	***
Heart failure	12	3	***	***
Hyperglycinemia, lactic acidosis, and seizures	2	2	***	***
Viral infection	2	2	***	***
Uremia	92	4	***	***
Kidney disease	28	3	***	***
2-Methyl-3-hydroxybutyryl-CoA dehydrogenase deficiency	3	2	***	***
Dengue fever	3	2	***	***

2,4-dienoyl-CoA reductase deficiency	4	2	***	***
Metabolic encephalomyopathic crises, recurrent, with rhabdomyolysis, cardiac arrhythmias, and neurodegeneration	4	2	***	***
Myocardial infarction	4	2	***	***
Refractory localization-related epilepsy	4	2	***	***
Hypermethioninemia	5	2	***	***
Infantile Liver Failure Syndrome 2	5	2	***	***
Pyruvate carboxylase deficiency	5	2	***	***
3-Methyl-crotonyl-glycinuria	6	2	***	***
Fructose-1,6-diphosphatase deficiency	6	2	***	***
Leigh's syndrome, subacute necrotizing encephalopathy, SNE	6	2	***	***
Mitochondrial trifunctional protein deficiency	6	2	***	***
Citrullinemia type II, neonatal-onset	7	2	***	***
3-Hydroxyacyl-CoA dehydrogenase deficiency	9	2	***	***
Obesity	745	6	***	***
3-Hydroxy-3-methylglutaryl-CoA lyase deficiency	11	2	***	***
3-Hydroxy-3-Methylglutaryl-CoA Synthase Deficiency	12	2	***	***
3-Hydroxyisobutyryl-coa hydrolase deficiency	2	1	**	**
3-Phosphoglycerate dehydrogenase deficiency	2	1	**	**
Alpha-aminoadipic and alpha-ketoadipic aciduria	2	1	**	**
Beckwith-Wiedemann Syndrome	2	1	**	**
Cerebral creatine deficiency syndrome 1	2	1	**	**
Cerebral creatine deficiency syndrome 3	2	1	**	**
Coenzyme Q10 deficiency, primary, 5	2	1	**	**
D-Glyceric acidura	2	1	**	**
Diabetes and Deafness, Maternally Inherited	2	1	**	**
GRACILE syndrome	2	1	**	**
Hawkinsinuria	2	1	**	**

Hyperinsulinemic hypoglycemia, familial, 1, HHF1	2	1	**	**
Hypoglycemia, familial neonatal	2	1	**	**
Iminoglycinuria	2	1	**	**
Leigh Syndrome, French Canadian Type	2	1	**	**
Maturity onset diabetes of the young, type 2	2	1	**	**
Myopathy with lactic acidosis, hereditary	2	1	**	**
Neu-Laxova Syndrome 1	2	1	**	**
Phosphoserine Aminotransferase Deficiency	2	1	**	**
Phosphoserine Phosphatase Deficiency	2	1	**	**
Pyridoxamine 5-prime-phosphate oxidase deficiency	2	1	**	**
Pyruvate dehydrogenase deficiency	2	1	**	**
Pyruvate dehydrogenase deficiency (E1)	2	1	**	**
Tyrosinemia I	2	1	**	**
Acute myelogenous leukemia	3	1	**	**
Addison's Disease	3	1	**	**
Carnitine transporter defect; primary systemic carnitine deficiency	3	1	**	**
D-Lactic Acidosis	3	1	**	**
Dicarboxylic aminoaciduria	3	1	**	**
Hyperlipoproteinemia	3	1	**	**
Juvenile myoclonic epilepsy	3	1	**	**
Lipodystrophy	3	1	**	**
Lysinuric protein intolerance	3	1	**	**
Methylmalonic aciduria mitochondrial encephelopathy Leigh-like	3	1	**	**
Mitochondrial complex I deficiency due to ACAD9 deficiency	3	1	**	**
Sarcosinemia	3	1	**	**
Short/branched chain acyl-CoA dehydrogenase deficiency	3	1	**	**

Tyrosinemia	3	1	**	**
Wolcott-Rallison syndrome	3	1	**	**
Continuous ambulatory peritoneal dialysis	4	1	**	*
Familial partial lipodystrophy	4	1	**	*
Fanconi Bickel syndrome	4	1	**	*
Glucagon deficiency	4	1	**	*
Growth hormone deficiency	4	1	**	*
L-2-Hydroxyglutaric aciduria	4	1	**	*
Leptin Deficiency or Dysfunction	4	1	**	*
Lipodystrophy, Congenital Generalized	4	1	**	*
Mitochondrial pyruvate carrier deficiency	4	1	**	*
Partial lipodystrophy	4	1	**	*
Cerebral creatine deficiency syndrome 2	5	1	**	*
Donohue Syndrome	5	1	**	*
Short-chain L-3-hydroxyacyl-CoA dehydrogenase deficiency	5	1	**	*
Carnitine palmitoyltransferase I deficiency	6	1	**	*
Myopathy, lactic acidosis, and sideroblastic anemia 1	6	1	**	*
Proprotein Convertase 1/3 Deficiency	6	1	**	*
Pyruvate dehydrogenase phosphatase deficiency	6	1	**	*
2-Ketoglutarate dehydrogenase complex deficiency	7	1	**	*
Diabetes mellitus type 1	7	1	**	*
Long-chain Fatty Acids, Defect in Transport of	7	1	**	*
Pearson Syndrome	7	1	**	*
Sulfite oxidase deficiency, ISOLATED	7	1	**	*
Stomach cancer	9	1	**	*
21-Hydroxylase deficiency	11	1	**	*
Primary hypomagnesemia	12	1	*	*

Alcoholism	13	1	*	*
Adrenal insufficiency, congenital, with 46,XY sex reversal, partial or complete	14	1	*	*
Adrenal hyperplasia, congenital, due to 3-beta-hydroxysteroid dehydrogenase 2 deficiency	18	1	*	*
Hemodialysis	19	1	*	*
Diabetes mellitus type 2	21	1	*	*

9.6. CSF COSY Spectrum

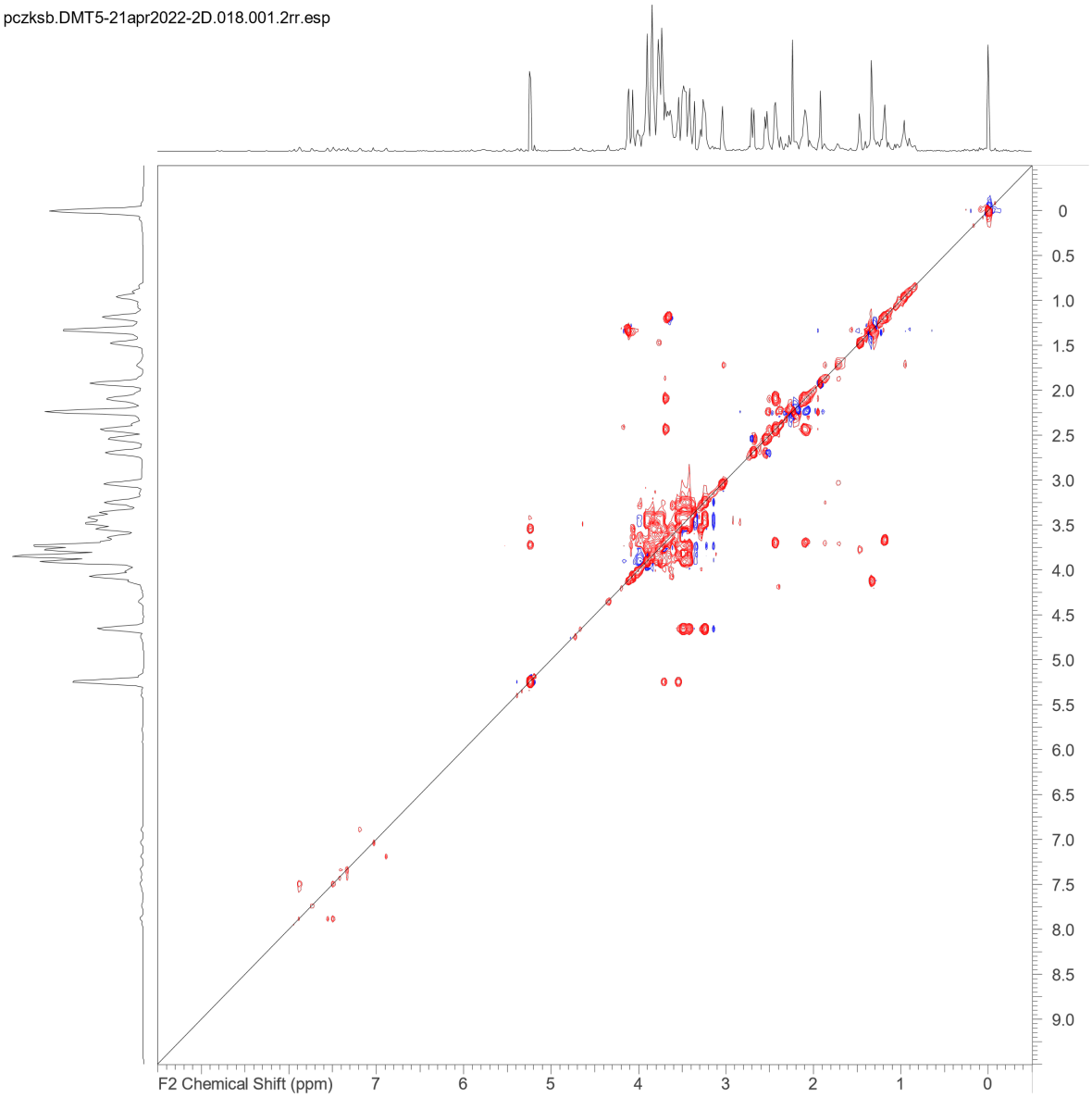

Figure 82 - COSY Full Spectrum of CSF

9.7. CSF COSY Spectrum 0.5 – 6ppm

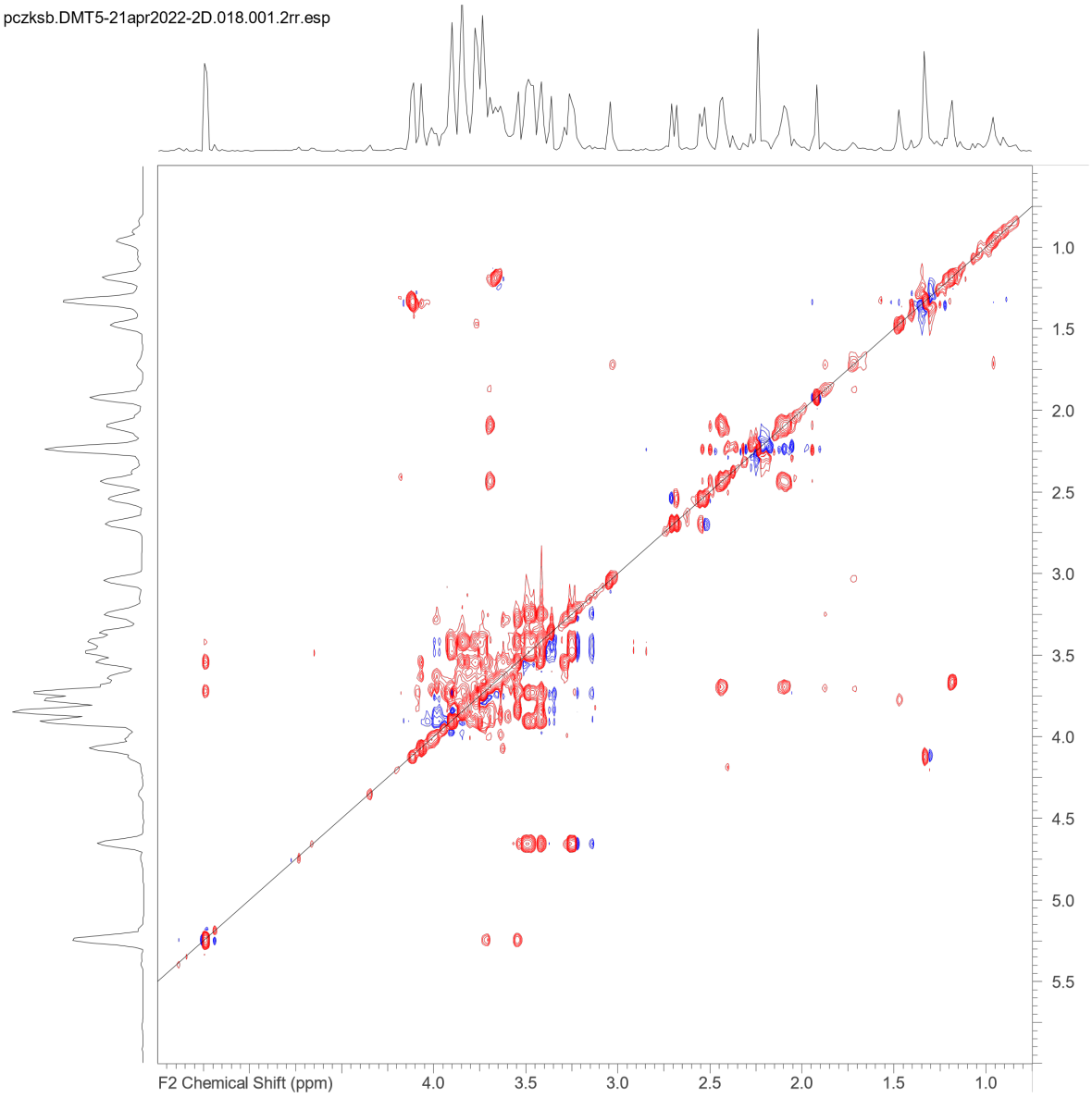

Figure 83 - CSF COSY Spectrum 0.5 – 6ppm

9.8. CSF COSY Spectrum 6.5 – 8.5ppm

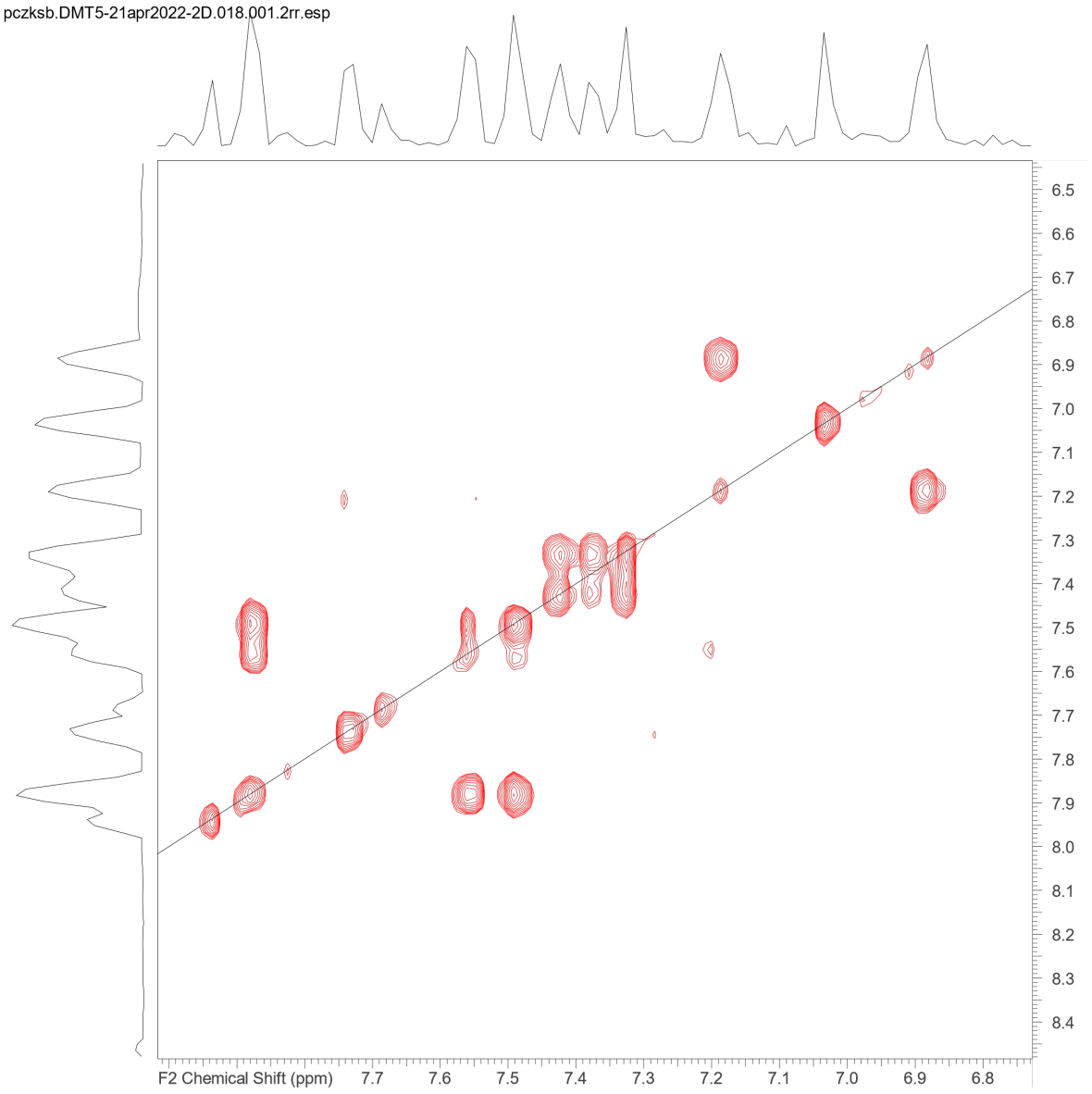

Figure 84 - CSF COSY Spectrum 6.5 – 8.5ppm

9.9. Other identified CSF metabolites at ^{1}H 800 MHz

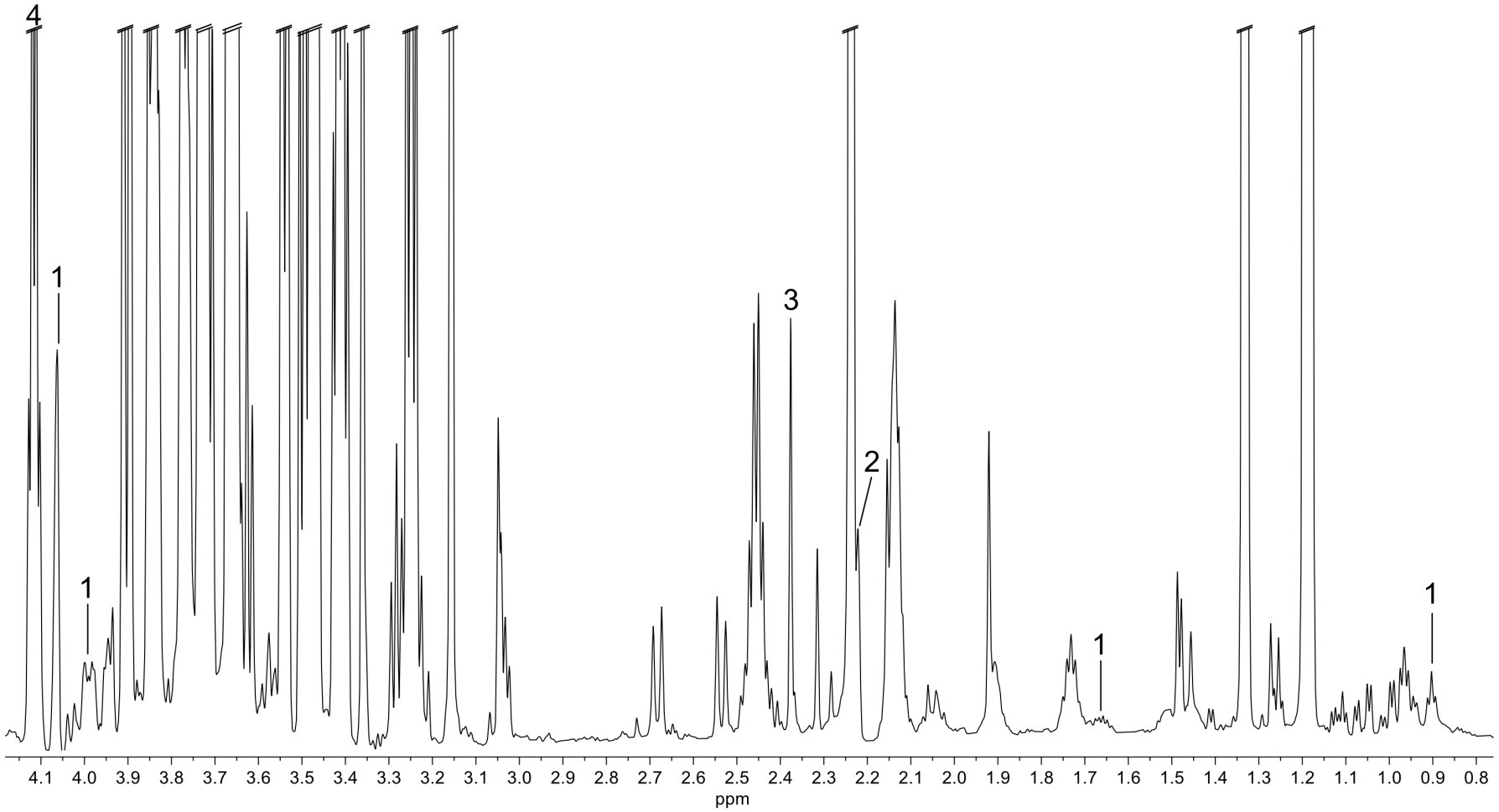

Figure 85- 800 MHz HF-NMR spectrometer with extra identified metabolites in a representative CSF sample. 1) 2-hydroxybutyric acid, 2) Acetone, 3) Pyruvic Acid, and 4) 3-hydroxybutyric acid.

9.10. OPLS-DA analysis of CSF of their age

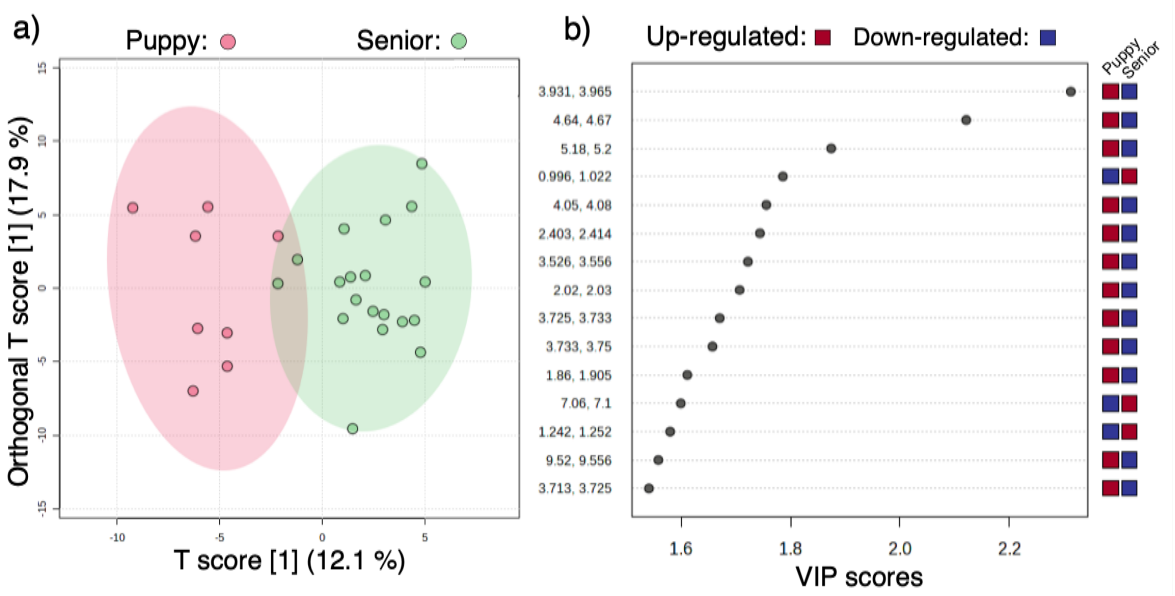

Figure 86 - OPLS-DA analysis of puppies with senior dogs. Q^2 of 0.521 ($p<0.001$), R^2 of 0.78 ($p = 0.05$).

9.11. bNMR CSF Enrichment Analysis

In total 26 (HMDB identified studies) diseases/ health conditions were identified with at least one metabolite being present in this study that could be used to detect different diseases. Only one disease, Lipoyltransferase 1 Deficiency, was significant and met the false discovery rate (FDR) correction significance. Three additional diseases also met the p-value threshold: leukaemia, Glucose transporter type 1 deficiency syndrome, and 2-ketoglutarate dehydrogenase complex deficiency.

Table 15 - Potential detectable diseases and health conditions using ^{1}H bNMR analysis of CSF identified during Enrichment Analysis.[211]

Disease and Health Conditions	Total Hits	Hits	P - Value	FDR
Lipoyltransferase 1 Deficiency	6	4	***	**
Leukemia	21	5	**	-
Glucose transporter type 1 deficiency syndrome	3	2	**	-
2-Ketoglutarate dehydrogenase complex deficiency	4	2	*	-
Epilepsy, early-onset, vitamin B6-dependent	8	2	-	-
Maple syrup urine disease	9	2	-	-
Meningitis	21	3	-	-
2,4-dienoyl-CoA reductase deficiency	2	1	-	-
Carnitine transporter defect; primary systemic carnitine deficiency	2	1	-	-
Cerebral creatine deficiency syndrome 2	2	1	-	-
D-Lactic Acidosis	2	1	-	-
Leigh's syndrome, subacute necrotizing encephalopathy, SNE	2	1	-	-
Long-chain Fatty Acids, Defect in Transport of	2	1	-	-
Propionic acidemia	2	1	-	-
Pyruvate dehydrogenase deficiency	2	1	-	-
Pyruvate dehydrogenase deficiency (E1)	2	1	-	-
Rett syndrome	2	1	-	-
Tuberculosis	2	1	-	-
Schizophrenia	25	3	-	-
Alzheimer's disease	56	5	-	-
Dicarboxylic aminoaciduria	3	1	-	-
Canavan disease	4	1	-	-
Perillyl alcohol administration for cancer treatment	4	1	-	-
Dementia	5	1	-	-
Tuberculous meningitis	7	1	-	-
Multiple sclerosis	17	1	-	-

9.12. Urine COSY Full Spectrum

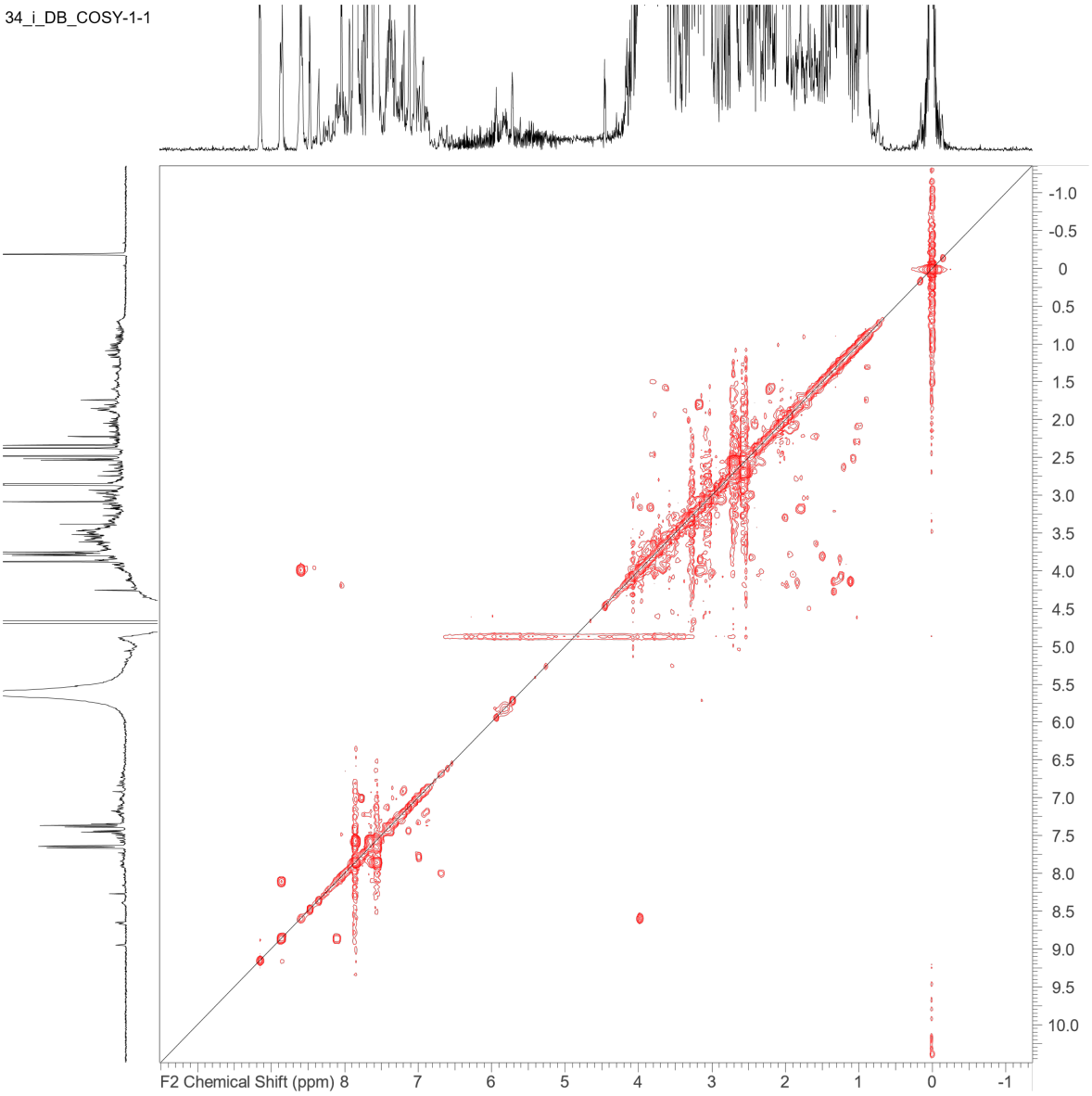

Figure 87 - Urine COSY

9.13. Urine COSY 6.5 – 9.5ppm spectrum

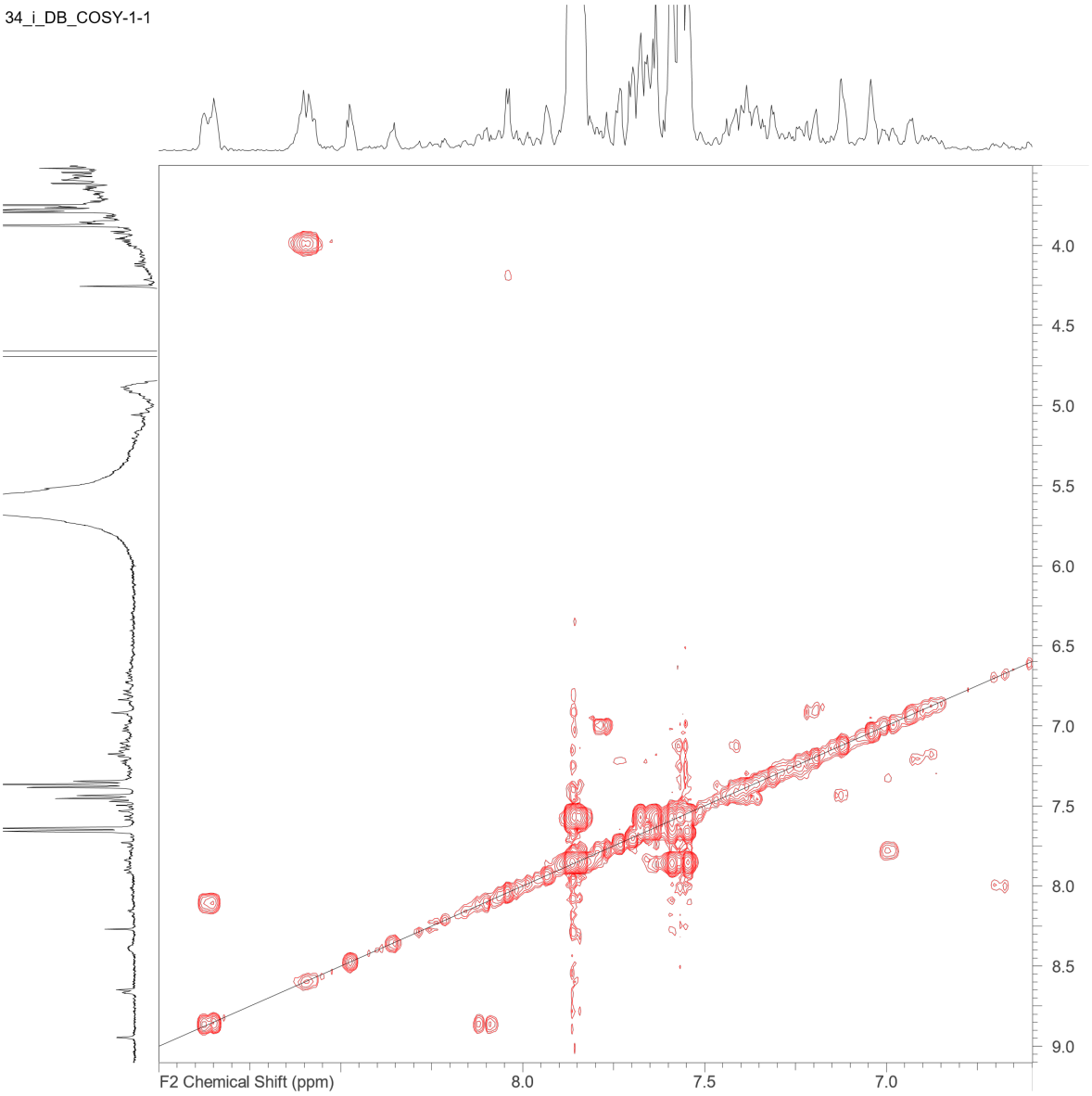

Figure 88 - COSY spectrum 6.5 - 9.5ppm

9.14. HSQC Diabetes

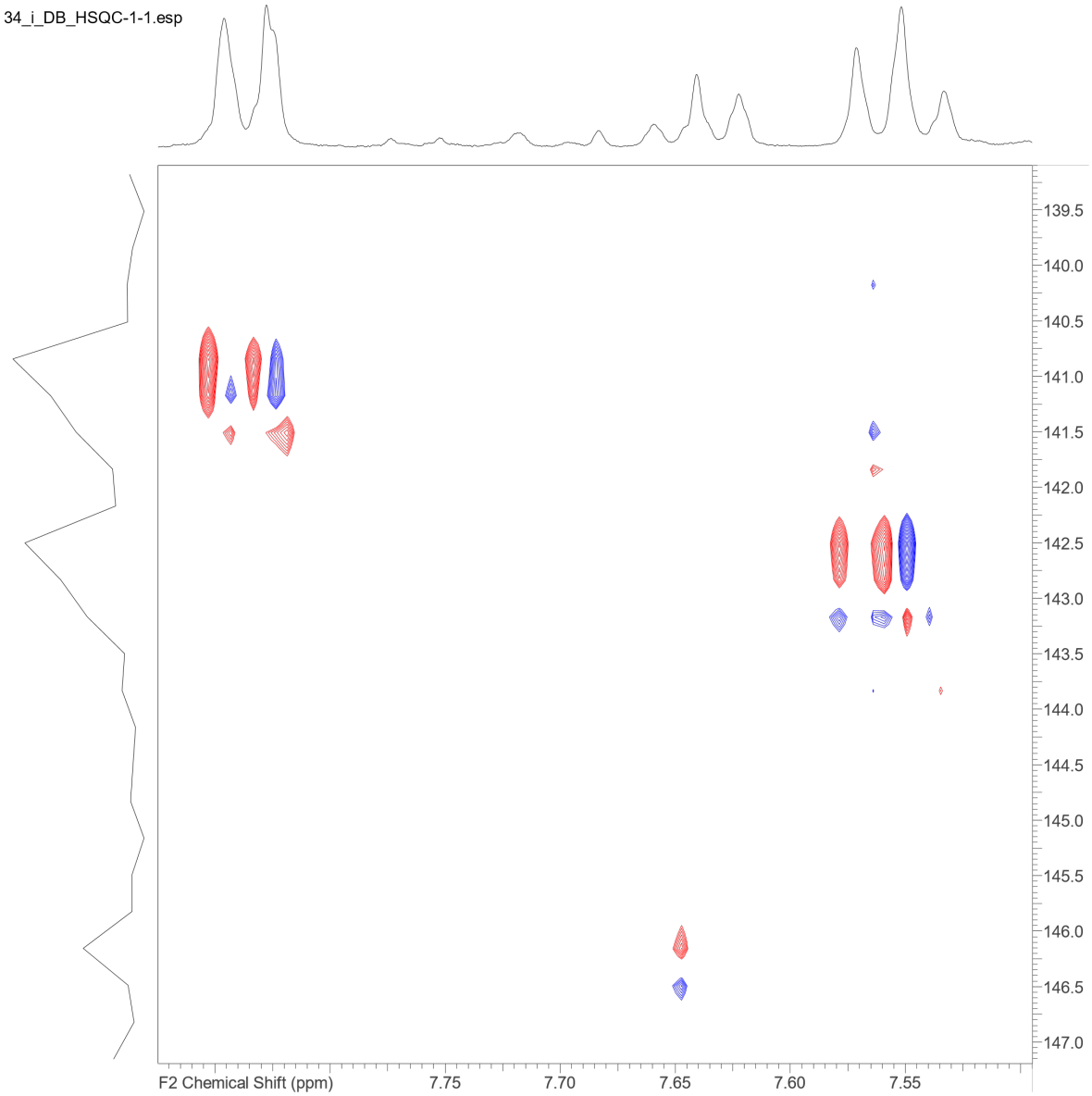

Figure 89 - Urine HSQC of sample 34 i

9.15. HSQC 3-4ppm

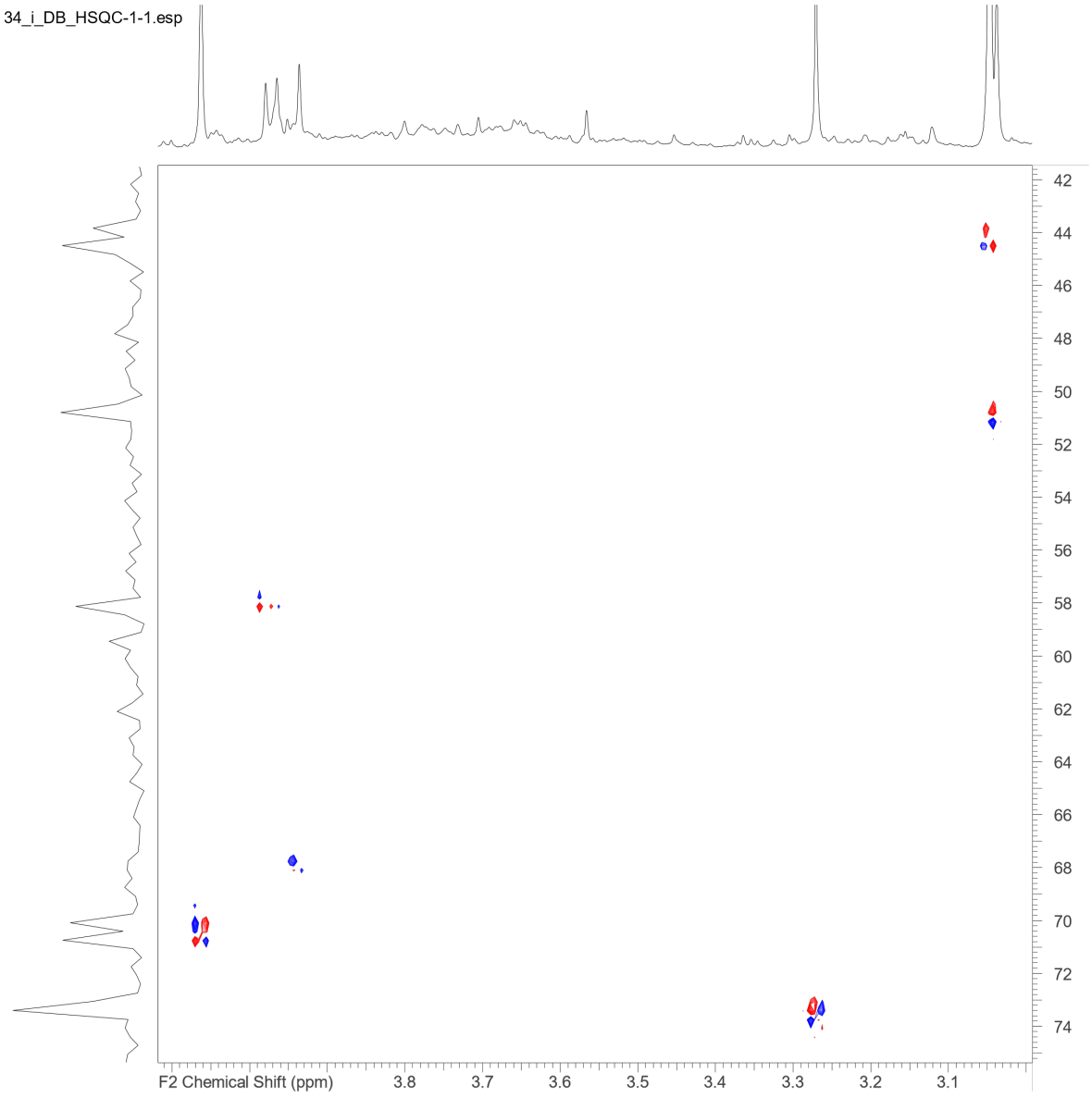

Figure 90 - 3-4ppm Urine

9.16. Medication and its Effect On Urine Metabolome

As observed in Figure 91a (left) and b (right), there is a large overlap between all medication groups and the separation that is observed is non-statistically significant suggesting overfitting of the data. From this, it was concluded that the medication had little to no influence, and no correction factor was applied to the data.

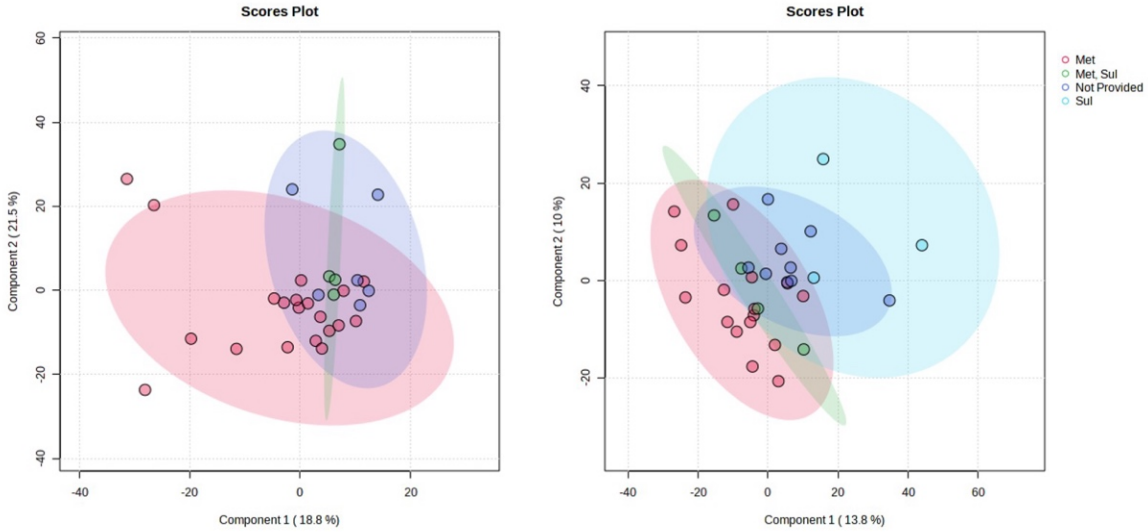

Figure 91 - PLS-DA plot of bNMR and HF-NMR of medication on urine.

bNMR p = 0.502 (left) and HF-NMR (right) p = 0.618 of medication types from samples. Metformin (red), Sulphonylureas (Light blue), Metaformin and Sulphonylureas (Green), and not provided (dark blue)

9.17. bNMR Urine Enrichment Analysis

Diseases identified through enrichment analysis of HMDB identified studies of diseases from bNMR urine metabolites.

Table 16 - MetaboAnalyst Enrichment analysis of Diseases associated with identified urine metabolites by bNMR

Disease / health status	Total	Hits	Raw p	FDR
Lung Cancer	33	14	***	***
Paraquat poisoning	7	7	***	***
Metabolites Affected By Age	11	7	***	***
Diabetes mellitus type 1	13	7	***	***
Colorectal cancer	34	9	***	***
Eosinophilic esophagitis	335	20	***	***
Tyrosinemia I	11	6	***	***
Rats Treated With Hgcl2	13	6	***	***
Schizophrenia	33	8	***	***
Rhabdomyolysis	4	4	***	***
Argininosuccinic aciduria	9	5	***	***

Maple syrup urine disease	19	6	***	***
Metabolites Affected By Diurnal Variation	6	4	***	***
Propionic acidemia	34	7	***	***
Rats Treated With Hydrazine	9	4	***	***
Peripheral Inflammatory Pain In The Rat (Fca Model)	10	4	***	***
Difference Between Normal Han-Wistar (Hw) And Sprague-Dawley (Sd) Rats	10	4	***	***
Phenylketonuria	21	5	***	***
Autosomal dominant polycystic kidney disease	43	6	***	**
Amish lethal microcephaly	7	3	***	**
Lipoyltransferase 1 Deficiency	8	3	***	**
Metabolites Affected By Gender	8	3	***	**
3-Methylglutaconic Aciduria type VI	3	2	**	*
Exposure To Tri-Butyl Phosphate (Tbp)	3	2	**	*
3-Methyl-crotonyl-glycinuria	4	2	**	*
Creatine Deficiency, Guanidinoacetate Methyltransferase Deficiency	4	2	**	*
Deafness, Onychodystrophy, Osteodystrophy, Mental Retardation, and Seizures Syndrome	6	2	**	-
Dimethylglycine Dehydrogenase Deficiency	6	2	**	-
Methylmalonate Semialdehyde Dehydrogenase Deficiency	6	2	**	-
Primary hypomagnesemia	7	2	**	-
Alzheimer's disease	23	3	*	-
Hartnup Disease	12	2	*	-
Cerebral creatine deficiency syndrome 1	2	1	*	-
Cerebral creatine deficiency syndrome 3	2	1	*	-
D-Glyceric acidemia	2	1	*	-
Pearson Syndrome	2	1	*	-
Pyruvate carboxylase deficiency	2	1	*	-
Trimethylaminuria	2	1	*	-
Cerebral creatine deficiency syndrome 2	3	1	-	-
Iminoglycinuria	3	1	-	-

Sarcosinemia	3	1	-	-
3-Methylglutaconic Aciduria (Type I)	3	1	-	-
Citrullinemia Type I	3	1	-	-
Hydroxyprolinemia | Hyperprolinemia, Type I | Hyperprolinemia, Type II | Iminoglycinuria	3	1	-	-
Hyperargininemia	3	1	-	-
Juvenile Myoclonic Epilepsy	3	1	-	-
Tyrosinemia III	3	1	-	-
Exposure To Tri-Phenyl Phosphate (Tpp)	3	1	-	-
3-Methylglutaconic Aciduria type V	4	1	-	-
Biotinidase deficiency	4	1	-	-
Carbamoyl Phosphate Synthetase Deficiency	4	1	-	-
Cystinuria	4	1	-	-
Fructose intolerance, hereditary	4	1	-	-
Hyperdibasic aminoaciduria I	4	1	-	-
Hyperlysinemia I, familial	4	1	-	-
Hyperlysinuria	4	1	-	-
Lysinuric protein intolerance	4	1	-	-
Tyrosinemia II	4	1	-	-
Dihydrolipoamide Dehydrogenase Deficiency	5	1	-	-
Duchenne Muscular Dystrophy	5	1	-	-
Hepatocellular carcinoma	5	1	-	-
Lysinuric Protein Intolerance (Lpi)	5	1	-	-
Ornithine Transcarbamylase Deficiency (Otc)	5	1	-	-
Renal Fanconi Syndrome	5	1	-	-
Perillyl alcohol administration for cancer treatment	57	3	-	-
Diabetes mellitus type 2	33	2	-	-
3-Hydroxy-3-methylglutaryl-CoA lyase deficiency	9	1	-	-
Anoxia	9	1	-	-
Methylmalonic Aciduria (Mma)	10	1	-	-
Fumarase deficiency	23	1	-	-
Obesity	184	1	-	-

9.18. Optimum bNMR Tubes

Common (^{1}H, ^{13}C, ^{15}N, and ^{19}F) Nuclear Magnetic Resonance Spectroscopy (NMR) uses 5 mm borosilicate glass tubes to contain a sample. Borosilicate glass is frequently used in NMR due to its low coefficient of thermal expansion and durability, as well as its high chemical resistance to corrosive environments. This composition results in the ideal material for common NMR nuclei, such as ^{1}H ^{13}C and ^{15}N, as its structure does not interfere with signals in the spectra; however, large broad signals arise during acquisition if using an interfering nucelli like ^{11}B.[342] When this is the case, quartz tubes are often used instead but are innately more fragile, prone to chipping and more expensive to produce than borosilicate NMR tubes.

Depending on the specification of the instrument and the purpose of the experiment, tubes can range in diameter, length, and frequency. Smaller diameter tubes are applied in situations where only a small sample volume is present (5μL); however, due to a lower abundance of magnetic nucelli present, a lower signal is achieved often leading to longer analysis times. The 10 mm diameter variant has a larger capacity (~4,000 μL) but is used less frequently due to the need for a specialised probe and additional issues with the homogeneity of the magnet.

Three main factors can alter spectra because of the tube; they are the composition of the tube, imperfections in the glass, and the balance of the tube. Concentricity is a measurement of the constancy of the tubes thickness, whereas camber refers to how straight it is. A large imbalance of concentricity and camber can reduce the homogeneity of a sample leading to inferior results. This is further exaggerated when imperfections in the glass can result in inadequate shimming [343]. Instruments can also be damaged because of insufficient tube quality. Examples of damage caused to the probe include large camber convexities that create tube wobble when spinning tubes and an uneven outer diameter (concentricity) that can cause tubes to slide around in the sample spinner.[342] Tubes that yield a higher signal-to-noise ratio (S/N) and a smaller peak width (PW), achieve the most preferable results. With the need to reduce costs in health care diagnostics and monitoring, the aim of this study is to compare various 5 mm borosilicate tubes, and to investigate the variability of tubes specifications on PW and S/N using benchtop NMR (bNMR).

9.18.1. Materials and Methods

All tubes (observed in Table 17) were purchased from Fisher Scientific and analysed using an Oxford Instruments (OI) 60MHz Pulsar benchtop NMR (bNMR) spectrometer (probe temperature 35˚C), with spectral analysis using MestReNova version 14.2.3. Creatine, urea, acetone, ethanol, sodium phosphate monobasic (Na_2HPO_4), sodium phosphate dibasic (NaH_2PO_4), 3-(Trimethylsilyl)propionic-2,2,3,3 acid sodium salt (TSP) were purchased from Sigma-Aldrich.

Table 17 - Product Information on examined NMR tubes

Experiment Identifier and Product Name	Frequency (MHz)	Camber (mm)	Concentricity (mm)	DO (mm)	DI (mm)	Cost per tube (£)
Tube A: Norell 505-P-7	200	0.04	0.01	4.97	4.2	5.16
Tube B: Norell 508-UP-7	500	0.013	0.005	4.97	4.2	10.84
Tube C: Norell XR-55TM-7	300	0.038	0.01	4.97	4.2	5.64
Tube D: Wilmad WG-BTNMR-7	45	0.051	0.076	4.95	4.09	1.08
Tube E: Wilmad 505-PS-8	100	0.051	0.076	4.9635	4.2	7.72
Tube F: Wilmad 505-PS-7	100	0.051	0.076	4.9635	4.2	7.70

The buffer solution was prepared using 0.2885g of sodium phosphate monobasic in 5mL of deuterium and 0.372g of sodium phosphate dibasic in 5mL of deuterium. Moreover, 100uL of the 7.1pH phosphate buffer solution was then added to each sample tube, followed by 50μL of TSP 0.5% of W/V, 50μL Sodium Azide 0.02% W/V, 100μL 0.009mg of Creatinine W/V, 100μL of acetone 0.03mL V/V and 100μL of Ethanol 0.02mL V/V. A WET-CP pulse sequence was used with 32 scans, a four-second relaxation relay, 16.697 μs pulse width, 32768 points and 5208 Hz width. All samples were referenced to TSP at δ = 0 ppm, before being manually phase corrected a baseline corrected. The acetone singlet (2.22 ppm) was then analysed for its PW at half height manually and its S/N automatically through the MestReNova software. Statistical analysis was then completed using Python 3.10. All samples were shimmed, tuned, and matched before analysis.

9.18.2. Results

A statistical measure of how well data points fit in a regression model (Table 18), was applied to measure the performance of tubes based on their metrics. An absence of correlation is displayed between the three main spectral features and the tube parameters, as shown in Table 18. A low correlation (44.7%) between cost per tube and signal to S/N displays the highest explanation of variance in data. These are suggestive that lower-cost tubes may be more cost-effective on bNMR.

Table 2: R^2 values of baseline noise, peak width and signal-to-noise against sample parameters.

Table 18 - R^2 values of baseline noise, peak width and signal-to-noise against sample parameters.

R^2 Value	Cost per tube	DO	DI	Concentricity	Camber	Frequency	Thickness of wall
Baseline Noise	0.0001	0.01	0.001	0.086	0.072	0.062	0.004
Peak Width	0.223	0.01	0.05	0.010	0.037	0.048	0.063
S/N	0.447	0.28	0.32	0.093	0.209	0.258	0.314

DO; Diameter Outer, DI; Diameter Inner, S/N; Signal to Noise.

The statistical significance of each category is shown in Table 19. The S/N has a statistically significant impact the with cost per tube, diameter outer (DO), diameter inner (DI), frequency and thickness of the wall. The baseline noise displays P-values above 0.05 (the statistical limit) for all tube parameters. This suggests that there is no strong statistical evidence to conclude that any of the sample parameters have a significant effect on the baseline noise. A similar outcome was also observed with the peak width at half height (peak width), where no significance is seen (DO, DI, concentricity, camber frequency and thickness of wall) except for the cost per tube where a potential significance is shown (0.04785). Statistical significance was observed for S/N for the cost per tube (0.00241), DO (0.02299), DI (0.01445), Frequency (0.03122) and the thickness of the tubes wall (0.01561). This suggests that these factors do have a significant relationship with S/N. Overall, the concentricity and camber did not seem to have a significant effect on the baseline noise, peak width or S/N.

Table 3: P-values of baseline noise, peak width, and signal-to-noise against sample parameters.

Table 19 - P-values of baseline noise, peak width, and signal-to-noise against sample parameters

P-value	Cost per tube	DO	DI	Concentricity	Camber	Frequency	Thickness of wall
Baseline Noise	0.98	0.67	0.90	0.24	0.28	0.32	0.81
Peak Width	0.048	0.67	0.36	0.69	0.44	0.38	0.31
S/N	0.002	0.023	0.014	0.22	0.056	0.03	0.016

DO; Diameter Outer, DI; Diameter Inner, S/N; Signal to Noise.

To calculate the tubes which produce the lowest peak width and highest S/N, a "quality" score (Equation 1) was devised. Where PW is the peak width at half height of the signal and the S/N is the signal-to-noise ratio of the signal compared to the background noise. This multiplies the peak width by the S/N ratio showing a higher quality score is associated with a smaller peak width and higher S/N. This score will be affected by the instruments' magnetic field strength, shim quality and potential sample preparation procedures. To avoid, this a standard operating procedure (SOP) for this procedure will avoid discrepancies between users. This could be applied in the same way instrument manufacturers want to discover the resolution of their devices.

$$Quality = PW \times {}^{S}/_{N} \qquad \text{Equation 18}$$

Equation 1 was applied in Figure 92 against the advertised frequency of each tube. The quality score between 45MHz and 300MHz showed little to no improvements between tubes; however, the 500MHz tube showed the greatest range, with both the highest and lowest quality score of an individual tube. This could have been caused from an anomaly in the data for a poor tube or hardware issues as previously mentioned. The 200 MHz tube (B) showed to be the most consistent tube.

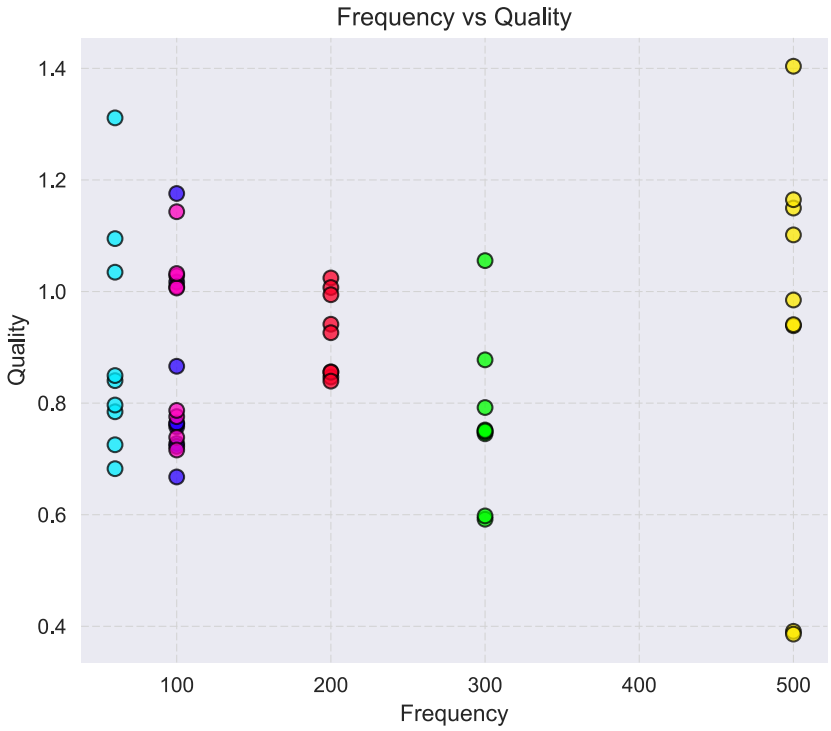

Figure 92 - A scatter graph showing the quality score of each tubes spectrum against the advertised frequency of the tube at 60 MHz. Key: red, tube A; yellow, tube B; green, tube C; light blue, tube D; dark blue, tube E; purple, tube F

A further equation, Equation 19, has been formulated to calculate the quality of a tube against the cost of a tube. This equation could be adapted so that the cost per tube is weighted accordingly to the user's requirements. In the example, shown in Figure 93, the cost per tube is weighted 1:1 so that the price has a large impact on the overall purchasing choice.

$$Value\ Quality = \frac{PW\ \times\ S\ /\ N}{Cost\ per\ tube} \qquad \text{Equation 19}$$

Equation 19 was further used in Figure 93 to display which tube was the most suitable for bNMR if the cost is a considerable impact on the consumables that are purchased. Overall tube D showed to be the most cost effective with tube B producing the lowest scores.

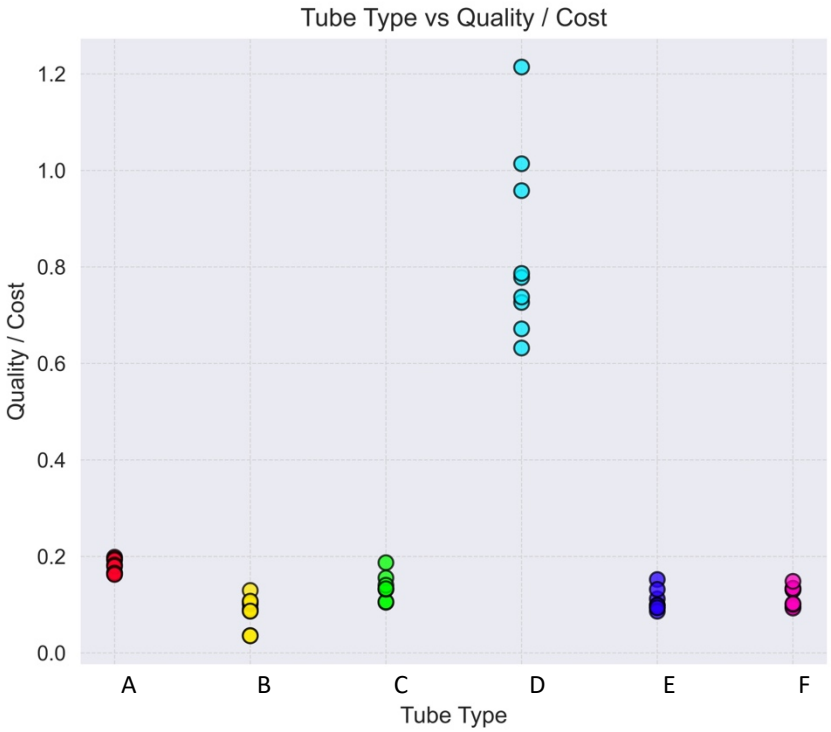

Figure 93 - A graph of the division of the quality score by the tube cost for each of the tested tube types.

Key: red, tube A; yellow, tube B; green, tube C; light blue, tube D; dark blue, tube E; purple, tube F.

9.18.3. Discussion

The requirements of a tube's quality could have a large impact on the choice that is made when purchasing consumables. From this preliminary study, key metrics advertised by tube manufacturers have little to no significant impact on the overall noise level of a spectrum. This is more likely to be attributed to the frequency of which bNMR spectrometers operate at. However, some effect is identified on the S/N and peak width that could be attributed to the tube thickness and the advertised suitable frequency of the tube. This significance is most likely attributed to the greater abundance of nuclei available with thinner-walled tubes. As displayed in Figure 93, tube D was the most economical tube for the quality of the spectrum. Due to the stringent costs seen in healthcare settings, the cost needed for an improved camber, concentricity or tube frequency does not yield an improvement that is most likely beneficial for cost-effective bNMR analysis. Future studies will need to be completed to replicate results at different operating frequencies to see where quality tubes should be employed.

Overall, there is no strong correlation between tube parameters and the quality of results. As a result, there is no significant benefit to buying more expensive tubes

for bNMR and so it is recommended to buy the more affordable tubes available unless a comparison study on higher field spectrometers is used. A new recommendation is devised to improve clarity when making purchases by implementing a quality score (Equation 1) in the description and advertisement of tubes at different field frequencies. This has been formulated to better inform purchasing requirements.

9.19. Chronic Kidney Disease assigned Urine ^{1}H NMR spectrum

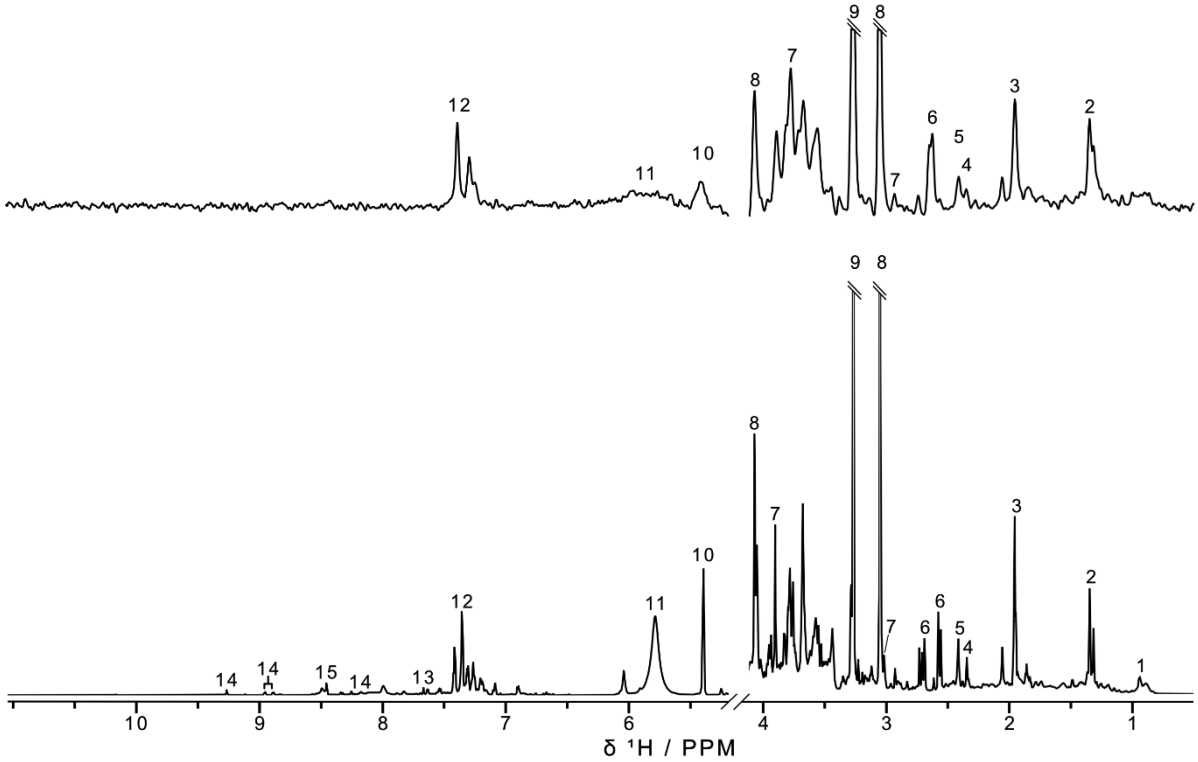

Figure 94 - Comparison of 60 MHz benchtop spectrometer (a) and 800 MHz high field spectrometer (b). The benchtop NMR spectrum has a much lower resolution and sensitivity compared to the high-field spectrum. The residual water signal has been removed from both spectra. The identified metabolites are as follows: 1. 2-Hydroxybutyrate, 2. Lactate, 3. Acetate, 4. Pyruvate, 5. Succinate, 6. Citrate, 7. Creatine, 8. Creatinine, 9. TMAO, 10. Allantoin, 11. Urea, 12. Phenylacetyl glutamine, 13. Hippurate, 14. Methylnicotinamide, 15. Formate.

9.20. Chronic Kidney Disease Urine COSY Spectrum

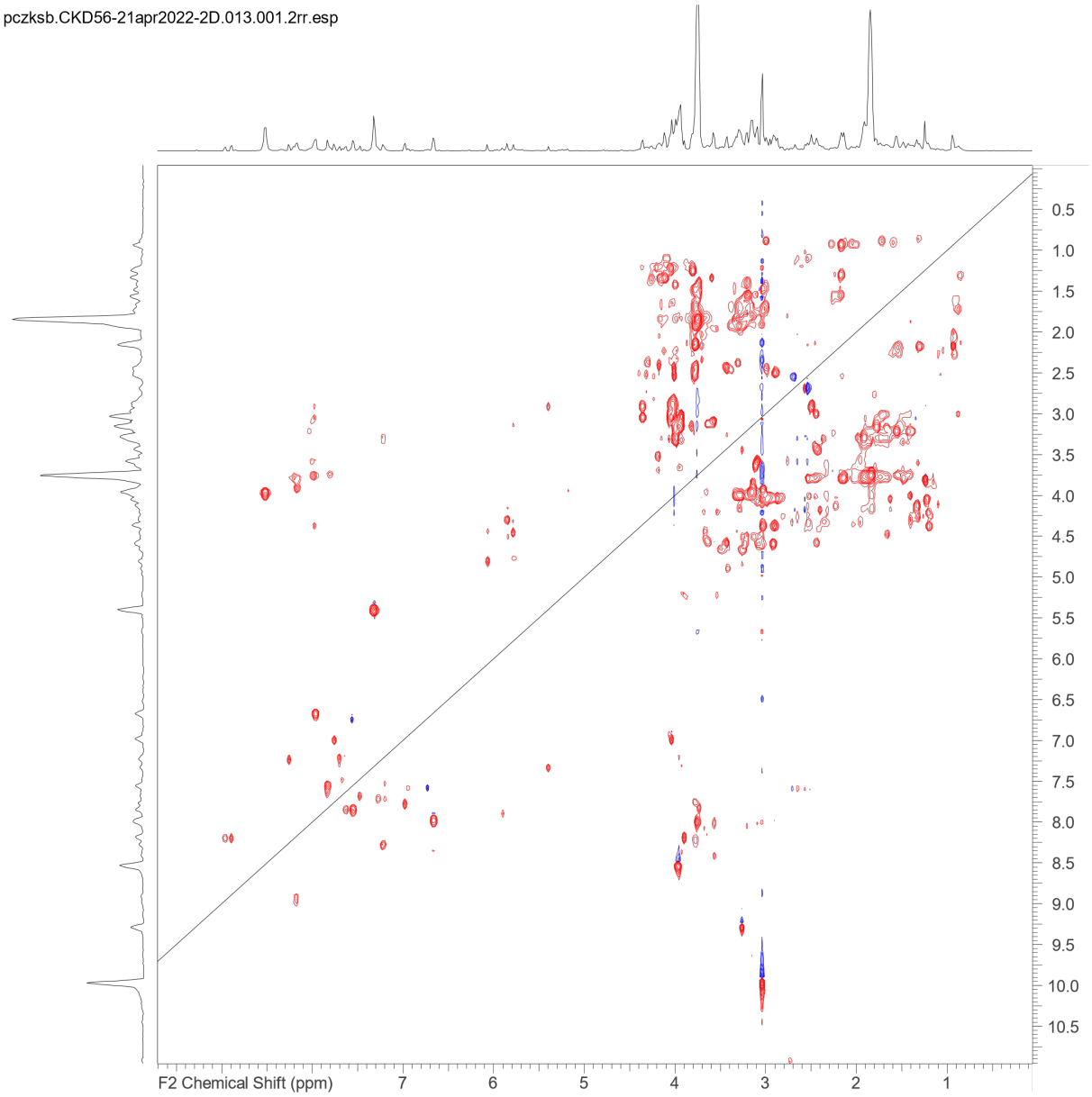

Figure 95 - Chronic Kidney Disease COSY Spectrum

9.21. Chronic Kidney Disease Urine COSY Spectrum (0.5 – 5ppm)

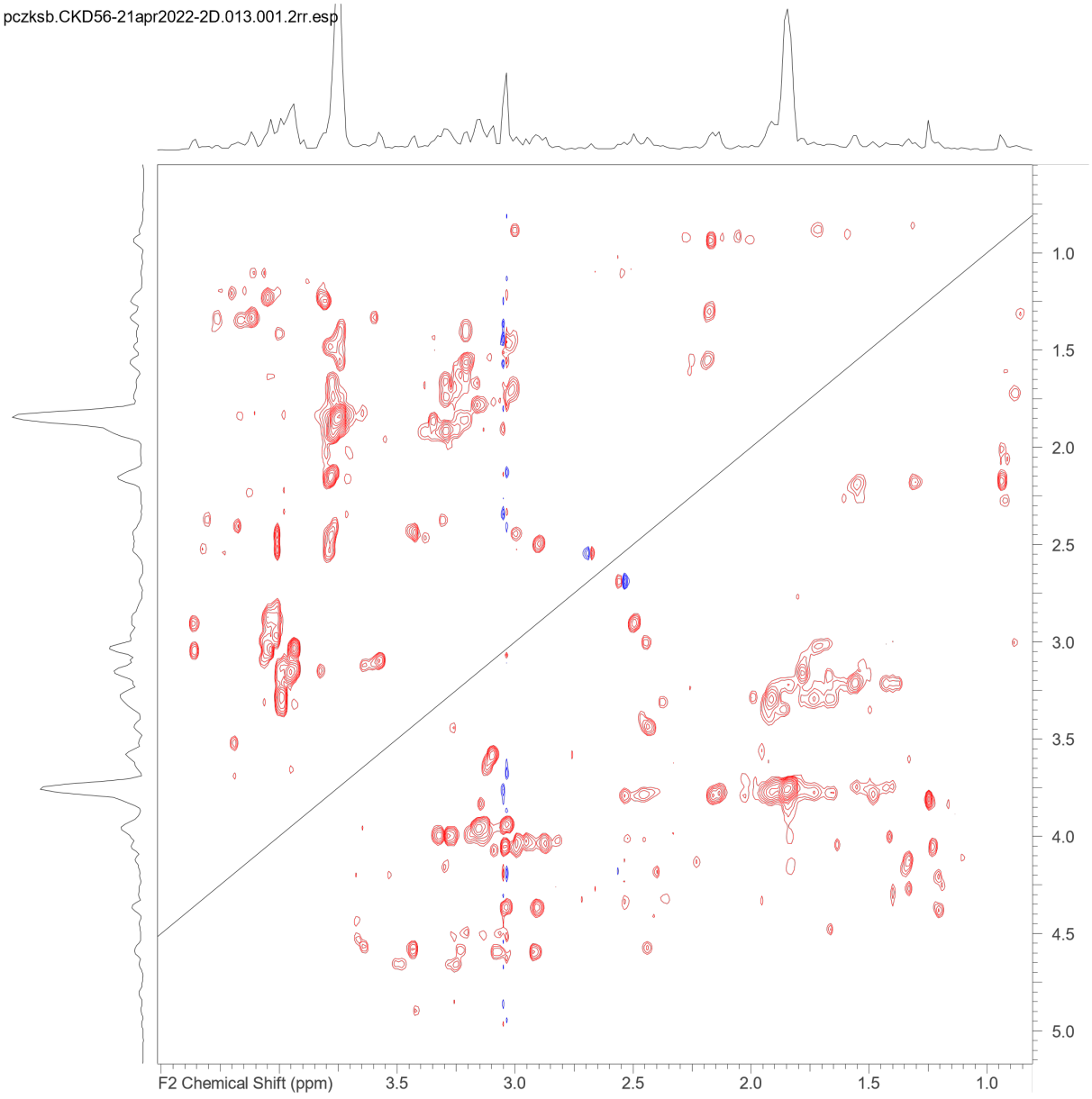

Figure 96 - Chronic Kidney Disease COSY Spectrum (0.5 – 5ppm)

9.22. Chronic Kidney Disease Urine COSY Spectrum (aromatic region)

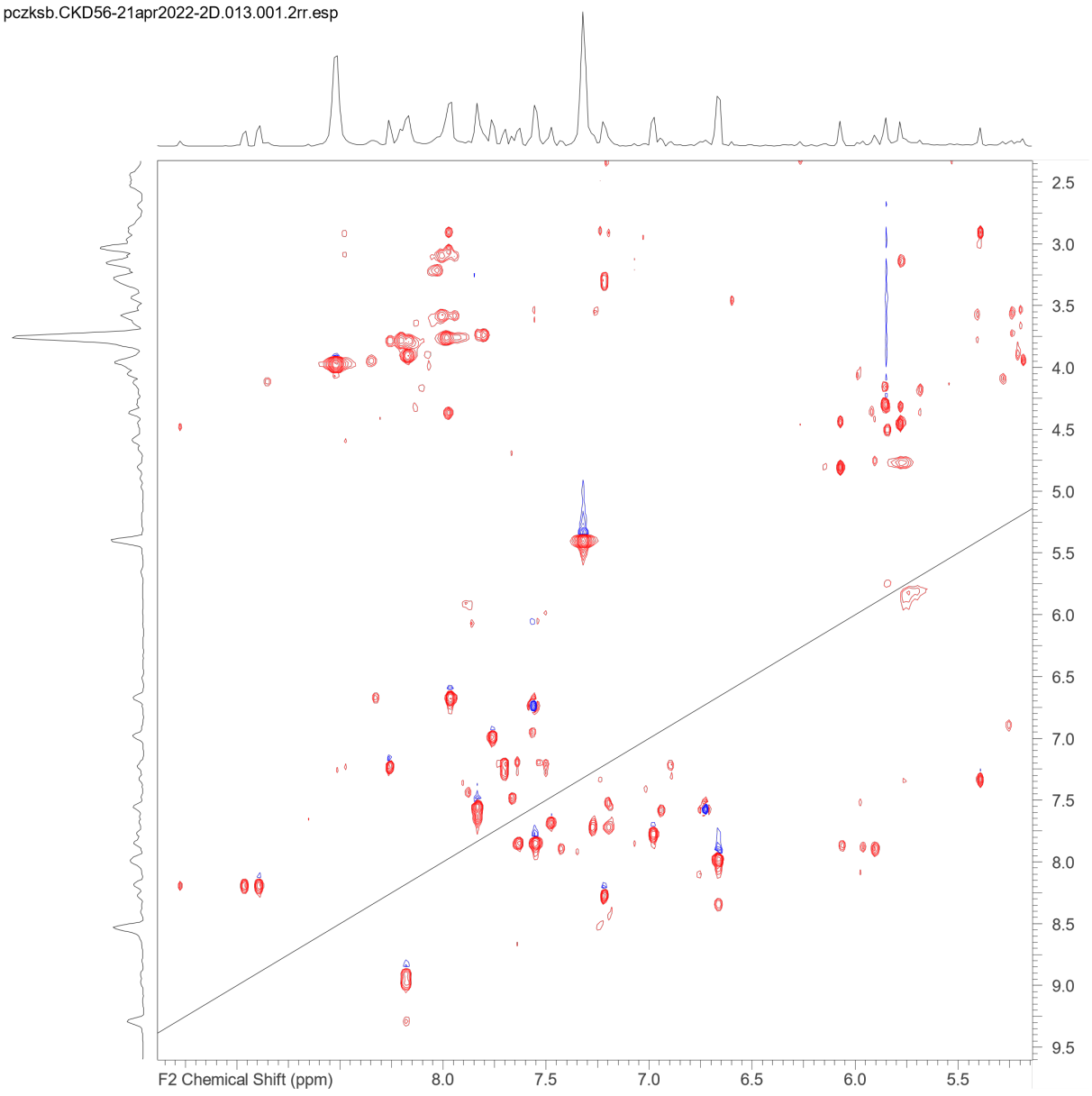

Figure 97 - Chronic Kidney Disease COSY Spectrum (aromatic)

9.23. Broth media obtained from bacteria culture cultivation annotated ^{1}H bNMR spectrum using WET-CP pulse sequence

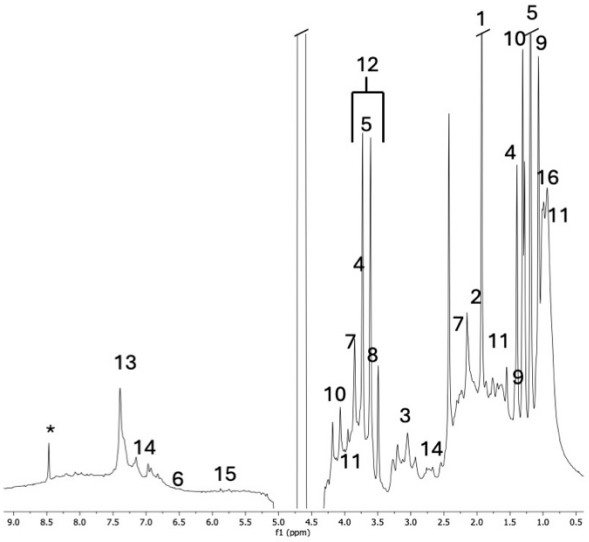

*Figure 98 - Annotated metabolites from microbiology media using WET-CP pulse sequence. 1) Acetate, 2) Acetoin, 3) Agmatine, 4) Alanine, 5) Ethanol, 6) Fumarate, 7) Glutamate, 8) Glycine, 9) Isoleucine, 10) Lactate, 11) Leucine, 12) Glucose, 13) Phenylalanine, 14) Tyrosine, 15) Uracil, 16) Valine, and *) Formate*

Samples were prepared following protocols set out in Chapter 7.

9.24. Broth media obtained from bacteria culture cultivation annotated ^{1}H HF-NMR spectrum using presaturation pulse sequence

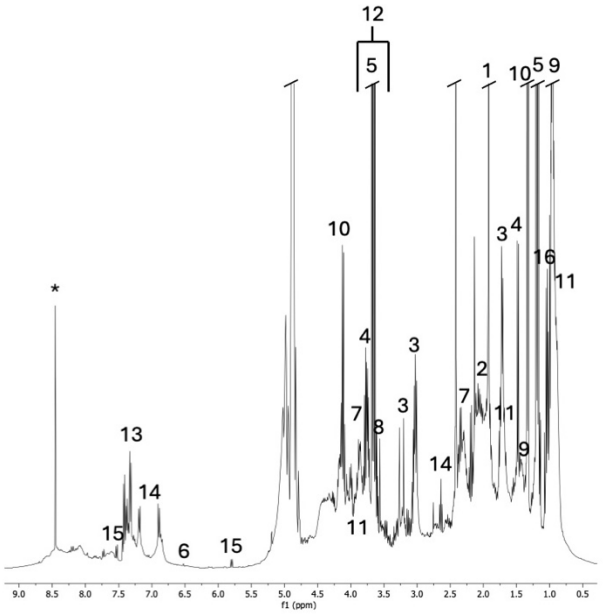

*Figure 99 - Annotated metabolites from microbiology media using presaturation pulse sequence. 1) Acetate, 2) Acetoin, 3) Agmatine, 4) Alanine, 5) Ethanol, 6) Fumarate, 7) Glutamate, 8) Glycine, 9) Isoleucine, 10) Lactate, 11) Leucine, 12) Glucose, 13) Phenylalanine, 14) Tyrosine, 15) Uracil, 16) Valine, and *) Formate*

Samples were prepared following protocols set out in in Chapter 7.

9.25. Blood Serum annotated ^{1}H bNMR spectrum using WASTED-II pulse sequence

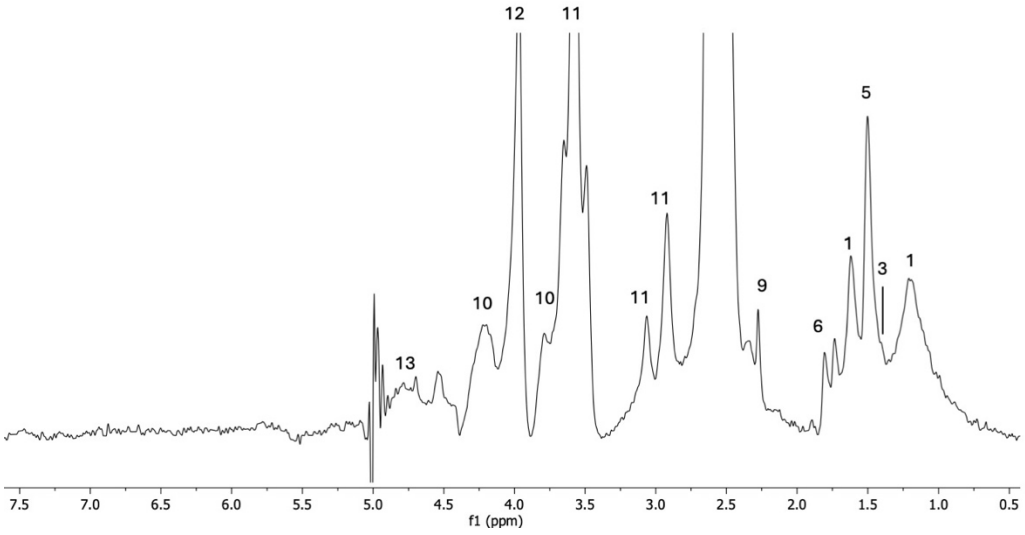

Figure 100 - Annotated metabolites from blood serum using bNMR WASTED-II pulse sequence.

The metabolites are: 1) Lipids, 2) Leucine, 3) Valine, 4) Isoleucine, 5) Lactate, 6) Alanine, 7) Lysine, 8) Acetone, 9) Acetate, 10) Proline, 11) EDTA, 12) Glycine, and 13) Glucose.

9.26. Blood Serum annotated ^{1}H HF-NMR spectrum using WASTED-II pulse sequence

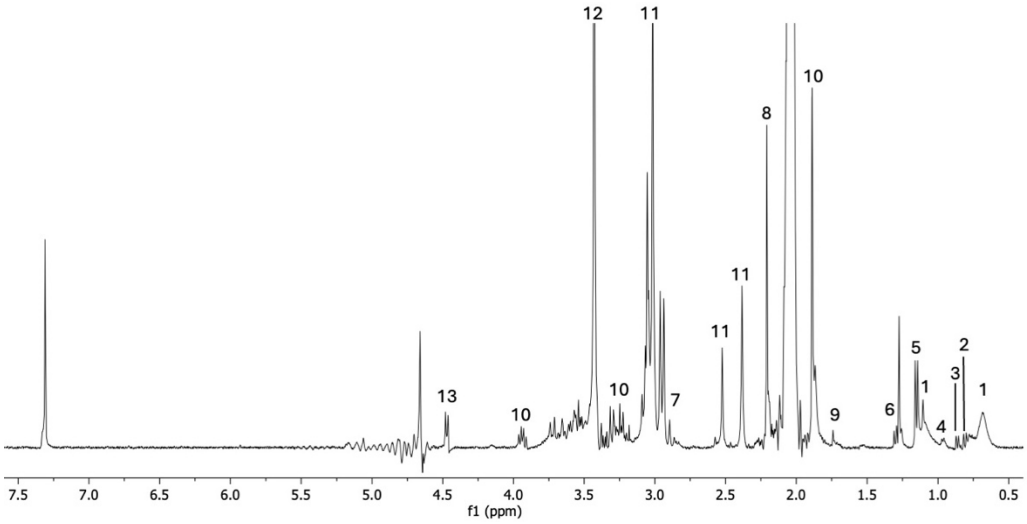

Figure 101 - Annotated metabolites from blood serum using HF-NMR WASTED-II pulse sequence.

The metabolites are: 1) Lipids, 2) Leucine, 3) Valine, 4) Isoleucine, 5) Lactate, 6) Alanine, 7) Lysine, 8) Acetone, 9) Acetate, 10) Proline, 11) EDTA, 12) Glycine, and 13) Glucose.

Reference

1. Stoye G, Warner M, Zaranko B. The past and future of UK health spending. 2024 [cited 2024 Jul 1];Available from: https://ifs.org.uk/publications/past-and-future-uk-health-spending
2. Global Health Expenditure Database [Internet]. [cited 2024 Jul 4];Available from: https://apps.who.int/nha/database/DocumentationCentre/Index/en
3. Why Our Future Health is important – Our Future Health [Internet]. [cited 2024 Oct 14];Available from: https://ourfuturehealth.org.uk/our-research-mission/why-our-future-health-important/
4. NHS Long Term Plan » Overview and summary [Internet]. [cited 2024 Jul 1];Available from: https://www.longtermplan.nhs.uk/online-version/overview-and-summary/
5. NHS Long Term Plan » Chapter 2: More NHS action on prevention and health inequalities [Internet]. [cited 2024 Jul 1];Available from: https://www.longtermplan.nhs.uk/online-version/chapter-2-more-nhs-action-on-prevention-and-health-inequalities/
6. NHS Long Term Plan » Chapter 1: A new service model for the 21st century [Internet]. [cited 2024 Jul 1];Available from: https://www.longtermplan.nhs.uk/online-version/chapter-1-a-new-service-model-for-the-21st-century/
7. Our Future Health: Most have high cholesterol, health project suggests - BBC News [Internet]. [cited 2024 Jul 1];Available from: https://www.bbc.co.uk/news/health-67303204
8. Our Future Health goes live to the public – Our Future Health [Internet]. [cited 2024 Oct 14];Available from: https://ourfuturehealth.org.uk/news/our-future-health-goes-live-to-the-public/
9. BVA – The value of veterinary care.
10. CPI INDEX 09.3.5.0 Veterinary and other services for pets 2015=100 - Office for National Statistics [Internet]. [cited 2024 Aug 27];Available from: https://www.ons.gov.uk/economy/inflationandpriceindices/timeseries/l7hh/mm23
11. Economy | Livestock Data for Decisions [Internet]. [cited 2024 Oct 15];Available from: https://livestockdata.org/research-themes/economy#

12. Asthma [Internet]. [cited 2024 Jul 2];Available from: https://www.who.int/news-room/fact-sheets/detail/asthma#
13. Respiratory High Impact Interventions Intervention Summary Cost of intervention / Return on investment Impact on demand Expected outcomes Resources.
14. Modifiable Risk Factors: High Impact Interventions. [cited 2024 Jul 2];Available from: https://portal.e-
15. Sim S, Choi Y, Park HS, Escribese M, Moreira A, Eguiluz-Gracia I, et al. Potential Metabolic Biomarkers in Adult Asthmatics. Metabolites 2021, Vol 11, Page 430 [Internet] 2021 [cited 2024 Jun 10];11(7):430. Available from: https://www.mdpi.com/2218-1989/11/7/430/htm
16. Majellano EC, Clark VL, Winter NA, Gibson PG, McDonald VM. Approaches to the assessment of severe asthma: barriers and strategies. J Asthma Allergy [Internet] 2019 [cited 2024 Jun 10];12:235. Available from: /pmc/articles/PMC6712210/
17. Asthma - NHS [Internet]. [cited 2024 Jun 12];Available from: https://www.nhs.uk/conditions/asthma/
18. Written evidence submitted by Our Future Health (IMH0081).
19. NHS England » NHS Diabetes Prevention Programme (NHS DPP) [Internet]. [cited 2024 Jul 2];Available from: https://www.england.nhs.uk/diabetes/diabetes-prevention/?msclkid=fdc49848d15a11ec921c629e1b68c832
20. Epilepsy [Internet]. [cited 2024 Jul 2];Available from: https://www.who.int/news-room/fact-sheets/detail/epilepsy
21. Heske L, Nødtvedt A, Jäderlund KH, Berendt M, Egenvall A. A cohort study of epilepsy among 665,000 insured dogs: Incidence, mortality and survival after diagnosis. The Veterinary Journal 2014;202(3):471–6.
22. Packer RMA, Berendt M, Bhatti S, Charalambous M, Cizinauskas S, De Risio L, et al. Inter-observer agreement of canine and feline paroxysmal event semiology and classification by veterinary neurology specialists and non-specialists. BMC Vet Res [Internet] 2015 [cited 2024 Jul 2];11(1):1–11. Available from: https://link.springer.com/articles/10.1186/s12917-015-0356-2
23. Hülsmeyer VI, Fischer A, Mandigers PJJ, DeRisio L, Berendt M, Rusbridge C, et al. International Veterinary Epilepsy Task Force's current understanding of idiopathic epilepsy of genetic or suspected genetic origin in purebred dogs.

BMC Veterinary Research 2015 11:1 [Internet] 2015 [cited 2024 Jul 2];11(1):1–28. Available from: https://link.springer.com/articles/10.1186/s12917-015-0463-0

24. Micheel CM, Nass SJ, Omenn GS, Trials C on the R of OBT for PPO in C, Services B on HC, Policy B on HS, et al. Omics-Based Clinical Discovery: Science, Technology, and Applications. 2012 [cited 2024 Dec 16];Available from: https://www.ncbi.nlm.nih.gov/books/NBK202165/
25. Maslov DP; L;, Balashova EE;, Lokhov PG, Trifonova OP, Maslov DL, Balashova EE, et al. Current State and Future Perspectives on Personalized Metabolomics. 2023 [cited 2024 Oct 21];Available from: https://doi.org/10.3390/metabo13010067
26. Lindon JC, Nicholson JK, Holmes E. The Handbook of Metabonomics and Metabolomics. The Handbook of Metabonomics and Metabolomics 2007;
27. Oliver SG, Winson MK, Kell DB, Baganz F. Systematic functional analysis of the yeast genome. Trends Biotechnol 1998;16(9):373–8.
28. What is metabolomics? | Metabolomics [Internet]. [cited 2024 Jul 4];Available from: https://www.ebi.ac.uk/training/online/courses/metabolomics-introduction/what-is/#
29. Lee J, Banerjee D. Metabolomics and the Microbiome as Biomarkers in Sepsis. Crit Care Clin 2020;36(1):105–13.
30. Definition of metabolic - NCI Dictionary of Cancer Terms - NCI [Internet]. [cited 2025 Mar 7];Available from: https://www.cancer.gov/publications/dictionaries/cancer-terms/def/metabolic
31. Nagana Gowda GA, Raftery D. NMR Based Metabolomics. Adv Exp Med Biol [Internet] 2021 [cited 2025 Mar 4];1280:19. Available from: https://pmc.ncbi.nlm.nih.gov/articles/PMC8816450/
32. Nicholson JK, O'flynn MP, Sadler PJ, Macleod AF, Juul SM, Sonksen PH. Proton-nuclear-magnetic-resonance studies of serum, plasma and urine from fasting normal and diabetic subjects. Biochem J 1984;217:365–75.
33. Holmes E, Antti H. Chemometric contributions to the evolution of metabonomics: mathematical solutions to characterising and interpreting complex biological NMR spectra. 2002 [cited 2024 Jul 10];Available from: www.rsc.org/analyst
34. 7.22C: Metabolomics - Biology LibreTexts [Internet]. [cited 2024 Jul 10];Available from:

https://bio.libretexts.org/Bookshelves/Microbiology/Microbiology_(Boundless)/07%3A_Microbial_Genetics/7.22%3A_Genomics_and_Proteomics/7.22C%3A__Metabolomics

35. Biomarkers for pancreatic cancer based on tissue and serum metabolomics analysis in a multicenter study | Enhanced Reader.
36. Kdadra M, Höckner S, Leung H, Kremer W, Schiffer E. Metabolomics Biomarkers of Prostate Cancer: A Systematic Review. Diagnostics [Internet] 2019 [cited 2024 Oct 10];9(1). Available from: /pmc/articles/PMC6468767/
37. Saiki S, Hatano T, Fujimaki M, Ishikawa KI, Mori A, Oji Y, et al. Decreased long-chain acylcarnitines from insufficient β-oxidation as potential early diagnostic markers for Parkinson's disease. Scientific Reports 2017 7:1 [Internet] 2017 [cited 2024 Oct 10];7(1):1–15. Available from: https://www.nature.com/articles/s41598-017-06767-y
38. Havelund JF, Andersen AD, Binzer M, Blaabjerg M, Heegaard NHH, Stenager E, et al. Changes in kynurenine pathway metabolism in Parkinson patients with L-DOPA-induced dyskinesia. J Neurochem 2017;142(5):756–66.
39. Yilmaz A, Geddes T, Han B, Bahado-Singh RO, Wilson GD, Imam K, et al. Diagnostic Biomarkers of Alzheimer's Disease as Identified in Saliva using 1H NMR-Based Metabolomics. Journal of Alzheimer's Disease 2017;58(2):355–9.
40. Zhu M, Han Y, Zhang Y, Zhang S, Wei C, Cong Z, et al. Metabolomics study of the biochemical changes in the plasma of myocardial infarction patients. Front Physiol [Internet] 2018 [cited 2024 Oct 10];9(AUG):340745. Available from: www.frontiersin.org
41. Li XS, Wang Z, Cajka T, Buffa JA, Nemet I, Hurd AG, et al. Untargeted metabolomics identifies trimethyllysine, a TMAO-producing nutrient precursor, as a predictor of incident cardiovascular disease risk. JCI Insight [Internet] 2018 [cited 2024 Oct 10];3(6). Available from: /pmc/articles/PMC5926943/
42. Aliu E, Kanungo S, Arnold GL. Amino acid disorders. Ann Transl Med [Internet] 2018 [cited 2024 Jul 12];6(24):471–471. Available from: /pmc/articles/PMC6331359/
43. Evans RD, Heather LC. Human metabolism: pathways and clinical aspects. Surgery (Oxford) 2019;37(6):302–9.

44. Organic Acids | EBSCO Research Starters [Internet]. [cited 2025 May 30];Available from: https://www.ebsco.com/research-starters/chemistry/organic-acids
45. Medical Definition of Biofluid [Internet]. [cited 2024 Dec 16];Available from: https://www.rxlist.com/biofluid/definition.htm
46. Teunissen CE, Kimble L, Bayoumy S, Bolsewig K, Burtscher F, Coppens S, et al. Methods to Discover and Validate Biofluid-Based Biomarkers in Neurodegenerative Dementias. Mol Cell Proteomics [Internet] 2023 [cited 2024 Dec 16];22(10):100629. Available from: https://pmc.ncbi.nlm.nih.gov/articles/PMC10594029/
47. Definition of red blood cell - NCI Dictionary of Cancer Terms - NCI [Internet]. [cited 2024 Sep 20];Available from: https://www.cancer.gov/publications/dictionaries/cancer-terms/def/red-blood-cell
48. Dean L. Blood and the cells it contains. 2005 [cited 2024 Sep 20];Available from: https://www.ncbi.nlm.nih.gov/books/NBK2263/
49. Hematology Glossary - Hematology.org [Internet]. [cited 2024 Sep 20];Available from: https://www.hematology.org/education/patients/blood-basics#
50. Qiu Q, Deng J, Deng H, Yao D, Yan Y, Ye S, et al. Association of the characteristics of the blood metabolome and gut microbiome with the outcome of methotrexate therapy in psoriasis. Front Immunol 2022;13:937539.
51. Lin CN, Huang CC, Huang KL, Lin KJ, Yen TC, Kuo HC. A metabolomic approach to identifying biomarkers in blood of Alzheimer's disease. Ann Clin Transl Neurol [Internet] 2019 [cited 2024 Sep 20];6(3):537. Available from: /pmc/articles/PMC6414491/
52. Yeo T, Sealey M, Zhou Y, Saldana L, Loveless S, Claridge TDW, et al. A blood-based metabolomics test to distinguish relapsing–remitting and secondary progressive multiple sclerosis: addressing practical considerations for clinical application. Scientific Reports 2020 10:1 [Internet] 2020 [cited 2024 Sep 20];10(1):1–12. Available from: https://www.nature.com/articles/s41598-020-69119-3
53. Larkin JR, Anthony S, Johanssen VA, Yeo T, Sealey M, Yates AG, et al. Metabolomic Biomarkers in Blood Samples Identify Cancers in a Mixed Population of Patients with Nonspecific Symptoms. Clinical Cancer Research

[Internet] 2022 [cited 2024 Sep 20];28(8):1651. Available from: /pmc/articles/PMC7613224/

54. Stringer KA, Younger JG, McHugh C, Yeomans L, Finkel MA, Puskarich MA, et al. Whole Blood Reveals More Metabolic Detail of the Human Metabolome than Serum as Measured by 1H-NMR Spectroscopy: Implications for Sepsis Metabolomics. Shock [Internet] 2015 [cited 2024 Sep 20];44(3):200. Available from: /pmc/articles/PMC4537695/
55. Checking your blood sugar levels | Diabetes testing | Diabetes UK [Internet]. [cited 2024 Sep 20];Available from: https://www.diabetes.org.uk/guide-to-diabetes/managing-your-diabetes/testing
56. Physiology of Urine Formation in the Nephrons | BIO103: Human Biology [Internet]. [cited 2024 Jul 8];Available from: https://courses.lumenlearning.com/suny-dutchess-ap1/chapter/physiology-of-urine-formation-in-the-nephrons/
57. Pregnancy Test: MedlinePlus Medical Test [Internet]. [cited 2024 Sep 20];Available from: https://medlineplus.gov/lab-tests/pregnancy-test/#
58. Yousri NA, Mook-Kanamori DO, Selim MMED, Takiddin AH, Al-Homsi H, Al-Mahmoud KAS, et al. A systems view of type 2 diabetes-associated metabolic perturbations in saliva, blood and urine at different timescales of glycaemic control. Diabetologia [Internet] 2015 [cited 2021 Dec 16];58(8):1855–67. Available from: https://link.springer.com/article/10.1007/s00125-015-3636-2
59. Friedrich N, Budde K, Suhre K, Völker U, John U, Felix SB, et al. Sex differences in urine metabolites related with risk of diabetes using NMR spectroscopy: results of the study of health in pomerania. Metabolomics [Internet] 2015 [cited 2021 Dec 16];11(5):1405–15. Available from: https://link.springer.com/article/10.1007/s11306-015-0795-6
60. Finch N, Percival B, Hunter E, Blagg RJ, Blackwell E, Sagar J, et al. Preliminary demonstration of benchtop NMR metabolic profiling of feline urine: chronic kidney disease as a case study. BMC Res Notes [Internet] 2021 [cited 2024 Jul 15];14(1):1–5. Available from: https://link.springer.com/articles/10.1186/s13104-021-05888-y
61. Protein in Urine: MedlinePlus Medical Test [Internet]. [cited 2024 Sep 20];Available from: https://medlineplus.gov/lab-tests/protein-in-urine/
62. Bouwman FH, Frisoni GB, Johnson SC, Chen X, Engelborghs S, Ikeuchi T, et al. Clinical application of CSF biomarkers for Alzheimer's disease: From

rationale to ratios. Alzheimer's & Dementia : Diagnosis, Assessment & Disease Monitoring [Internet] 2022 [cited 2024 Sep 20];14(1). Available from: /pmc/articles/PMC9044123/

63. Diagnostics in infectious encephalitis | Encephalitis International [Internet]. [cited 2024 Sep 20];Available from: https://www.encephalitis.info/diagnosis-of-encephalitis/diagnostics-in-infectious-encephalitis/
64. Meningitis [Internet]. [cited 2024 Sep 20];Available from: https://www.who.int/news-room/fact-sheets/detail/meningitis
65. Deisenhammer F, Zetterberg H, Fitzner B, Zettl UK. The cerebrospinal fluid in multiple sclerosis. Front Immunol [Internet] 2019 [cited 2024 Sep 20];10(APR):438156. Available from: www.frontiersin.org
66. Telano LN, Baker S. Physiology, Cerebral Spinal Fluid. StatPearls [Internet] 2023 [cited 2024 Sep 20];Available from: https://www.ncbi.nlm.nih.gov/books/NBK519007/
67. De Risio L, Muñana K. A practical guide to seizure disorders in dogs and cats. 2022;356.
68. Grootveld M, Page G, Bhogadia M, Edgar M. Updates and Original Case Studies Focused on the NMR-Linked Metabolomics Analysis of Human Oral Fluids Part I: Emerging Platforms and Perspectives. Applied Sciences (Switzerland) [Internet] 2022 [cited 2024 Sep 19];12(3):1235. Available from: https://www.mdpi.com/2076-3417/12/3/1235/htm
69. Percival BC, Wann A, Taylor S, Edgar M, Gibson M, Grootveld M, et al. Metabolomics Distinction of Cigarette Smokers from Non-Smokers Using Non-Stationary Benchtop Nuclear Magnetic Resonance (NMR) Analysis of Human Saliva. 2022 [cited 2024 Sep 20];Available from: https://www.intechopen.com/chapters/79699
70. Lee JM, Garon E, Wong DT. Salivary diagnostics. Orthod Craniofac Res [Internet] 2009 [cited 2024 Sep 20];12(3):206. Available from: /pmc/articles/PMC2909324/
71. Fan G, Qin X, Streblow DN, Hoyos CM, Hansel DE. Comparison of SARS-CoV-2 PCR-Based Detection Using Saliva or Nasopharyngeal Swab Specimens in Asymptomatic Populations. Microbiol Spectr [Internet] 2021 [cited 2024 Sep 20];9(1). Available from: https://pubmed.ncbi.nlm.nih.gov/34431689/

72. Edgar M, Kuhn S, Page G, Grootveld M. Computational simulation of 1H NMR profiles of complex biofluid analyte mixtures at differential operating frequencies: Applications to low-field benchtop spectra. Magnetic Resonance in Chemistry [Internet] 2022 [cited 2024 Jul 15];60(12):1097–112. Available from: https://onlinelibrary.wiley.com/doi/full/10.1002/mrc.5236
73. 4.3: Raman Spectroscopy - Chemistry LibreTexts [Internet]. [cited 2025 Jun 1];Available from: https://chem.libretexts.org/Bookshelves/Analytical_Chemistry/Physical_Methods_in_Chemistry_and_Nano_Science_(Barron)/04%3A_Chemical_Speciation/4.03%3A_Raman_Spectroscopy
74. Wang TL, Chiang H hua K, Lu H hsin, Hung Y da. SERS quantitative urine creatinine measurement of human subject. https://doi.org/101117/12591393 [Internet] 2005 [cited 2025 Feb 28];5703:17–24. Available from: https://www.spiedigitallibrary.org/conference-proceedings-of-spie/5703/0000/SERS-quantitative-urine-creatinine-measurement-of-human-subject/10.1117/12.591393.full
75. Hsu PH, Tsai TH, Chiang HK. In vivo blood lactic acid monitoring using microdialysis and surface-enhanced Raman spectroscopy. https://doi.org/101117/12794798 [Internet] 2008 [cited 2025 Feb 28];7040:139–46. Available from: https://www.spiedigitallibrary.org/conference-proceedings-of-spie/7040/70400R/In-vivo-blood-lactic-acid-monitoring-using-microdialysis-and-surface/10.1117/12.794798.full
76. Liu J, Cai C, Wang Y, Liu Y, Huang L, Tian T, et al. A Biomimetic Plasmonic Nanoreactor for Reliable Metabolite Detection. Advanced Science [Internet] 2020 [cited 2025 Feb 28];7(10):1903730. Available from: https://onlinelibrary.wiley.com/doi/full/10.1002/advs.201903730
77. Lima C, Muhamadali H, Goodacre R. The Role of Raman Spectroscopy within Quantitative Metabolomics. Annual Review of Analytical Chemistry [Internet] 2021 [cited 2025 Feb 28];14(Volume 14, 2021):323–45. Available from: https://www.annualreviews.org/content/journals/10.1146/annurev-anchem-091420-092323
78. Martens J, Berden G, Van Outersterp RE, Kluijtmans LAJ, Engelke UF, Van Karnebeek CDM, et al. Molecular identification in metabolomics using infrared ion spectroscopy. Scientific Reports 2017 7:1 [Internet] 2017 [cited 2025 Feb

28];7(1):1–5. Available from: https://www.nature.com/articles/s41598-017-03387-4

79. 4.4: UV-Visible Spectroscopy - Chemistry LibreTexts [Internet]. [cited 2025 Jun 1];Available from: https://chem.libretexts.org/Bookshelves/Analytical_Chemistry/Physical_Methods_in_Chemistry_and_Nano_Science_(Barron)/04%3A_Chemical_Speciation/4.04%3A_UV-Visible_Spectroscopy
80. Ray P, Steckl AJ. Label-Free Optical Detection of Multiple Biomarkers in Sweat, Plasma, Urine, and Saliva. ACS Sens [Internet] 2019 [cited 2025 Mar 4];4(5):1346–57. Available from: https://pubs.acs.org/doi/full/10.1021/acssensors.9b00301
81. Wang Q, He H, Li B, Lin H, Zhang Y, Zhang J, et al. UV–Vis and ATR–FTIR spectroscopic investigations of postmortem interval based on the changes in rabbit plasma. PLoS One [Internet] 2017 [cited 2025 Mar 4];12(7):e0182161. Available from: https://pmc.ncbi.nlm.nih.gov/articles/PMC5533326/
82. Comparison of NMR and MS | Metabolomics [Internet]. [cited 2024 Jul 9];Available from: https://www.ebi.ac.uk/training/online/courses/metabolomics-introduction/designing-a-metabolomics-study/comparison-of-nmr-and-ms/
83. Sample Preparation for Mass Spectrometry | Thermo Fisher Scientific - UK [Internet]. [cited 2024 Sep 20];Available from: https://www.thermofisher.com/uk/en/home/life-science/protein-biology/protein-biology-learning-center/protein-biology-resource-library/pierce-protein-methods/sample-preparation-mass-spectrometry.html
84. Fiehn O. Metabolomics by Gas Chromatography-Mass Spectrometry: the combination of targeted and untargeted profiling. Current protocols in molecular biology / edited by Frederick M Ausubel . [et al] [Internet] 2016 [cited 2025 Feb 28];114:30.4.1. Available from: https://pmc.ncbi.nlm.nih.gov/articles/PMC4829120/
85. Wang DC, Sun CH, Liu LY, Sun XH, Jin XW, Song WL, et al. Serum fatty acid profiles using GC-MS and multivariate statistical analysis: potential biomarkers of Alzheimer's disease. Neurobiol Aging 2012;33(6):1057–66.
86. Vemuri R, Shinde T, Gundamaraju R, Gondalia S V., Karpe A V., Beale DJ, et al. Lactobacillus acidophilus DDS-1 Modulates the Gut Microbiota and Improves Metabolic Profiles in Aging Mice. Nutrients 2018, Vol 10, Page 1255

[Internet] 2018 [cited 2025 Mar 4];10(9):1255. Available from: https://www.mdpi.com/2072-6643/10/9/1255/htm

87. Phillips M, Cataneo RN, Chaturvedi A, Danaher PJ, Devadiga A, Legendre DA, et al. Effect of influenza vaccination on oxidative stress products in breath. J Breath Res [Internet] 2010 [cited 2025 Mar 4];4(2):026001. Available from: https://iopscience.iop.org/article/10.1088/1752-7155/4/2/026001
88. LC-MS Metabolomics Analysis | Thermo Fisher Scientific - UK [Internet]. [cited 2025 Mar 4];Available from: https://www.thermofisher.com/uk/en/home/industrial/mass-spectrometry/mass-spectrometry-learning-center/mass-spectrometry-applications-area/metabolomics-mass-spectrometry/practical-guide-metabolomics/lc-ms-metabolomics-analysis.html
89. McGarrah RW, Crown SB, Zhang GF, Shah SH, Newgard CB. Cardiovascular metabolomics. Circ Res [Internet] 2018 [cited 2025 Mar 4];122(9):1238–58. Available from: https://www.ahajournals.org/doi/10.1161/CIRCRESAHA.117.311002
90. Pradhan SS, Thota SM, Rajaratnam S, Bhagavatham SKS, Pulukool SK, Rathnakumar S, et al. Integrated multi-omics analysis of Huntington disease identifies pathways that modulate protein aggregation. DMM Disease Models and Mechanisms [Internet] 2022 [cited 2025 Mar 4];15(10). Available from: https://dx.doi.org/10.1242/dmm.049492
91. Chu Z, Zhao T, Zhang Z, Chu CH, Cai K, Wu J, et al. Untargeted Metabolomics Analysis of Gingival Tissue in Patients with Severe Periodontitis. J Proteome Res [Internet] 2024 [cited 2025 Mar 4];23(1):3–15. Available from: https://pubs.acs.org/doi/abs/10.1021/acs.jproteome.3c00105
92. Zhang W, Ramautar R. CE-MS for metabolomics: Developments and applications in the period 2018–2020. Electrophoresis [Internet] 2020 [cited 2025 Mar 4];42(4):381. Available from: https://pmc.ncbi.nlm.nih.gov/articles/PMC7891659/
93. Soga T. Advances in capillary electrophoresis mass spectrometry for metabolomics. TrAC Trends in Analytical Chemistry 2023;158:116883.
94. Beale DJ, Pinu FR, Kouremenos KA, Poojary MM, Narayana VK, Boughton BA, et al. Review of recent developments in GC–MS approaches to metabolomics-based research. Metabolomics [Internet] 2018 [cited 2025 Mar

4];14(11):1–31. Available from: https://link.springer.com/article/10.1007/s11306-018-1449-2

95. Rates | Harvard Center for Mass Spectrometry [Internet]. [cited 2024 Sep 20];Available from: https://massspec.fas.harvard.edu/pages/rates
96. Levitt MH. Spin dynamics : basics of nuclear magnetic resonance. 2008 [cited 2022 Oct 19];714. Available from: https://www.wiley.com/en-gb/Spin+Dynamics%3A+Basics+of+Nuclear+Magnetic+Resonance%2C+2nd+Edition-p-9781118681848
97. Keeler James. Understanding NMR spectroscopy. 2010;511.
98. Hore PJ. Nuclear magnetic resonance. :112.
99. Hore PJ, Jones JA (Jonathan A), Wimperis S. NMR : the toolkit : how pulse sequences work. :120.
100. Emwas AH, Roy R, McKay RT, Tenori L, Saccenti E, Nagana Gowda GA, et al. NMR Spectroscopy for Metabolomics Research. Metabolites [Internet] 2019 [cited 2025 Mar 7];9(7):123. Available from: https://pmc.ncbi.nlm.nih.gov/articles/PMC6680826/
101. Wishart DS. NMR metabolomics: A look ahead. Journal of Magnetic Resonance 2019;306:155–61.
102. Nagana Gowda GA, Raftery D. Quantitating metabolites in protein precipitated serum using NMR spectroscopy. Anal Chem [Internet] 2014 [cited 2025 Mar 7];86(11):5433–40. Available from: https://pubs.acs.org/doi/full/10.1021/ac5005103
103. McPherson RA., Pincus MR. Henry's clinical diagnosis and management by laboratory methods. 2021;1666.
104. NMR Magnets | Superconducting Magnets | Bruker [Internet]. [cited 2024 Sep 19];Available from: https://www.bruker.com/en/products-and-solutions/mr/nmr/ascend-nmr-magnets.html
105. Nightingale Health's biomarkers | Nightingale Health [Internet]. [cited 2024 Aug 9];Available from: https://research.nightingalehealth.com/biomarkers
106. Castaing-Cordier T, Bouillaud D, Farjon J, Giraudeau P. Recent advances in benchtop NMR spectroscopy and its applications. Annu Rep NMR Spectrosc 2021;103:191–258.
107. What is Benchtop NMR? [Internet]. [cited 2024 Sep 19];Available from: https://nmr.oxinst.com/what-is-benchtop-nmr

108. Percival BC, Grootveld M, Gibson M, Osman Y, Molinari M, Jafari F, et al. Low-Field, Benchtop NMR Spectroscopy as a Potential Tool for Point-of-Care Diagnostics of Metabolic Conditions: Validation, Protocols and Computational Models. High Throughput [Internet] 2019 [cited 2024 Jul 12];8(1). Available from: /pmc/articles/PMC6480726/
109. Edgar M, Percival BC, Gibson M, Jafari F, Grootveld M. Low-field benchtop NMR spectroscopy as a potential non-stationary tool for point-of-care urinary metabolite tracking in diabetic conditions. Diabetes Res Clin Pract 2021;171:108554.
110. Leenders J, Grootveld M, Percival B, Gibson M, Casanova F, Wilson PB. Benchtop Low-Frequency 60 MHz NMR Analysis of Urine: A Comparative Metabolomics Investigation. Metabolites 2020, Vol 10, Page 155 [Internet] 2020 [cited 2024 Jul 15];10(4):155. Available from: https://www.mdpi.com/2218-1989/10/4/155/htm
111. Comella-del-Barrio P, Izquierdo-Garcia JL, Gautier J, Doresca MJC, Campos-Olivas R, Santiveri CM, et al. Urine NMR-based TB metabolic fingerprinting for the diagnosis of TB in children. Scientific Reports 2021 11:1 [Internet] 2021 [cited 2024 Jul 15];11(1):1–11. Available from: https://www.nature.com/articles/s41598-021-91545-0
112. Ruiz-Cabello J, Sevilla IA, Olaizola E, Bezos J, Miguel-Coello AB, Muñoz-Mendoza M, et al. Benchtop nuclear magnetic resonance-based metabolomic approach for the diagnosis of bovine tuberculosis. Transbound Emerg Dis [Internet] 2022;69:859–70. Available from: https://onlinelibrary.wiley.com/doi/10.1111/tbed.14365
113. Izquierdo-Garcia JL, Comella-del-Barrio P, Campos-Olivas R, Villar-Hernández R, Prat-Aymerich C, De Souza-Galvão ML, et al. Discovery and validation of an NMR-based metabolomic profile in urine as TB biomarker. Scientific Reports 2020 10:1 [Internet] 2020 [cited 2024 Jul 15];10(1):1–13. Available from: https://www.nature.com/articles/s41598-020-78999-4
114. Song Z, Ohnishi Y, Osada S, Gan L, Jiang J, Hu Z, et al. Application of Benchtop NMR for Metabolomics Study Using Feces of Mice with DSS-Induced Colitis. Metabolites [Internet] 2023 [cited 2024 Aug 12];13(5). Available from: /pmc/articles/PMC10224185/
115. PubMed [Internet]. [cited 2024 Dec 17];Available from: https://pubmed.ncbi.nlm.nih.gov/

116. Scopus | Abstract and citation database | Elsevier [Internet]. [cited 2024 Dec 17];Available from: https://www.elsevier.com/products/scopus
117. Document Search - Web of Science Core Collection [Internet]. [cited 2024 Dec 17];Available from: https://www.webofscience.com/wos/woscc/basic-search
118. Zotero | Your personal research assistant [Internet]. [cited 2024 Dec 16];Available from: https://www.zotero.org/
119. Rayyan: AI-Powered Systematic Review Management Platform [Internet]. [cited 2024 Dec 16];Available from: https://www.rayyan.ai/
120. Gunning Y, Davies KS, Kemsley EK. Authentication of saffron using 60 MHz 1H NMR spectroscopy. Food Chem 2023;404:134649.
121. Jakes W, Gerdova A, Defernez M, Watson AD, McCallum C, Limer E, et al. Authentication of beef versus horse meat using 60 MHz 1H NMR spectroscopy. Food Chem [Internet] 2015 [cited 2024 Dec 16];175:1–9. Available from: https://pubmed.ncbi.nlm.nih.gov/25577043/
122. Gunning Y, Defernez M, Watson AD, Beadman N, Colquhoun IJ, Le Gall G, et al. 16-O-methylcafestol is present in ground roast Arabica coffees: Implications for authenticity testing. Food Chem 2018;248:52–60.
123. Ozbay M, Arslan FN, Gorur G. Low-field 1H-NMR spectroscopy allied with chemometrics for recognition of botanical origin and adulteration of honeys. European Food Research and Technology [Internet] 2024 [cited 2024 Dec 16];1–12. Available from: https://link.springer.com/article/10.1007/s00217-024-04617-6
124. Khilare V, Tiknaik A, Prakash B, Ughade B, Korhale G, Nalage D, et al. Multiple tests on saffron find new adulterant materials and reveal that Ist grade saffron is rare in the market. Food Chem 2019;272:635–42.
125. Ordoudi SA, Cagliani LR, Melidou D, Tsimidou MZ, Consonni R. Uncovering a challenging case of adulterated commercial saffron. Food Control 2017;81:147–55.
126. Husaini A, Anam Ul Haq S, Amir W, Ahmad Dedmari M. The menace of saffron adulteration: Low-cost rapid identification of fake look-alike saffron using Foldscope and machine learning technology. [cited 2023 Apr 4];Available from: https://www.researchgate.net/publication/362710109

127. Gouilleux B, Farjon J, Giraudeau P. Gradient-based pulse sequences for benchtop NMR spectroscopy. Journal of Magnetic Resonance 2020;319:106810.
128. Silva Terra AI, Taylor DA, Halse ME. Hyperpolarised benchtop NMR spectroscopy for analytical applications. Prog Nucl Magn Reson Spectrosc [Internet] 2024 [cited 2024 Dec 16];144–145:153–78. Available from: https://pubmed.ncbi.nlm.nih.gov/39645349/
129. Richardson PM, Iali W, Roy SS, Rayner PJ, Halse ME, Duckett SB. Rapid 13C NMR hyperpolarization delivered from para-hydrogen enables the low concentration detection and quantification of sugars. Chem Sci [Internet] 2019 [cited 2024 Dec 16];10(45):10607–19. Available from: https://pubs.rsc.org/en/content/articlehtml/2019/sc/c9sc03450a
130. Silva Terra AI, Rossetto M, Dickson CL, Peat G, Uhrín D, Halse ME. Enhancing 19F Benchtop NMR Spectroscopy by Combining para-Hydrogen Hyperpolarization and Multiplet Refocusing. ACS Measurement Science Au [Internet] 2023 [cited 2024 Dec 16];3(1):73–81. Available from: https://pubs.acs.org/doi/full/10.1021/acsmeasuresciau.2c00055
131. Nowroozi A, Shahlaei M, Kobarfard F. Simultaneous Determination of Multicomponent Dosage Forms Using Benchtop NMR Spectroscopy: Application to Phenytoin-Phenobarbital Combination. Iran J Pharm Res [Internet] 2022 [cited 2024 Dec 16];21(1):e127040. Available from: https://pmc.ncbi.nlm.nih.gov/articles/PMC10024314/
132. Lee Y, Matviychuk Y, Bogun B, Johnson CS, Holland DJ. Quantification of mixtures of analogues of illicit substances by benchtop NMR spectroscopy. Journal of Magnetic Resonance 2022;335:107138.
133. Araneda JF, Chu T, Leclerc MC, Riegel SD, Spingarn N. Quantitative analysis of cannabinoids using benchtop NMR instruments. Analytical Methods [Internet] 2020 [cited 2024 Dec 16];12(40):4853–7. Available from: https://pubs.rsc.org/en/content/articlehtml/2020/ay/d0ay01511c
134. Wu N, Danoun S, Balayssac S, Malet-Martino M, Lamoureux C, Gilard V. Synthetic cannabinoids in e-liquids: A proton and fluorine NMR analysis from a conventional spectrometer to a compact one. Forensic Sci Int [Internet] 2021 [cited 2024 Dec 16];324. Available from: https://pubmed.ncbi.nlm.nih.gov/33993010/

135. Gouilleux B, Charrier B, Danieli E, Dumez JN, Akoka S, Felpin FX, et al. Real-time reaction monitoring by ultrafast 2D NMR on a benchtop spectrometer. Analyst [Internet] 2015 [cited 2024 Dec 16];140(23):7854–8. Available from: https://pubs.rsc.org/en/content/articlehtml/2015/an/c5an01998b
136. Sagmeister P, Poms J, Williams JD, Kappe CO. Multivariate analysis of inline benchtop NMR data enables rapid optimization of a complex nitration in flow. React Chem Eng [Internet] 2020 [cited 2024 Dec 16];5(4):677–84. Available from: https://pubs.rsc.org/en/content/articlehtml/2020/re/d0re00048e
137. Claaßen C, Mack K, Rother D. Benchtop NMR for Online Reaction Monitoring of the Biocatalytic Synthesis of Aromatic Amino Alcohols. ChemCatChem [Internet] 2020 [cited 2024 Dec 16];12(4):1190–9. Available from: https://onlinelibrary.wiley.com/doi/full/10.1002/cctc.201901910
138. Jeong HJ, Min S, Baek J, Kim J, Chung J, Jeong K. Real-Time Reaction Monitoring of Azide-Alkyne Cycloadditions Using Benchtop NMR-Based Signal Amplification by Reversible Exchange (SABRE). ACS Measurement Science Au [Internet] 2023 [cited 2024 Dec 16];3(2):134–42. Available from: https://pubs.acs.org/doi/full/10.1021/acsmeasuresciau.2c00065
139. Block F, May A, Wetzel K, Adels K, Elbers G, Schulze M, et al. What is the best spectroscopic method for simultaneous analysis of organic acids and (poly)saccharides in biological matrices: Example of Aloe vera extracts? Talanta Open 2023;7:100220.
140. Peez N, Rinesch T, Kolz J, Imhof W. Applicable and cost-efficient microplastic analysis by quantitative 1H-NMR spectroscopy using benchtop NMR and NoD methods. Magnetic Resonance in Chemistry [Internet] 2022 [cited 2024 Dec 16];60(1):172–83. Available from: https://onlinelibrary.wiley.com/doi/full/10.1002/mrc.5210
141. Chen P, Zhuang S, Chen W, Chen Z, Li R, Chen F, et al. Facile identification of fluorosurfactant category in aqueous film-forming foam concentrates via optimized 19F NMR. Magnetic Resonance Letters 2024;4(3):100097.
142. Tang B, Chong K, Ragauskas AJ, Evans R. Quantitative Low-Field 19F Nuclear Magnetic Resonance Analysis of Carbonyl Groups in Pyrolysis Oils. ChemSusChem [Internet] 2023 [cited 2024 Dec 16];16(17):e202300625. Available from: https://onlinelibrary.wiley.com/doi/full/10.1002/cssc.202300625

143. Makarova K, Sajkowska-Kozielewicz JJ, Zawada K, Olchowik-Grabarek E, Ciach MA, Gogolewski K, et al. Harvest time affects antioxidant capacity, total polyphenol and flavonoid content of Polish St John's wort's (Hypericum perforatum L.) flowers. Scientific Reports 2021 11:1 [Internet] 2021 [cited 2024 Dec 16];11(1):1–12. Available from: https://www.nature.com/articles/s41598-021-83409-4
144. Heerah K, Waclawek S, Konzuk J, Longstaffe JG. Benchtop 19F NMR spectroscopy as a practical tool for testing of remedial technologies for the degradation of perfluorooctanoic acid, a persistent organic pollutant. Magnetic Resonance in Chemistry [Internet] 2020 [cited 2024 Dec 16];58(12):1160–7. Available from: https://onlinelibrary.wiley.com/doi/full/10.1002/mrc.5005
145. Stocchero M, Cannet C, Napoli C, Demetrio E, Baraldi E, Giordano G. Low-Field Benchtop NMR to Discover Early-Onset Sepsis: A Proof of Concept. Metabolites [Internet] 2023 [cited 2024 Dec 16];13(9):1029. Available from: https://www.mdpi.com/2218-1989/13/9/1029/htm
146. Stolz M, Schlawne C, Hoffmann J, Hartmann V, Marini I, Fritsche A, et al. Feasibility of precise and reliable glucose quantification in human whole blood samples by 1 tesla benchtop NMR. NMR Biomed [Internet] 2020 [cited 2024 Dec 16];33(9):e4358. Available from: https://onlinelibrary.wiley.com/doi/full/10.1002/nbm.4358
147. Diabetes Facets and Figures | International Diabetes Federation [Internet]. [cited 2023 Nov 22];Available from: https://idf.org/about-diabetes/diabetes-facts-figures/
148. 1.1 TB incidence [Internet]. [cited 2024 Aug 12];Available from: https://www.who.int/teams/global-tuberculosis-programme/tb-reports/global-tuberculosis-report-2023/tb-disease-burden/1-1-tb-incidence
149. 1.2 TB mortality [Internet]. [cited 2024 Aug 12];Available from: https://www.who.int/teams/global-tuberculosis-programme/tb-reports/global-tuberculosis-report-2023/tb-disease-burden/1-2-tb-mortality
150. The top 10 causes of death [Internet]. [cited 2024 Aug 12];Available from: https://www.who.int/news-room/fact-sheets/detail/the-top-10-causes-of-death#
151. Ulcerative colitis - Symptoms, diagnosis and treatment | BMJ Best Practice [Internet]. [cited 2024 Aug 12];Available from: https://bestpractice.bmj.com/topics/en-gb/43

152. Ross SJ, Polzin DJ, Osborne CA. Clinical progression of early chronic renal failure and implications for management. Consultations in Feline Internal Medicine [Internet] 2006 [cited 2024 Aug 12];389–98. Available from: https://experts.umn.edu/en/publications/clinical-progression-of-early-chronic-renal-failure-and-implicati
153. Gouilleux B, Charrier B, Akoka S, Giraudeau P. Gradient-based solvent suppression methods on a benchtop spectrometer. Magnetic Resonance in Chemistry [Internet] 2017 [cited 2024 Jul 16];55(2):91–8. Available from: https://onlinelibrary.wiley.com/doi/full/10.1002/mrc.4493
154. Krishnan V V., Murali N. Radiation damping in modern NMR experiments: Progress and challenges. Prog Nucl Magn Reson Spectrosc 2013;68:41–57.
155. Williams DH. Spectroscopic methods in organic chemistry / Dudley H. Williams, Ian Fleming. 2008 [cited 2024 Mar 1];Available from: https://encore.lib.warwick.ac.uk/iii/encore/record/C__Rb2217852__Sspectroscopic%20methods%20organic%20chemistry__Orightresult__U__X2?lang=eng&suite=cobalt
156. Chemical shift - Labster [Internet]. [cited 2024 Sep 4];Available from: https://theory.labster.com/chemshift/
157. Chechik V, Carter E, Murphy D. Electron Paramagnetic Resonance. 1st ed. Oxford: Oxford Chemistry Primers; 2016.
158. T1 relaxation - Questions and Answers in MRI [Internet]. [cited 2024 Oct 1];Available from: https://mriquestions.com/what-is-t1.html
159. Direction of inversion pulse - Questions and Answers in MRI [Internet]. [cited 2024 Sep 27];Available from: https://mriquestions.com/direction-of-180deg-pulse.html
160. Aguilar JA, Nilsson M, Bodenhausen G, Morris GA. Spin echo NMR spectra without J modulation. Chem Commun [Internet] 2012 [cited 2024 Feb 15];48:811–3. Available from: www.rsc.org/chemcomm
161. Mckay RT. How the 1D-NOESY suppresses solvent signal in metabonomics NMR spectroscopy: An examination of the pulse sequence components and evolution. Concepts in Magnetic Resonance Part A [Internet] 2011 [cited 2024 Mar 21];38A(5):197–220. Available from: https://onlinelibrary.wiley.com/doi/full/10.1002/cmr.a.20223
162. Balaram P, Bothner-By AA, Dadok J. Negative Nuclear Overhauser Effects as Probes of Macromolecular Structure. J Am Chem Soc [Internet] 1972 [cited

2024 Aug 15];94(11):4015–7. Available from: https://pubs.acs.org/doi/abs/10.1021/ja00766a063

163. Zheng G, Price WS. Solvent signal suppression in NMR. Prog Nucl Magn Reson Spectrosc 2010;56(3):267–88.
164. Berger Stefan, Braun Siegmar. 200 and more NMR experiments : a practical course. 2011 [cited 2024 Aug 13];838. Available from: https://www.wiley.com/en-us/200+and+More+NMR+Experiments%3A+A+Practical+Course-p-9783527310678
165. Aguilar JA, Kenwright SJ. Robust NMR water signal suppression for demanding analytical applications †. Analyst [Internet] 2015 [cited 2024 Feb 16];141:236. Available from: www.rsc.org/analyst
166. Aguilar JA;, Aguilar JA, Kenwright SJ. Robust NMR water signal suppression for demanding analytical applications 5.0 4.0 3.0 ppm Residual H 2 O Robust NMR water signal suppression for demanding analytical applications. J Name [Internet] 2013 [cited 2024 Aug 14];00:1–3. Available from: www.rsc.org/
167. Le Guennec A, Tayyari F, Edison AS. Alternatives to Nuclear Overhauser Enhancement Spectroscopy Presat and Carr–Purcell–Meiboom–Gill Presat for NMR-Based Metabolomics. Anal Chem [Internet] 2017 [cited 2024 Aug 13];89(17):8582. Available from: /pmc/articles/PMC5588096/
168. University of Ottawa NMR Facility Blog: COSY vs TOCSY [Internet]. [cited 2024 Oct 4];Available from: https://u-of-o-nmr-facility.blogspot.com/2008/06/cosy-vs-tocsy.html
169. University of Ottawa NMR Facility Blog: Search results for HSQC [Internet]. [cited 2024 Oct 7];Available from: https://u-of-o-nmr-facility.blogspot.com/search?q=HSQC
170. Shimming - Questions and Answers in MRI [Internet]. [cited 2024 Aug 28];Available from: https://mriquestions.com/routine-shimming.html
171. Magnetic shimming - Questions and Answers in MRI [Internet]. [cited 2024 Aug 28];Available from: https://mriquestions.com/why-shimming.html
172. Second Order Shimming of High Field Magnets s medical.
173. Mckay RT. How the 1D-NOESY suppresses solvent signal in metabonomics NMR spectroscopy: An examination of the pulse sequence components and evolution. Concepts Magn Reson Part A Bridg Educ Res 2011;38 A(5):197–220.

174. Percival B, Gibson M, Leenders J, Wilson PB, Grootveld M. Univariate and Multivariate Statistical Approaches to the Analysis and Interpretation of NMR-based Metabolomics Datasets of Increasing Complexity. RSC Theoretical and Computational Chemistry Series [Internet] 2020 [cited 2024 Aug 28];2021-January(20):1–40. Available from: https://books.rsc.org/books/edited-volume/808/chapter/551125/Univariate-and-Multivariate-Statistical-Approaches
175. Walsh MC, Brennan L, Malthouse JPG, Roche HM, Gibney MJ. Effect of acute dietary standardization on the urinary, plasma, and salivary metabolomic profiles of healthy humans. Am J Clin Nutr 2006;84(3):531–9.
176. Xia J, Psychogios N, Young N, Wishart DS. MetaboAnalyst: a web server for metabolomic data analysis and interpretation. Nucleic Acids Res [Internet] 2009 [cited 2023 Oct 27];37(suppl_2):W652–60. Available from: https://dx.doi.org/10.1093/nar/gkp356
177. Dog population in the UK 2024 | Statista [Internet]. [cited 2024 Oct 31];Available from: https://www.statista.com/statistics/515379/dogs-population-in-the-united-kingdom-uk/#
178. PET PAINS: OVER A FIFTH OF DOG AND CAT OWNERS PUT OFF VET VISITS DUE TO INCREASED COSTS - Co-op [Internet]. [cited 2024 Oct 31];Available from: https://www.co-operative.coop/media/news-releases/pet-pains-over-a-fifth-of-dog-and-cat-owners-put-off-vet-visits-due-to
179. Veterinary Industry Trends in the UK and Europe [Internet]. [cited 2024 Oct 31];Available from: https://www.vetstoria.com/blog/exploring-the-world-of-veterinary-medicine-key-facts-and-trends-of-2023-for-veterinarians-in-the-uk-and-globally/
180. Sánchez-Vizcaíno F, Noble PJM, Jones PH, Menacere T, Buchan I, Reynolds S, et al. Demographics of dogs, cats, and rabbits attending veterinary practices in Great Britain as recorded in their electronic health records. BMC Vet Res [Internet] 2017 [cited 2024 Oct 31];13(1):1–13. Available from: https://bmcvetres.biomedcentral.com/articles/10.1186/s12917-017-1138-9
181. Vets raise concerns as 1 in 5 pets not receiving veterinary treatment in time due to cost-of-living crisis | British Veterinary Association [Internet]. [cited 2024 Oct 31];Available from: https://www.bva.co.uk/news-and-blog/news-article/vets-raise-concerns-as-1-in-5-pets-not-receiving-veterinary-treatment-in-time-due-to-cost-of-living-crisis/

182. Epilepsy – Seizure Types, Symptoms and Treatment Options [Internet]. [cited 2022 Aug 2];Available from: https://www.aans.org/en/Patients/Neurosurgical-Conditions-and-Treatments/Epilepsy
183. True C, Pilossoph Z. Cost of Veterinary Care in 2023 - Pet Care Blog – Dog and Cat Health Advice and More | Healthy Paws [Internet]. Healthy Paws [cited 2024 Oct 31];Available from: https://www.healthypawspetinsurance.com/blog/cost-of-veterinary-care
184. Heske L, Nødtvedt A, Jäderlund KH, Berendt M, Egenvall A. A cohort study of epilepsy among 665,000 insured dogs: Incidence, mortality and survival after diagnosis. The Veterinary Journal 2014;202(3):471–6.
185. Epilepsy in dogs | Dog health | The Kennel Club [Internet]. [cited 2024 Oct 31];Available from: https://www.thekennelclub.org.uk/health-and-dog-care/health/health-and-care/a-z-of-health-and-care-issues/epilepsy/#
186. Jaggy A, Bernardini M. Idiopathic epilepsy in 125 dogs: A long-term study. Clinical and electroencephalographic findings. Journal of Small Animal Practice 1998;39(1):23–9.
187. Suñol A, Garcia-Pertierra S, Faller KME. Cerebrospinal fluid analysis in dogs: Main patterns and prevalence of albuminocytological dissociation. Veterinary Record [Internet] 2021 [cited 2024 Aug 29];188(5):N/A-N/A. Available from: https://onlinelibrary.wiley.com/doi/full/10.1002/vetr.27
188. Cerebrospinal Fluid Collection and Examination | VCA Animal Hospitals [Internet]. [cited 2024 Aug 29];Available from: https://vcahospitals.com/know-your-pet/cerebrospinal-fluid-collection-and-examination
189. Czarniak N, Kamińska J, Matowicka-Karna J, Koper-Lenkiewicz OM. Cerebrospinal Fluid–Basic Concepts Review. Biomedicines [Internet] 2023 [cited 2024 Aug 29];11(5). Available from: /pmc/articles/PMC10216641/
190. Telano LN, Baker S. Physiology, Cerebral Spinal Fluid. StatPearls [Internet] 2023 [cited 2024 Nov 1];Available from: https://www.ncbi.nlm.nih.gov/books/NBK519007/
191. Khasawneh AH, Garling RJ, Harris CA. Cerebrospinal fluid circulation: What do we know and how do we know it? Brain Circ [Internet] 2018 [cited 2024 Nov 22];4(1):14. Available from: https://pmc.ncbi.nlm.nih.gov/articles/PMC6057699/

192. Neuro-Diagnostic Tests Fact Sheet - Davies Veterinary Specialists [Internet]. [cited 2022 Feb 10];Available from: https://vetspecialists.co.uk/fact-sheets-post/neuro-diagnostic-tests-fact-sheet/
193. Stoop MP, Coulier L, Rosenling T, Shi S, Smolinska AM, Buydens L, et al. Quantitative Proteomics and Metabolomics Analysis of Normal Human Cerebrospinal Fluid Samples*. Molecular & Cellular Proteomics 2010;9(9):2063–75.
194. Aguilar-Castillo MJ, Cabezudo-García P, García-Martín G, Lopez-Moreno Y, Estivill-Torrús G, Ciano-Petersen NL, et al. A Systematic Review of the Predictive and Diagnostic Uses of Neuroinflammation Biomarkers for Epileptogenesis. International Journal of Molecular Sciences 2024, Vol 25, Page 6488 [Internet] 2024 [cited 2024 Nov 1];25(12):6488. Available from: https://www.mdpi.com/1422-0067/25/12/6488/htm
195. Banote RK, Akel S, Zelano J. Blood biomarkers in epilepsy. Acta Neurol Scand [Internet] 2022 [cited 2024 Nov 1];146(4):362. Available from: https://pmc.ncbi.nlm.nih.gov/articles/PMC9790299/
196. Banote RK, Håkansson S, Zetterberg H, Zelano J. CSF biomarkers in patients with epilepsy in Alzheimer's disease: a nation-wide study. Brain Commun [Internet] 2022 [cited 2024 Nov 1];4(4). Available from: https://dx.doi.org/10.1093/braincomms/fcac210
197. Hanin A, Lambrecq V, Denis JA, Imbert-Bismut F, Rucheton B, Lamari F, et al. Cerebrospinal fluid and blood biomarkers of status epilepticus. Epilepsia [Internet] 2020 [cited 2024 Nov 1];61(1):6–18. Available from: https://onlinelibrary.wiley.com/doi/full/10.1111/epi.16405
198. Kobylarek D, Iwanowski P, Lewandowska Z, Limphaibool N, Szafranek S, Labrzycka A, et al. Advances in the potential biomarkers of epilepsy. Front Neurol [Internet] 2019 [cited 2024 Nov 1];10(JUL):450539. Available from: www.frontiersin.org
199. Langenbruch L, Wiendl H, Groß C, Kovac S. Diagnostic utility of cerebrospinal fluid (CSF) findings in seizures and epilepsy with and without autoimmune-associated disease. Seizure 2021;91:233–43.
200. Mastrangelo M, Manti F, Ricciardi G, Cinnante EMC, Cameli N, Beatrice A, et al. The diagnostic and prognostic role of cerebrospinal fluid biomarkers in glucose transporter 1 deficiency: a systematic review. European Journal of

Pediatrics 2024 183:9 [Internet] 2024 [cited 2024 Nov 1];183(9):3665–78. Available from: https://link.springer.com/article/10.1007/s00431-024-05657-6

201. Simani L, Sadeghi M, Ryan F, Dehghani M, Niknazar S. Elevated Blood-Based Brain Biomarker Levels in Patients with Epileptic Seizures: A Systematic Review and Meta-analysis. ACS Chem Neurosci [Internet] 2020 [cited 2024 Nov 1];11(24):4048–59. Available from: https://pubs.acs.org/doi/full/10.1021/acschemneuro.0c00492
202. Dev P, Cyriac M, Chakravarty K, Pathak A. Blood and CSF biomarkers for post-stroke epilepsy: a systematic review. Acta Epileptologica [Internet] 2022 [cited 2024 Nov 1];4(1):1–9. Available from: https://aepi.biomedcentral.com/articles/10.1186/s42494-022-00091-3
203. Raoof R, Jimenez-Mateos EM, Bauer S, Tackenberg B, Rosenow F, Lang J, et al. Cerebrospinal fluid microRNAs are potential biomarkers of temporal lobe epilepsy and status epilepticus. Scientific Reports 2017 7:1 [Internet] 2017 [cited 2024 Nov 1];7(1):1–17. Available from: https://www.nature.com/articles/s41598-017-02969-6
204. Yakimov AM, Timechko EE, Areshkina IG, Usoltseva AA, Yakovleva KD, Kantimirova EA, et al. MicroRNAs as Biomarkers of Surgical Outcome in Mesial Temporal Lobe Epilepsy: A Systematic Review. International Journal of Molecular Sciences 2023, Vol 24, Page 5694 [Internet] 2023 [cited 2024 Nov 1];24(6):5694. Available from: https://www.mdpi.com/1422-0067/24/6/5694/htm
205. pandas - Python Data Analysis Library [Internet]. [cited 2024 Nov 4];Available from: https://pandas.pydata.org/
206. NumPy - [Internet]. [cited 2024 Nov 4];Available from: https://numpy.org/
207. Matplotlib — Visualization with Python [Internet]. [cited 2024 Nov 4];Available from: https://matplotlib.org/
208. SciPy - [Internet]. [cited 2024 Nov 4];Available from: https://scipy.org/
209. statsmodels 0.14.4 [Internet]. [cited 2024 Nov 4];Available from: https://www.statsmodels.org/stable/index.html
210. MetaboAnalyst [Internet]. [cited 2024 Nov 4];Available from: https://www.metaboanalyst.ca/
211. Human Metabolome Database [Internet]. [cited 2024 Jun 19];Available from: https://hmdb.ca/

212. Albrecht B, Voronina E, Schipke C, Peters O, Parr MK, Díaz-Hernández MD, et al. Pursuing Experimental Reproducibility: An Efficient Protocol for the Preparation of Cerebrospinal Fluid Samples for NMR-Based Metabolomics and Analysis of Sample Degradation. Metabolites [Internet] 2020 [cited 2024 Nov 4];10(6):251. Available from: https://pmc.ncbi.nlm.nih.gov/articles/PMC7345835/
213. Hasegawa T, Sumita M, Horitani Y, Tamai R, Tanaka K, Komori M, et al. Gas Chromatography-Mass Spectrometry-Based Metabolic Profiling of Cerebrospinal Fluid from Epileptic Dogs. J Vet Med Sci 2014;76(4):517–22.
214. Bernini P, Bertini I, Luchinat C, Nincheri P, Staderini S, Turano P. Standard operating procedures for pre-analytical handling of blood and urine for metabolomic studies and biobanks. J Biomol NMR [Internet] 2011 [cited 2024 Apr 23];49(3–4):231–43. Available from: https://link.springer.com/article/10.1007/s10858-011-9489-1
215. Tashjian RS, Vinters H V., Yong WH. Biobanking of Cerebrospinal Fluid. Methods Mol Biol [Internet] 2019 [cited 2024 Apr 23];1897:107. Available from: /pmc/articles/PMC6918832/
216. McNally MA, Hartman AL. Ketone Bodies in Epilepsy. J Neurochem [Internet] 2012 [cited 2025 Oct 18];121(1):28. Available from: https://pmc.ncbi.nlm.nih.gov/articles/PMC3969728/
217. Mariani CL, Nye CJ, Ruterbories L, Tokarz DA, Green L, Lau J, et al. Cerebrospinal fluid lactate concentrations in dogs with seizure disorders. J Vet Intern Med [Internet] 2020 [cited 2025 Oct 18];34(6):2562. Available from: https://pmc.ncbi.nlm.nih.gov/articles/PMC7694838/
218. Asthma - What Is Asthma? | NHLBI, NIH [Internet]. [cited 2024 Jun 12];Available from: https://www.nhlbi.nih.gov/health/asthma
219. What is asthma? | Asthma + Lung UK [Internet]. [cited 2024 Jun 12];Available from: https://www.asthmaandlung.org.uk/conditions/asthma/what-asthma
220. Types of asthma | Asthma + Lung UK [Internet]. [cited 2024 Nov 29];Available from: https://www.asthmaandlung.org.uk/conditions/asthma/types-asthma
221. Respiratory Health Initiative [Internet]. [cited 2024 Nov 29];Available from: https://respiratoryhealth.org/
222. Levy ML, Fleming L, Bush A. Asthma deaths in children in the UK: the last straw! British Journal of General Practice [Internet] 2024 [cited 2024 Nov 29];74(743):244–5. Available from: https://bjgp.org/content/74/743/244

223. Mukherjee M, Stoddart A, Gupta RP, Nwaru BI, Farr A, Heaven M, et al. The epidemiology, healthcare and societal burden and costs of asthma in the UK and its member nations: Analyses of standalone and linked national databases. BMC Med [Internet] 2016 [cited 2024 Nov 29];14(1):1–15. Available from: https://bmcmedicine.biomedcentral.com/articles/10.1186/s12916-016-0657-8
224. Iacobucci G. Asthma deaths rise 33% in past decade in England and Wales. BMJ [Internet] 2019 [cited 2024 Jun 12];366:l5108. Available from: https://www.bmj.com/content/366/bmj.l5108
225. NHS England » Respiratory disease [Internet]. [cited 2024 Dec 2];Available from: https://www.england.nhs.uk/ourwork/clinical-policy/respiratory-disease/
226. NHS England » Respiratory high impact interventions [Internet]. [cited 2024 Dec 2];Available from: https://www.england.nhs.uk/ourwork/prevention/secondary-prevention/respiratory-high-impact-interventions/
227. Cao Y, Chen S, Chen X, Zou W, Liu Z, Wu Y, et al. Global trends in the incidence and mortality of asthma from 1990 to 2019: An age-period-cohort analysis using the global burden of disease study 2019. Front Public Health 2022;10:1036674.
228. 2024 Severe Asthma Guide - Global Initiative for Asthma - GINA [Internet]. [cited 2024 Dec 2];Available from: https://ginasthma.org/severe-asthma/
229. Specialist asthma care | Asthma + Lung UK [Internet]. [cited 2024 Nov 29];Available from: https://www.asthmaandlung.org.uk/conditions/asthma/specialist-asthma-care
230. Asthma - Diagnosis - NHS [Internet]. [cited 2024 Nov 29];Available from: https://www.nhs.uk/conditions/asthma/diagnosis/
231. Kirenga BJ, Schwartz JI, Jong C De, van der Molen T, Okot-Nwang M. Guidance on the diagnosis and management of asthma among adults in resource limited settings. Afr Health Sci [Internet] 2015 [cited 2024 Jun 10];15(4):1189. Available from: /pmc/articles/PMC4765426/
232. Our asthma reports | Asthma + Lung UK [Internet]. [cited 2024 Jun 10];Available from: https://www.asthmaandlung.org.uk/about-us/our-latest-work/our-asthma-reports

233. Maniscalco M, Sofia M, De Laurentiis G, Paris D, Melck D, Motta A. Exploring Airway Diseases by NMR-Based Metabonomics: A Review of Application to Exhaled Breath Condensate. J Biomed Biotechnol [Internet] 2011 [cited 2024 Dec 4];2011:403260. Available from: https://pmc.ncbi.nlm.nih.gov/articles/PMC3061220/
234. Motta A, Paris D, D'Amato M, Melck D, Calabrese C, Vitale C, et al. NMR metabolomic analysis of exhaled breath condensate of asthmatic patients at two different temperatures. J Proteome Res [Internet] 2014 [cited 2024 Jun 10];13(12):6107–20. Available from: https://pubs.acs.org/doi/full/10.1021/pr5010407
235. Loureiro CC, Duarte IF, Gomes J, Carrola J, Barros AS, Gil AM, et al. Urinary metabolomic changes as a predictive biomarker of asthma exacerbation. Journal of Allergy and Clinical Immunology [Internet] 2014 [cited 2024 Jun 10];133(1):261-263.e5. Available from: http://www.jacionline.org/article/S0091674913017144/fulltext
236. Saude EJ, Skappak CD, Regush S, Cook K, Ben-Zvi A, Becker A, et al. Metabolomic profiling of asthma: Diagnostic utility of urine nuclear magnetic resonance spectroscopy. Journal of Allergy and Clinical Immunology 2011;127(3):757-764.e6.
237. Mamtimin B, Hizbulla M, Kurbantay N, You L, Yan X, Upur H. An magnetic resonance-based plasma metabonomic investigation on abnormal Savda in different complicated diseases. Journal of Traditional Chinese Medicine 2014;34(2):166–72.
238. Jung J, Kim SH, Lee HS, Choi GS, Jung YS, Ryu DH, et al. Serum metabolomics reveals pathways and biomarkers associated with asthma pathogenesis. Clinical & Experimental Allergy [Internet] 2013 [cited 2024 Jun 10];43(4):425–33. Available from: https://onlinelibrary.wiley.com/doi/full/10.1111/cea.12089
239. Farraia M, cavaleiro ruFo J, castro MenDes F, Boechat J, Farraia M. Metabolic interactions in asthma. Eur Ann AllErgy Clin immunol 51(5).
240. Kelly RS, Dahlin A, McGeachie MJ, Qiu W, Sordillo J, Wan ES, et al. Asthma Metabolomics and the Potential for Integrative Omics in Research and the Clinic. Chest [Internet] 2016 [cited 2024 Dec 4];151(2):262. Available from: https://pmc.ncbi.nlm.nih.gov/articles/PMC5310123/

241. Warner JO. The Blood Lung Function Test. https://doi.org/101164/rccm2303002 2012;167(11):1465–6.
242. Chang C, Guo ZG, He B, Yao WZ. Metabolic alterations in the sera of Chinese patients with mild persistent asthma: a GC-MS-based metabolomics analysis. Acta Pharmacol Sin [Internet] 2015 [cited 2024 Jun 10];36(11):1356. Available from: /pmc/articles/PMC4635323/
243. Yamauchi K, Ogasawara M. The Role of Histamine in the Pathophysiology of Asthma and the Clinical Efficacy of Antihistamines in Asthma Therapy. Int J Mol Sci [Internet] 2019 [cited 2025 Oct 18];20(7). Available from: https://pubmed.ncbi.nlm.nih.gov/30965592/
244. Cottrill KA, Stephenson ST, Mohammad AF, Kim SO, McCarty NA, Kamaleswaran R, et al. Exacerbation-prone pediatric asthma is associated with arginine, lysine, and methionine pathway alterations. Journal of Allergy and Clinical Immunology [Internet] 2023 [cited 2025 Oct 18];151(1):118-127.e10. Available from: https://www.sciencedirect.com/science/article/pii/S0091674922011277
245. Fogarty A, Broadfield E, Lewis S, Lawson N, Britton J. Amino acids and asthma: a case-control study. European Respiratory Journal [Internet] 2004 [cited 2025 Oct 18];23(4):565–8. Available from: https://publications.ersnet.org/content/erj/23/4/565
246. Appel D, Rubenstein R, Schrager K, Williams MH. Lactic acidosis in severe asthma. Am J Med [Internet] 1983 [cited 2025 Oct 18];75(4):580–4. Available from: https://www.amjmed.com/action/showFullText?pii=0002934383904369
247. Narendra DK, Khurana S. Asthma and Hyperglycemia: Exploring the Interconnected Pathways. Diagnostics [Internet] 2024 [cited 2025 Oct 18];14(17):1869. Available from: https://pmc.ncbi.nlm.nih.gov/articles/PMC11393853/
248. Kim JM, Im YN, Chung YJ, Youm J ho, Im SY, Han MK, et al. Glutamine deficiency shifts the asthmatic state toward neutrophilic airway inflammation. Allergy [Internet] 2022 [cited 2025 Oct 18];77(4):1180–91. Available from: https://pubmed.ncbi.nlm.nih.gov/34601745/
249. Kharroubi AT, Darwish HM. Diabetes mellitus: The epidemic of the century. World J Diabetes [Internet] 2015 [cited 2022 Mar 23];6(6):850. Available from: /pmc/articles/PMC4478580/

250. National Diabetes Audit - Report 2 Complications and Mortality, 2017-18 - NHS Digital [Internet]. 2019 [cited 2022 Mar 15];Available from: https://digital.nhs.uk/data-and-information/publications/statistical/national-diabetes-audit/report-2--complications-and-mortality-2017-18#
251. Raffel LJ, Goodarzi MO. Diabetes Mellitus [Internet]. Elsevier; 2014. Available from: https://www.sciencedirect.com/science/article/pii/B9780128012383055586
252. Cnop M, Welsh N, Jonas JC, Jörns A, Lenzen S, Eizirik DL. Mechanisms of pancreatic beta-cell death in type 1 and type 2 diabetes: many differences, few similarities. Diabetes [Internet] 2005 [cited 2022 Mar 15];54 Suppl 2(SUPPL. 2). Available from: https://pubmed.ncbi.nlm.nih.gov/16306347/
253. Diabetes Footcare - OHID [Internet]. [cited 2022 Jan 25];Available from: https://fingertips.phe.org.uk/profile/diabetes-footcare
254. National Diabetes Audit - Report 2 Complications and Mortality, 2017-18 - NHS Digital [Internet]. 2019 [cited 2022 Jan 25];Available from: https://digital.nhs.uk/data-and-information/publications/statistical/national-diabetes-audit/report-2--complications-and-mortality-2017-18
255. Ilonen J, Lempainen J, Veijola R. The heterogeneous pathogenesis of type 1 diabetes mellitus. Nature Reviews Endocrinology 2019 15:11 [Internet] 2019 [cited 2022 Mar 15];15(11):635–50. Available from: https://www.nature.com/articles/s41574-019-0254-y
256. Papatheodorou K, Banach M, Bekiari E, Rizzo M, Edmonds M. Complications of Diabetes 2017. J Diabetes Res 2018;2018.
257. Sapra A, Bhandari P. Diabetes Mellitus. StatPearls [Internet] 2021 [cited 2022 Mar 15];Available from: https://www.ncbi.nlm.nih.gov/books/NBK551501/
258. Ingerski LM, Anderson BJ, Dolan LM, Hood KK. Blood Glucose Monitoring and Glycemic Control in Adolescence: Contribution of Diabetes-Specific Responsibility and Family Conflict. Journal of Adolescent Health 2010;47(2):191–7.
259. The National Diabetes Audit (NDA) provides a comprehensive view of diabetes care in England and Wales and measures the effectiveness of diabetes healthcare against NICE Clinical Guidelines and NICE Quality Standards. 2018 [cited 2022 Mar 15];Available from: www.digital.nhs.uk
260. undefined, DM N, S G, J L, P C, O C, et al. The effect of intensive treatment of diabetes on the development and progression of long-term complications

in insulin-dependent diabetes mellitus. N Engl J Med [Internet] 1993 [cited 2022 Mar 23];329(14):977–86. Available from: http://content.nejm.org/cgi/content/full/329/14/977

261. Iglay K, Hannachi H, Howie PJ, Xu J, Li X, Engel SS, et al. Prevalence and co-prevalence of comorbidities among patients with type 2 diabetes mellitus. Curr Med Res Opin [Internet] 2016 [cited 2022 Mar 15];32(7):1243–52. Available from: https://www.tandfonline.com/doi/abs/10.1185/03007995.2016.1168291
262. Sherling DH, Perumareddi P, Hennekens CH. Metabolic Syndrome: Clinical and Policy Implications of the New Silent Killer. J Cardiovasc Pharmacol Ther [Internet] 2017 [cited 2022 Mar 15];22(4):365–7. Available from: https://journals.sagepub.com/doi/full/10.1177/1074248416686187
263. Whicher CA, O'Neill S, Holt RIG. Diabetes in the UK: 2019. Diabetic Medicine [Internet] 2020 [cited 2022 Mar 15];37(2):242–7. Available from: https://onlinelibrary.wiley.com/doi/full/10.1111/dme.14225
264. DiMeglio LA, Evans-Molina C, Oram RA. Type 1 diabetes. Lancet [Internet] 2018;391(10138):2449–62. Available from: https://pubmed.ncbi.nlm.nih.gov/29916386
265. Chen C, Zhao XL, Li ZH, Zhu ZG, Qian SH, Flewitt AJ. Current and Emerging Technology for Continuous Glucose Monitoring. Sensors 2017, Vol 17, Page 182 [Internet] 2017 [cited 2022 Mar 15];17(1):182. Available from: https://www.mdpi.com/1424-8220/17/1/182/htm
266. Rajaei E, Jalali MT, Shahrabi S, Asnafi AA, Pezeshki SMS. HLAs in Autoimmune Diseases: Dependable Diagnostic Biomarkers? Curr Rheumatol Rev 2019;15(4):269–76.
267. How many people in the UK have diabetes? [Internet]. [cited 2024 Nov 19];Available from: https://www.diabetes.org.uk/about-us/about-the-charity/our-strategy/statistics#
268. 2. Classification and Diagnosis of Diabetes: Standards of Medical Care in Diabetes-2019. Diabetes Care [Internet] 2019 [cited 2022 Mar 15];42(Suppl 1):S13–28. Available from: https://pubmed.ncbi.nlm.nih.gov/30559228/
269. National Diabetes Audit Report 1 Care Processes and Treatment Targets 2017-18 - NHS Digital [Internet]. [cited 2022 Jan 25];Available from: https://digital.nhs.uk/data-and-information/publications/statistical/national-

diabetes-audit/report-1-care-processes-and-treatment-targets-2017-18-short-report

270. Glucose Tolerance Test [Internet]. [cited 2022 Mar 15];Available from: https://www.diabetes.co.uk/oral-glucose-tolerance-test.html
271. Harreiter J, Roden M. Diabetes mellitus – Definition, Klassifikation, Diagnose, Screening und Prävention (Update 2019). Wien Klin Wochenschr [Internet] 2019;131(1):6–15. Available from: https://doi.org/10.1007/s00508-019-1450-4
272. Oh TK, Han S, Oh AY, Kim S, Ryu JH. Chronic hyperglycemia with elevated glycated hemoglobin level and its association with postoperative acute kidney injury after a major laparoscopic abdominal surgery in diabetes patients. J Anesth [Internet] 2018 [cited 2022 Mar 15];32(5):740–7. Available from: https://pubmed.ncbi.nlm.nih.gov/30218160/
273. Knowler WC, Edelstein SL, Goldberg RB, Ackermann RT, Crandall JP, Florez JC, et al. HbA1c as a predictor of diabetes and as an outcome in the diabetes prevention program: a randomized clinical trial. Diabetes Care [Internet] 2015 [cited 2022 Mar 15];38(1):51–8. Available from: https://pubmed.ncbi.nlm.nih.gov/25336746/
274. Welsh KJ, Kirkman MS, Sacks DB. Role of Glycated Proteins in the Diagnosis and Management of Diabetes: Research Gaps and Future Directions. Diabetes Care [Internet] 2016 [cited 2022 Mar 15];39(8):1299–306. Available from: https://diabetesjournals.org/care/article/39/8/1299/37126/Role-of-Glycated-Proteins-in-the-Diagnosis-and
275. Goldstein DE, Little RR, Lorenz RA, Malone JI, Nathan D, Peterson CM, et al. Tests of Glycemia in Diabetes. Diabetes Care [Internet] 2004;27(7):1761. Available from: http://care.diabetesjournals.org/content/27/7/1761.abstract
276. What is HbA1c? | Blood Test | Target Levels | Diabetes UK [Internet]. [cited 2022 Mar 15];Available from: https://www.diabetes.org.uk/guide-to-diabetes/managing-your-diabetes/hba1c
277. Würtz P, Tiainen M, Mäkinen VP, Kangas AJ, Soininen P, Saltevo J, et al. Circulating metabolite predictors of glycemia in middle-aged men and women. Diabetes Care [Internet] 2012 [cited 2022 Mar 15];35(8):1749–56. Available from: /pmc/articles/PMC3402262/
278. Lu J, Xie G, Jia W, Jia W. Metabolomics in human type 2 diabetes research.

279. Lotta LA, Scott RA, Sharp SJ, Burgess S, Luan J, Tillin T, et al. Genetic Predisposition to an Impaired Metabolism of the Branched-Chain Amino Acids and Risk of Type 2 Diabetes: A Mendelian Randomisation Analysis. PLoS Med [Internet] 2016 [cited 2022 Mar 15];13(11):e1002179. Available from: https://journals.plos.org/plosmedicine/article?id=10.1371/journal.pmed.1002179
280. Zhao X, Han Q, Liu Y, Sun C, Gang X, Wang G. The Relationship between Branched-Chain Amino Acid Related Metabolomic Signature and Insulin Resistance: A Systematic Review. J Diabetes Res 2016;2016.
281. Fasting Plasma Glucose Test [Internet]. [cited 2022 Mar 15];Available from: https://www.diabetes.co.uk/fasting-plasma-glucose-test.html
282. Tirosh A, Shai I, Tekes-Manova D, Israeli E, Pereg D, Shochat T, et al. Normal Fasting Plasma Glucose Levels and Type 2 Diabetes in Young Men. http://dx.doi.org/101056/NEJMoa050080 [Internet] 2009 [cited 2022 Mar 15];353(14):1454–62. Available from: https://www.nejm.org/doi/full/10.1056/NEJMoa050080
283. Brunzell JD, Robertson RP, Lerner RL, Hazzard WR, Ensinck JW, Bierman EL, et al. Relationships Between Fasting Plasma Glucose Levels and Insulin Secretion During Intravenous Glucose Tolerance Tests. J Clin Endocrinol Metab [Internet] 1976 [cited 2022 Mar 15];42(2):222–9. Available from: https://academic.oup.com/jcem/article/42/2/222/2685175
284. Jang C, Oh SF, Wada S, Rowe GC, Liu L, Chan MC, et al. A branched-chain amino acid metabolite drives vascular fatty acid transport and causes insulin resistance. Nat Med [Internet] 2016;22(4):421–6. Available from: https://doi.org/10.1038/nm.4057
285. Weight loss surgery for type 2 diabetes | Diabetes UK [Internet]. [cited 2023 Nov 22];Available from: https://www.diabetes.org.uk/guide-to-diabetes/managing-your-diabetes/treating-your-diabetes/weight-loss-surgery
286. Welbourn RB (Richard B, Dendrite Clinical Systems., National Bariatric Surgery Registry. Second registry report 2014. 2014;295.
287. Home | Bariatric Surgeon Reporting Website [Internet]. [cited 2024 Nov 21];Available from: https://nbsr.e-dendrite.com/
288. Bariatric Surgery Statistics & Facts - 2024 - Renew Bariatrics [Internet]. [cited 2024 Nov 21];Available from: https://renewbariatrics.com/bariatric-surgery-statistics/

289. Courcoulas A, Coley RY, Clark JM, McBride CL, Cirelli E, McTigue K, et al. Interventions and Operations 5 Years after Bariatric Surgery in a Cohort from the US National Patient-Centered Clinical Research Network Bariatric Study. JAMA Surg [Internet] 2020 [cited 2023 Nov 21];155(3):194–204. Available from: https://www.niddk.nih.gov/health-information/weight-management/bariatric-surgery/side-effects
290. Weight loss surgery - NHS [Internet]. [cited 2023 Nov 21];Available from: https://www.nhs.uk/conditions/weight-loss-surgery/
291. Compare Bariatric Procedures - Which Procedure Is Right For You? [Internet]. [cited 2024 Nov 21];Available from: https://renewbariatrics.com/procedures/compare/
292. Park JY. Weight Loss Prediction after Metabolic and Bariatric Surgery. J Obes Metab Syndr [Internet] 2023 [cited 2023 Nov 21];32(1):46. Available from: /pmc/articles/PMC10088553/
293. Aron-Wisnewsky J, Sokolovska N, Liu Y, Comaneshter DS, Vinker S, Pecht T, et al. The advanced-DiaRem score improves prediction of diabetes remission 1 year post-Roux-en-Y gastric bypass. Diabetologia [Internet] 2017 [cited 2023 Nov 21];60(10):1892–902. Available from: https://link.springer.com/article/10.1007/s00125-017-4371-7
294. Lee WJ, Chong K, Chen SC, Zachariah J, Ser KH, Lee YC, et al. Preoperative Prediction of Type 2 Diabetes Remission After Gastric Bypass Surgery: a Comparison of DiaRem Scores and ABCD Scores. Obes Surg [Internet] 2016 [cited 2023 Nov 21];26(10):2418–24. Available from: https://link.springer.com/article/10.1007/s11695-016-2120-5
295. Aminian A, Brethauer SA, Kashyap SR, Kirwan JP, Schauer PR. DiaRem score: External validation. Lancet Diabetes Endocrinol [Internet] 2014 [cited 2023 Nov 21];2(1):12–3. Available from: http://www.thelancet.com/article/S221385871370202X/fulltext
296. Lopes TIB, Geloneze B, Pareja JC, Calixto AR, Ferreira MMC, Marsaioli AJ. “Omics” Prospective Monitoring of Bariatric Surgery: Roux-En-Y Gastric Bypass Outcomes Using Mixed-Meal Tolerance Test and Time-Resolved 1H NMR-Based Metabolomics. https://home.liebertpub.com/omi [Internet] 2016 [cited 2023 Nov 21];20(7):415–23. Available from: https://www.liebertpub.com/doi/10.1089/omi.2016.0061

297. Percival BC, Grootveld M, Gibson M, Osman Y, Molinari M, Jafari F, et al. Low-field, benchtop NMR spectroscopy as a potential tool for point-of-care diagnostics of metabolic conditions: Validation, protocols and computational models. High Throughput 2019;8(1).
298. Leenders J, Grootveld M, Percival B, Gibson M, Casanova F, Wilson PB. Benchtop low-frequency 60 MHz NMR analysis of urine: A comparative metabolomics investigation. Metabolites 2020;10(4).
299. Grootveld M, Percival B, Gibson M, Osman Y, Edgar M, Molinari M, et al. Progress in low-field benchtop NMR spectroscopy in chemical and biochemical analysis. Anal Chim Acta 2019;1067:11–30.
300. Finch N, Percival B, Hunter E, Blagg RJ, Blackwell E, Sagar J, et al. Preliminary demonstration of benchtop NMR metabolic profiling of feline urine: chronic kidney disease as a case study. BMC Res Notes [Internet] 2021 [cited 2023 Nov 21];14(1):469. Available from: /pmc/articles/PMC8708514/
301. Grootveld M, Percival B, Gibson M, Osman Y, Edgar M, Molinari M, et al. Progress in Low Field Benchtop NMR Spectroscopy in Chemical and Biochemical Analysis 1.
302. Garcia E, Wolak-Dinsmore J, Wang Z, Li XS, Bennett DW, Connelly MA, et al. NMR quantification of trimethylamine-N-oxide in human serum and plasma in the clinical laboratory setting. Clin Biochem 2017;50(16–17):947–55.
303. Types of Gastric Surgery [Internet]. [cited 2024 Nov 20];Available from: https://app.biorender.com/biorender-templates/figures/all/t-66703b201c7de84ccc00a6a7-types-of-gastric-surgery
304. WMA Declaration of Helsinki – Ethical Principles for Medical Research Involving Human Participants – WMA – The World Medical Association [Internet]. [cited 2024 Nov 18];Available from: https://www.wma.net/policies-post/wma-declaration-of-helsinki/
305. Estimate of Bariatric Surgery Numbers, 2011-2021 | American Society for Metabolic and Bariatric Surgery [Internet]. [cited 2023 Nov 20];Available from: https://asmbs.org/resources/estimate-of-bariatric-surgery-numbers
306. Samczuk P, Hady HR, Adamska-Patruno E, Citko A, Dadan J, Barbas C, et al. In-and-Out Molecular Changes Linked to the Type 2 Diabetes Remission after Bariatric Surgery: An Influence of Gut Microbes on Mitochondria Metabolism. [cited 2023 Nov 21];Available from: www.mdpi.com/journal/ijms

307. Chang Tan H, Hsu JW, Kovalik JP, Eng A, Hoong Chan W, Meng Khoo C, et al. Branched-Chain Amino Acid Oxidation Is Elevated in Adults with Morbid Obesity and Decreases Significantly after Sleeve Gastrectomy. [cited 2023 Nov 21];Available from: https://doi.org/10.1093/jn/nxaa298.
308. Kwon Y, Jang M, Lee Y, Ha J, Park S. Metabolomic Analysis of the Improvements in Insulin Secretion and Resistance After Sleeve Gastrectomy: Implications of the Novel Biomarkers. Obes Surg 2021;31(1):43–52.
309. Ramos-Molina B, Castellano-Castillo D, Alcaide-Torres J, Pastor O, De Luna D Iaz R, Salas-Salvad J, et al. Differential effects of restrictive and malabsorptive bariatric surgery procedures on the serum lipidome in obese subjects. J Clin Lipidol [Internet] 2018 [cited 2023 Nov 21];12:1502–12. Available from: https://doi.org/10.1016/j.jacl.2018.07.006
310. Kayser BD, Lhomme M, Dao MC, Ichou F, Bouillot JL, Prifti E, et al. Serum lipidomics reveals early differential effects of gastric bypass compared with banding on phospholipids and sphingolipids independent of differences in weight loss. Int J Obes 2017;41(6):917–25.
311. Vaz M, Pereira SS, Monteiro MP. Metabolomic signatures after bariatric surgery – a systematic review. Reviews in Endocrine and Metabolic Disorders 2021 23:3 [Internet] 2021 [cited 2023 Nov 20];23(3):503–19. Available from: https://link.springer.com/article/10.1007/s11154-021-09695-5
312. Ha J, Jang M, Kwon YK, Park YS, Park DJ, Lee JH, et al. Metabolomic profiles predict diabetes remission after bariatric surgery. J Clin Med 2020;9(12):1–12.
313. Lee WJ, Almulaifi A, Chong K, Chen SC, Tsou JJ, Ser KH, et al. The Effect and Predictive Score of Gastric Bypass and Sleeve Gastrectomy on Type 2 Diabetes Mellitus Patients with BMI < 30 kg/m2. Obes Surg 2015;25(10):1772–8.
314. Park JY. Prediction of type 2 diabetes remission after bariatric or metabolic surgery. J Obes Metab Syndr2018;27(4):213–22.
315. Elsayed NA, Aleppo G, Aroda VR, Bannuru RR, Brown FM, Bruemmer D, et al. 2. Classification and Diagnosis of Diabetes: Standards of Care in Diabetes-2023. 2022 [cited 2024 Jul 30];Available from: https://doi.org/10.2337/dc23-S002
316. Del Coco L, Vergara D, De Matteis S, Mensà E, Sabbatinelli J, Prattichizzo F, et al. NMR-Based Metabolomic Approach Tracks Potential Serum Biomarkers

of Disease Progression in Patients with Type 2 Diabetes Mellitus. Journal of Clinical Medicine 2019, Vol 8, Page 720 [Internet] 2019 [cited 2022 Mar 16];8(5):720. Available from: https://www.mdpi.com/2077-0383/8/5/720/htm

317. Del Coco L, Vergara D, De Matteis S, Mensà E, Sabbatinelli J, Prattichizzo F, et al. NMR-Based Metabolomic Approach Tracks Potential Serum Biomarkers of Disease Progression in Patients with Type 2 Diabetes Mellitus. Journal of Clinical Medicine 2019, Vol 8, Page 720 [Internet] 2019;8(5):720. Available from: https://www.mdpi.com/2077-0383/8/5/720/htm
318. Long J, Yang Z, Wang L, Han Y, Peng C, Yan C, et al. Metabolite biomarkers of type 2 diabetes mellitus and pre-diabetes: a systematic review and meta-analysis. BMC Endocr Disord [Internet] 2020 [cited 2024 Jul 29];20(1):1–17. Available from: https://bmcendocrdisord.biomedcentral.com/articles/10.1186/s12902-020-00653-x
319. Wang-Sattler R, Yu Z, Herder C, Messias AC, Floegel A, He Y, et al. Novel biomarkers for pre-diabetes identified by metabolomics. Mol Syst Biol [Internet] 2012 [cited 2024 Jul 29];8:615. Available from: https://www.embopress.org/doi/10.1038/msb.2012.43
320. Gu X, Al Dubayee M, Alshahrani A, Masood A, Benabdelkamel H, Zahra M, et al. Distinctive Metabolomics Patterns Associated With Insulin Resistance and Type 2 Diabetes Mellitus. Front Mol Biosci [Internet] 2020 [cited 2024 Jul 29];7:609806. Available from: www.metaboanalyst.ca
321. Alves A, Bassot A, Bulteau AL, Pirola L, Morio B. Glycine Metabolism and Its Alterations in Obesity and Metabolic Diseases. Nutrients [Internet] 2019 [cited 2025 Oct 18];11(6):1356. Available from: https://pmc.ncbi.nlm.nih.gov/articles/PMC6627940/
322. Thaker V V., Kwee LC, Chen H, Bahnson J, Ilkayeva O, Muehlbauer MJ, et al. Metabolite signature of diabetes remission in individuals with obesity undergoing weight loss interventions. Obesity (Silver Spring) [Internet] 2023 [cited 2025 Oct 18];32(2):304. Available from: https://pmc.ncbi.nlm.nih.gov/articles/PMC11201087/
323. Friedrich N, Budde K, Wolf T, Jungnickel A, Grotevendt A, Dreßler M, et al. Short-term changes of the urine metabolome after bariatric surgery. OMICS [Internet] 2012 [cited 2025 Oct 18];16(11):612–20. Available from: https://pubmed.ncbi.nlm.nih.gov/23095112/

324. Friedrich N, Budde K, Wolf T, Jungnickel A, Grotevendt A, Dreßler M, et al. Short-term changes of the urine metabolome after bariatric surgery. OMICS [Internet] 2012 [cited 2025 Oct 18];16(11):612–20. Available from: https://pubmed.ncbi.nlm.nih.gov/23095112/
325. Rizo-Roca D, Henderson JD, Zierath JR. Metabolomics in cardiometabolic diseases: Key biomarkers and therapeutic implications for insulin resistance and diabetes. J Intern Med [Internet] 2025 [cited 2025 Oct 18];297(6):584. Available from: https://pmc.ncbi.nlm.nih.gov/articles/PMC12087830/
326. Li J V., Ashrafian H, Sarafian M, Homola D, Rushton L, Barker G, et al. Roux-en-Y gastric bypass-induced bacterial perturbation contributes to altered host-bacterial co-metabolic phenotype. Microbiome [Internet] 2021 [cited 2025 Oct 18];9(1):139. Available from: https://pmc.ncbi.nlm.nih.gov/articles/PMC8201742/
327. Lee SJ, Park YS, Kim YJ, Han SU, Hwang GS, Han Y, et al. Changes in trimethylamine-n-oxide levels in obese patients following laparoscopic roux-en-y gastric bypass or sleeve gastrectomy in a korean obesity surgical treatment study (Kobess). J Clin Med [Internet] 2021 [cited 2025 Oct 18];10(21):5091. Available from: https://pmc.ncbi.nlm.nih.gov/articles/PMC8584728/
328. Boshier PR, Fehervari M, Markar SR, Purkayastha S, Spanel P, Smith D, et al. Variation in Exhaled Acetone and Other Ketones in Patients Undergoing Bariatric Surgery: a Prospective Cross-sectional Study. Obes Surg [Internet] 2018 [cited 2025 Oct 18];28(8):2439–46. Available from: https://link.springer.com/article/10.1007/s11695-018-3180-5
329. Boshier PR, Fehervari M, Markar SR, Purkayastha S, Spanel P, Smith D, et al. Variation in Exhaled Acetone and Other Ketones in Patients Undergoing Bariatric Surgery: a Prospective Cross-sectional Study. Obes Surg [Internet] 2018 [cited 2025 Oct 18];28(8):2439–46. Available from: https://link.springer.com/article/10.1007/s11695-018-3180-5
330. Mo H, Raftery D. Pre-SAT180, a Simple and Effective Method for Residual Water Suppression. J Magn Reson [Internet] 2008 [cited 2024 Feb 9];190(1):1. Available from: /pmc/articles/PMC2662483/
331. Cho K, Chung JY, Cho SK, Shin HW, Jang IJ, Park JW, et al. Antihyperglycemic mechanism of metformin occurs via the AMPK/LXRα/POMC pathway. Scientific Reports 2015 5:1 [Internet] 2015

[cited 2024 Feb 9];5(1):1–7. Available from: https://www.nature.com/articles/srep08145

332. Pelantová H, Bugáňová M, Holubová M, Šedivá B, Zemenová J, Sýkora D, et al. Urinary metabolomic profiling in mice with diet-induced obesity and type 2 diabetes mellitus after treatment with metformin, vildagliptin and their combination. Mol Cell Endocrinol 2016;431:88–100.
333. Park JE, Jeong GH, Lee IK, Yoon YR, Liu KH, Gu N, et al. A Pharmacometabolomic Approach to Predict Response to Metformin in Early-Phase Type 2 Diabetes Mellitus Patients. Molecules 2018, Vol 23, Page 1579 [Internet] 2018 [cited 2024 Feb 9];23(7):1579. Available from: https://www.mdpi.com/1420-3049/23/7/1579/htm
334. Garcia-Galiano D, Borges BC, Allen SJ, Elias CF. PI3K signalling in leptin receptor cells: Role in growth and reproduction. J Neuroendocrinol [Internet] 2019 [cited 2024 Feb 9];31(5):e12685. Available from: https://onlinelibrary.wiley.com/doi/full/10.1111/jne.12685
335. John CM, Yusof NISM, Aziz SHA, Fauzi FM. Maternal Cognitive Impairment Associated with Gestational Diabetes Mellitus—A Review of Potential Contributing Mechanisms. International Journal of Molecular Sciences 2018, Vol 19, Page 3894 [Internet] 2018 [cited 2024 Feb 9];19(12):3894. Available from: https://www.mdpi.com/1422-0067/19/12/3894/htm
336. Różańska D, Regulska-Ilow B. The significance of anthocyanins in the prevention and treatment of type 2 diabetes. Advances in Clinical and Experimental Medicine 2018;27(1):135–42.
337. Glosse P, Föller M. AMP-Activated Protein Kinase (AMPK)-Dependent Regulation of Renal Transport. International Journal of Molecular Sciences 2018, Vol 19, Page 3481 [Internet] 2018 [cited 2024 Feb 9];19(11):3481. Available from: https://www.mdpi.com/1422-0067/19/11/3481/htm
338. Hirosumi J, Tuncman G, Chang L, Görgün CZ, Uysal KT, Maeda K, et al. A central role for JNK in obesity and insulin resistance. Nature 2002 420:6913 [Internet] 2002 [cited 2024 Feb 9];420(6913):333–6. Available from: https://www.nature.com/articles/nature01137
339. Andersson-Hall U, Gustavsson C, Pedersen A, Malmodin D, Joelsson L, Holmäng A. Higher Concentrations of BCAAs and 3-HIB Are Associated with Insulin Resistance in the Transition from Gestational Diabetes to Type 2

Diabetes. J Diabetes Res [Internet] 2018 [cited 2024 Aug 6];2018(1):4207067. Available from: https://onlinelibrary.wiley.com/doi/full/10.1155/2018/4207067

340. Kujala UM, Peltonen M, Laine MK, Kaprio J, Heinonen OJ, Sundvall J, et al. Branched-chain amino acid levels are related with surrogates of disturbed lipid metabolism among older men. Front Med (Lausanne) [Internet] 2016 [cited 2024 Aug 6];3(NOV):215721. Available from: www.frontiersin.org
341. Pang Z, Wang G, Wang C, Zhang W, Liu J, Wang F. Serum Metabolomics Analysis of Asthma in Different Inflammatory Phenotypes: A Cross-Sectional Study in Northeast China. Biomed Res Int [Internet] 2018 [cited 2024 Jun 10];2018(1):2860521. Available from: https://onlinelibrary.wiley.com/doi/full/10.1155/2018/2860521
342. Sample Preparation - SSPPS NMR Facility - UC San Diego [Internet]. [cited 2021 Dec 23];Available from: http://sopnmr.ucsd.edu/sample-preparation.htm
343. Boron NMR [Internet]. [cited 2022 Jan 27];Available from: http://chem.ch.huji.ac.il/nmr/techniques/1d/row2/b.html